Advancing reliability information for Wave Energy Converters

Philipp Rudolf Thies

School of Engineering, Mathematics and Physical Science

University of Exeter

I certify that all material in this thesis which is not my own work has been identified and that no material has previously been submitted and approved for the award of a degree by this or any other University.

. . . . . .

A thesis submitted for the degree of

Doctor of Philosophy in Renewable Energy

August 2012

Abstract

Marine renewable energy promises to provide a significant contribution to the future electricity supply. It is estimated that 17% of today's UK electricity demand could be generated from wave and tidal sources. The ambition to harvest this resource is in the public interest, as it eases the pressures on energy security, holds the potential to reduce carbon emissions and has the prospect to create a new UK industry sector worth £15 billion. From an engineering perspective, marine energy is one of the least developed renewable energy technologies and has to be regarded as unproven. The reliability of components and devices in the harsh marine environment is one of the main engineering challenges. Reliability assessments and the assurance of acceptable reliability levels are dependant on the adequacy of failure information, which is scantily available for marine energy.

This thesis shows that large failure rate uncertainties impede the reliability assessment for wave energy converters and how a suite of experimental, numerical and statistical methods can be applied to improve scarcely available reliability information. The analysis of component load conditions identifies fatigue as failure mode of concern and the fatigue life of mooring lines and marine power cables is quantified in a floating wave energy application. A Bayesian statistical approach and dedicated service-simulation component testing is proposed, and implemented to improve the quality of reliability estimates and to provide relevant data and assurance.

The methods presented, along with the results, will assist reliability assessment and design during early development stages, and will inform the prediction of maintenance requirements during operation. Reliable marine energy systems will be the technical enabler for the successful transition of prototype devices to a commercially viable marine energy industry.

Acknowledgements

It is with the greatest humbleness that I receive this PhD. It is the result of great personal, intellectual and mental efforts. As such, it required not only the commitment and perseverance of myself, but of several others who supported, advised, criticised, helped and encouraged me along the way.

My team of supervisors at the University of Exeter, Prof. George H. Smith, Dr Lars Johanning and Prof. Julian Wolfram showed me the ropes of academia, challenged my ideas and supported me on my quest to become an independent researcher. I am extremely grateful for the numerous opportunities they have provided for me, as well as their continuous and valuable thoughts. Further, I want to acknowledge and thank my external examiners, Prof. Feargal Brennan (Cranfield University) and Prof. Alexander Day (University of Strathclyde) and my internal examiner Dr Khurram Wadee.

I would also like to thank an enthusiastic and innovative team of engineers (Dave Parish, Ian Faulks and Tom Clifford) and the invaluable team of PhD students who became and are becoming Dr along side me (Ian Ashton, Andrew Vickers, Angus Vantoch-Wood, Alfonso Ramallo). I also express my sincere gratitude to Wendy Campbell at the ASU reception who always has a smiling encouragement to offer.

I would also like to mention the support from all the organisations I had the opportunity to work with along the way, including Orcina, JDR Cable Systems, Det Norske Veritas, Wave Energy Centre and Event Horizon.

This research was made possible through PhD studentship funding provided by the Engineering and Physical Sciences Research Council under its SuperGen Marine Phase 2 initiative. My work also benefited from funds available through the Peninsula Research Institute for Marine Renewable Energy (PRIMaRE) funded by the South West Regional Development Agency

(SWRDA) and the European Regional Development Fund (ERDF) Competitiveness and Convergence Programme. The Institution of Engineering and Technology (IET) awarded me with a Postgraduate Scholarship in 2010 which also helped this research.

On a personal note, my parents Sylvia Thies and Rudolph Brueckner-Thies own all the credit of bringing up a restless, inquisitive, demanding child and giving me confidence and trust.

Most importantly, I am forever indebted to my wife Heinke and our son Joshua for all the love, joy and spirit you bring to my life. I have received an incredible amount of unconditional support and generosity from Heinke. Thank you for your courage, patience and love during this period. Above all, I am grateful to share this dance of life with you.

Contents

List of Figures

List of Tables

Nomenclature

Roman Symbols

A	Availability
b_{max}	maximum vertical acceleration
C_D	hydrodynamic drag coefficient
C_M	hydrodynamic mass coefficient
$C(p, v)$	damping load
D	fatigue damage
D	water depth
d	diameter [m]
D_a	distribution percentage for category a
d	water depth
E	Young's modulus[GPa]
EA	Tensile stiffness [N]
EI	Bending stiffness [Nm^2]
F	Force [N]
f	force per unit length [$\frac{N}{m}$]
$f(t)$	time to failure probability density function
F_a	difference factor previous; new item
F_g	gravitational force
$F(p, v, t)$	external load
$F(t)$	Failure probability function
F_v	viscous force
g	gravitational constant [$\frac{m}{s^2}$]
H	wave height [m]
h	height [m]
H_s	significant wave height [m]
$h(t)$	hazard rate function
k	axial stiffness[$\frac{N}{m}$]
k	wave number [$\frac{1}{m}$]
KC	Keulegan-Carpenter number
l	lenght [m]
M	bending moment [Nm]
m	mass of cable
m	number of active blocks
$M(p, a)$	inertia load
N	number of load cycles
n	number of blocks
S	stress amplitude
s	scale factor

t test time

T_p wave peak period

w unit weight of cable in water

$\dot{u}$ wave particle acceleration $[\frac{m}{s^2}]$

L wave length [m]

T wave period [s]

u wave particle velocity $[\frac{m}{s}]$

Greek Symbols

α Weibull scale parameter

β Weibull shape parameter

Δ displacement force [kN]

Δp pressure differential

η wave elevation [m]

Γ Gamma function

κ curvature $[\frac{1}{m}]$

λ failure rate

ω angular frequency $[\frac{\text{rad}}{s}]$

ρ density $[\frac{kg}{m^3}]$

Θ rotational angle [degree]

Θ Weibull location parameter

Subscripts

$_D$ drag

$_I$ inertia

λ_b base failure rate

λ_{EQUIP} failure rate of equipment

λ_f field failure rate

λ_G generic failure rate

λ_p predicted failure rate

π_A application stress factor

π_E environmental loading factor

π_Q quality factor

Acronyms

AWS Archimedes Wave Swing

cdf cumulative distribution function

DMaC Dynamic Marine Component test rig

DOF degrees of freedom

EPR ethylene propylene rubber

EPSRC Engineering and Physical Sciences Research Council

L Load

LIMPET Land Installed Marine Power Energy Transmitter

MAE mean absolute error

MBL minimum break load

MBR minimum bend radius [m]

MRL mean residual life

MTTF mean time to failure

OWC Oscillating water column

pdf probability density function

Pr Probability

R Reliability

S Strength

SWMTF South West Mooring Test Facility

T Time to failure

t time

WD Wavedragon

XLPE cross-linked polyethylene

Part I

Research question

Chapter 1

Introduction

1.1 Research context

Marine renewable energy is a promising energy resource, which is envisaged to play an important role as a future energy source. For the UK it is estimated that wave and tidal energy could provide up to 17% of the current electricity demand. This would help to guarantee the security of energy supply and significantly reduce carbon emissions. Beyond that, marine renewable energy holds the opportunity to create a new and successful UK industry sector of global importance which is estimated to be worth £15 billion (DECC, 2010).

The importance of device reliability is rooted in the economic impact failures and downtimes may have. It is important to note that reliability is not a simple performance characteristic. Reliability itself is influenced by a multitude of design decisions, operational conditions and maintenance strategies, which in turn effect overall cost of energy. Several input parameters for a generic wave energy conversion cost model are either influenced or driven by reliability considerations. The device design and its reliability characteristics govern how much of the annual available wave resource can be captured and what costs are incurred through operation and maintenance.

Figure 1.1 illustrates the key parameters that are influenced by reliability aspects and how they relate to the unit cost of energy. For example, a key feature of the device characteristics is the failure behaviour, such as the Mean time to failure (MTTF) which, in turn, influences the availability of the device and the expected annual electricity

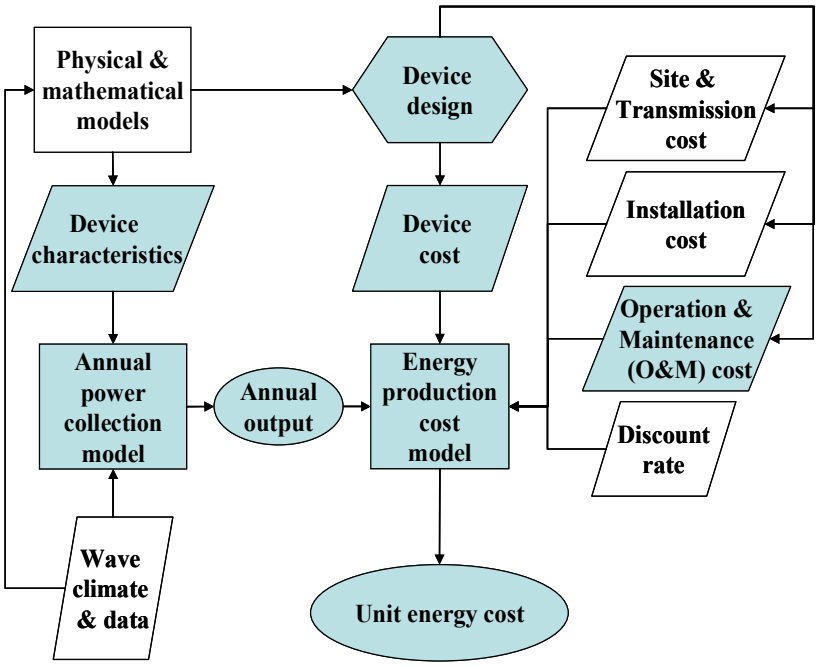

Figure 1.1: Generic cost model for wave energy conversion - parameters influenced by reliability are shaded, based on Rudd (2003).

output. The device design is heavily dependant on the aspired reliability level and determines the device cost. Moreover, depending on the type and frequency of failure, operation and maintenance (O&M) activities are also driven by reliability.

Given the importance of reliability considerations one might assume that the reliability can be reasonably well estimated. Still, the technological risk and uncertainty about the reliability of marine energy systems is identified as a potential barrier in a report from RenewableUK (2010). A survey among original manufacturing companies involved in the sector and large utilities who are potential end-users of devices emphasised this as a main concern. In this context, one of the recommendations of the Marine Energy Action Plan 2010 for the UK (DECC, 2010) is to provide funding for improving the performance, reliability and survivability of MECs, focussing on "enabling components" such as foundations and moorings, power take-offs and wet-mateable power connectors.

1.2 Funding objectives

The research presented in this thesis is part of a wider research consortium. The Sustainable Power Generation and Supply (SuperGen) programme, funded by the Engineering and Physical Sciences Research Council (EPSRC) is a research initiative that explores future energy supplies of the United Kingdom. The Marine Energy consortium was started in 2003 with a Phase 1 programme which lasted until 2007.

The general aim was "to increase knowledge and understanding of the extraction of energy from the sea in order to reduce investment risk and uncertainty" (SuperGen, 2007). The task was to conduct generic research for the benefit of all participating stakeholders. A total of 13 work packages were defined to undertake the research, spanning from energy resource appraisal over engineering guidance, economics, moorings and foundations to full-scale field validation.

The work for this thesis has been funded under the SuperGen Marine Phase 2 (2007-2011). The core participating universities are The University of Edinburgh, Heriot Watt University, Lancaster University, Queen's University of Belfast and Strathclyde University. The University of Exeter is one of the affiliated universities. A total of ten

different workstreams have been defined building on the results and research questions obtained in phase 1. Workstream 8 is concerned with the reliability of marine energy devices. It focusses on the challenge of how to predict and assess the long term reliability of marine energy systems. During Phase 1 an initial failure rate database has been established. However, the failure rate data was not sufficiently verified for many of the critical components as not enough devices have been field tested and reliability data is often not published. The aims of this work stream as defined in SuperGen (2007), phase 2 are:

- to assess the effect of uncertainty on the calculations of device reliability and availability,
- to evaluate and adapt reliability methodologies from other industries for application to marine energy converters.

From the outlined research context three implications emerge for this thesis.

1. The research contribution shall be *generic* to meet the research objectives set out under the SuperGen initiative.
2. The uncertainties regarding device reliability shall be assessed.
3. Reliability methods used in other industries shall be applied to the marine energy case.

In an applied science such as reliability engineering it is challenging to follow the provision of generic research. For this thesis it was sought to focus on components and sub-systems that would generically apply to as many devices as possible. The evolution of wave energy devices has been described as a succession of three generations from atshore over nearshore to floating offshore devices (de O. Falcão, 2004). In this respect, all floating wave energy converters have a requirement to be moored to the seabed and to be electrically connected via marine cables, which makes moorings and marine power cables fundamental first choice system components of all third generation devices. The physical investigations presented in chapter 6 determine the load conditions for these components in experimental and field conditions.

The effect of failure rate uncertainties on the predicted system reliability is presented as part of the reliability assessment in chapter 3. Furthermore this thesis aims

to provide a methodology how the available reliability information for a particular component/device can be compiled and subsequently improved in order to decrease uncertainties (chapter 4).

A service-simulation component test approach that is being applied in other industries has been adapted for the marine energy application and is proposed in (chapter 7). It aims to replicate field load conditions in a controlled laboratory environment to inform the design and to ensure/improve component reliability.

1.3 Related work

In this section the literature related to the reliability of WECs is briefly presented. The work reviewed here has been published in three areas: Economic assessments, Standards and guidelines and reliability assessments.

Economic assessments aim to calculate a unit cost of energy and thus require some consideration of reliability/availability.

Thorpe (1999) reports some reliability and availability considerations for a shoreline, a nearshore and an offshore wave energy device in the light of unit costs of energy. Some failure rate data is presented for the OSPREY OWC device but not further discussed. Related availability figures of 95-98% appear optimistically high. The report emphasises the importance of demonstration schemes to prove system survivability and reliability to the extent that initial deployments should have the main objective to demonstrate this, rather than favourable generation costs.

An extensive feasibility study carried out by the American EPRI institute (Previsic & Bedard, 2004; Previsic *et al.*, 2004a,b) for a potential deployment of wave energy devices off the Californian coast assessed a number of devices and explicitly queried device developers on device survivability and potential failure modes. Yet, no quantitative reliability assessment has been conducted and the economic model simply assumes an availability factor $A = 0.85$ for the pilot plant and $A = 0.95$ for a commercial wave farm.

Dunnett & Wallace (2009) conducted a performance assessment for three types of wave devices at different locations off the Canadian coast. Their production calculations

assumes a device availability $A = 100\%$, i.e. potential down time and repair are not considered, making the results overly optimistic.

Further feasibility studies by Dalton *et al.* (2010) investigate the economic viability for wave projects in Ireland, Portugal and North America. The presented method considered both, the cost and the operational conditions in detail, but potential costs associated with the reliability of devices are only accounted for as a lump sum capital cost between $3 - 5\%$ of the investment cost. These figures are mere assumptions, but highlighted the sensitivity of cost models to an increased annual O&M cost. While the 3% case predicted a required feed-in tariff of 0.37€/kWh the higher assumption of 5% O&M cost required a tariff of 0.43€/kWh to achieve an economically attractive internal rate of return (IRR) of 10%.

The second strand of publications is concerned with standards and guidelines to ensure and validate the reliability of WECs. To inform the engineering design and certification of wave energy devices, existing standards from the offshore oil and gas industry have been adapted to suit the requirements of this new technology.

A review of applicable standards and guidelines that are applicable for the design and operation of MECs has been carried out by The Minerals Management Service (MMS) (PCCI, 2009). The MMS is a subsidiary of the U.S. Department of the Interior and is responsible for the permit and regulation of marine energy projects in US waters.

Three standards and guidelines have been revised or are in the process of being issued to cover the pertinent aspects of MECs. While these guidelines cover the entire field of device design, testing, certification, performance, production, operation and maintenance only those which explicitly refer to device reliability are listed in the following:

- The class society Det Norske Veritas DNV (2005) has issued guidelines which propose an integrated qualification process to accompany the device design and development to reach acceptable reliability levels. This guideline in particular discusses some of the additional reliability issues that may arise for typical components used in WECs such as moorings, electrical and mechanical equipment, instrumentation and umbilicals. Fatigue is considered to be one of the main failure mechanisms to determine the design.

- The European Marine Energy Centre (EMEC) has issued a guide for the reliability, maintainability and survivability of MECs (Starling, 2009). It provides an overview of important factors and lists a number of techniques that may be used. The report particularly highlights the relevance of system and component testing prior to device installation, but remains rather general and qualitative.

- Since 2007, the International Electrotechnical Commission (IEC) has put the Task Committee TC-114 in place that develops international standards for marine energy conversion systems. The standards will cover system definition, requirements for design and safety, performance measurement of devices, resource characterisation and assessment, electrical power quality, manufacturing and testing. Publications are planned from 2012 onwards (Peacock, 2011).

Few works have been devoted to quantify the reliability of MECs. Two reports commissioned for the Energy Technology Support Unit [ETSU] (AME, 1992; YARD, 1980) assessed the reliability and availability for a selection of wave energy devices. Namely, these are the Belfast, NEL and Vickers Oscillating Water Columns (OWC), the Lancaster Clam and the Salter Duck in YARD (1980). The devices considered in AME (1992) are the Edinburgh Duck, NEL OWC, Bristol Cylinder and the circular SEA-clam. For these early reliability simulations, adapted failure rate data from other industries was used, but no field data from WECs was incorporated. Both submerged bottom-mounted and floating devices were assessed through Failure Mode and Effect Analysis (FMEA). The result was a ranking of the assessed devices. As no directly applicable failure rate data was available, a simple environmental adjustment was used, where component failure rates for bottom-standing devices were multiplied with a factor of 2. Floating devices were considered to be more exposed to wave loading and were multiplied with a factor of 4. Consequently, for the reliability comparison, bottom-standing designs were ranked higher, i.e. judged to have a better system- reliability, than floating devices. The authors emphasise the caveat, that the failure rates used are of limited quality and that "Confidence in their absolute value is low (...)" (YARD, 1980, p. 2.4).

Another early publication by Hudson *et al.* (1980) identifies and describes some general material aspects which are likely to effect the reliability of WECs. The main

issues that should be considered for WECs are impact loading and fracture, corrosion, fatigue, wear, fretting and marine fouling. Structural loading and fracture calculations undertaken in the (wind) offshore industry consider actual load conditions as a combination of wind, wave and current induced forces. For a 20 year lifetime prediction, load cycles amount to 10^9 cycles, making fatigue a major concern when considering reliability (Schaumann *et al.*, 2004). In the case of wave energy, load carrying and exposed components, such as moorings, bearings and marine power cables are most prone to fatigue failures.

An overview into the difficulties and potential solutions to the reliability assessment of marine energy converters has been presented by Wolfram (2006). He reviewed the different types of marine energy converters and the available techniques to assess their reliability and suggested a database approach where failure rate data is adjusted for the altered environment. He concludes that reliability and availability estimation for MECs "(...) is complex and involves many inputs that have uncertainties which are difficult to quantify." Two propositions made in this paper have been followed in the research for this thesis:

1. The application of a Bayesian statistical approach to reduce the uncertainty of failure rate estimates when additional information, such as field failure data become available.

2. Development of component reliability test programmes for marine renewable conversion systems.

In conclusion all three types of appraisals, economic studies, design standards and performance assessments, face a lack of applicable reliability data. The design standards rely on the detailed technical assessment and evaluation through, e.g. reliability assessments. If the confidence in the underlying information, i.e. failure rates, is low the standards impose higher safety factors, which in turn might lead to an unacceptably high unit cost of energy.

The economic studies also rely on the performance assessments to determine a unit cost of energy. As the reviewed appraisals show, reliability issues and the associated reduced availability of devices is difficult to quantify and is thus not considered or tends to be overly optimistic.

From this review, the clear research requirement arises to improve the reliability information for marine renewable energy.

1.4 Wave energy test centres

The present thesis contributes to a research and development landscape where components for marine renewable devices are being more and more extensively tested, both in the field and under controlled laboratory conditions. There are several test centres that aim to bridge the gap between lab-based prototype devices and full-scale field deployment (Mueller *et al.*, 2010). Field test sites have the purpose to demonstrate the installation and operation of marine energy devices and assess their field performance, while laboratory test stands allow the investigation of critical sub-systems, such as the power take off or moorings.

There are a number of field test sites around the world which may be broadly distinguished regarding the type of device (tidal/wave) that may be tested. Moreover the sites accommodate different sizes, allowing scaled and/or full scale devices. A recent development are so called 'nursery' intermediate scale wave and tidal sites to facilitate installation and testing in more moderate conditions (EMEC, 2011b; FaB Test, 2011). Table 1.1 provides a non-exhaustive list of field test sites devoted to the deployment of WECs.

Full scale sites in the UK are the European Marine Energy Centre (EMEC) located in Orkney, Scotland and the Wave Hub development off St. Ives in Cornwall. EMEC offers one wave energy and one tidal energy test berth which have seen a number of deployments since 2004 while WaveHub allows the connection of small arrays in 4 berths of up to 5MW capacity each.

Off the Irish coast lies the Galway Bay test site which holds two berths for $\frac{1}{4}$-scale wave devices. A full scale test site is under development at Belmullet and is expected to be operational in 2013.

In the United States the Northwest National Marine Renewable Energy Center (NNMREC) plans an Ocean Test Berth which will initially be a mobile installation that is subsequently extended to a grid connected site. Similarly, the Hawaii National Marine Energy Center (HINMREC) develops a full-scale test site on Maui and operates two

medium scale-sites on Oahu, for which an extension up to four berths with a capacity of up to 2MW is planned.

Table 1.1: Wave energy field test sites, information after (EMEC, 2011a,c; FaB Test, 2011; Johanning *et al.*, 2011; Mueller *et al.*, 2010; SWRDA, 2011).

Name	Location	Capacity	Scale	Status
Wave Hub	Cornwall, UK	4 berths, 20MW	Full scale	Deployment planned 2012
Falmouth Bay test site	Cornwall, UK	3 MW	Scaled & full scale	Commissioning test site, operational
South West Mooring Test facility	Cornwall, UK	1 berth	$\frac{1}{3}$ scale	Operational
EMEC Billia Croo	Orkney, Scotland	5 berths, 2.2MW	Full scale	7 installations since 2004
EMEC Scapa Flow	Orkney, Scotland	1 berth 75 kW	Nursery site	under development
Galway Bay Test site	Ireland	1 berth	$\frac{1}{3} - \frac{1}{5}$ scale	2 installations
Nissum Bredning	Denmark	1 berth	$\frac{1}{4}$ scale	>30 tests
Lysekil test site	Sweden	10 berths, 10kW	Small scale	Array of 10 installed
NNMREC Ocean Test Berth	Oregon, USA	5 berths	Full scale	Operational
HWMREC Kaneohe test site,	Hawaii, USA	2 berths	medium scale	1 installation, plans for 4 berths, 2MW

Field test sites are crucial to gain experience with the installation, operation and maintenance of devices and to gather necessary component loading information. However, unexpected and frequent failures are a common occurrence for new unproven technologies. A trial and error approach might be acceptable if the associated cost and consequence have a limited, tolerable extent. For the wave energy case field failures provide valuable information and 'lessons learnt', but unless the project investor has

included enough contingency to buffer the cost of failures the project is at risk. The history of wave energy development has seen multiple examples of devices that suffered severe or catastrophic failures and impeded the further development of these devices. These range from devices that sunk during deployment to severe or catastrophic failures during operation. Examples of sunken devices are the OSPREY (Scotland Herald, 1995) and the Trident device (Hopson, 2009) while Pelamis suffered severe failures that ended its first commercial deployment in Portugal (Snieckus, 2010). Incidents of catastrophic failures during operation have been reported for the Oceanlinx floating OWC (Arnold, 2010) and the Wave Dragon overtopping device (Tedd, 2007)).

As a result reliability and survivability of devices are recognised as key characteristics that must be satisfied by any WEC technology that has the aspiration to proceed to the commercial development stage. Yet, the dilemma is that the required experience and demonstration is often sought through field installations, both at scaled sizes and full scale. The field installations itself are fraught with the risk of failure and have high cost attributed to them, which in most cases did not allow a supporting reliability programme to be carried out on the key components and sub-systems of the WEC.

This lack of reliability centred investigation and development of existing and new components for the wave energy application is slowly now being recognised and has sparked the planning and implementation of dedicated laboratory-based large-scale reliability test rigs. These reliability test stands allow to utilise the operational and load experience from the field to test, improve and demonstrate the reliability of components before devices are being deployed in commercial-scale numbers.

One of the first proponents for dedicated laboratory test rigs was Salter (2003a,b) who wanted to "provide a facility to expose (...) any new components and subassemblies at sea before they are chosen for use". His design of a floating platform was ambitious as it aimed not only to replicate the load conditions but also the marine environment of several components at once, including steel girth, seals, cables, belts, hydrofoils, anti-fouling coatings and electric enclosures. As a result his idea was not realised. Mueller & Wallace (2008) also emphasise that to ensure the component reliability of WECs, " (...) extensive testing to failure in representative conditions" is needed.

One of the few examples of full-scale test stands is the rig that was constructed to test the hydraulic power take-off of the Pelamis WEC (Henderson, 2006; Yemm, 2003). The power module of the Pelamis device was exercised by an externally mounted 1MW hydraulic actuation system that replicated the heave and sway wave force and motions experienced at sea. The main objectives of this test effort were to:

- provide evidence of the power conversion efficiency,
- verify the power take-off control algorithms,
- to test the function of the power module components, particularly seal performance,
- to gain experience in assembling and operating the power take-off.

Thus, the intention of the three month cycle test was not to provoke failures by accelerated testing, but rather "(...) to increase confidence in reliability before the first offshore test" (Yemm, 2003).

Another test example is the performance test for a new device concept called Aegir Dynamo (Al-Habaibeh *et al.*, 2010). The power take-off system is tested under realistic, simulated wave force conditions in one degree of freedom. The test rig is a hydraulic linear piston, rated at 55kW hydraulic power with a maximum force of 63.8kN, replicating random wave profiles up to 3m (Ocean Navitas, 2007). This linear test rig served to evaluate the performance of the linear generator power take-off system, but no reliability investigations have been carried out.

The National Renewable Energy Centre (Narec) is currently developing a test rig to replicate the specific offshore load conditions for wind and tidal drivetrains at full-scale (Grimwade, 2010), named the Nautilus Testing Facility. This includes components such as the drive shafts, bearings, gearbox, generator and the power converters equipment. The test rig will be capable to emulate both mechanical and electrical loads. It is designed for a maximum generator capacity of 3MW, with an envisaged investment cost of 15.4 million €.

From these examples and the lack of other published failure-induced testing, it appears that testing efforts are mainly concerned with the functionality and performance of the power take-off system. Furthermore a tendency to demonstrate the reliability of

systems and components is apparent in the testing approach undertaken, rather than accelerating the reliability test in order to induce failures. While this is a suitable approach to convey confidence, it does not investigate the physical limits of the components (i.e. reliability limits). This important disparity is highlighted by O'Connor (2008), who states that in order to come to meaningful results in a cost- and time-effective way "... we must test to cause failures, not test to demonstrate successful achievement".

This thesis makes a contribution in advancing the component reliability testing for wave energy converters. The work presented in this thesis contributed to the development and successful implementation of the dynamic marine component test rig (DMaC) that replicates the physical loading of components to enable a targeted reliability testing under realistic conditions. The DMaC is a unique facility that will support the necessary reliability improvement and demonstration for marine energy components.

Furthermore, the physical load measurements and simulations presented in this thesis for mooring lines and power cables in a marine renewable application inform present and future component design decisions and test efforts.

Additionally, the Bayesian statistical methods presented in this thesis allow to continuously update and improve component failure rates and thus the system reliability estimates as more reliability information becomes available.

1.5 Aim of the research

The motivation for this work is that from an engineering point of view, marine energy is one of the least developed renewable energy technologies and has to be regarded as unproven. The main engineering challenge is being recognised as the reliability of components and devices. "Survivability and reliability represent key challenges for marine renewables, due to the economic consequences of catastrophic failures and/or long periods of unavailability" (Callaghan & Boud, 2006, p. 25). In their review of research requirements for the marine renewable sector, Mueller *et al.* (2010) also identify survivability and reliability as two of the major challenges that must be overcome to advance device deployments at an economically feasible commercial scale.

The objective of the research in this thesis is to develop and apply methods to establish and improve reliability information for marine energy converters. The original research proposal *Reliability of Marine Energy Converters* has been subsequently constricted and narrowed to the research question: How can sparsely available reliability information be improved and utilised more efficiently for wave energy converters?

This thesis aims to make a contribution to the engineering science that will advance the reliability of marine energy converters. While the methods and concepts presented in the following are applicable to wave and tidal devices, the research and analysis is centred around floating wave energy applications. The reason for this restriction being that i) the strength of the marine research group at the University of Exeter lies in the fields of wave resources and station keeping of floating devices and ii) other research institutes with strong roots in the reliability of wind energy applications are conducting research regarding the reliability of tidal energy devices, namely those are Durham University and Heriot-Watt University, which are both part of the SuperGen consortium.

The presented research has investigated and applied a suite of experimental, numerical and statistical methods with the aim to assess the reliability of marine devices and components prior to, and during, their field deployment. These methods will assist and inform both the design at early development stages and the maintenance requirements anticipated during operation.

1.6 Contribution to knowledge

This thesis makes the following contributions to knowledge in the field of marine energy converter reliability:

- Reliability-centred review of wave energy technologies
- Reliability assessment of typical hydraulic wave energy converter
- Evaluation of failure rate uncertainties
- Application of Bayesian statistical techniques to marine energy components
- Application of a service simulation component testing approach to marine renewable energy
- Estimation of realistic in-service loads for mooring components and marine power cables
- Estimation of fatigue load spectrum and fatigue life for WEC mooring lines and marine power cables
- Advancement of component reliability testing for wave energy converters through contributions to the successful design, development and implementation of a marine component test rig for dynamic loads

1.7 Content and structure

The distinctive parts of the thesis are mapped in figure 1.2. The different chapters emerge from the central research question how reliability information for wave energy devices may be improved.

The process and rationale of specifying the research question is presented in Part I. Chapter 1 has introduced the research context together with the motivation and objectives for this this research. Chapter 2 briefly defines and reviews key reliability concepts and reviews a selection of wave energy converters from a reliability perspective.

In Part II different approaches are presented that can be applied to generate or improve reliability information. Chapter 3 presents a systematic reliability assessment of a notional hydraulic wave energy converter based on publicly available failure rate data. The results of this assessment highlight several issues that would be faced by an external agency in developing realistic reliability estimates when using generic data:

- inappropriate or insufficient data,
- environmental adjustment factors and system behaviour are uncertain,
- reliability results tend to be unfavourable and uncertain.

As a consequence, the available data and information are not sufficient to conduct a robust quantitative reliability assessment. At the outset of this PhD research project it was regarded as one of the objectives to quantitatively compare the reliability performance of different types of devices. In consideration of the scarcity of appropriate failure rate data the accurate estimation of component reliability was identified as research focus.

Chapter 4 is concerned with the benefits and pitfalls of the methods based on the application of Bayesian statistics, which allow an updating procedure of existing failure rate information using additional information such as expert knowledge or test results. A practical procedure to reduce the failure rate uncertainty through Bayesian updating is presented.

Part III presents the physical and numerical investigations in order to implement a service simulation test approach. At this point the view of the study is narrowed down

from a system view to moorings and marine power cables. These components will be critical for all third generation floating MEC, as they have a requirement to be moored to the seabed and to be electrically connected through power cables. The operational load conditions of these components are determined to identify the characteristic load patterns. Two different type of load data were used for the analysis:

- Mooring loads acquired during wave tank tests of a cylindrical floating Oscillating Water Column (OWC)
- Numerical modelling of power cable loads, based on tank test information

The experimental and modelling procedures are presented in chapter 5, together with the design rationale and specifications for a novel Dynamic Marine component test rig that aims to facilitate a service simulation test approach.

The analysis and results of the expected load conditions of mooring lines and marine power cables in wave energy applications are described in chapter 6. Both the maximum operational load conditions and the fatigue life of these two components are estimated.

A further core objective of this thesis is to replicate the load regime of components in physical reliability tests. The results of initial tests with a marine power umbilical, that were carried out on the purpose built dynamic component test rig as a collaborative test effort with a marine power cable manufacturer, are given in chapter 7.

Part IV concludes with a discussion of the main findings, summarises the conclusion of the presented work and identifies areas for further investigations.

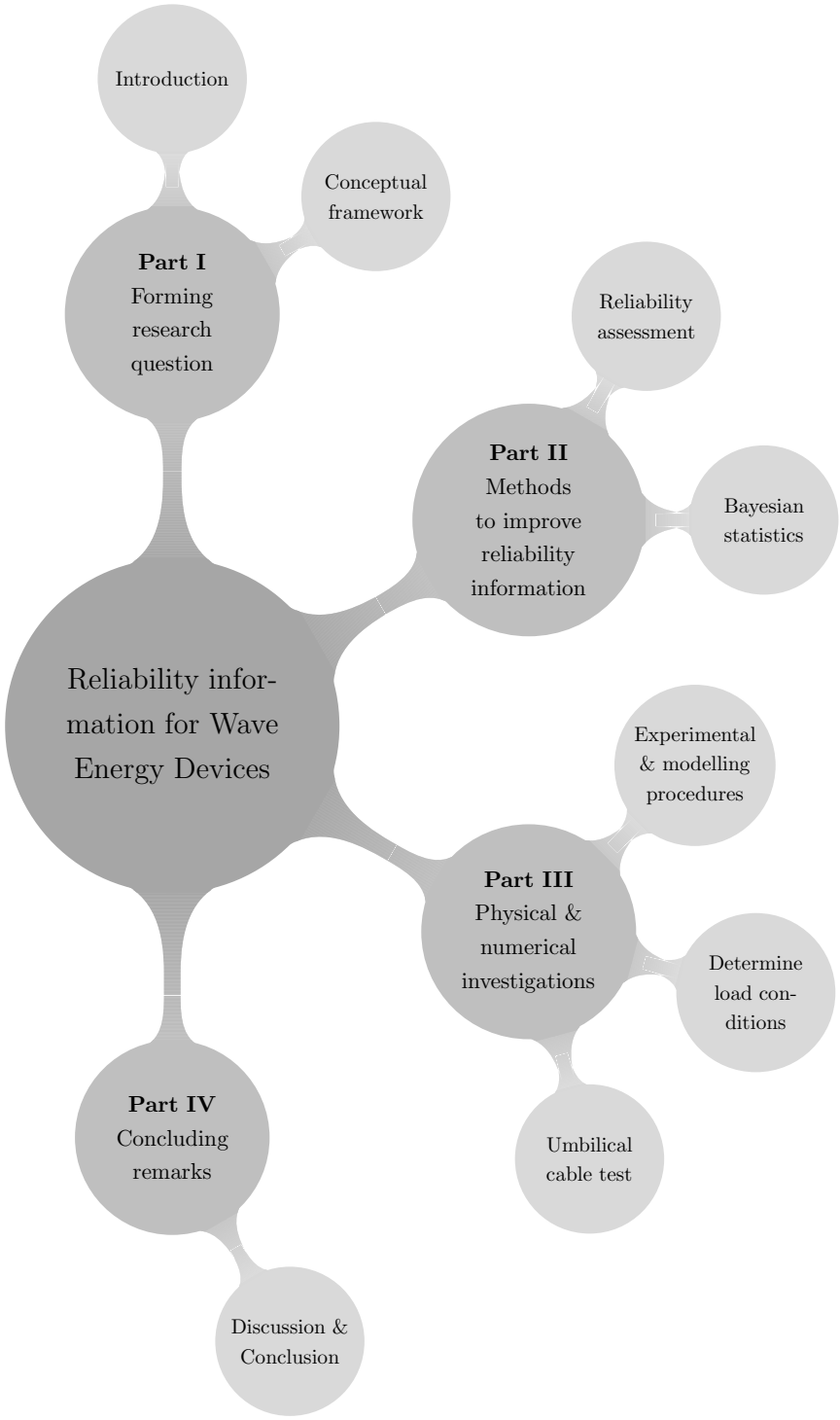

Figure 1.2: Thesis content mindmap.

Chapter 2

Conceptual framework

2.1 Reliability concepts

This section briefly presents the most important reliability concepts and methodologies which are essential for the following chapters and in order to identify an appropriate approach to assess the reliability of WECs.

2.1.1 Definition

Reliability is defined as "the ability of an item to perform a required function under stated conditions for a stated period of time" (BS 5760-4:2003, 2003). The qualitative interpretation is that the item is free from operational failures. In quantitative terms, the reliability is given as the probability the function is performed for specified conditions and time.

Thus, four aspects need to be defined to make a statement about the reliability of an item:

- The probability that the item will operate,
- the function that is required,
- the operational and environmental conditions,
- and the period of time the function is required for.

The probability that the item will operate is usually given in the form of a point estimate, i.e. a single number. A more precise probability statement would give some

consideration to the uncertainty of the probability estimate and would therefore also comprise at least confidence intervals and the relevant probability distribution.

An item can have different types of function and failures which has strong implications for the reliability definition (Yang, 2007, p. 10). A *binary state function* is either a success or a failure (e.g. a light bulb). A *multi state function* can be a success, a partial success or a failure (e.g. a pump which can have a reduced output as partial success). The type of function is closely linked to the failure definition. A *soft failure* describes a partial loss of function (e.g. through degradation) while a *hard failure* is the complete loss of function. Reliability models that assume a binary state function are a simplification of reality as they are not capable of modelling a range of function states (Hudson & Kapur, 1982).

The operating conditions influence the reliability and should therefore be stated. They comprise the type (e.g. mechanical, electrical, thermal) and level of stress, the use rate, operating profiles and environmental conditions.

The time period specified over which the item should perform its function may be e.g. the design life, the warranty period or envisaged maintenance intervals. The unit of time is measured in the unit of interest that is linked to a failure mechanism, e.g. operational time [h], calendar time [h], number of load cycles, mileage [km] or number of switching operations.

Two fundamental approaches to reliability analysis are generally distinguished, the *physical* and the *actuarial* approach (comp. e.g. Rausand & Høyland (2004, p.3)). The physical approach is largely applied for structures and is thus often referred to as structural reliability analysis. With this approach the strength of an item has to withstand a certain load. Both the strength and the load are modelled as random variables. The reliability of an item is mathematically defined as probability that the load L does not exceed the item's strength S (see equation 2.1). If the physical parameters vary with time, load and strength are modelled as time dependant variables $L(t)$ and $S(t)$. The time to failure, T, is then defined as the point in time when the load exceeds the strength ($T = min\{t; S(t) < L(t)\}$). The time dependent reliability function $R(t)$ can then be written as in equation 2.2. The physical approach is illustrated in figure 2.1.

$$R = Pr(S > L) \tag{2.1}$$

$$R(t) = Pr(T > t) \tag{2.2}$$

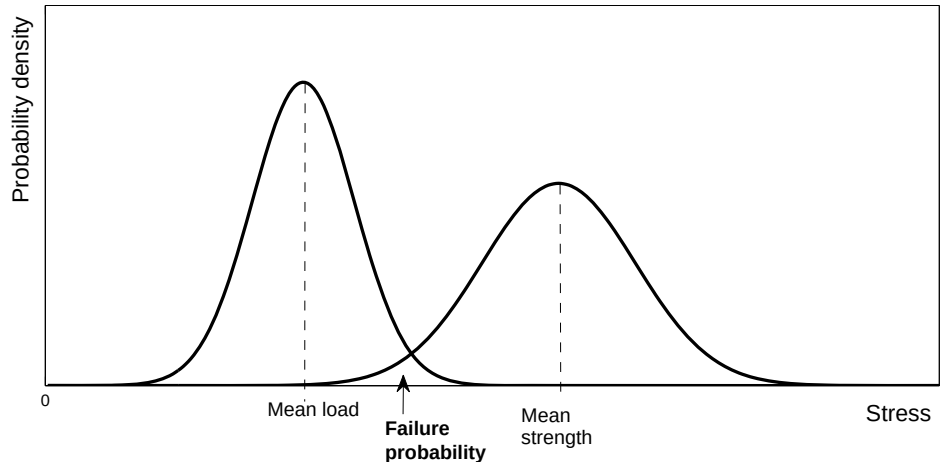

Figure 2.1: Structural reliability approach, load and strength as random variables, based on Rausand & Høyland (2004).

For the actuarial approach the information about the physical quantities of strength and load is aggregated into a probability density function $f(t)$ that describes the time to failure, i.e. the physical loadings are not modelled explicitly. The data to derive suitable probability distributions for $f(t)$ usually stems from dedicated life tests or field use data. The most commonly used reliability measures, such as the reliability function $R(t)$, the hazard rate function $h(t)$ and the mean time to failure $MTTF$ are derived from the probability function $f(t)$ as shown in the following section 2.1.2.

2.1.2 Reliability measures

There are a number of reliability measures that pursue different objectives, depending on the type of item, i.e. repairable or non repairable, and the performance characteristic one is interested in. The mathematical foundation of these measures is well described (Martz & Waller, 1982; Rausand & Høyland, 2004; Yang, 2007) and is only briefly presented here to provide the necessary theoretical framework.

The reliability measures hinge on the statistical concept of probability density function (pdf) and cumulative distribution function (cdf). The measures are defined as a

combination of pdfs and cdfs. Apart from choosing a suitable reliability measure the crucial choice is which type of statistical distribution is considered most appropriate and for what reasons. A multitude of distributions can be found in the literature, but the exponential- and Weibull distribution are most widely used in the reliability community. The former is referred to due to the ease of use and the statistical simplicity and the latter is used due to its flexibility in modelling a range of different distribution shapes.

In this section four measures of reliability are presented, namely the reliability function $R(t)$, the hazard rate function $h(t)$ and the mean time to failure (MTTF) together with two types of distribution, the exponential and the Weibull distribution.

2.1.2.1 Reliability function R(t)

The reliability function describes the probability of success, i.e. that the item performs its function under given environmental and operating conditions. It is worth noting that the exact specification of environmental and operating conditions is one of the main sources of uncertainty if failure data is to be used, as the data source often does not coincide with the application at hand. The failure time T is modelled as random variable with a supposed distribution $f(\tau)$ as the pdf of T. The probability of failure is defined as

$$Pr(T \leq t) = \int_0^t f(\tau)d\tau = F(t), \quad t \geq 0 \tag{2.3}$$

$F(t)$ is the probability that the item fails by time t and is by definition a cdf. Because the reliability function $R(t)$ is the probability of success it is the compliment of the failure probability, i.e. $R(t) = 1 - F(t)$, or more formally written:

$$R(t) = Pr(T \geq t) = \int_t^\infty f(\tau)d\tau = 1 - F(t) \tag{2.4}$$

In summary, the reliability function $R(t)$ represents the probability the item does *not* fail, i.e. that it survives for a particular time interval $[0, t]$. For this reason $R(t)$ is also referred to as *survivor function*.

2.1.2.2 Hazard rate function h(t)

The hazard rate $h(t)$ describes the question at what rate failures occur within a particular time interval $[t_1, t_2]$, if no failure has occurred up to t_1. When the time interval is thought to be infinitesimal small and approaches zero it is referred to as the instantaneous failure rate which is defined as:

$$h(t) = \lim_{\Delta t \to 0} \frac{R(t) - R(t + \Delta t)}{\Delta t R(t)} \tag{2.5}$$

$$= -\frac{dlnR(t)}{dt} = \frac{f(t)}{R(t)} \tag{2.6}$$

with $\frac{-dR(t)}{dt} = \frac{dF(t)}{dt} = f(t)$

The hazard rate is of relevance, because it describes the failure behaviour of an item over its lifetime. The failure rate can either decrease, be constant or increase. Typically, the hazard rate over the entire lifetime of an item exhibits all three behaviour types, illustrated by the bathtub curve in figure 2.2. Empirical evidence obtained from the failure data of several products suggests three distinct periods during the 'life' of a product (O'Connor, 2008):

- Early failures with decreasing hazard rate during the early life of a product
- Random failures during the useful life of the product, with approximately constant hazard rate
- Wear-out failures or ageing failures exhibiting increasing hazard rates

All three distributions, the failure pdf $f(t)$, the reliability function $R(t)$ and the hazard rate function $h(t)$ are related through the Equations 2.7. Expanding and integrating equation 2.7 to equation 2.8 yields an expression for the reliability function $R(t)$ given in 2.9.

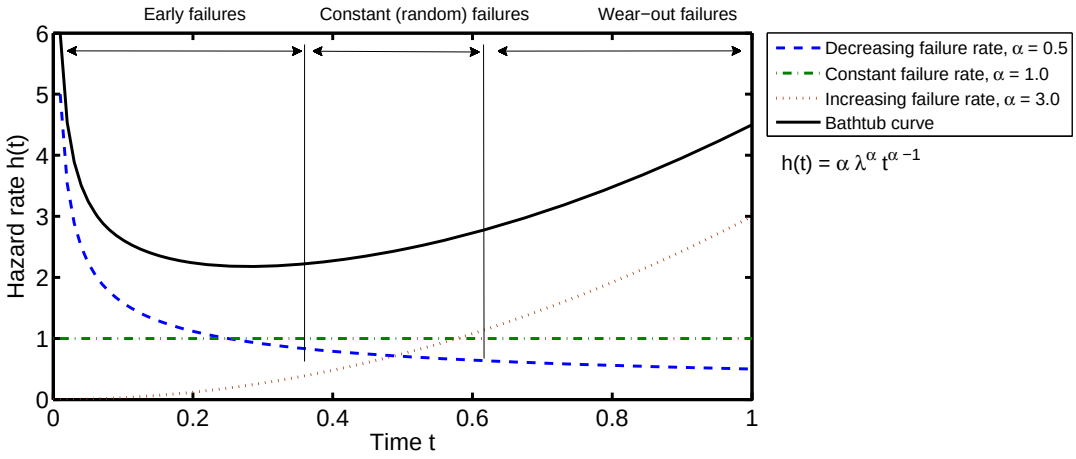

Figure 2.2: Bathtub curve failure rate behaviour, modelled as 2-parameter Weibull distribution with $\lambda = 1$.

$$h(t) = \frac{f(t)}{R(t)} \tag{2.7}$$

$$\int_0^t h(x)dx = -\int_0^t \frac{dR(x)/dx}{R(x)}dx = -lnR(x)|_0^t \tag{2.8}$$

$$= -lnR(t) + lnR(0) = -lnR(t)$$

$$R(t) = exp\left[-\int_0^t h(x)dx\right] \tag{2.9}$$

Combining equation 2.7 and 2.9 yields an expression to define the probability function $f(t)$ in terms of the hazard rate $h(t)$:

$$f(t) = h(t)\ exp\left[-\int_0^t h(x)dx\right] \tag{2.10}$$

2.1.2.3 Mean time to failure MTTF

The mean time to failure (MTTF) represents the life expectancy value for an item that is not repaired and is defined as:

$$MTTF(T) = \int_0^\infty R(t) \tag{2.11}$$

If the item is repaired after each failure the MTTF is termed as mean time between failures (MTBF).

If the mean time to failure is calculated for an item that has not failed until time t, this is known as mean residual life (MRL):

$$MRL(t) = \mu(t) = \frac{1}{R(t)} \int_t^\infty R(x)dx \tag{2.12}$$

In the case where $t = 0$, i.e. the item is new, the MRL is equal to the MTTF.

2.1.2.4 Context of reliability measures

The reliability measures are commonly used to describe and quantify the performance characteristics of a component or system. The presented measures aggregate different failure modes and mechanisms in a single parameter which is convenient to measure performance against targets or to compare different types of components and systems.

These reliability measures are established through statistical analysis of recorded failure events to identify the most suitable statistical distribution. For wave energy converters there is not enough experience to date to establish specific reliability measures for this novel application. In this situation, one can refer to a combined approach to assess, estimate and update application specific reliability measures.

1. One can refer to available failure rate information and seek to adjust to facilitate an initial reliability assessment. This approach is presented in chapter 3.

2. It is also possible to quantify specific failure modes if additional information is available. Chapterr̃efsec:DetermineLoadCond presents the calculation of fatigue life based on available load information

3. Another approach to continuously update reliability measures with additional information is the Bayesian statistical approach presented in chapter 4. Useful information to establish a best estimate for the reliability measure may be field failures; specific failure mode estimates; expert knowledge or results from dedicated tests, such as the service simulation approach proposed in section 5.3.

In this thesis all three approaches are presented in an attempt to advance the reliability information for marine energy converters in a situation of data scarcity. It aims to provide and demonstrate a suite of experimental, numerical and statistical methods to establish, quantify and incorporate reliability information for marine energy converters.

2.1.3 Failure distributions

2.1.3.1 Exponential distribution

The exponential distribution is used in cases where a constant failure rate model is appropriate. It stems from the assumption of a homogeneous Poisson process, which states that the item is subjected to a random number of 'shocks' during a certain time interval and that the item fails upon receiving a shock but does not fail otherwise. The exponential pdf is defined as:

$$f(t;\lambda) = \lambda e^{-\lambda t}, \quad \text{for } t \geq 0 \ , \ \lambda > 0 \tag{2.13}$$

Where λ denotes the failure rate of the item. According to equation 2.4 the reliability function of the exponential distribution is:

$$R(t;\lambda) = \int_t^\infty f(\tau)d\tau = e^{-\lambda t} \quad \text{for } t > 0 \tag{2.14}$$

The hazard rate follows from equation 2.7 giving just a simple constant hazard rate, often referred to as failure rate:

$$h(t;\lambda) = \frac{f(t)}{R(t)} = \frac{\lambda e^{-\lambda t}}{e^{-\lambda t}} = \lambda \tag{2.15}$$

Finally the MTTF for the exponential distribution, as defined in equation 2.11, is:

$$MTTF = \int_0^\infty R(t)dt = \int_0^\infty e^{-\lambda t} = \frac{1}{\lambda} \tag{2.16}$$

The exponential failure distribution implies a number of assumptions which are worth noting (Rausand & Høyland, 2004):

- The MRL is equal to the MTTF, i.e. a used item is as good as a new one.
- Because the reliability function and the MTTF function are relatively simple for the exponential case the only data that is required to determine them is the period of time and the encountered number of failures during that time.
- The exponential failure distribution does only model the failure rate behaviour at the bottom of the bathtub-curve, i.e. early failures and failure mechanisms related to the age of the item are not considered. Thus this distribution is not suitable to describe early life failures or wear-out failures.

The probability density function *pdf*, cumulative $F(t)$ and reliability function $R(t)$ of the exponential distribution are shown in figure 2.3 for values of $\lambda = 0.5$. Hence the item is assumed to fail once for every two units of time.

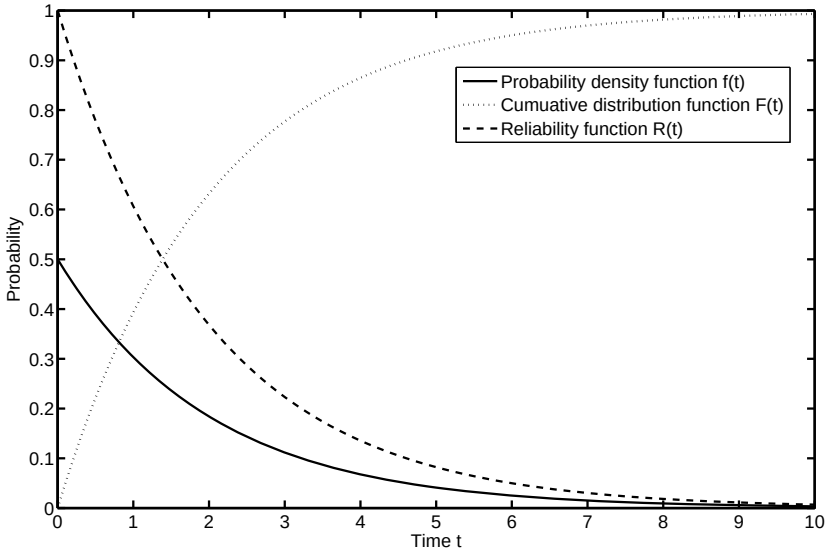

Figure 2.3: Exponential life distribution, probability density function f(t), cumulative distribution function F(t) and reliability function R(t); $\lambda = 0.5$.

2.1.3.2 Weibull distribution

The Weibull distribution has been proposed to statistically model a wide range of applications (Weibull, 1951). It is one of he most widely used distributions in reliability applications as it is very flexible and the choice of different distribution parameters allows to model a multitude of failure behaviours. The Weibull distribution thus provides a good statistical fit to most of the data collected in the field.

The probability of failure using a three parameter Weibull distribution function F(t) is defined as:

$$F(t;\alpha,\beta,\Theta) = 1 - e^{-\left(\frac{t-\Theta}{\alpha}\right)^{\beta}} \tag{2.17}$$

Different characteristics of the distribution are controlled through each parameter. The exponent β governs the shape of the distribution and is hence referred to as *shape parameter*. The scale of the distribution is controlled by the *scale parameter* α. A

change of α while the other parameters are kept constant has the same effect as if the x-axis would be scaled, i.e. for larger values the distribution is stretched out whereas smaller values compress the distribution. The location, or x-offset of the distribution, also referred to as the 'guaranteed life' is controlled by the location parameter Θ.

For the reliability function R(t) the Weibull distribution is then written as:

$$R(t;\alpha,\beta,\Theta) = 1 - F(t) = e^{-\left(\frac{t-\Theta}{\alpha}\right)^{\beta}} \tag{2.18}$$

The derivative of equation 2.17 yields the Weibull pdf:

$$f(t;\alpha,\beta,\Theta) = \frac{\partial F}{\partial t} = \frac{\beta}{\alpha}\left(\frac{t-\Theta}{\alpha}\right)^{\beta-1} e^{-\left(\frac{t-\Theta}{\alpha}\right)^{\beta}} \tag{2.19}$$

And finally the Weibull hazard rate is found substituting equation 2.18 and 2.19 in equation 2.7.

$$\begin{aligned} h(t;\alpha,\beta,\Theta) &= \frac{f(t)}{R(t)} \\ &= \frac{\beta}{\alpha}\left(\frac{t-\Theta}{\alpha}\right)^{\beta-1} \end{aligned} \tag{2.20}$$

All three Weibull distribution functions are plotted in figure 2.4 showing the effect of different shape parameter values β, while the scale parameter α and the location parameter Θ are fixed. All three plots show the versatility of the distribution, but in particular figure 2.4(c) highlights the degree of control β has on the hazard rate function $h(t)$. This property of the Weibull distribution makes it ideal to model the reliability behaviour shown through the empirical bathtub curves.

The reliability measure MTTF was defined in equation 2.11 and for a Weibull distribution it yields:

$$\begin{aligned} MTTF &= \int_0^{\infty} R(t)dt = \int_0^{\infty} e^{-\left(\frac{t-\Theta}{\alpha}\right)^{\beta}} dt \\ &= \Theta + \alpha\Gamma\left(\frac{\beta+1}{\beta}\right) \end{aligned} \tag{2.21}$$

Where the gamma function Γ is defined as (Papula, 2003, p. 393):

$$\Gamma(n) = \int_0^\infty e^{-x} x^{n-1} dx \quad (n > 0) \tag{2.22}$$

It is further worth noting that if the three parameter Weibull distribution is used, it implies that no failures are possible until time $t = \theta$ has elapsed. Thus θ is an addend in the MTTF equation 2.21.

2.1.4 Reliability prediction methods

Predicting the reliability of products and systems is desirable to assess if an acceptable reliability level can be achieved, what maintenance activities can be expected and what life cycle cost is incurred. Reliability predictions thus inform the decisions made during the design process. Particular applications include (EPSMA, 2005):

- Identification of design weaknesses
- Comparison of design alternatives
- Data provision for reliability and availability assessments
- Planning of operation and maintenance strategies
- Establishing reliability test objectives

Even though reliability predictions are necessary, they may be the subject of considerable criticism due to two main limitations (O'Connor, 2008). Firstly, the failure rate models are point estimates, based on available data. Therefore, in a strict sense they are only valid for the assessed system and the environmental and operating conditions that prevailed during the data collection. For example, the deviation of field failure rates from reliability predictions is found to be small for ground electronics whereas significant errors occur for aviation applications due to differing environmental stresses (White & Bernstein, 2008). Similarly to this, failure rates are also influenced by factors like operational characteristics, maintenance regimes, measurement techniques and failure definitions. As a conclusion "a reliability prediction should never be assumed to represent the expected field reliability as measured by the user" (Mil-Hdbk-217F, 1995, 3-2).

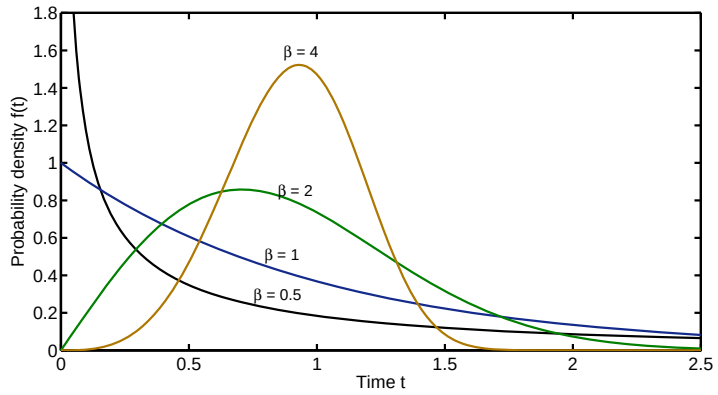

(a) Probability density function f(t)

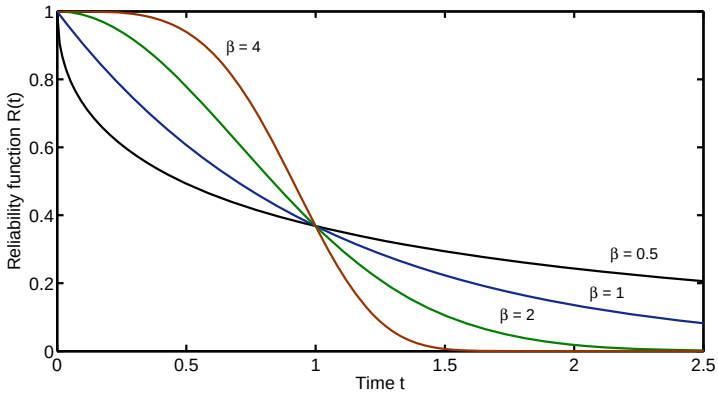

(b) Reliability function R(t)

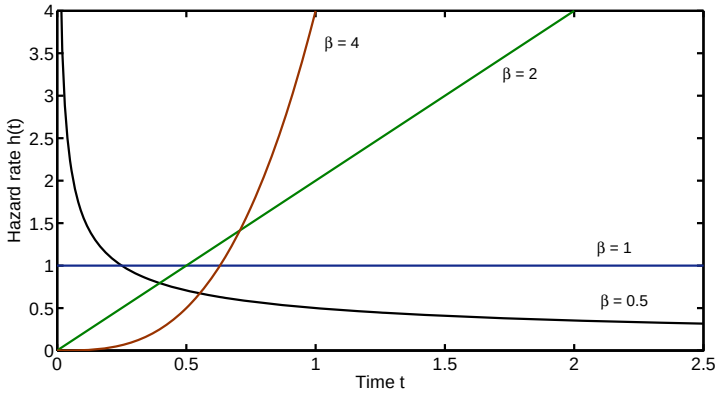

(c) Hazard rate function h(t)

Figure 2.4: Weibull distribution functions for different shape parameters β with scale parameter $\alpha = 1$ and location parameter $\Theta = 0$.

The second limitation is the continuous industrial development of new machinery and processes that impede reliability predictions. Assessments that are based on past data ignore any reliability improvement that might have taken place. Thus, past data for future reliability predictions tend to result in more pessimistic failure rates, i.e. would lead to a more conservative system design.

However, if these shortcomings are recognised reliability predictions are a valuable tool to support decision making, improve the design and to increase the reliability of a system. This leads to a multitude of different reliability prediction techniques which can be classified into three concept types (Foucher *et al.*, 2002):

- Statistical methods following a 'bottom-up' approach
- Similarity analysis methods following a top-down approach which are based on external failure databases
- Physics of failure methods following a bottom-up approach.

2.1.4.1 Bottom-up statistical methods

A reliability prediction that uses bottom-up statistical methods is based on component failure data that has been collected in the field, has been established through laboratory experiments or has been supplied by manufacturers. A component failure rate is established through statistical curve fitting using e.g. the probability distributions described in section 2.1.3. The bottom-up statistical approach is widely used and a range of industry-specific analysis procedures have been developed. The common feature is not only the statistical derivation of failure rates, but two types of analysis procedures that originate from the Military Handbook 217 (Mil-Hdbk-217F, 1995), the *parts count* and the *part stress* method.

The *part stress* analysis prediction method is applicable to late design phases. Beside detailed stress analysis information, it requires knowledge of environmental conditions, quality applications, maximum ratings, complexity levels, temperature and other application-related factors. The basic calculation procedure to obtain a failure rate prediction λ_p, is the multiplication of a base failure rate λ_b with operational and environmental stress factors π, so-called influence factors (see equation 2.23). Typical environmental loading factors π_E are shown in table 2.1.

Table 2.1: Environmental load factors π_E for part stress analysis approach (Mil-Hdbk-217F, 1995, 5.1.1-3).

Environment	Symbol	Factor	Description
Ground, benign	G_B	0.38	Laboratory environment, readily accessible to maintenance
Ground, fixed	G_F	2.5	Conditions not ideal, e.g. unheated building
Ground, mobile	G_M	4.2	Equipment installed on vehicles
Naval, sheltered	N_S	4.0	Sheltered, below deck conditions, weather protected
Naval, unsheltered	N_U	5.7	Unprotected, shipborne equipment, weather exposed
Naval, undersea, unsheltered	N_{UU}	6.3	Equipment immersed in salt water
Naval, submarine	N_{SB}	4.0	Equipment installed in submarines

$$\lambda_P = \lambda_B \cdot \pi_Q \cdot \pi_E \cdot \pi_A \tag{2.23}$$

Where λ_p = predicted failure rate, λ_b = base failure rate, π_E = environmental loading factor, π_Q = quality factor and π_A = application stress factor.

The *parts count* prediction method is applicable to early design phases where typically little information about the design and its specifications is known. Required information comprises generic part types, part quality levels and the equipment environment. To obtain the failure rate of equipment λ_{EQUIP}, a generic failure rate λ_G for each part is multiplied by a quality factor π_Q. The sum is then calculated for all parts, see equation 2.24. The resulting failure rate expresses the failure rate of a series system. Thus, for redundant systems λ_{EQUIP} may also be interpreted as the upper failure rate boundary. The parts count method is applicable if the entire equipment is used in one particular environment. In the case of units that operate in different environments, the equation has to be applied separately to each individual unit.

$$\lambda_{EQUIP} = \sum_{i=1}^{n} N_i \cdot (\lambda_G \cdot \pi_Q)_i \tag{2.24}$$

Where λ_{EQUIP} = total equipment failure rate, λ_G = generic failure rate of i-th generic part, π_Q = quality factor of i-th generic part, N_i = quantity of i-th generic part and n = number of different part categories.

2.1.4.2 Similarity top-down methods

In the case of extensive (often proprietary) reliability databases a reliability prediction can be performed with so-called similarity analysis methods. The concept of a similarity analysis is to compare (sub-) systems which are already in service and have a reliability track record with the newly developed system, i.e. the previous knowledge of a particular system is used to estimate the reliability of a similar system or product (Hitziger, 2007).

The process involves determining a similarity measure between the existing and new system, rather than the direct assignment of reliability estimates. Gullo (1999) describes a similarity approach to predict the component failure rate in the aviation industry. This method was developed to reduce the uncertainty of reliability predictions through the use of field failure data of components in service. This has led to the Honeywell In-Service Reliability Assessment Program (HIRAP) to predict and assess the reliability of aviation components. The main consecutive steps of a similarity prediction are:

1. Collection and assessment of field failure data
2. Creation of in-service failure rate database with physical model categories describing failure causes
3. Similarity comparison to identify and quantify characteristic differences
4. Calculation of failure rate prediction (equation 2.25)

$$\lambda_P = \lambda_f \sum_{a=1}^{n} (D_a \cdot F_a) \tag{2.25}$$

Where λ_p = predicted failure rate, λ_f = field failure rate of similar component, D_a =distribution percentage for physical model category a, F_a = difference factor between previous and new item, n = total number physical model categories.

This approach is expanded by Limbourg *et al.* (2006) who predict the failure distribution of new automotive components using data from similar in-service components and expert knowledge. The expert elicitation is used to establish the similarity transformation factor. The presented case study reaches satisfactory levels of accuracy, but requires detailed failure rate data of in-service components. The reported case uses more than 200 records which were collected over an eight year period.

2.1.4.3 Physics of failure bottom-up methods

The physics of failure (PoF) methodology for reliability predictions is described by Pecht & Jie (2009) as an approach that combines the knowledge about component loading and potential failure mechanisms to estimate component reliability. This approach aims to identify and model the governing failure mechanisms based on the fundamental physical principals. Thus it may be classified as a bottom-up approach that requires detailed knowledge of both the component material and the environment the component is subjected to throughout its life. This comprises the exact material- and design properties, the operating environment as well as operational loads.

The methodology of the PoF approach has been summarised in White & Bernstein (2008) as a sequence of six steps:

1. Identification of potential failure mechanisms
2. Finding the dominant root cause of failure through highly accelerated stress testing of the component
3. Identification of dominant failure mechanisms
4. Modelling of dominant failure mechanisms
5. Combining data from accelerated tests and observed statistical distributions
6. Developing equations that describe the dominant failure mechanism and its expected MTTF.

The failure mechanisms comprise the full spectrum of structural, mechanical, electrical, chemical and thermal processes. Dasgupta & Pecht (1991) define four conceptual failure models that may be used to describe the physical failure mechanisms:

- The *stress-strength* model assumes the component only fails, if the applied stress exceeds the component's strength. The operational stress is assumed to have no other effect on the component.

- In a *damage-endurance* model, applied stress causes damage in the component and that accumulates irreversibly over time. Fatigue, wear and corrosion are examples of this failure model, where the damage does not influence the actual performance but the component fails if the accumulated damage exceeds the endurance limit. Another example, where damage-endurance models are applicable is the electromigration failure of integrated circuits where metal ions are transported through the influence of an electric field (Pierce & Brusius, 1997).

- If a component is not operational and fails in the event it is needed, this is considered through a *challenge-response* failure model.

- The *tolerance-requirement* failure model describes the case that a component/system is operating out of the specified performance tolerance.

A good example where the Pof approach has been implemented to estimate a failure rate distribution based on the underlying failure mechanisms is The Mechanical Reliability Handbook (MechRel, 2004). It covers different failure modes for seals, valves, bearings, pumps and electric motors. The failure rates are estimated through the consideration of operating environment effects onto the system at the part-, rather than the sub-system level. The physics of failure are investigated for each particular application. Based on quantitative estimates of stresses and associated material behaviour, the expected failure mechanisms are quantitatively modelled through engineering equations for every part/component/assembly. The resulting failure rates are time dependent and need to be combined for a specified period of time to obtain a valid total equipment failure rate. The failure rate prediction equations have to be validated by additional failure rate tests.

2.1.4.4 Discussion of reliability prediction models

One of the objectives of this thesis is to conduct a reliability analysis for an entire wave energy converter system. Consequently a suitable method of reliability prediction needed to be identified. This section discusses the methods outlined above in this view.

Table 2.2 compares some of the main criteria for all three general reliability prediction approaches. The bottom-up statistical methods require the least detailed information and can be performed with relative ease, but do not offer an absolute reliability. The top-down reliability approach necessitates detailed information of similar components and systems to be conducted while the Pof approach is based on the understanding of the fundamental failure mechanisms and load characteristic for each individual part. These more complex approaches offer an absolute reliability estimate but require information that has not been gained in the marine renewable case, as yet.

Table 2.2: Comparison of reliability prediction methods, based on Foucher *et al.* (2002).

Method	Data input	Accuracy	Required resources
Bottom-up statistical	Component type, count and quality level; operating environment; system environment	Relative	Small
Top-down similarity	Failure rates of similar components, main differences	Absolute	Medium
Bottom-up physics of failure	Material- and design properties, assembly process, loading and operating environment	Absolute	Large

After reviewing the different approaches and the associated analysis tools a bottom-up statistical method was chosen, using the Reliability Block Diagram analysis. The reasoning for this choice is twofold. Firstly, after consideration of the available information, which mainly comprises failure rate databases of components, a reliability analysis for a complete wave energy system is only feasible using a bottom-up statistical approach. The two other approaches both would require detailed information on the component specification and loading, which was not available in the early phase of the PhD. In fact the lack of the specific loading and information inspired some of the test efforts for this thesis.

Secondly, the objective of a system reliability analysis is to identify the most critical components which would need further more detailed analysis. Thus the method requiring limited resources is chosen over the other methods which could be employed

at later stages to critical sub-systems and components when more detailed load information becomes available.

2.1.5 Reliability Block Diagram

A Reliability Block Diagram (RBD) depicts the system components as interconnected blocks. Each block may represent a single component or a number of components grouped into a sub-system. Depending on the functional system layout, the different blocks are either connected in series or in parallel.

- If all components need to be functional for an operating system, the blocks are arranged in series.
- If the system stays operational with at least one non-failed component the blocks are connected in parallel.

The reliability calculations using such RBDs are based on the assumption that component failures are independent, i.e. the failure of one component does not affect the performance of others. This is not necessarily the case in reality, where e.g. parallel systems share the load. If one of the items fails, the other two would operate at a higher load and thus may incur a higher failure probability. This is called a positive dependence failure (Rausand & Høyland, 2004, p. 215). However positive dependencies, such as cascading failures or 'common cause' failures, may still be modelled in Reliability Block Diagrams when the underlying interrelationships are identified and additional functional blocks are incorporated.

An example where common cause failures must be considered is, if the redundancy level of a system may be overcome by an external event. A redundant power take-off does not satisfy the assumption of independent failures if a flooding of the same compartment leads to failure of both systems. This common cause failure would then have to be modelled as an additional 'hypothetical' component modelled as in-series with the components exposed to the common cause failure. The proportion the common cause failure has in comparison to the independent failure is denoted after Fleming *et al.* (1986) as β-factor:

$$\beta = \frac{\lambda_{CC}}{\lambda} \tag{2.26}$$

Where λ_{CC} denotes the probability of occurrence for a common cause failure.

For the case of independent failures, table 2.3 shows the configuration layouts and the applicable formula for reliability calculations for some basic cases. More realistic and more complex systems may be built through a combination of in-series and parallel configurations. Thus the overall system can be modelled as a composition of the given basic cases (Ayyub & McCuen, 2003, p.537ff).

Table 2.3: Reliability Block Diagram calculations for basic system configurations, based on O'Connor (2008, p.170).

Configuration		System reliability for n blocks
		-
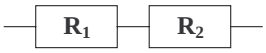		$R_{System} = \prod_{i=1}^{n} R_i$
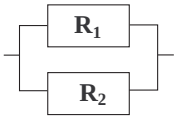	Active	$R_{System} = 1 - \prod_{i=1}^{n} (1 - R_i)$
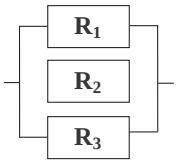	Active 1/3	$R_{System} = 1 - \prod_{i=1}^{n} (1 - R_i)$
	Active 2/3	$R_{System} = 1 - \sum_{i=0}^{m-1} \binom{n}{i} R^i (1 - R)^{n-i}$
	n = number of blocks; m = number of active blocks ('m out of n')	

2.2 Technology review of wave energy converters

One of the peculiarities of wave energy is the vast number of technologies and concepts that have been proposed and are being utilised to produce useful energy from waves, typically electricity. Clément *et al.* (2002) report over 1,000 patents for wave energy converter techniques. The *Marine and Hydrokinetic Database* (U.S. Department of Energy, 2011) lists a total of 134 different wave energy devices. Thus, neither an exhaustive list of devices nor a complete review is attempted here. The technology review which is presented in the following rather presents some of the most advanced technologies to be found in the literature (Cruz, 2008; de O. Falcão, 2010; Drew *et al.*, 2009; Salter *et al.*, 2002), which have achieved at least prototype status.

The aim of this review is to explicate pertinent reliability aspects of the four distinct technology approaches. For each technology a brief technical description of the working principle is coupled with reported and/or potential reliability concerns. The technologies considered are Oscillating Water Columns with air turbines, direct drive linear generator point absorbers, hydraulic systems and overtopping devices employing low-head water turbines as power-take off.

In order to set these technologies and operating principles into context they are preceded by a brief review of classification criteria, as well as a generic appraisal of wave loads for different converter types.

2.2.1 Classification

The large variety of different types of WEC is generally classified with regard to four basic characteristics (de O. Falcão, 2010; Graw, 1995; Harris *et al.*, 2004; Thorpe, 1999):

1. Deployment location,
2. device orientation,
3. operating principle,
4. and power take-off.

The *location* where a WEC is installed can be at the shore, near the shore or offshore and represents an important design decision which determines the required structure and operating principle. This classification is commonly applied in economic assessments as the location heavily influences both installation and operation and maintenance (O&M) cost. Shoreline devices are fixed to, or embedded in the shoreline itself and offer the advantage of relative easy installation and maintenance with permanent access. On the downside, the shoreline location experiences a wave regime which is considerably less powerful compared to offshore locations due to energy dissipation in shallow water. Near shore devices are installed in moderate water depths (up to 20m) and within moderate distance to shore (up to 20km) (Scarr *et al.*, 2001, p.6). They combine increased wave power levels with relative ease of marine access and short subsea interconnection requirements.

A distinction with regard to water depth is typically made through the 'deepwater criterion' (Chakrabarti, 2005a, p. 86) which relates the physical water depth d to the

incident wave length L. Deep water is defined as $\frac{d}{L} \geq \frac{1}{2}$. The water depth is referred to as 'intermediate' when $\frac{1}{20} < \frac{d}{L} < \frac{1}{2}$ and the criterion for shallow water thus is $\frac{d}{L} \leq \frac{1}{20}$. The wave length L depends on the wave period T, which for deep water is given by:

$$L_{deep} = \frac{gT^2}{2\pi} \tag{2.27}$$

Thus, for a typical wave period of $T = 8s$ deep water would describe water depth larger than 50m, and shallow water for water depth less than 5m.

Devices located offshore are exposed to the most powerful wave regime, as energy dissipation mechanisms are negligible at these depths. The devices need to be at or near the water surface to extract the majority of the available energy. Thus, devices typically require a floating or semi-submerged structure together with a mooring arrangement and electrical transmission cables that cross the water column.

Regarding the reliability aspect of the different installation locations it can be argued, that with increased distance from shore the design level for system reliability needs to increase. The reason for this are the extremely increased costs for accessing and repairing offshore devices. A cost review for the wind industry SDC (2005) found that the O&M cost for turbines escalated from 15£/kW installed capacity for onshore locations to 35-42 £/kW for offshore wind farms. In this respect, table 2.4 makes a qualitative comparison between the location, wave regime, O&M strategy and reliability levels required for typical devices. In general, where access is difficult and e.g. restricted by weather windows (Walker *et al.*, 2011), reliability target levels need to be higher to reach acceptable levels of system availability.

The *orientation* of a device relates to the position and its relative length in relation to the direction and length of the incoming wave. This differentiation is useful to compare capture efficiencies, mooring requirements and control strategies. Usually three different configurations are distinguished, which are shown in figure 2.5:

- Point Absorber - Device is smaller than the incident wave length, capturing energy from a larger wave front than the absorber's size.

Table 2.4: Qualitative comparison of location and related reliability aspects for different wave energy devices.

Location	Wave resource	Access	Reliability level required
Offshore, submerged	High energy	Divers or retrieval	High
Offshore, floating	High energy	On board or pulled into harbour	Medium-high
Nearshore, floating	Medium energy	By boat, large platform	Medium
At shore	Reduced energy	Land-based but remote	Low-medium

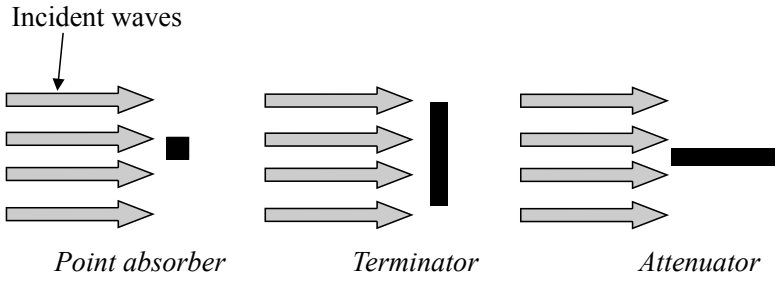

Figure 2.5: Device orientation - point absorber, terminator and attenuator, based on Graw (1995).

- Terminator - Principal axis positioned perpendicular to the wave direction, potentially capturing all energy of the incoming wave crest.
- Attenuator - Principal axis positioned parallel to the wave direction and the energy is captured as it propagates along the device.

A further classification that proofs useful for this thesis is the distinction of motion dependent and motion independent devices which has been suggested by Johanning *et al.* (2006). Devices of the terminator type are mostly motion independent, while point absorbers and attenuators rely on the relative motion of the structure and reaction point for their power conversion.

2.2.2 Wave loads

From a reliability perspective it is of interest to classify the different devices regarding the type and magnitude of the expected forces on the structure and its components.

Loads are generally distinct as either static or dynamic. Chakrabarti (2005a) describes the different load types for offshore structures. Static loads are typically caused by the structural or operational weight and hydrostatic loads whereas dynamic loads are induced through wind and waves. The dynamic, environmental loads can be further separated as either steady type or oscillatory type, depending on the time scale the load fluctuates. If a load can be considered static for a certain time, e.g. an hourly interval, it is regarded as steady, whereas a continuous fluctuation in the considered time frame is described by an oscillatory load. Influences such as wind and current loads are typically considered as steady load for offshore structures, but may also require an assessment as oscillatory load, e.g. to determine the cyclic loading of wind or tidal turbine blades (Deyuan *et al.*, 2003; Faudot & Dahlhaug, 2011). Another example for a steady dynamic load are wave drift loads caused by the mean wave direction, that may lead to spatial offsets of moored structures and are varying slowly.

The motion response of the structure as a result of the induced forces leads to a dynamic oscillatory load. The oscillation frequency depends on the natural response period of the structure for each of its six degrees of freedom. The motion response is usually modelled with Response Amplitude Operators (RAOs) which can be determined experimentally or via numerical simulation.

Additionally the wave motions cause wave loads on the structure which fluctuate at wave frequency. As wave energy converters are located in high energy wave locations the wave force will be the governing load component.

Wave forces are estimated following two different approaches, depending on the criterion if the size of the structure relative to the incident wavelength L is considered 'small and slender' or 'large'. For small structures Morison's equation is used whereas wave forces for large structures are calculated using diffraction theory. In order to determine which approach applies, the value of the diffraction parameter must be consulted. It describes how much the structure interferes and bends the incoming waves, i.e. how much diffraction occurs. The diffraction parameter is defined by Chakrabarti (2005a, p. 164) as $\frac{\pi D}{L}$. D denotes the characteristic dimension of the structure that opposes the wave front, L is the wavelength and π denotes the mathematical constant. For values of $\frac{\pi D}{L} < 0.5$ structures are regarded as 'small' and if $\frac{\pi D}{L} > 0.5$, they are considered to be 'large'.

2.2.2.1 Morison's equation

The loading on a small and slender marine structure as a combined effect of the velocity and acceleration of water particles is estimated with the empirical Morison's equation (Chakrabarti, 2005a; DNV, 2005), first presented by Morison *et al.* (1950).

The horizontal force F_{Mor} per unit length of the structure is estimated after Morison's equation as:

$$F_{Mor} = \rho C_M \frac{\pi D^2}{4} \dot{u} + \frac{1}{2} \rho C_D D |u| u \tag{2.28}$$

$$F_{Mor} = F_I + F_D \tag{2.29}$$

Where ρ denotes the density of water, u is the wave particle velocity, $\dot{u}$ denotes the wave particle acceleration, C_M and C_D are the hydrodynamic coefficients for mass and drag, which depend on the cross-section and are determined through model tests. Typical values for cylindrical shapes, using linear wave theory, are stated in Techet (2004) as $C_M \approx 2$ and $C_D \approx 1.4$. The hydrodynamic coefficients used here are for illustrative purposes and would have to be estimated for each device individually.

The choice of linear wave theory in this context requires justification, as a number of wave theories are being applied for the design of offshore structures (compare e.g. Holthuijsen (2007) and Tucker (1991)). Non-linear wave theories such as Stoke's second and fifth order theory or the stream function theory are more appropriate to model non-linear waves, where wave steepness and elevation do not follow the simple sinusoidal motion assumed by linear wave theory. Therefore, the objective for the calculations presented in the following is not to estimate the load conditions during storm or extreme waves where the application of non-linear theory would be required. The simplified assessment presented here uses linear wave theory to gauge the wave loads for operational sea states, i.e. for moderate wave heights, for different generic device types. Chakrabarti (2005b, p.102) discusses the applicability of wave theories and supports the choice of linear theory for situations of low, swell dominated sea states (1 year storms) and for fatigue analysis of inertia dominated structures.

Equation 2.29 comprises two parts, the inertia force element F_I and the drag force element F_D. The inertia is proportional to the volume of the structure, i.e. proportional to the square of the width that opposes the wave front, $F_I \propto D^2$. The drag term depends on the cross-sectional area of the structure with regards to incident wave direction, i.e. it is only proportional to the width of the structure, $F_D \propto D$. Consequently, for structures with high values of D, within the limit for 'small' structures, the horizontal forces will be dominated by the inertia component while the drag element becomes almost negligible. At the other extreme with very small values for D the horizontal wave force is largely governed by the drag force component.

Morison's equation can be further expanded when the particle velocity and acceleration are explicitly stated as the derivatives of the wave elevation $\eta(x,t)$:

$$\eta(x,z,t) = \frac{H}{2} cos(kx - \omega t) \tag{2.30}$$

$$u(x=0,t) = \frac{H}{2} \frac{cosh\,[k(z+d)]}{sinh(kd)} cos(\omega t) \tag{2.31}$$

$$\frac{\partial u}{\partial t}(0,z,t) = \frac{H\omega^2}{2} \frac{cosh\,[k(z+d)]}{sinh(kd)} sin(\omega t) \tag{2.32}$$

Integration along the vertical dimension z along the structure over the water depth d then yields expressions for the resultant inertial force $F_I(t)$ and the drag force as a function of time $F_D(t)$:

$$F_I(t) = \rho C_M \frac{\pi}{4} D^2 \frac{H}{2k} \omega^2 sin(\omega t) \tag{2.33}$$

$$F_D(t) = \frac{1}{2} \rho C_D D \frac{H^2 \omega^2}{4} \frac{\left[\frac{sinh(2kd)}{4} + \frac{kd}{2}\right]}{ksinh^2(kd)} cos(\omega t)|cos(\omega t)| \tag{2.34}$$

Where k denotes the wave number, defined as $k = \frac{2\pi}{L}$.

Equations 2.33 and 2.34 show the dependence of the wave force on the incident wave height H. While the inertial force is proportional to the wave height $F_I \propto H$, the drag force is proportional to the square of the wave height $F_D \propto H^2$.

The maximum forces $F_{I,\,max}$ $F_{D,\,max}$ can then be computed as:

$$F_{I,\,max} = \frac{\pi}{4} C_M \rho D^2 \omega^2 \frac{H}{2k} \tag{2.35}$$

$$F_{D,\,max} = \frac{1}{2} \rho C_D D \omega^2 \frac{H^2}{4} \frac{\left[\frac{sinh(2kd)}{4} + \frac{kd}{2}\right]}{ksinh^2(kd)} \tag{2.36}$$

2.2.2.2 Diffraction theory

For large structures, i.e. for diffraction parameters $\frac{\pi D}{L} > 0.5$, diffraction theory becomes applicable to estimate the wave loads on the structure. In such conditions it is assumed, that the flow does not separate from the structure and can be described by the potential flow assumption (Chakrabarti, 2005a, p. 160). A number of numerical models have been developed to solve this problem, most of which are based on the Boundary Element Method (BEM) also referred to as panel methods. McCabe (2004) summarises the procedure to derive the fluid potential: "The division of the body surface into a discrete number of panels transforms the overall surface integral into a set of integral equations, one for each panel. Each panel is taken to be a fluid source (or singularity), which has an effect on every other panel source, all contributing to the flow over the surface."

Much work has been devoted to the numerical modelling of WECs using panel method software such as WAMIT or AQUADYN, examples of which are presented in

Cruz *et al.* (2008).

For the objective here, to attribute the principal wave loads to the different converter types, an empirical equation that has been derived by Jeffrey *et al.* (1976) shall be used to estimate the horizontal wave force. For the Duck device, a terminator type device, for which the diffraction theory applies, the horizontal wave force per unit length of the device is calculated as:

$$F_{Term} = \rho g D C_f H \tag{2.37}$$

where C_f is the force coefficient, with values for the Duck device around $C_f \approx 0.5$

Experimental results for the horizontal forces reported in Jeffrey *et al.* (1976) showed good agreement with the values estimated through equation 2.37.

2.2.2.3 Wave load estimation

The question which wave load theory, Morison's equation of diffraction theory, is applicable can also be resolved with the help of non-dimensional charts that plot the diffraction parameter $\pi\frac{D}{L}$ against $\frac{H}{D}$ (Chakrabarti, 2005a, p. 164). The latter is a measure of the Keulegan-Carpenter number KC which describes the relative contribution of drag forces and inertial force. In the deep water case the KC number is defined as $KC = \pi\frac{H}{D}$.

To revert back to the device classification with regard to their orientation as shown in figure 2.5, it is necessary to identify the applicable wave load theory for each type of device in order to estimate the wave loads. To provide an example here, for each capture type the dimensions of a real device are selected as reference width D that opposes the wave front. For the attenuator type this is $D_{Att} = 3.5m$, based on the Pelamis P1 device; for the point absorber $D_{Point} = 11m$ based on OPT's PB150; and for the terminator $D_{Term} = 300m$ is chosen based on the Wavedragon dimensions.

The non-dimensional values $\pi\frac{D}{L}$ and $\frac{H}{D}$ are calculated for a set of wave heights H across a range of wave periods $T = [4, 6, \ldots, 18, 20]$. The wavelength L is calculated after equation 2.27 for deep water. The results for $H = 3m$ and $H = 15m$ are shown in figure 2.6.

A terminator type of device with a large characteristic width D falls in the application regime of the diffraction theory, as the calculated diffraction parameter is greater than 0.5. For the attenuator device, Morison's equation is applicable, as $\pi\frac{D}{L} < 0.5$. In case of the point absorber Morison's equation is applicable in most cases. Only for small wave heights, $H \leq 3$ and small wave periods $T = [4, 6]$ diffraction theory becomes applicable.

For each of the generic devices a simplified calculation of the expected wave forces has been performed using Morison's equation (2.29) for the attenuator and point absorber, and using the approximation for diffraction theory (equation 2.37) for the terminator type. The calculation results are plotted in figure 2.6. The maximum levels of horizontal force for each of the devices in various wave heights H is depicted in figure 2.7. For small wave heights, the devices are separated by approximately an order of magnitude in maximal wave force. The terminator exhibits the highest loads (in the $10^7 N$ range), followed by the point absorber ($10^6 N$ range) and the attenuator ($10^5 N$ range). An increase in wave height generally results in an increased horizontal force. However, the attenuator shows a relatively larger force increase compared to the other devices, this is due to the increased drag force at larger wave heights, as $F_D \propto H^2$ (equation 2.34). A note of caution must be raised here for the attenuator type. The presented case assumes the device is able to 'weathervane' into the incident waves, reducing the cross-sectional area that opposes the waves. This might not be always possible in realistic conditions when there are multiple wave directions, e.g. a combination of long-period swell from a westerly direction and locally generated wind waves from a northerly direction. Such a situation will induce wave forces at the larger cross-section orientated orthogonal to the wave direction.

The relative contribution of drag force F_D to the total horizontal force F_{Mor} is illustrated in figure 2.8, which shows the time series for two different wave heights, $H = 5m$ (2.8(a)) and $H = 15m$ (2.8(b)). It is consistent with the earlier statement that the point absorber is subject to larger loads, as $D_{Point} > D_{Attenuator}$, and that increased wave heights lead to a load increase. Yet, the plots reveal two further aspects.

Firstly, considering the peak force for the point absorber in the lower sea state, figure 2.8(a), the drag force is not governing the total force, but gains in influence for

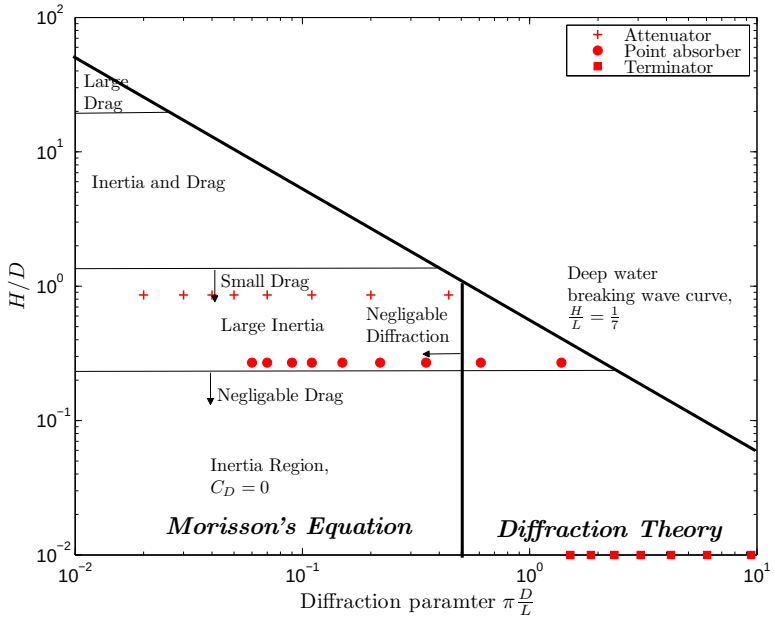

(a) H=3m

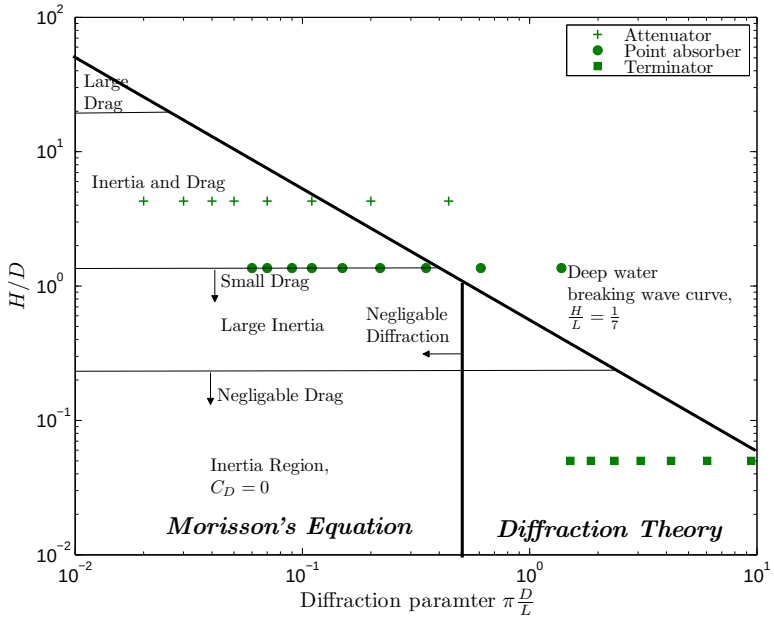

(b) H=15m

Figure 2.6: Wave load theory application ranges for different wave energy converter types. Non-dimensional boundaries for wave load theories after Chakrabarti (2005a, p. 146), data shows values for a set of wave periods $T = [4, 6, \ldots, 18, 20]$ for each device type.

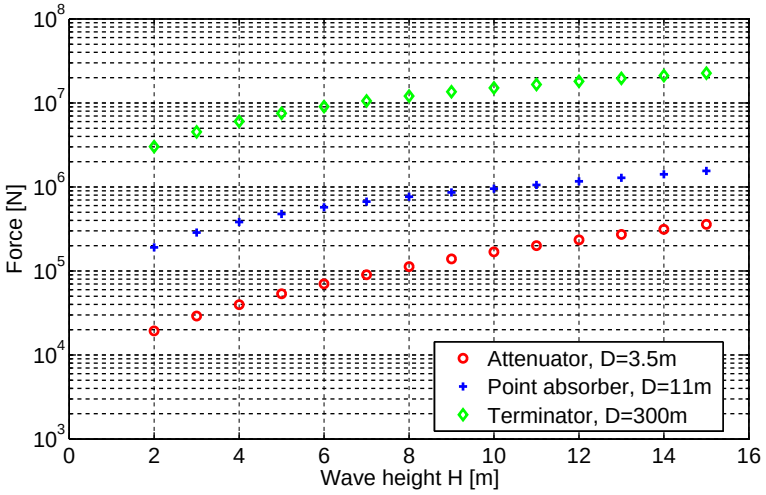

Figure 2.7: Wave height dependence of horizontal wave forces for different types of devices. Plot shows force per unit length for a variation in wave height H whilst wave period $T = 10s$. Attenuator ($D = 3.5m$) and point absorber ($D = 11m$) force is calculated using Morison's equation (2.29); Terminator ($D = 300m$) values computed with approximation for diffraction theory (equation 2.37).

the larger sea state, (2.8(b)). In case of the attenuator, the drag force already largely contributes to the total peak force in the lower sea state and dominates the total force for the larger wave height.

The quantitative increase of the drag force for both sea states can be expressed as the ratio $\zeta = \frac{F_D(15m)}{F_D(5m)}$. Furthermore, in order to compare the relative increase in drag force for both sea states between attenuator and point absorber one may write the ratio Z (equation 2.38). Hence, an increase in wave height H by a factor of 3, increases the drag force for the attenuator by twice as much as for the point absorber.

$$Z = \frac{\zeta_{Attenuator}}{\zeta_{Point}} = \frac{\frac{3.6 \cdot 10^5}{5.4 \cdot 10^4}}{\frac{1.6 \cdot 10^6}{4.8 \cdot 10^5}} = \frac{6.7}{3.3} \approx 2 \tag{2.38}$$

Secondly, the time series exhibits the cyclic, oscillatory nature of the wave force, which largely follows the wave period T. It must be noted though, that the presented calculations after Morison's equation are somewhat simplified. Forces caused by breaking waves, slamming of the devices and non-linear effects and the motion response of the device are *not* considered. It is therefore evident, that the presented wave loads do

not describe the full hydrodynamic behaviour of the device. This is usually described and modelled by Response Amplitude Operators (RAO) which describe the first order motions of the device. It must be stressed that the assessment of the hydrodynamic behaviour is of crucial importance for any marine structure , but is not the pivotal matter of this thesis. For a more detailed hydrodynamic assessment of WECs, the interested reader is referred to De Backer (2009); Thomas (2008) for the hydrodynamic design optimisation and the evaluation of slamming loads, to the work of Payne (2008) for guidance on hydrodynamic experiments, as well as to Brito-Melo *et al.* (1999); Eriksson *et al.* (2005) for a detailed hydrodynamic modelling of OWCs and direct drive wave energy converters.

The preceding explanations regarding the governing parameters for the expected structural wave forces allow the following conclusions for the different types of devices:

- The transferred loads for a terminator type of device will be maximal as it directly opposes the incoming wave front with a large width D.

- The attenuator is mainly subjected to inertial forces. However for larger wave heights H, the drag force component increases. Hence the wave force for the attenuator in the case of small waves is $F_{Att,\,\mathrm{smallH}} \propto D^2$ and $F_{Att,\,\mathrm{smallH}} \propto H$. For large wave heights such as the depicted $H = 15m$, $F_{Att,\,\mathrm{largeH}} \propto D$ and $F_{Att,\,\mathrm{largeH}} \propto H^2$.

- In case of the point absorber the wave forces are largely driven by inertial forces and drag forces are small. Thus, the wave force for point absorbers follows $F_{Point} \propto D^2$ and $F_{Point} \propto h$.

- As $D_{Att} < D_{Point}$, in comparison between the two, the inertial force and indeed the total wave force is much larger for the point absorber $F_{Att} << F_{Point}$.

- From a reliability perspective, motion independent systems require a high structural strength as they are subject to large steady forces, such as drift forces, but are less exhibited to highly cyclic dynamic loads. Motion dependent devices are typically smaller structures, requiring less structural strength as steady forces are not as large as for terminators. However, they rely on oscillatory motion to drive

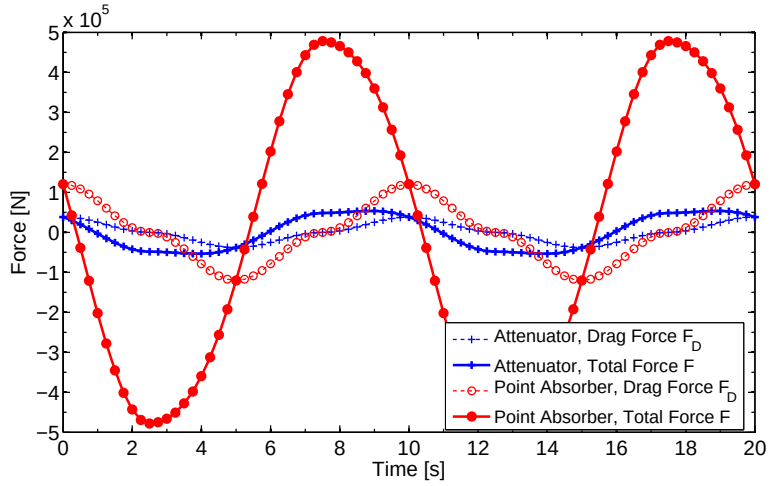

(a) $H = 5m$, $T = 10s$

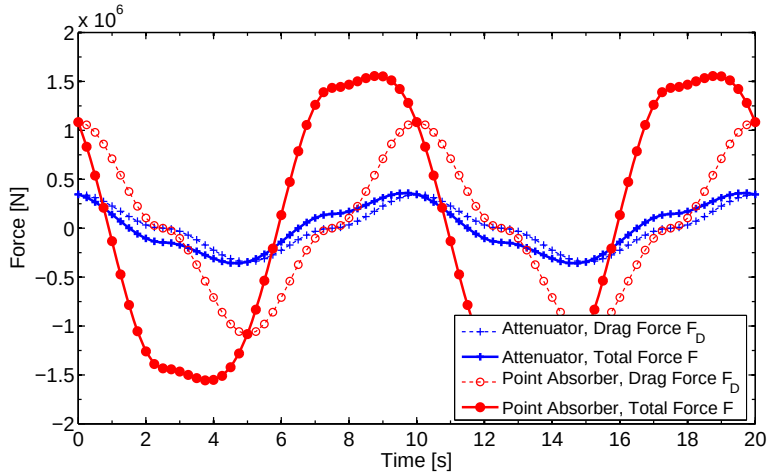

(b) $H = 15m$, $T = 10s$

Figure 2.8: Time series of horizontal force and drag force contribution after Morison's equation for two types of wave energy converters in medium 2.8(a) and large wave height 2.8(b); $T = 10s$.

the power take-off mechanism and are subject to increasing drag forces with increased wave heights, which was shown to be proportional to the square of the wave height.

- The motion response of a motion dependent device will be close to the incident wave period, while a motion independent device as most terminator types, will respond at much larger response periods (i.e. lower natural frequencies). As a result motion dependent devices will experience more load cycles compared to relatively large, motion independent devices.

2.2.3 Operating principle and energy conversion

The elemental process of wave energy conversion can be generalised as a "$(\cdots)$ force (or torque) produced in a system by an incident wave [that] causes relative motion between an absorber and a reaction point, which acts directly on, or drives a working fluid through, a generator prime mover" (Brooke, 2003, p. 27). The passage of the wave induces an oscillating low frequency, high force movement with frequencies in the range of $f = 0.05 - 0.5$Hz. This motion response then needs to be matched with the operating range of the power take off system. Conventional electrical generators are designed to operate with low torque, high frequency unidirectional rotation and necessitate another conversion step. The conversion chain from wave energy to electricity can thus be divided into three phases (see figure 2.9).

The primary conversion from wave energy to energy in a working fluid or potential/kinetic energy is often attained by an oscillating system, making use of the periodic wave movement. The oscillating system can use air, water, hydraulic fluids or mechanical linkage to transmit the kinetic and/or potential energy.

Apart from the direct drive linear generator systems, a secondary conversion is required to gain a more useful form of energy, namely mechanical energy of a rotating shaft to provide the high speed, low torque motion required to drive an electric generator. This secondary step may be achieved via air- or water turbines, hydraulic motors or mechanical gears to drive a rotational shaft.

In order to generate electricity the tertiary conversion step uses electric generators to convert the rotational energy into electricity.

The energy conversion in case of linear generator power requires less conversion steps. The wave-induced motion of the prime mover is directly converted into electrical energy. Thus the linear generator has a separate flow path in figure 2.9. The linear generator directly converts the mechanical motion into electricity.

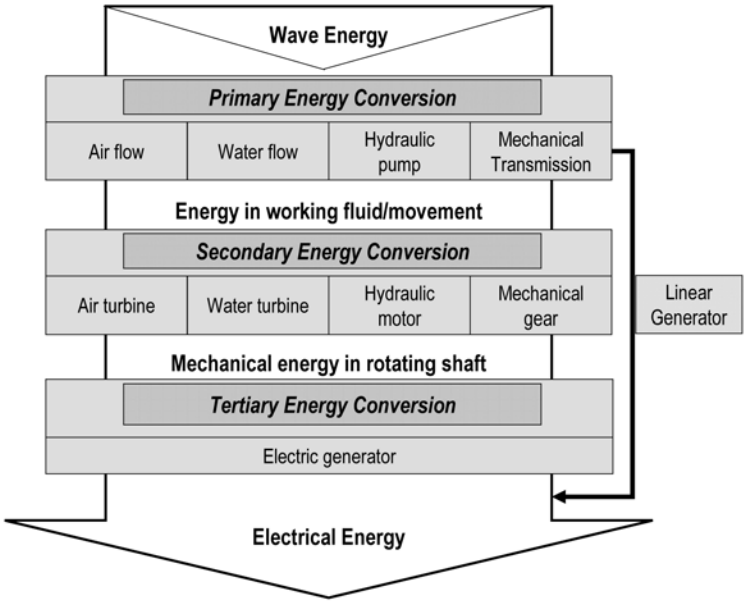

Figure 2.9: Schematic energy conversion path for wave energy converters.

Cruz (2008, p.5) regards the Oscillating water column (OWC), the Archimedes Wave Swing (AWS), the Pelamis and the Wavedragon (WD) device as the four main technologies at full scale, which are currently competing for commercial deployment. An earlier, in-depth assessment of WECs by the American Electric Power Research Institute (EPRI) came to a similar conclusion (Bedard et al., 2005, p. 14). As those four devices also represent the four different power conversion mechanisms, i.e. air turbines (OWC), direct drive linear generators (AWS), hydraulic systems (Pelamis) as well as low head water turbines (WD), these devices will be presented in some more detail in the following.

2.2.4 Oscillating Water Column

The Oscillating Water Columns (OWC) design was the first full-scale devices to be built, as it could be erected at shore. They consist of a chamber that is open to the sea. Through the heave motion of incoming waves the air in the chamber is pressurised and depressurised. This results in an air flow that reciprocates at wave frequency and is forced through an air turbine. The principle and typical power take-off via a Wells turbine is illustrated in figure 2.10.

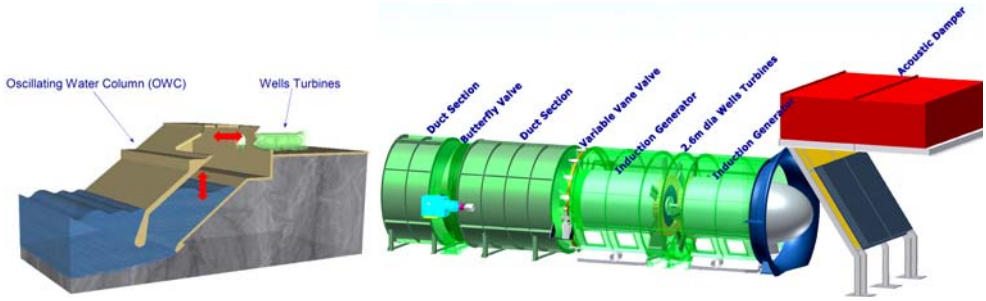

Figure 2.10: Operating principle (left) and turbine/generator set (right) of LIMPET Oscillating Water Column, reproduced from Mackie (2004, p.4).

Three of the most prominent devices at full-scale are the LIMPET (Boake *et al.*, 2002), Pico (de O. Falcão, 2000) and Oceanlinx device (Denniss, 2009). A detailed comparison and evaluation of the different OWC systems can be found in a study compiled for the Carbon Trust (Webb *et al.*, 2005).

The operation of the LIMPET (Land Installed Marine Power Energy Transmitter) was mainly hampered by the reduced energy climate close to the shoreline. While about 20 kW/m was estimated to prevail at the collector, only 12 kW/m could be measured in operation. As the LIMPET is a shore based device, the maintenance regime foresees weekly visual checks and regular maintenance activities (e.g. grease of bearings). Beyond that, during the first two years of operation some unplanned maintenance occurrences were reported in (Mackie, 2004; WAVEGEN, 2002).

- Blockage of collector
- Vibration loosening of bolts and screws
- Vane valve flutter

- Seizure of the butterfly valve shaft bearings
- Storm damage, water ingress

For the Pico plant, the following operational problems were encountered (Brito-Melo *et al.*, 2007; Neumann *et al.*, 2007):

- Excessive vibrations in the turbo-generator set at higher turbine speeds $n > 1,200rpm$.
- Power electronic equipment and transformers had to be renovated and relocated outside the plant due to the aggressive marine environment in the plant.
- The guide vane stator on the atmospheric side of the turbine failed due to material fatigue.

Some of these issues are due to the long marine exposure of the mechanical and electrical equipment, but the vibrations and failure of guide vanes are design-related issue. The design appears to follow the requirements for conventional unidirectional turbines and fell short to accommodate the conditions in a bidirectional, OWC turbine. The failure of the guide vane stator was attributed to pressure oscillations caused by vortex shedding under turbine stall conditions on the atmospheric side of the turbine (Brito-Melo *et al.*, 2007). The problem was resolved with a new reinforced set of guide vanes. The original and failed guide vanes are pictured in figure 2.11.

(a) Before operation (b) Failed, pictured 10/2009

Figure 2.11: Guide vane stator failure Pico Oscillating Water Column, figure 2.11(a) is taken from de O. Falcão (2000).

The OceanLinx device was continuously developed from a nearshore device to an offshore floating platform. Not much operational information is available, but the so

called MK-3 device, a pre-commercial scale floating platform with 2 turbines, broke free of its catenary moorings and sunk in May 2010 (Hasham, 2010).

2.2.5 Direct drive linear generator

Linear generators can be directly connected to a prime mover of a wave energy device to generate electricity. The advantage over conventional high speed rotating generators is that the movement is directly converted into electricity and no secondary energy conversion is necessary. The appeal is a more reliable power conversion, as there are fewer parts to fail and less maintenance requirements as the number of moving parts is reduced (Spooner & Mueller, 2001). However, the disadvantage of this technology is that the output voltage varies in frequency and amplitude which necessitates a further electrical conversion before the electricity can be fed into the grid (Eriksson *et al.*, 2005).

A number of point absorbers operate with linear generators. The more prominent devices are the Archimedes Wave Swing (AWS) (Polinder *et al.*, 2005; Valério *et al.*, 2007), Trident energy (Clifton *et al.*, 2010) and the Seabased floating buoy developed at Uppsala University (Danielsson, 2006; Waters *et al.*, 2007). The concept of these devices is identical in the sense that a linear generator is coupled to a heaving prime mover that follows the wave movement. The moving part of the generator is called the translator and consists of permanent magnets that pass through the stator where a current is induced as shown in figure 2.12. The devices vary in the arrangement of the floater. The AWS is designed as completely submerged, bottom-mounted device with an oscillating heaving, air-filled cylindrical chamber. The Seabased device consists of a floating buoy which is connected to the linear generator by a wire rope, while the Trident energy design aims to built a raised platform for the linear generator which is being driven by floaters underneath the platform.

Two of the devices suffered from delays and difficulties during the offshore deployment. The 2MW AWS prototype was deployed off the northern Portuguese coast in 2004, but this was preceded by two failed attempts in 2002 and 2003. During the deployment the control cubicle was flooded which led to the failure of crucial control and communication components. As a results the device was only operational, i.e. feeding electricity into the grid, for 15mins, before the testing was halted by Enersis, the funder of the project (Mill, 2004). The device is currently being redesigned by the

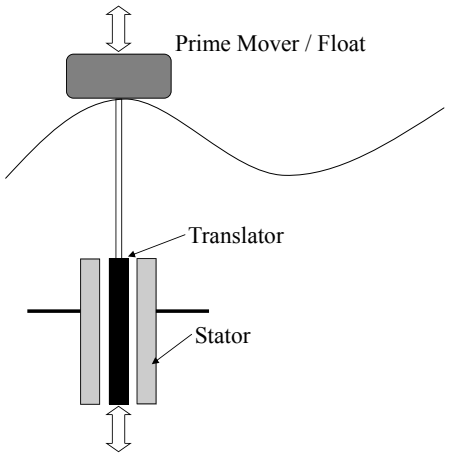

Figure 2.12: Simplified operating principle for linear generator wave energy converters.

AWS ocean energy consortium. The Trident energy device capsized and sunk five miles offshore while it was being towed to its installation site on the 20th September 2009 (Bond, 2009). Both examples underline the challenge of offshore deployments and the careful planning it requires, but are not informative regarding the reliability of linear generators in wave applications.

A known reliability challenge for linear generators are the bearings that guide the translator and maintain the air gap between the translator and the stator. This is due to large attractive force between the translator and stator, the large amount of translator cycles for a typical year of operation and the fact that conventional mechanical bearings require regular maintenance (Polinder *et al.*, 2007). Plain contact polymer bearings are being investigated by Caraher (2011); Caraher *et al.* (2010) who performed application specific testing of different bearing materials and point out the need to base the bearing system design on empirical test data.

Linear generators are thus a promising power conversion mechanism for wave energy converters but require further work and development to overcome in particular the reliability concerns of bearings.

2.2.6 Hydraulic system

Hydraulic power take-offs are being considered in wave energy applications, because the are well suited to the high force, low frequency conditions present in the primary energy conversion step.

Pelamis is a floating device, rated at 750kW and installed in offshore locations and employs hydraulic systems to generate electricity from waves. The device consists of a number of partly submerged cylinders connected with hinged joints. The waves cause the cylinders to move relative to each other in two degrees of freedom, heave and sway (Henderson, 2006). The device can be classed as attenuator, as it is a slender, long device with a diameter of 4m and a length of 180m in case of the P2 device, that progressively absorbs the energy as it passes down the device.

Figure 2.13 shows the schematic layout of the hydraulic power system used in the Pelamis device. The system comprises two independent hydraulic cycles, each of which is driven by one cylinder in the heave axis and another cylinder in the sway axis. A simple heaving buoy would be driven by a single hydraulic ram. The hydraulic cylinders are driven by the relative movements of the floating structure and pump the working fluid through control manifolds into high-pressure accumulators. The high-pressure fluid drives hydraulic motors that are coupled to electric generators which feed into a step-up transformer.

Regarding the reliability of the PTO machinery, a number of redundancies are apparent in this configuration (Yemm, 2003):

- Three power conversion modules are operating independently, i.e. are in parallel.
- Two generators rated at 125 kW each are installed within each of the three power modules.
- Two independent hydraulic systems, with one heave/sway axis each.

Apart from offshore environmental operating conditions of the machinery, in particular the hydraulic cylinders are subject to reliability issues as they absorb the incident wave forces as a primary energy conversion step. They effectively act as compressing pistons which is contrary to their conventional deployment as actuators and results in much higher cycle frequency and reversed, less controlled loadings.

Some of the detrimental effects that should be considered for hydraulic cylinders are (DNV, 2005, p. 55)

- Fatigue and buckling of piston rod
- Wear mechanisms of seals, pins and bearings

- Hydraulic fluid contamination, e.g. by seawater and bacterial growth

The abrasive wear of piston ring seals for a heaving buoy configuration has been modelled by Yang & Moan (2011); Yang *et al.* (2010a). They conclude that high frequency oscillations due to the compressibility of the oil significantly increase the travelled distance of the piston ring and thereby accelerate the wear of the ring seal. Moreover average wear rates for different sea states are calculated. It is shown that the wear rate is affected by both significant wave height H_s and wave period T_p. Still the model is somewhat simplified as it assumes that all horizontal side loads are absorbed by bearings and that other seal failure modes such as corrosive and adhesive wear, surface fatigue and fretting are not modelled.

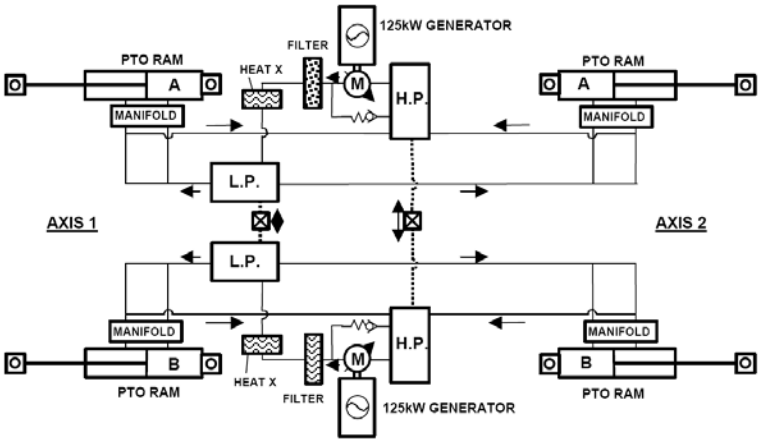

Figure 2.13: Hydraulic power conversion system schematic of Pelamis wave energy converter taken from(Yemm, 2003).

During the deployment of three Pelamis machines in 2008 in Aguacadora, Portugal an increased wear rate was discovered for the main cylindrical bearings of the hydraulic cylinders. As a root cause undesired lateral movement of the bearing face have been identified (Pelamis, 2011) that has not been expected from preceding development testing.

The design has been subsequently changed from the two-axis hinged joints to a single universal joint, thus all bearings are on the same axis and are covered by a low-friction liner (Snieckus, 2010).

The hydraulic power take-off is a good example of how existing and well-known components may be applied for wave energy converters, but the altered loading must be understood and considered in order to evaluate and ensure component reliability.

2.2.7 Water turbine

Low head water turbines are a well established technology for hydropower plants. They may also be used in overtopping WECs where the waves run over the structure and the water is collected in an elevated reservoir from which the turbine is fed and drives an electric generator.

One of the most advanced overtopping devices is the Wave Dragon (WD). The potential rated power output ranges between 4-10 MW depending on the site specific wave climate. Compared to other devices the structural dimensions with 300m width and 170m length are large. The device can be classified as a terminator, as the structural dimensions are large compared to the wavelength. The device consists of three main components (Christensen *et al.*, 2005):

- The main structure comprising ramp and water storage reservoir
- Two wave reflectors, fixed to the main structure, focus incoming waves onto the ramp
- Several low head Kaplan turbines (16-18), modified for variable speed operation.

As the WD is a terminator-type device, the wave forces on the structure and moorings are expected to be large. After over 15,000 hours of sea trials with a 1:4.5 prototype, in January 2005 a force transducer in the main mooring line failed during a large storm (Christensen *et al.*, 2005) and the device broke free (figure 2.14).

Nevertheless, the device has been at sea for en extended period of time and several reliability and maintenance issues have been identified by Tedd (2007) and Christensen *et al.* (2005):

- Turbine bearings were intruded by salt water and began to corrode.
- The turbine draft tubes made from black steel and coated with epoxy paint experienced significant marine growth whereas a silicone based antifouling coating inhibited almost all marine growth.

(a) Failed force transducer

(b) Wavedagon stranded in storm conditions

Figure 2.14: Mooring failure of Wavedragon device, reproduced from Christensen *et al.* (2005).

- Maintenance activities on board and accessing the device could only be carried out in calm weather conditions most likely during the summer month.
- For electrical components Ingress Protection Rating IP66 (protected against dust and low pressure jets of water) was not sufficient. The sea water spray overcame existing protections and attacked exposed sealing by corrosion.

2.2.8 Common reliability aspect

The environmental influences and material phenomena that effect the reliability of wave energy converters have been described by Hudson *et al.* (1980) and Wolfram (2006) and a list of the most pertinent aspects is given in table 2.5. The listed potential failure mechanisms are a result of the operational and environmental factors. Even though most of these phenomena are well known and understood, it appears from the technology review, that the specific application to actual devices is fraught with difficulty and field failures are often not averted.

The different technologies listed above may be separated in two distinct design approaches:

New, unproven technology As wave energy conversion is an unprecedented energy generation, new technological solutions and components are engineered to suit this

application. The invention of the Wells turbine for OWCs and linear generators fall into this approach.

Proven technology in new application Components and technologies which are widely used and regarded as proven are applied for wave energy applications. Examples are the use of hydraulic systems and water turbines.

Most of the failures and reliability issues described above are due to the fact that actual load conditions in the field are not well understood and the associated reliability is difficult to predict. For proven technologies in new applications it is crucial to understand how the component reliability is affected by the environmental- and load conditions. New technology has to be developed and tested appropriately to validate the design and demonstrate its performance.

While new technology always has the association of possible failures while it is being developed, components that have been proven in other fields might be expected to perform accordingly in the new application. While the former is a reasonable precaution, the latter expectation might not be the case when a proven technology is placed into a radically different operating environment.

The research question emerging from this is to understand how the system reliability can be estimated for new or proven technology in wave energy applications. Chapter 3 presents such a reliability assessment for a typical hydraulic wave energy converter.

Table 2.5: Environmental influences and material aspects for wave energy converters, based on Hudson *et al.* (1980); Wolfram (2006).

Environmental influences	Material aspects
External water pressure	Corrosion
Damp, saline atmosphere	Fatigue
Temperature variations	Corrosion fatigue
Cyclic motions and accelerations	Stray current corrosion
Inaccessibility	Wear and fretting fatigue
Human factors	Marine fouling
	Impact loading and fracture

Part II

Methods to improve reliability and reliability information

Chapter 3

Reliability assessment for wave energy converters

3.1 Methodology

Reliability assessment and analysis play an important role in the performance assessment of a system evaluating performance measures regarding system reliability, availability and maintainability (RAM). Two general approaches to determine system performance measures are distinguished (Ramani & Trivedi, 2000):

1. *Measurement-based* techniques require measured data from prototypes or real systems (e.g. generated electricity or recorded failures) and use statistical inference techniques to determine the general systems performance.

2. *Model-based* assessments require a system model that has to be established, specifying random variables and system characteristics in order to derive performance measures. They can be further classified into simulation and analytical methodologies.

The record of occurring failures and the documentation of the prevalent operating environment, maintenance schedule and failure modes form the basis for robust measurement-based reliability assessment. As an example, Tavner *et al.* (2007) conducted a reliability analysis for the wind industry, using failure records from 6,000 turbines collected over a 11-year period. This amount of data allows for statistically

significant inferences. The early stage of the wave energy sector means there is no significant operational experience and a lack of failure records. Furthermore, the reliability data and experience gained during the few deployments are not publicly available, as they are seen as major competitive advantages over other developers (Flinn & Bittencourt, 2008).

This lack of specific failure data does not allow a measurement based reliability analysis and one has to revert to a model-based approach and the associated reliability prediction methods described in section 2.1.4. Nevertheless, the situation of scarce reliability data is not uncommon for new and high technology products. O'Connor (2008, p.163) points out that in such circumstances reliability modelling has to follow a practical approach to identify the reliability objectives and assess the risk of the analysed technology, rather than determining an exact reliability figure. Therefore the development of a reliability model is of avail, as it displays a picture of functional interdependencies and provides the framework for developing quantitative system reliability estimates to guide the design trade-off process.

In the following, the reliability assessment is conducted by means of a Reliability Block Diagram (RBD). The rationale for this choice over other methods is that RBD analysis can be performed with the input of basic information, such as system layout and component failure rates. Other methods would need much more detailed information, for both the system layout and the associated failure rates, which could not be found in the public domain.

The reliability assessment comprises the following six primary steps:

1. Development of a system block model (section 3.1.1, 3.2.2)
2. Collection of component failure rates from reliability databases (section 3.1.2)
3. Adjustment of failure rates towards the expected application / environmental effects (section 3.1.3, 3.2.1)
4. Data input to the system model and reliability calculation (section 3.2.3-3.2.6)
5. Result analysis (section 3.2.7)
6. Uncertainty estimation (section 3.1.4)

3.1.1 System Block Diagram

The purpose of a WEC system is the generation of electricity. Despite the different designs and working principles, Wolfram (2006) points out that there are considerable similarities in the functional layout and logical design of WECs. Most converters comprise of four sub-systems, which are illustrated as generic RBD in figure 3.1. For the system to be functional, i.e. to generate electricity, each of the following sub-system blocks must be operational:

- *Mooring* - For near shore and offshore devices the mooring assembly warrants the station keeping of the device.
- *Structure* - The structure provides shelter for the power machinery, maintains the system's level of buoyancy and withstands applied loadings.
- *Power take-off* (PTO) - The PTO converts the wave energy into electricity. Depending on the device design different conversion principles are used (hydraulic; air- or water turbines; direct drive generators).
- *Power transmission* - The generated electricity is typically transmitted to shore where it is fed into the electricity grid.

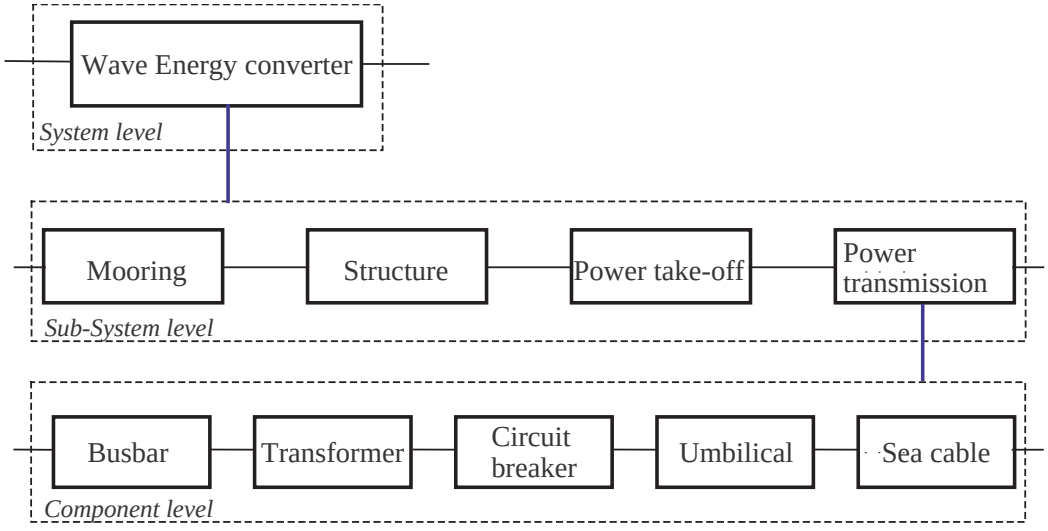

Figure 3.1: Generic wave energy converter reliability block diagram: system-, subsystem and component level.

Each sub-system consists of a number of components which themselves are assembled from parts. The transmission sub-system for offshore applications for example can be further divided into the following components:

- Busbar that provides the electrical connection within the device;
- Transformer to increases the voltage level;
- Circuit breaker to enable the separation of the device from the grid;
- Umbilical cable to transfer data and electricity to and from the device;
- Sea cable to conduct electricity to the shore grid station.

The component levels of the other subsystems are device-specific, depending on device design and location and are shown for a floating hydraulic device as case study in section 3.2.

3.1.2 Reliability databases

Several databases provide reliability information about components and sub-systems that is needed to populate the RBD. Rausand & Høyland (2004, p. 562) distinguish three different types of databases (see also table 3.1):

- *Component failure event databases* (Type I): Failure and maintenance data is recorded for particular components. The data can be used for maintenance planning or system modifications.
- *Accident and incident databases* (Type II): Accidents/incidents description may be used to derive component failure information.
- *Component reliability databases* (Type III): Provide failure rate estimates for single components and in some cases failure rate distributions and repair times.

A number of authors (Akhmedjanov, 2001; Funnemark *et al.*, 2006; OGP, 2010; Sharp *et al.*, 2005; Vintr, 2007) have compared the range of different reliability databases. The US Military Handbook Reliability Prediction of Electronic Equipment (MIL-HDBK-217F) and the Offshore Reliability Data (OREDA) Handbook appear to be the most frequently used data source for reliability prediction and assessment. With regards to

assessing the reliability in a marine environment the OREDA database is the reference of choice as the data is recorded in a marine offshore environment. The handbook is briefly described in the following.

The OREDA project has been collecting equipment failure data in the offshore oil and gas industry since 1981. It provides information about failure modes, failure rates and repair times. OREDA handbooks are considered to contain high quality reliability data, because the data has been collected over a long period of operational time using a standardised, consistent procedure. It covers a range of machinery, mechanical-, control- and subsea equipment and components which are listed in table 3.2. The physical boundaries of each component are specified and the failure/repair data are presented with detailed statistical measures of the sample population. This includes the number of samples, the operational time covered, the mean failure rate and the 90% confidence bounds of the mean failure rate.

Despite the high data quality, the application towards WECs involves uncertainties. The components would be operating in an unmanned installation in contrast to manned oil & gas installations where regular and appropriate maintenance can be carried out. Furthermore, it is likely that the equipment operating in a WEC is more exposed to marine conditions than this would be the case for the original OREDA data (Flinn & Bittencourt, 2008). Moreover, the complete database is only available to the member companies and partners working on their behalf.

Only limited, more generic, data is published through the OREDA Handbooks (1984, 1992, 1997, 2002, 2009). This restrictive dissemination of failure rate data emphasises the fact that detailed, high-quality data is regarded as valuable asset and a major competitive advantage.

3.1.3 Data quality and adjustment

Database failure rates always require interpretation and adjustment to be used in reliability assessments. The analyst needs to make a judgement regarding the quality and applicability of the data. This comprises aspects such as assumptions during data collections, environmental-, loading- and operating conditions, levels of quality or manufacturing experience which all have an impact on failure rates and thus need to be considered. Consequently, even in cases where failure rates are quoted as exact figures

Table 3.1: Data bank sources for reliability assessments, based on (OGP, 2010; Rausand & Høyland, 2004; Sharp *et al.*, 2005).

Name	Components covered	Type*
OREDA Offshore Reliability Data	Topside and subsea hardware offshore oil and gas	III
MIL-HDBK-217F	Reliability Prediction of military electronic equipment	III
EPRD Electronic parts reliability data Reliability Information Analysis Center (RIAC)	Electronic parts	III
NPRD-95 Non-electronic Parts Reliability Data	Mechanical and electro-mechanical	III
FARADIP Failure rate data in perspective	Microelectronic, electric, electro-mechanical, mechanical and hydraulic	III
FMD-97 Failure Mode/Mechanism Distributions	Electronic, electrical, mechanical and electro-mechanical	I
SR-332 (RIAC)	Reliability prediction for electronic equipment (Telcordia Technologies)	I
MechRel Handbook of Reliability Prediction	Mechanical equipment, mainly military applications	I
Subsea Master	Subsea oil/gas production systems	I
Well Master	Down hole and drilling equipment	I
CCPS Process reliability data (American Institute of Chemical Engineers(AIChE))	Process equipment	III
PERD Process equipment Reliability Data (AIChE)	Process equipment	III
EIReDA European Industry Reliability data	Nuclear power plant equipment	III
CORDS Component Reliability Data System	Components in Canadian Nuclear power plants	III
IEEE 500-1984	Electrical, electronic, sensing components and mechanical equipment from nuclear plants	III
RAC PRISM	Non electronic parts, mechanical and electromechanical	III
GIDEP Government Industry Data Exchange Programme	Primarily military equipment	III
TRACS	Military vehicle reliability data	III
T-Book	Nuclear power plant equipment	III
SIRENS Subsea Investigation and Reporting of Events Network	Lessons learned database, subsea equipment	II

* I = Component failure event; II = Accident; III = Component reliability.

Table 3.2: Equipment covered in the OREDA database (SINTEF, 2002).

Rotating machinery	Mechanical equipment	Control & Safety	Subsea equipment
Combustion engines	Cranes	Control Logic Units	Control systems
Compressors	Heat exchangers	Fire & Gas detectors	Flowlines
Electric generators	Heaters and Boilers	Process sensors	Manifolds
Electric motors	Loading arms	Nozzles	Pipelines
Gas turbines	Swivels	Power transformers	Risers
Pumps	Turrets	Valves	Running tools
Steam turbines	Vessels		Templates
Turbo expanders	Winches		Wellheads & X-mas Trees

(i.e. point estimates rather than confidence bounds) they should always be understood as failure rate *probabilities*.

In this section three potential aspects are outlined which have been considered in the judgement and adjustment of failure rates:

- Failure rate data source
- Operating/environmental conditions
- Failure mode

3.1.3.1 Source of reliability information

The source of reliability information can be classified into four different types (Smith, 2005, p.46):

1. Site/company specific data, collected from similar equipment on similar sites
2. Industry specific data, collected within a particular industry environment
3. Generic data, a combination of various applications, drawn from several sources
4. Failure rate data based on expert judgement

If possible, site specific data is preferred as it is usually the most applicable data source. In the assessment, care has been taken to indicate the type of data source, as it gives a qualitative measure of how much confidence can be placed in the individual failure rates. Reliability predictions using industry or even generic data may vary by as much as an order of magnitude and would need to be validated over time through actual operational experience and/or component testing.

3.1.3.2 Operating and environmental conditions

The adjustment of failure rates to account for operating and environmental influences that have not been prevalent during the failure rate collection is widely used in reliability predictions. The part stress analysis proposed in the MIL-HDBK-217F (section 2.1.4.1) involves a simple multiplication of base failure rates with empirical factors.

The factors are given for electronic parts and components, where the base failure rate has been established through laboratory experiments. The difficulty lies in the determination and applicability of those factors towards the wave energy application. For example, if industry specific failure rates are used for an electric component of a WEC (e.g. circuit breaker) these factors cannot simply be applied. Therefore, the factors have been recalculated to enable an adjustment regarding the difference of distinct environmental conditions, which are considered more applicable.

As an example, the factor for a ground benign application is $G_B = 0.38$ and a naval sheltered environment implies a factor of $N_S = 4.0$ (see table 2.1, p. 58). If the component failure rate has been established in a ground benign environment, rather than applying the given factor N_S to a WEC component, the ratio of those two factors is more appropriate, as it expresses the level of stress increase due to the less benign environment:

$$\pi_{G_B \to N_S} = \frac{N_S}{G_B} = \frac{4.0}{0.35} = 10.5 \tag{3.1}$$

Hence, a generic failure rate established in a benign ground environment could be adjusted towards a WEC environment with a multiplication of 10.5. The same procedure can be justified for other combinations of base failure rate- and application environments. Table 3.3 presents a matrix of factors that can be used to adjust failure

rates from various environments towards the environment that is encountered by WEC applications.

Following this adjustment approach, the stress level in maritime conditions is rated about $10-15$ times higher than in benign laboratory conditions G_B, between $1.5-2.5$ higher in ground fixed G_F, and $1-1.5$ times higher than in mobile applications G_M. The conversion from a sheltered marine environment N_S to an unsheltered N_U or undersea N_{UU} marine condition, as it might be necessary for the application of the OREDA data towards WEC, implies a factor of $1.4-1.6$. Such environmental adjustment factors represent an accumulation of varying failure modes that are being expected for a particular environment. However, the actual change from a benign ground environment towards maritime, sheltered conditions implies a multitude of unspecified failure causes. Possible additional stressors are for example corrosion, temperature, maintenance intervals and vibration. The chemical processing industry has developed an approach where failure rates are adjusted with failure mode specific factors.

Table 3.3: Environmental loading adjustment factors for different base failure rate environments. Own calculations after (Mil-Hdbk-217F, 1995, 5.1.1-3 ff). Values rounded to two valid digits.

Field Environment	Factor	Base failure rate environment						
		G_B	G_F	G_M	N_S	N_U	N_{UU}	N_{SB}
		0.38	2.50	4.20	4.00	5.70	6.30	4.00
		Loading adjustment factor matrix						
Ground, benign G_B	0.38	1.00	0.15	0.09	0.10	0.07	0.06	0.10
Ground, fixed G_F	2.50	6.58	1.00	0.60	0.63	0.44	0.40	0.63
Ground, mobile G_M	4.20	11.05	1.68	1.00	1.05	0.74	0.67	1.05
Naval, sheltered N_S	4.00	10.53	1.60	0.95	1.00	0.70	0.63	1.00
Naval, unsheltered N_U	5.70	15.00	2.28	1.36	1.43	1.00	0.90	1.43
Naval, undersea N_{UU}	6.30	16.58	2.52	1.50	1.58	1.11	1.00	1.58
Naval, submarine N_{SB}	4.00	10.53	1.60	0.95	1.00	0.70	0.63	1.00

3.1.3.3 Specific failure modes

The sourced failure rate may also be assessed with regard to the prevailing failure modes. For a specific component the failure causes are identified and subsequently quantified, so that particular failure rate influences can be considered. The prerequisite

to derive cause specific failure rate adjustments is a highly detailed data collection, which specifies the exact failure modes and environmental conditions. Adjustment factors for specific failure modes that have been determined in the processing industry are listed in table 3.4.

Table 3.4: Failure mode specific adjustment factors after Debray *et al.* (2004).

Failure rate influences	Adjustment factors	
	Instruments	Valves
Corrosion	1.07	1.14
Erosion	1.14	1.28
Fouling, plugging	1.07	1.14
Temperature extremes	1.07	1.07
Vibration	1.42	1.21
Corrosive atmosphere	1.21	1.21
Dirty atmosphere	1.07	1.07
High temperature/humidity	1.07	1.07
Exposed to mechanical damage	1.07	1.07
Inaccessible for inspection	1.07	1.07

3.1.4 Uncertainty of failure rates

The term *uncertainty* can be pragmatically defined as a situation where the available quantitative and qualitative information does not suffice to numerically describe, prescribe or predict a system with its behaviour and characteristics (Zimmermann, 2000).

The type of uncertainty is commonly classified as aleatory or epistemic uncertainty (Oberkampf *et al.*, 2004). *Aleatory uncertainty* describes random, irreducible or stochastic uncertainty that characterises the inherent variation of physical systems or the environment under consideration. *Epistemic* uncertainty refers to a reducible, subjective, state of knowledge or model uncertainty describing a lack of knowledge, data or information. The categorisation into either of the above groups implies either a) that the uncertainty can be decreased through additional knowledge (epistemic) or b) it is irreducible (aleatory).

O'Connor (1995, p. 1356) points out that whenever the reliability of a system is predicted, it is essential to identify and account for the uncertainty inherit to these

predictions. This is particularly the case if new components, new materials and different operating environments increase the prediction uncertainty. The main source of failure rate uncertainty for WECs appears to be the lack of knowledge with regard to inadequate or missing experimental and operational data. This manifests itself in the use of generic, rather than device/operation specific reliability failure rate data, which can often not be directly applied. Furthermore the detailed specification of components and sub-systems is generally not publicly available.

Two aspects of epistemic failure rate uncertainty are explored in the following:

- The variation of failure rate levels
- The probability distribution and parameters which depend on the knowledge of failure types and mechanisms.

3.1.4.1 Mean failure rate variation

There are only few studies that compare predicted failure rates with actual field failure rates to give an indication of prediction uncertainties. Cox & Tait (1998, p. 193ff.) report two cases where detailed surveys have been conducted.

In the first study, operational failure rates for a ten year period in a processing plant are compared with previously predicted failure rate levels. The ratio r_F of actual rate to predicted rate is reported to stay largely within $0 < r_F < 4$. The most extreme case of divergence exhibited a factor of $r_F > 1000$. Such large deviations were reasoned through unexpected failure modes that were not considered during the initial analysis. Other discrepancies were mainly caused by maintenance shortfalls (e.g. erroneous replacement, calibration and undetected degradation) and imprecise failure definition for deteriorating components.

The second comparative study (Cox & Tait, 1998) considered failure records for mechanical, electrical and electronic equipment. About 2/3 of the investigated cases did not exceed a factor $r_F = 2$ and almost all cases (93%) did not exceed $r_F = 4$.

A study for electronic components by Smith (2005) suggests to treat predicted failure rates as random variables with confidence intervals. The upper/lower boundaries of a 90% confidence interval of the expected component field failure rate can be calculated by multiplying/dividing the predicted mean failure rate by a factor of 3.5 in the case

of site specific data, a factor of 5 in the case of industry specific data, and a factor of 8 if generic failure rate data is used. This failure rate adjustment is a simplified procedure which is only valid for original data that has not been described statistically. The mean failure rates presented in reliability databases can generally not be adjusted to determine confidence intervals, as the original sample is unknown.

Another approach is proposed by Flinn & Bittencourt (2008) who use uncertainty bands to account for different data source qualities, i.e. to introduce upper and lower boundaries for point estimates. The given values are only preliminary and are subject of further investigation:

- $\pm 10\%$ for site and industry specific data
- $\pm 30\%$ for generic data sources
- $\pm 50\%$ for failure rates derived by expert judgment

An incomplete analysis where potential failure modes are overlooked can have serious impact, as this source of uncertainty is not considered in probabilistic risk assessments (Cox & Baybutt, 1981). This risk can only be reduced through quality control of the analysis together with dedicated research and testing programs.

In most engineering disciplines (in)accuracies of a factor of 10 are not acceptable. However, it may be deemed as a reasonable accuracy in the realm of probabilistic reliability assessments. As an example, a failure rate data bank, set up by the International Energy Agency (Cadwallader, 2001), compares equipment and instrumentation failure rates between different fusion test reactors. It classifies values that agree within a factor of 3 as "good", within a factor of 10 as "fair" and values that differ by more than a factor of 10 as "poor" comparison. Similarly, Zio (2009, p.314) applies variations up to a factor of 10 in a failure rate uncertainty analysis.

Two implications may be drawn from the above cases:

1. One of the main objectives during the development phase should be to reveal all likely, and possibly unknown failure modes. This is particularly the case for

components that are established in other industries/environments but may be subject to new failure modes if deployed in a MEC.

2. When the critical failure modes are established and quantified, the described studies exhibit failure rate variability factor of up to four when all failure modes are identified. Yet, failure rate data that agrees within a factor of 10 might be considered as sufficient for probabilistic calculations.

3.1.4.2 Failure rate distribution

The initial assumption in most reliability assessments is a constant failure rate, modelled by an exponential distribution, which only covers the 'bottom-part' of the bathtub curve (see figure 2.2, p. 50). This assumption is also made for the initial reliability assessment and results presented in section 3.2.7.2. A constant failure rate implies that the failure mechanism is time-independent. This is arguably not the case for failure mechanisms like fatigue, wear and corrosion (Wolfram, 2006). The Weibull distribution, introduced in section 2.1.3.2, equation 2.18 allows to model the system reliability for different types of failure rate behaviour.

In principle, three different types of failure rate behaviour occur, which are represented by the Bathtub curve (see section 2.1.2.2, figure 2.2).

1. Early failures with decreasing failure rate over time ($\alpha < 1$)
2. Random failures during the useful life of the system, showing constant failure rates ($\alpha = 1$)
3. Wear-out failures or ageing failures exhibiting increasing failure rates over time ($\alpha > 1$)

3.2 Case study: Notional hydraulic wave energy converter

The methodology outlined in section 3.1 is in the following applied to a case study. The objective is to assess the reliability of a wave energy converter in order to identify potentially critical components and derive a reliability estimate. An analysis using Reliability Block Diagrams was chosen as it offers a good visual representation of the system, making the analysis accessible and comprehensible. Furthermore, it must be

noted that such an analysis is deterministic and does not take account of individual occurring incidents. This is considered acceptable as the detailed information required for a state-space model could not be obtained.

The applied approach is based on the assumption of independent failures with constant failure rates. The source and type of failure rate information are assessed and adjusted accordingly. The case study investigates the reliability of a floating hydraulic wave energy converter as sufficiently detailed technical information (see section 2.2.6) could be obtained for this type of device.

3.2.1 Reliability data and adjustment

The data used for the following reliability assessment is collected from various sources and databases, given in table 3.1, page 96. An already existing embryonic database compiled by Dorrell (2004) was extended and failure rate adjustments accounting for data sources, environmental loading conditions and failure modes were used. The adjustment of the base failure rate λ_B in order to estimate the failure rate of the component λ_C follows three consecutive steps (see also equation 3.2):

1. Sourcing of base failure rate data λ_B and additional information
2. Choice and application of environmental factor π_E
3. Application of specific failure mode factor π_{FM}, if applicable

$$\lambda_C = \lambda_B \cdot \pi_E \cdot \pi_{FM} \tag{3.2}$$

During the adjustment a double consideration of stressors is likely to occur, but intended. As an example, the environmental factor for a marine environment already implies the failure mode of corrosion. In the case of a component, that is particular susceptible to corrosion this can be accounted by an additional failure mode factor. Consequently, the adjustment of failure rates is always subject to interpretation and judgement of the analyst. Where double consideration of stressors occurs, the resulting failure rates tend to be more pessimistic.

A detailed example for the adjustment procedure is demonstrated for a hydraulic cylinder:

1. The base failure rate λ_B for a hydraulic cylinder is sourced from AME (1992) and is given as $\lambda_{B,\ hydraulic\ Cylinder} = 0.087/a$, where 1/a denotes per annum. In this case the failure mode, rating and the number of observed items are not specified. Thus, it is classed as a generic mean failure rate.

2. The given base failure rate is generic, but from a marine application so no environmental factor is applied.

3. As the system application (frequent, cyclic operation under medium-low loads) of the cylinder is contrary to its usual application (few high load applications with longer no-use periods) the application of an additional failure mode factor due to wear and fatigue seems appropriate. The altered cylinder operation and the occurring loads were simulated in a component test of the Pelamis power take-off module (Yemm, 2003), but the actual results are not publicly available. Alternatively, Green & Bourne (1978) have suggested factors to account for different loading capacities. If the application is considered as a more extreme loading, a factor $\pi_{FM} = 2$ can be used, representing 120% capacity loading. This results in the following component failure rate for the hydraulic cylinder:

$$\lambda_{c,\ hydr.\ Cylinder} = \lambda_{B,\ hydr.\ Cylinder} \cdot \pi_{FM} = 0.087/a \cdot 2 = 0.174/a \tag{3.3}$$

This crude adaptation of often generic data leads to reliability estimates that should be regarded as an indication, rather than exact values. Nevertheless, the failure rate adjustment considers the degree of information that is available and should allow an identification of those components tending to exhibit high failure rates or high degrees of uncertainty. This can be due to the fact, that the components are either not commonly employed in the marine environment and only generic data exists or that they are subjected to particular harsh environmental/operational conditions.

3.2.2 System Block Diagram

As stated earlier, the illustrative hydraulic wave energy converter comprises the following four sub-systems:

- Mooring: Assuming a slack-moored device.
- Structure: A thin-walled 20mm steel structure is assumed for the main structure.

- Power take-off system: This subsystem comprises a hydraulic system with a total of six parallel units to provide redundancy.
- Power transmission: This consists of power transformation within the device and transmission to shore via subsea cable.

Mooring, Structure and Power transmission are assumed to operate in series (figure 3.2), i.e. if one of these sub-systems fail, the converter is not able to produce electricity. The power take-off comprises six independent hydraulic cycles which are configured in parallel. Thus, power production is maintained at reduced level if one or more of the hydraulic units fail.

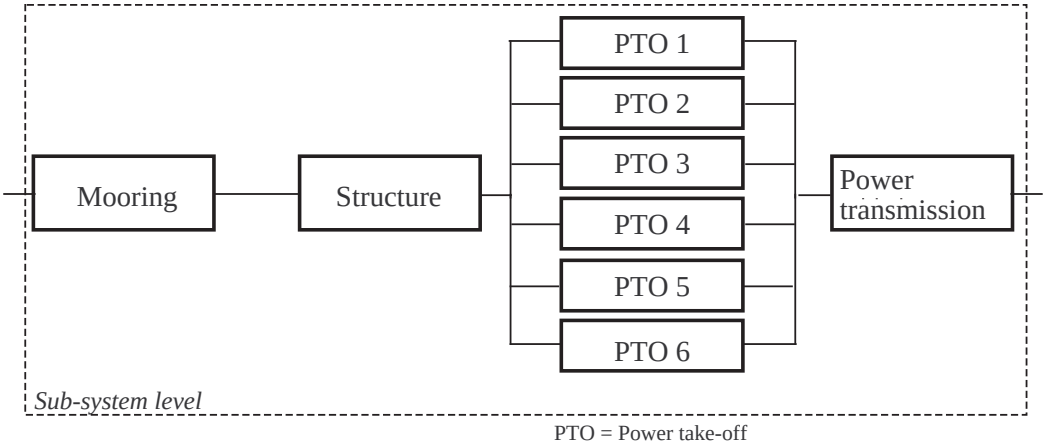

Figure 3.2: Wave energy converter sub-system reliability block diagram.

Each of the sub-systems is dissected further into components and parts. At this level, commercially available components are considered. For example a generator is regarded as single component, even though it consists of several other parts and can be regarded as a system on its own. The level of detail is therefore chosen due to practical necessity, as failure rates are usually given for particular components/sub-assemblies.

3.2.3 Mooring

The mooring of the converter will not only depend on the type of device and the design chosen but will be site-specific to account e.g. for different soil and current characteristics of the installation site. Without going into the details of a particular mooring

design, on a generic component level three required components can be identified; the anchor to hold the mooring in position, the mooring cable (or chain/rope) and the attachment to the device. No representative failure rates could be found for those single components, thus the mooring sub-system is modelled as in-series RBD system of individual mooring lines. A typical mooring configuration is a three-leg mooring setup which is shown as RBD in figure 3.3.

Figure 3.3: Mooring sub-system reliability block diagram.

The failure rate information is sourced from incidents and mooring failures that have been continuously monitored for Floating Production Systems (FPS) in the offshore oil and gas industry. FPS are used to receive, process and store crude oil at offshore production wells in deep water. Most of these vessels are moored to a central turret within the hull (Oil and Gas UK, 2009). This allows the FPS to rotate freely around the point of mooring to direct the bow into the prevailing wave, current or wind direction in order to minimise loadings, a design which is also found for some floating wave energy devices.

A report issued by the Health and Safety Executive (HSE) states that a failure of FPS mooring systems in the North Sea occurred once every 5.4 years in the period from 1980-1998 and once every 8.8 operating years considering the period from 1980-2001 (Noble Denton, 2006, p.175). This equals to failure rates of $\lambda_{Mooring\ FPS,\ 1998} = 0.185/a$ for the former figure and $\lambda_{Mooring\ FPS,\ 2001} = 0.114/a$ for the more recent report.

There are significant differences in mooring designs for WECs. The required safety factor is higher in the oil industry due to the potential loss of life and risk of large environmental pollution as consequence of failure (Harris *et al.*, 2004). These risks are not apparent for unmanned WEC, so the safety factors could be reduced but could result in higher failure rates. Thus, the stated mooring failure rate is likely to be a lower bound for WECs. Beyond the requirement of safe station keeping, which is the main concern for conventional floating offshore systems, the mooring system of a WEC

influences the device motion and response to wave action and thus can have a direct impact on the energy extraction efficiency (Johanning *et al.*, 2007).

As these differences are difficult to quantify in terms of failure rates at this stage, this assessment applies the more conservative failure rate of $\lambda_{C\ Mooring} = 0.185/a$ at sub-system level. If further three mooring assemblies are assumed for the entire mooring system the failure rate can be calculated as the sum of the individual mooring lines (equations 3.4).

$$\lambda_{Mooring} = \sum (\lambda_{C,\ Mooring}) = 0.555/a \tag{3.4}$$

3.2.4 Structure

The structural sub-system can be regarded as in-series configuration of hull, connection joints and seals. The seals protect the hydraulic cylinders which transfer the wave motion onto the hydraulic system. Assuming that three power modules are connected accordingly to adjacent steel tubes, requires a total of six connection joints. The steel wall of the power modules and the steel tubes can be considered as hull. The simplified RBD of the structural sub-system is shown in figure 3.4.

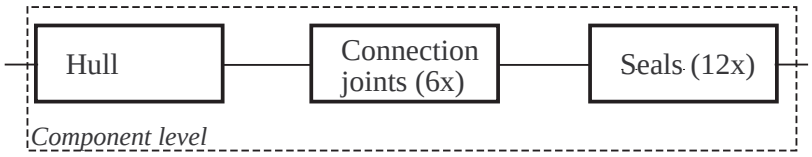

Figure 3.4: Structure component reliability block diagram.

3.2.4.1 Structural hull

No structural failure rate could be found in the consulted databases as the structure is highly device and wave-load dependent. Accident and failure rate information is available for Aframax tankers (Papanikolaou & Eliopoulou, 2006). Assuming the comparability of single hulled oil tankers and the structural housing of the WEC, an indication of expected failure rates can be established. The average structural failure rate which satisfies the constant failure rate assumption is calculated as $\lambda_{SF\ Aframax} = 0.011/a$. Due to the smaller area and the less corrosive internal environment in case of a WEC the applied failure rate is decreased by an order of magnitude. Hence, the non-accidental

structural failure rate is estimated at $\lambda_{Hull} = \lambda_{SF\ Aframax} \cdot 0.1 = 0.001/a$.

3.2.4.2 Connection joints

It is difficult to estimate the failure rate of joints, as hardly any information is available on the detailed design and on expected loads. An approximation is obtained through the mechanical linkage failure rate that has been estimated for the Circular Sea Clam, a WEC proposed in 1978 (AME, 1992). The device consisted of 12 circular connected steel tubes with attached flexible air bags as PTO mechanism. The failure rate of the mechanical linkage is already factored for an unprotected shipboard environment and given as $\lambda_{Joint,\ SC} = 0.63/a$. Assuming only six connections for the illustrative device, the suitable fraction of $\lambda_{C,\ Joints} = \lambda_{Joint,\ SC} \cdot 0.5 = 0.315/a$, is used as failure rate for the joint connections.

It must be mentioned, that the used base failure rate is certainly specific to the Sea Clam device. Therefore, it carries a large degree of epistemic uncertainty. This example highlights the dilemma for reliability analyses when bespoke designs, scarce information and uncertain loadings occur in combination, as it is more often than not the case for WECs.

3.2.4.3 Seals

A generic failure rate is available for rolling rubber seals $\lambda_{B,\ Seal} = 0.0364/a$ (AME, 1992). It is already adjusted for marine use, but the inverse application of rams with significantly higher cycle frequency is not accounted for, so an additional capacity factor $\pi_{Capacity} = 2$ is applied resulting in:

$\lambda_{C,\ Seal} = \lambda_{B,\ Seal} \cdot \pi_{Capacity} = 0.07/a$. For the entire structural subsystem this yields:

$$\lambda_{Structure} = \lambda_{Hull} + \lambda_{Joints} + 12 \cdot \lambda_{C,\ Seal} = 1.19/a \tag{3.5}$$

3.2.5 Power take-off system

A number of proposed converter designs utilise hydraulic power take-off (PTO) systems. The main components of such a hydraulic system are described to a sufficient level of

detail by Yemm (2003). The named system components are used as a basis for this case study. The hydraulic sub-system consist of hydraulic cylinders, manifold, accumulator, hydraulic motor and electric generator. A generic in-series configuration is shown in figure 3.5.

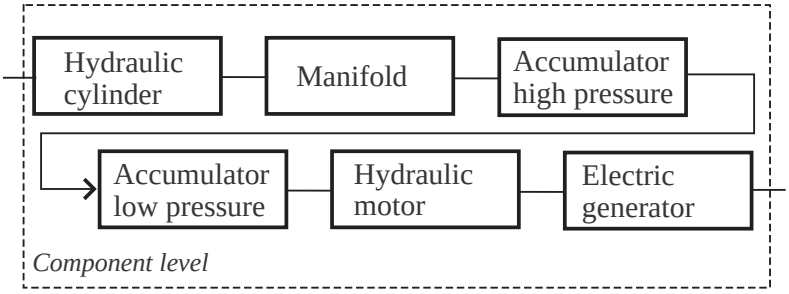

Figure 3.5: Hydraulic power take-off component reliability block diagram.

Industry specific and generic failure rates could be obtained for all components. Table 3.5 lists the base failure rates, data source, respective adjustment factors and resulting failure rates for the modelled PTO. Each hydraulic unit is modelled as series of components, hence the failure rate for each PTO unit is calculated as sum of the adjusted component failure rates (equation 3.6).

$$\lambda_{PTO} = \sum (\lambda_{C,\ PTO}) = 2.42/a \tag{3.6}$$

3.2.6 Power transmission

The power transmission system is modelled as a series configuration of five main components. As shown earlier in figure 3.1 it comprises busbar, transformer, circuit breaker, umbilical cable and sea cable.

The 415 V busbar, interconnects the power modules to the transformer. An environmental factor of $\pi_E = 2.3$ is applied to the base failure rate to account for the less sheltered environment in a naval unsheltered instead of a ground benign environment.

The failure rates for transformer and circuit breaker have been obtained from SINTEF (2002), an industry-specific database. The individual failure rates are adjusted by a factor of $\pi_E = 1.4$, as they are not installed on a stable platform but on a floating device.

Table 3.5: Power take-off sub-system, component failure rates and adjustment.

Component	Base failure rate λ_B [1/a]	Source	Adjusting factor π	Component failure rate λ_C [1/a]
Hydraulic cylinder	0.087	AME, 1992	2.8	0.24
	Adjustment higher pressure $\pi_C = 2$; marine unsheltered, $\pi_E = 1.4$			
Manifold	0.002	AME, 1992	2	0.004
	Adjusted for higher working pressure, $\pi_C = 2$			
Accumulator high/low p	0.263	FARADIP, 2006	1.6	0.42
	Mean value adjusted for naval sheltered environment, $\pi_E = 1.6$			
Hydraulic motor	0.107	FARADIP, 2006	1.6	0.17
	Geometric mean, adjusted for naval sheltered environment, $\pi_E = 1.6$			
Electric generator	1.588	OREDA, 2002	1	1.59
	Critical failure, mean value, not adjusted			

Table 3.6: Power transmission sub-system, component failure rates and adjustment.

Component	Base failure rate λ_B [1/a]	Source	Adjusting factor π	Component failure rate λ_C [1/a]
415V busbar	0.004	YARD, 1980	2.3	0.01
	Adjusted for marine unsheltered, $\pi_E = 2.3$			
Transformer	0.053	OREDA, 2002	1.4	0.07
	Voltage: 441V - 5.5/6.6kV, adjusted for naval unsheltered, $\pi_E = 1.40$			
Circuit breaker	0.184	OREDA, 2002	1.4	0.26
	Voltage: 441V - 5.5/6.6kV Adjusted for naval unsheltered $\pi_E = 1.4$			
Umbilical	0.037	AME, 1992	1	0.04
	Dynamic umbilical			
Sea cable	0.15	AME, 1992	0.6	0.09
	400kV, failure per 10km length, adjusted for lower capacity $\pi_C = 0.6$			

The failure rate for the umbilical cable is sourced from AME (1992) and is given as 0.04 failures/year.

The specific failure rate for the sea cable (per 10 km cable length) is reduced by $\pi_C = 0.6$, as the given capacity (400 kV) is not reached in this application with only 11kV voltage level. Table 3.6 summarises the component failure rates for the power transmission system. The resulting failure rate for power transmission sub-system is calculated as:

$$\lambda_{Power\ transmission} = \sum (\lambda_{C,\ Power\ transmission}) = 0.47/a \tag{3.7}$$

3.2.7 System reliability

So far, the analysis was aimed at the estimation of failure rates. As a next step it is necessary to establish the reliability values which account for the system configuration in order to describe the system behaviour and to identify critical components and sub-systems.

3.2.7.1 Reliability calculation

The WEC system is modelled as a combination of series and parallel components as shown in figure 3.2. The calculations are performed based on the assumptions that:

- failures are independent,
- failure rate probability functions follow an exponential distribution, i.e. a constant failure rate with time is assumed for the model,
- there is no intervention/repair in the event of failures,
- the reliability is modelled for one year of continuous deployment.

The constant failure rate assumption follows the underlying assumption of most databases. It is further supposed that the system is not repaired within a 12 month period because few to limited data and experience exists on the necessary repair and access times which are highly site- and resource dependant. Furthermore, one year is generally regarded as the shortest practical maintenance interval (Wolfram, 2006, p. 65). This time period schedules device access during larger weather windows in

summer. Consequently, in the absence of remote interventions, the 12 month period can be considered as the yardstick for system reliability.

The reliability for each sub-system follows the exponential distribution (equation 3.8) with failure rate λ and time t.

$$R(t) = e^{-\lambda t} \tag{3.8}$$

In case of the six parallel PTO units the calculation needs to account for the number of active units to determine the reliability values for all possible generating capacities between 'm out of n' hydraulic units. The PTO fails if less units than specified are operational. The probability $F(t)$ that the PTO fails until time t can be calculated as the binomial cdf (O'Connor, 2008).

$$F_{PTO}(t) = Pr(T < t) = \sum_{i=0}^{m-1} \binom{n}{i} R^i \left(1 - R\right)^{n-i} \tag{3.9}$$

Thus the reliability R(t) follows as:

$$R_{PTO} = 1 - \sum_{i=0}^{m-1} \binom{n}{i} R^i \left(1 - R\right)^{n-i} \tag{3.10}$$

Once all sub-system reliabilities are computed, the system reliability R_{System} is the product of the respective reliabilities of the in-series blocks:

$$R_{System} = \prod_{i=1}^{n} R_i \tag{3.11}$$

3.2.7.2 Reliability plots

The results of the above reliability calculations are presented in three subsequent reliability plots.

- Comparison of sub-system reliabilities (figure 3.6)
- Comparison of different PTO configurations (figure 3.7)
- Reliability of overall system (figure 3.8)

To begin with, the reliability estimates of the different sub-systems in figure 3.6, the power transmission and the mooring sub-system exhibit the highest reliability values after one year of operating time $R(8760) \approx 0.6$. The structure- and hydraulic power take-off sub-system indicate significantly lower levels of reliability $R(8760) < 0.3$ after 12 months.

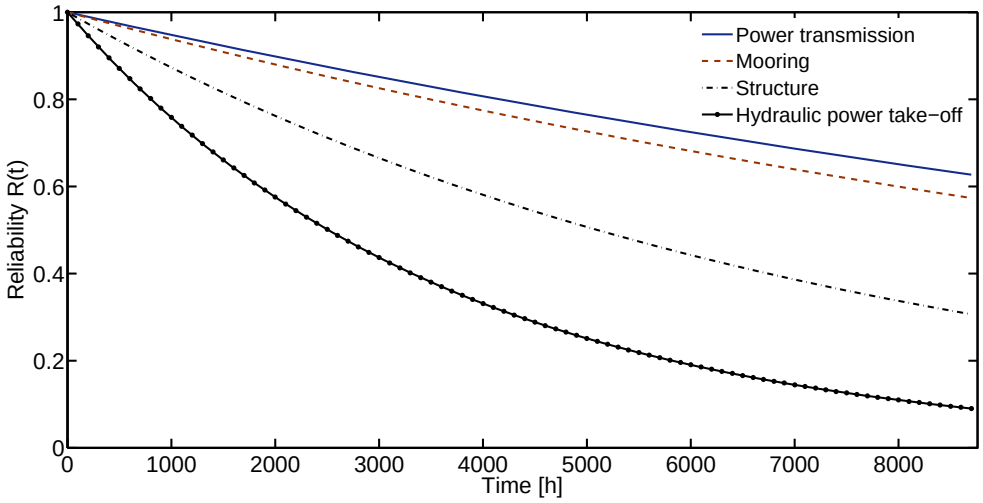

Figure 3.6: Sub-system reliability.

In particular the hydraulic PTO (considering a single hydraulic cycle) exhibits a low reliability under the assumptions and data used. Yet, the WEC system can maintain electricity production if a PTO unit fails, as all six PTO units are in a parallel configuration which increases the reliability of the PTO sub-system. However, no unit is redundant in a strict sense as a failure of one unit has the consequence of reduced power output for the overall system.

The reliability for different power production requirements is shown in figure 3.7. If a reduced power output of 1 out of 6 ('1oo6') units is accepted the reliability after one year of operation is $R_{PTO,1oo6}(8,760) > 0.4$. If at least three PTO units shall be operational, this is only the case up to 3,500 operational hours, i.e. $R_{PTO,3oo6}(3,500) > 0.4$. The reliability for a full power output, i.e. all six PTO shall be operational, decreases quickly and is only 0.03 after 2,000 operational hours.

Following the formulae stated in table 2.3, the system reliability for an in-series configuration is determined through the multiplication of the individual sub-system

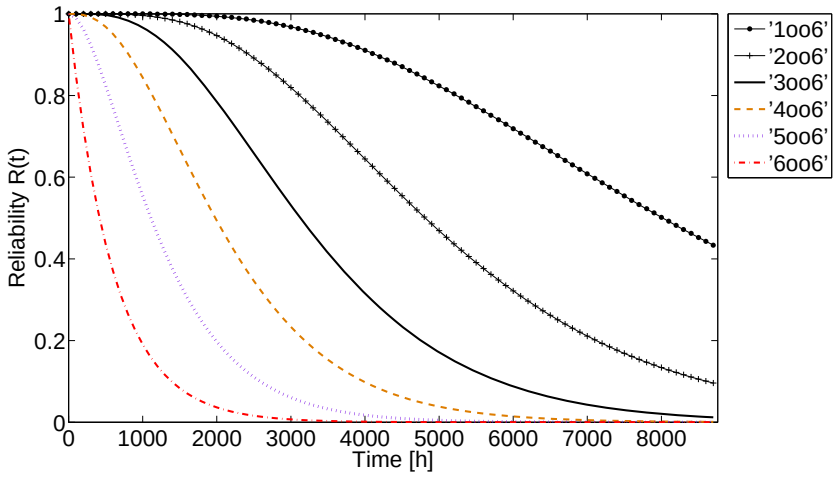

Figure 3.7: Reliability of hydraulic power take-off sub-system for different configurations.

reliabilities. The reliability plot of the overall system is depicted in figure 3.8. It also shows how a reduced power requirement increases the reliability of the overall system through the redundancy of the PTO units. After 3,000 hours, the reliability for different generating capacities is as follows:

$$R_{Sys,1oo6}(3,000) = 0.43;\ R_{Sys,4oo6}(3,000) = 0.05;\ R_{Sys,6oo6}(3,000) = 0.001.$$

One aspect of criticism which is raised with regard to reliability predictions are the large uncertainties of failure rates. In the presented analysis this is reflected by the rather crude adjustments and subjective judgement of failure rates. Yet, the uncertainties are not made explicit. Therefore, the likely extent of failure rate uncertainty and the potential impacts this may have on the system reliability estimates are investigated in the following section.

3.2.8 Modelling failure rate uncertainty

One method to account for the inherit variability of component failure rates is to model the uncertainty by failure rate probability distribution functions. Compared to simple point estimates, the degree of uncertainty is reflected in the system reliability calculations (Zafiropoulos & Dialynas, 2004).

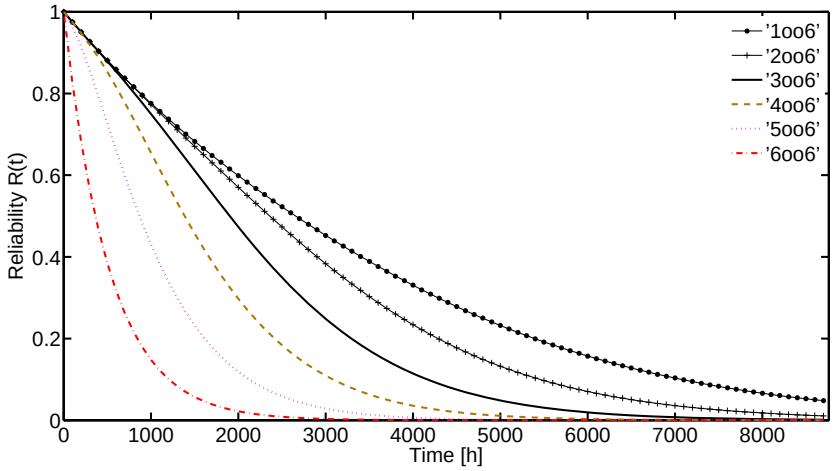

Figure 3.8: System reliability.

The model that is proposed here aims to extend the Reliability Block Diagram presented in section 3.2.2 by making the uncertainties of the underlying failure rates explicit with regard to i) failure rate level and ii) failure rate behaviour, as described in section 3.1.4.

3.2.8.1 Model parameters

The sub-system reliabilities are assumed to follow a two-parameter Weibull distribution with the failure rate λ as scale parameter and α as the shape parameter (equation 3.12). The location parameter Θ from the 3 parameter Weibull distribution (compare equation 2.18, p. 54) which guarantees a minimum failure free time is simply $\Theta = 0$. The values for λ are adopted from the mean failure rates λ_{Mean} from the presented case study.

$$R(t) = e^{-(\lambda t)^{\alpha}} \tag{3.12}$$

In order to estimate the effect of lack of knowledge of the exact failure rates the analysis is undertaken for higher and lower bounds. A lower (λ_{Lower}) bound is defined as $\lambda_{Mean} \cdot 0.5$ and the upper failure rate (λ_{Upper}) is calculated as $\lambda_{Mean} \cdot 2$ (Cox & Tait, 1998). The effect of different failure rate *behaviours* is modelled with the Weibull

shape parameters α. The values are based on experience with wind turbine failures (Stiesdal & Madsen, 2005) where early failures are modelled by $\alpha_1 = 0.5$; the useful life (constant failure rate) is modelled with $\alpha_2 = 1$ and wear-out failures use $\alpha_3 = 3$. The failure rate parameters are summarised in table 3.7.

Table 3.7: Summary of failure rate parameters.

Failure level				
Sub-system	Mooring	Structure	Power take-off	Transmission
$\lambda_{Mean}\,[1/a]$	0.56	1.19	2.42	0.47
Failure behaviour (Stiesdal & Madsen, 2005)				
Type	Early	Constant	Wear-out	
α	0.5	1.0	3.0	

A reliability model has been implemented to demonstrate the effect of the stated uncertainties on system reliability for three cases:

- Case 1 - Uncertain failure rate level. The different failure rate levels are propagated through the model while the failure rate with time is constant, i.e. $\alpha = 1$.
- Case 2 - Uncertain failure rate behaviour. While the failure rate level is assumed to be at the mean level the system reliability is computed for different shape parameters α.
- Case 3 - Combined effect of failure rate level variation and failure rate behaviour variability.

3.2.8.2 Model results

The system reliabilities for the failure rate *levels* are shown in figure 3.9. The reliability (survivor) function R(t) describes the probability that the system does not fail (i.e. survive) in the given time interval (here 1 year). The uncertainty that is introduced through moderately different failure rate levels leads to a considerable range of possible system reliability. For example at $Time = 2,000h$ a spread of 0.5 is present which will be presented in the following as $\Delta R(2,000h) = 0.5$. The spread decreases to $\Delta R(4,000h) = 0.35$ and to $\Delta R(6,000h) = 0.2$.

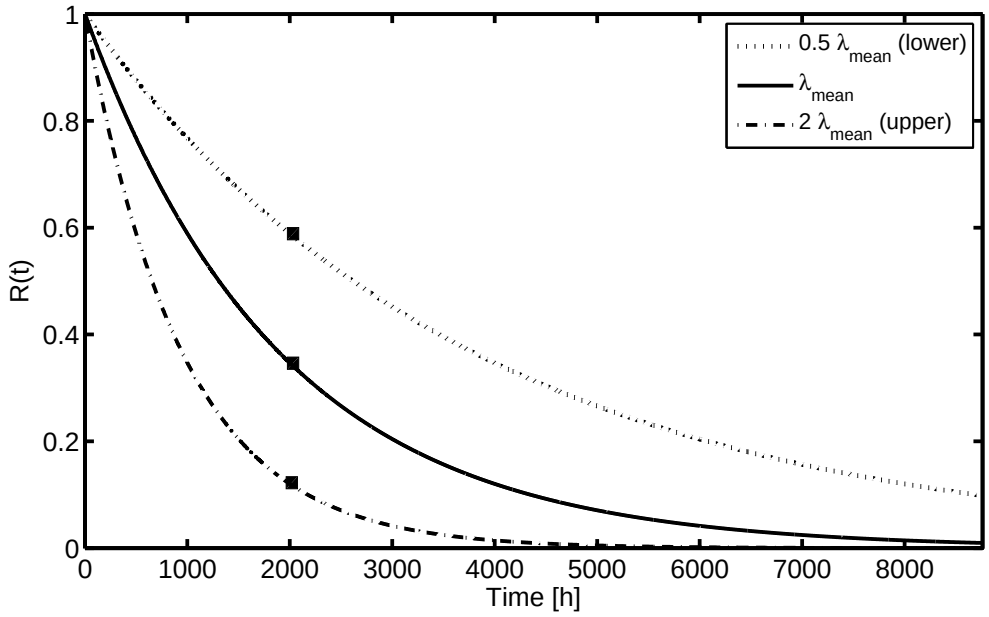

Figure 3.9: Case 1 - System reliability of in-series subsystems for different failure rate levels (λ).

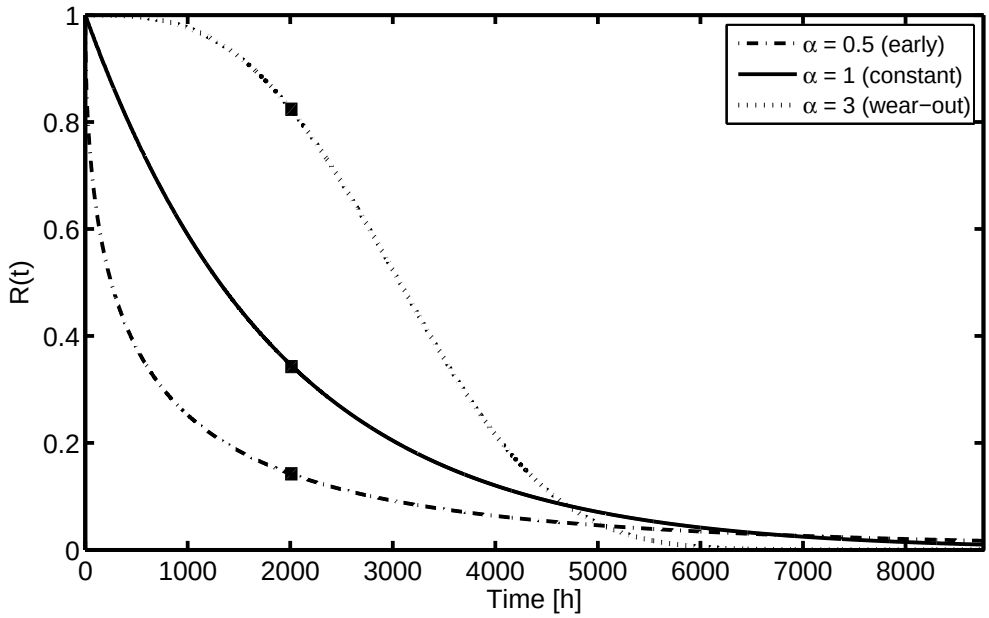

Figure 3.10: Case 2 - System reliability of in-series subsystems for different failure rate behaviour parameters (α).

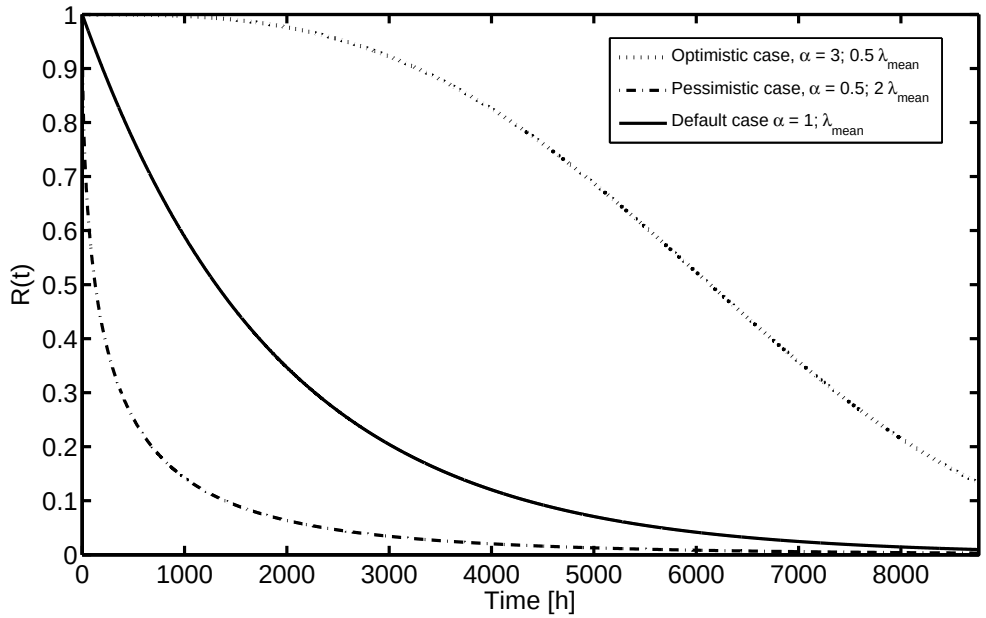

Figure 3.11: Case 3 - System reliability of in-series subsystems for optimistic, constant mean failure rate and pessimistic case.

The system reliability for different failure rate *behaviours* (figure 3.10) exhibits a larger divergence at the beginning with $\Delta R(2,000h) = 0.7$ and decreases soon with $\Delta R(4,000h) = 0.15$.

The different failure levels and behaviours have been further combined to an optimistic and pessimistic scenario (case 3). The optimistic setting which may be advocated by device developers, assumes the lower bound of the mean failure rate and wear-out failures. The pessimistic setting, possibly used by insurance companies assumes the higher mean failure rate level and early failure behaviour as input. The resulting system reliabilities are shown in figure 3.11. Considering the variation across the full time range, it is not easy to make a statement about the realistic reliability of the system. As a consequence of these variations, a simple constant failure rate assumption may significantly over- or underestimate the system reliability. Therefore, a reliability assessment that is based on generic data with a constant failure rate assumption clearly is not robust, as it does not include considerations of existing variations in the failure rate level and behaviour.

3.3 Discussion of results

In the first instance, the results for the system reliability presented in section 3.2.7 are validated through the actual system design of the converter. The power take-off is being identified as the least reliable individual sub-system. Thus, a redundancy of this sub-system leads to an improvement in the overall system reliability. This redundancy is certainly the case in the hydraulic power take-off design which was used for the presented case study. Each power module has two individual, independent hydraulic cycles and with a total of three power modules, the redundancy level is increased to a total of six parallel units.

The absolute reliability values of the sub-systems and consequently the overall system are low, i.e. significantly lower than $R(8,760h) = 0.5$ and would hardly be acceptable for a commercial device. These very conservative values are attributed to two main reasons:

- The available failure rates are rather pessimistic and largely stem from dated sources.
- The adjustment of failure rates has been conservative throughout the analysis.

Moreover, for some failures, e.g. seal leakage, the device could stay operational for additional hours without repair. Nevertheless, these kinds of failures were included, as they make repair activities necessary. Thus, the displayed values could be termed as 'theoretical reliability levels'. The 'practical reliability' would be significantly higher, as e.g. minor failures are accumulated until repair activities are planned. These theoretical reliability values underline the need for high quality information, the investigation and improvement of high failure sub-systems and the benefits of redundant configuration to establish high reliability without instantaneous intervention.

The comparison of the sub-systems shows that in particular the device structure and the power module exhibit low reliability values. This illustrates how even the application of "crude" data can be used to identify those areas where component reliability would need to be improved, or better failure rate estimates are required.

The presented results shed also light on a fundamental question that has to be answered during the design process. The designer has to find a balance between the reliability level of the individual components and the amount of redundancy in the system configuration. There are two strategies:

- Relying on highly reliable components that require only a low degree of redundancy, i.e. aiming for in-series configuration.
- Accepting less reliable components with increased redundancy, i.e. aiming for parallel configuration.

Many applications in the oil and gas industry combine these two possibilities, in that highly reliable components are employed in a redundant configuration. As an example, the mooring design often allows for significant redundancy, so in case of a mooring line failure the remaining mooring lines still have the capacity to withstand the expected loads (Choi *et al.*, 2006). While such an approach to employ highly reliable components in a redundant configuration is desirable in safety critical applications it considerably increases the capital cost of the system. For wave energy converters this will only be possible for early prototypes, but not for commercial installations. A practicable approach may be to employ an increased degree of component reliability and reliability (i.e. increased safety factors) for the first devices to gather not only operational experience but also to reduce the uncertainties regarding environmental loads and occurring component failure rates. Subsequently the design could be further developed towards a lean but robust configuration.

If the potential failure rate uncertainties are considered in the reliability prediction, a large range of values is possible. In particular figure 3.11 displays the uncertainty with which the calculated reliability estimates are fraught. However, the depicted uncertainties may be regarded as the accumulated uncertainties across the 'life' of a MEC. In this respect, the 'early failure' regime is most applicable for the first couple of years when the device enters operational service. Following the empirical experience expressed through the bathtub curve, the constant failure regime would be applicable during the 'useful life'. Finally, as soon as degradation becomes the governing failure mechanism, the device enters the 'wear-out' failure rate regime with increasing hazard rate. Hence the cases presented with $\alpha = 3$ would apply to the late stage in the

operational life of the device, while the case with $\alpha = 0.5$ relates to the reliability that might be expected in during the initial first years.

Yet, the challenge is to attribute a time or a number of load cycles to each of these phases. This would allow a more detailed description of the device reliability. This however is not attainable with the reliability information contained in the underlying data basis where a simple constant failure rate is the default case. Detailed load and failure data of individual device failures would be necessary to develop a suitable failure distribution model for the different life stages.

All in all, the reliability information that could be ascertained from a detailed survey of literature and data base sources is not sufficient to conduct a robust and meaningful reliability assessment for marine energy converters. Even an informative comparison of device reliabilities which focuses on the relative reliability between devices, as it has been attempted by Delorm *et al.* (2011) for different tidal turbine designs, is questionable. The outcomes are largely biased through the initial assumptions such as operational environment and the underlying data that is chosen. Furthermore, in the case of wave energy converters, the specific design and system configuration is in most cases not in the public domain.

Following these considerations it is concluded for this thesis, that the marine renewable energy sector is at such an early stage, that much improved reliability information is required to robustly quantify the system reliability. This in turn is needed to be able to inform the design and to subsequently be able to improve the device reliability. Thus the research question is specified as:

"How to advance the reliability information for wave energy converters?"

The subsequent chapters explore and apply the following methods that have the potential to improve the reliability information of wave energy converters:

- a Bayesian statistical framework,
- experimental and numerical load investigations
- and service simulation testing.

Chapter 4

Bayesian statistical framework

> "*Given* the number of times in which an unknown event has happened and failed: *Required* the chance that the probability of its happening in a single trial lies somewhere between any two degrees of probability that can be named." Bayes, 1763 after (Barnard & Bayes, 1958)

There are two distinct frameworks of statistical data analysis i) the classical, frequentist approach and ii) the Bayesian approach. Both approaches are being applied to reliability applications, although the classical analysis dominates the literature and is more widely applied (Tobias, 2006).

Classical frequentist approach The conventional statistical method is to restrict the information for the analysis to a relevant set of data that has been obtained. The reliability parameters are considered as fixed (i.e. a true value exists, but is unknown), while the data constitutes sample points of the population. The derived parameter estimates are usually stated in conjunction with confidence intervals.

Bayesian approach This method makes use of all prior information and knowledge to establish the so-called *prior distribution* of the reliability parameters. The current, obtained data is then used to adjust the earlier distribution, which leads to the so-called *posterior distribution*. The fundamental difference between the classical and the Bayesian approach lies in the treatment of the parameters as the Bayesian methodology treats the reliability parameters as random variables.

The above explanation outlines the characteristics of the two approaches but does not highlight the reasoning for or against a particular approach. Weise & Wöger (1992) give a pointed rationale to when the Bayesian approach should be chosen:

> "Conventional statistics fail in cases when observable information cannot be gained. (...) By understanding probability as a numerical description of the state of incomplete knowledge based on any kind of rational relevant information available, Bayesian statistics offer a probability statement for the actual unknown non-random value of a quantity."

Classical statistical methods for reliability analysis require actual operating or experimental test data from components which are difficult to obtain for the marine renewable energy case. This is partly due to a lack of operating experience and partly due to intellectual property issues in a competitive market. In such a setting, Bayesian methods allow the analyst to combine available operating data with supplementary information, likely to inform a reliability analysis. Such additional information could come from previous tests, operating data of similar equipment/ in different environments, expert judgement and other sources. Hence, there are good reasons to advocate the use of Bayesian statistics for the assessment of MECs, the most prominent being the capability to treat scarce data.

In the following, the Bayesian approach is briefly outlined and compared to the classical statistical approach. The two approaches are based on fundamentally different assumptions with regard to notions of probability, interpretation of estimates and availability of data that need to be considered to reason the decision for one or the other approach.

4.1 Bayes' theorem

The statistical Bayesian model consists of two parts (Hamada *et al.*, 2008, p.15), i) the prior information and ii) the likelihood function. The prior distribution expresses the knowledge about the parameters of interest before any experimental data has been obtained/analysed. The likelihood function describes the data that has been obtained form a test/experiment, usually this is derived from the sampling distribution of test results. Both elements, prior distribution and likelihood function are then combined

to compute the posterior distribution. This resulting distribution describes the uncertainty (degree of belief) of the parameter after the test data has been considered.

Bayes' theorem is central to the application of Bayesian probability methods. It relates the probability that the event or hypothesis (H_k) is true given the data/events (D) to the probability of the data if the hypothesis was true ($\Pr(D \mid H_k)$). Mathematically this is generally stated as (comp. e.g. Rausand & Høyland, 2004, p.540):

$$\Pr(H_k|D) = \frac{\Pr(D \mid H_k)\Pr(H_k)}{\sum_{i=1}^{\infty}(\Pr(D \mid H_i)\Pr(H_i))} \tag{4.1}$$

With $H_1, H_2, ..., H_n$ as mutually exclusive and exhaustive events, stemming from a sample space S with $Pr\left(\cup_{i=1}^{\infty} H_i\right) = 1$; $H_i \cap H_k = \varnothing$ for i $\neq$ k; $\Pr(H_i) > 0$ for each i; and D as an event in S with $\Pr(D) > 0$.

A qualitative statement of this theorem in the discrete case is:

$$Posterior\ probability = \frac{(Likelihood) * (Prior\ probability)}{\sum((Likelihood) * (Prior\ probability))} \tag{4.2}$$

Or if the theorem is expressed in form of probability density functions with regard to the failure rate λ it can be rewritten as:

$$g(\lambda \mid x) = \frac{f(x \mid \lambda)\ g(\lambda)}{\int_0^{\infty} f(x \mid \lambda)\ g(\lambda)\mathrm{d}\lambda} \tag{4.3}$$

Where $g(\lambda \mid x)$ is the posterior distribution for λ given the recorded data x, $g(\lambda)$ is the prior distribution of the failure rate λ and $f(x \mid \lambda)$ is the likelihood function for the observed data x given the unknown failure rate λ.

In summary, the *prior* probability represents the state of knowledge about the failure rate, before any current/recent data has been analysed. The *likelihood* probability describes the data (failure events) recorded e.g. from experimental tests. The normalised product of prior- and likelihood probability yields the *posterior* probability, which represents the state of knowledge about the failure rate incorporating the new data.

4.2 Comparison of frequentist and Bayesian statistical approach

The discourse on the choice of statistical methods for reliability revolves around three main areas where the Bayesian approach fundamentally differs from the classical statistical approach. Namely, these are the concept of probability, the meaning of the derived parameter estimates and the applicability in the case of scarce data. The Bayesian approach to reliability applications is described in detail in Hamada *et al.* (2008); Martz & Waller (1982) while the classical approach is covered e.g. in Barlow & Proschan (1975); Meeker & Escobar (1998).

Table 4.1 summarises the main differences between the Bayesian and Frequentist approach which will be outlined in the following.

Table 4.1: Comparison of Frequentist and Bayesian statistical inference, based on Martz & Waller (1982, p.169).

Attribute	Frequentist	Bayesian
Reliability parameter	Unknown constant	Random variable
Reasoning	Inductive	Deductive
Past experience	Not considered	Explicitly considered
Interval estimate	Confidence interval	Probability interval
Availability of data	Large sample size required	Small sample size sufficient if relevant experience exists

4.2.1 Notion of probability

The traditional viewpoint of probability theory regards experiments in relation to specific events (e.g. survival or failure of a component) and their success rate while repeating the experiment. Well-known examples for these are the classic 'game experiments' such as drawing cards/balls with an assigned probability, rolling a dice or tossing a coin. Martz & Waller (1982, p.163) highlight that the central and distinct attribute of this frequency notion is the idea that "(...) the probability of an event can be empirically established by conducting a sufficiently large series of repeated trials in which the event can occur."

In strong contrast to that, Bayesian inference is based on the concept of subjective probability i.e. the subjective state of knowledge about a parameter, given the available information. This knowledge state is often referred to as a degree of belief. This interpretation of probability allows to integrate information that is available before the actual experimental data/results have been obtained.

In a reliability context such additional information can stem from physical or chemical theory of failure mechanisms, earlier qualification or prototype tests, computational models, precedent experience with similar equipment, generic reliability information as well as engineering judgement and experiences (Hamada *et al.*, 2008). More specifically for the marine renewable energy application this information could arise e.g. from wave tank tests during the design period, prototype tests, reliability information from related industries that use similar equipment (e.g. failure rate databases such as the OREDA handbook), specific component tests, generic failure rate data (e.g. FARADIP) or the engineering judgement form experienced marine engineers.

It is argued that subjectivity is present in any statistical analysis (Martz & Waller, 1982). This is particularly true for the assumptions taken in reliability applications (e.g. type of failure distribution/mechanism). In a nutshell, Bayesian inference addresses subjective elements in a transparent, explicit manner while the classical approach strives to avoid subjective factors. In cases where objective information (e.g. failure data) is scarce a reliability analysis may only be possible with the consideration of subjective information.

4.2.2 Interpretation of statistical estimates

Reliability is most commonly estimated either as the probability that an item does not fail for a specified period or as the time until it does fail (BS 5769-0:1986, 1986, p.10). The latter is the case for the mean time to failure (MTTF) and mean time between failures (MTBF). If we were interested in the MTTF of a component the frequentist approach would understand the unknown parameter as a fixed constant and derive a statistical inference in three steps:

1. Determining a point estimator, e.g. $\hat{MTTF}$ from the available sample data, using e.g. the least square or Maximum likelihood method.

2. Obtaining the corresponding sampling distribution, covering all sampling possibilities.

3. Calculating a confidence interval that describes the difference between the true value of MTTF and the point estimate $\hat{MTTF}$, given a significance level α (typically $\alpha = 5\%$). The confidence interval includes the true value of MTTF with a certainty of $1 - \alpha$.

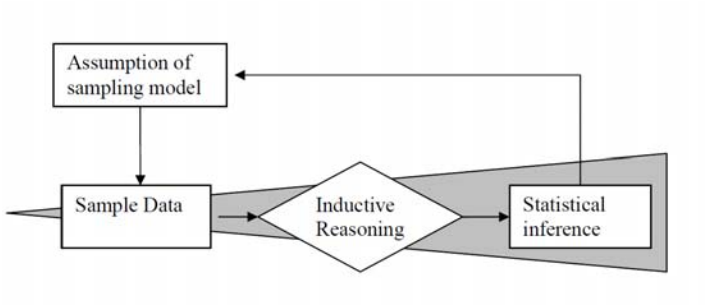

(a) Inductive inference - Classical sampling theory

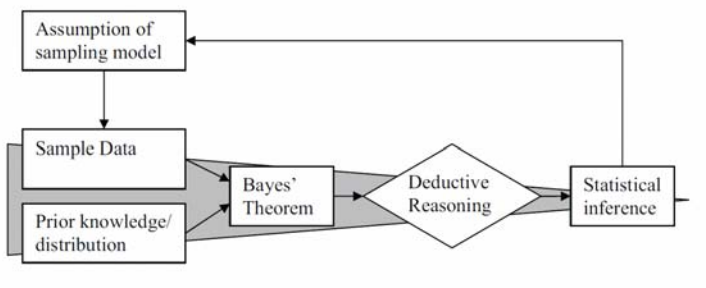

(b) Deductive inference - Bayesian theory

Figure 4.1: Schematic inference procedure, based on Martz & Waller (1982, p.166).

The inference procedure of this sampling method may also be depicted as shown in 4.1(a). A suitable sampling model is assumed with regard to the experiment and the expected data. The sample data and inductive reasoning (i.e. using the particular events and observations to derive a generalisation) is used to generate inferences about the parameters of interest in the previously assumed sampling model. A commonly estimated parameter is e.g. the mean estimate of MTTF within a 95% confidence interval.

The confidence intervals that have been computed in this way "(...) *cannot* be interpreted as a probability statement" (Martz & Waller, 1982) about the MTTF, because the MTTF is not a random variable, but a fixed constant. In other words the confidence interval is not a statement about the probability of the unknown parameter but only specifies the boundaries and an associated confidence level that the true value lies within those boundaries.

This attribute makes the application of frequentist statistics inconvenient for reliability purposes where various confidence intervals have to be combined, e.g. in the case where the system reliability shall be computed from the confidence intervals of the various components.

Opposed to this, Bayesian inference uses deductive reasoning, i.e. aims to make specific conclusions derived from generalised assumptions and observed events (see 4.1(b)). The parameter of interest is understood as a random variable and is assigned a prior distribution. This prior distribution describes the knowledge (or ignorance) about the parameter of interest before the actual sample data is analysed.

Using both the prior knowledge and the observed sample data the posterior distribution is calculated via Bayes' theorem. The reasoning here is deductive, because from the posterior distribution more specific inferences are drawn. As an example, the mean of the posterior distribution is a specific point estimator for the parameter of interest, derived from the more general prior distribution.

The diverse interpretation of statistical estimates might be regarded as a distinction without difference but it poses implications on the ability to compute system reliability estimates from component reliability and the meaning of derived reliability estimates.

4.2.3 Availability of data

In the case of large sample sizes classical and Bayesian inferences yield similar results, if the different notion of probability is put aside. In the case of scarce test data though, Bayesian interval estimates with a meaningful prior distribution are known to often yield better results (Hamada *et al.*, 2008, p. 17), i.e. narrower intervals compared to the classical estimates.

As discussed in section 4.2.1 the assumption of "hypothetical repetitions of (...) test procedures"(Winterbottom, 1984) is waived for the Bayesian methodology, allowing the integration of additionally available information and knowledge. This extension of usable information is particularly useful in the case of scarce data or complex environmental- and loading conditions which are hardly ever identical. For the marine energy case this means e.g. that there might not be two devices which will fail in exactly the same manner but the reliability information could be jointly used in a Bayesian approach.

4.3 Critique of the Bayesian approach

Within the framework of a Bayesian approach data that is available previous to the actual experiment (prior data) can be considered and is potentially highly relevant for the outcome of the analysis. If not assessed correctly though, there is a possibility that the posterior results are being biased towards prior reliability information and away from the obtained test data (Krivtsov & Wasiloff, 2000, p.315). For engineering applications caution is required to prevent that wishful thinking is contained in the prior information and in turn influences the conclusions. This is particularly the case where the prior information dominates the results because experimental data is limited (Meeker & Escobar, 1998, p.363).

Thus, the main difficulties in performing a Bayesian reliability analysis lie in the choice, determination and justification of the prior distribution (Martz & Waller, 1982, p.185). If the prior distribution dominates the posterior distribution the entire analysis could be condemned based on the argument that a biased prior was chosen to achieve a particular result. Items that are prone to such criticism are in particular the type of prior distribution, the data sources leading to the prior distribution as well as the quantification of subjective information. Consequently, the selection of prior distributions remains a key criticism of the Bayesian approach, unless it is conducted in a transparent, comprehensible way and with just reasoning.

There are two types of prior distributions distinguished with regard to their information content (Hamada *et al.*, 2008, p.28). If not much information about the parameter of interest is available before the experiments then the distribution is called

noninformative. Other common designations are diffuse or vague distribution as not much is known and the parameter data has a large spread. If in the contrary case the prior information is very specific and allows to render the prior distribution more precisely, it is called *informative*.

The prior distribution has to reconcile opposing positions. On the one hand it should be robust against criticism, on the other hand it should represent the best knowledge about the parameter. If a prior is purposely chosen to contain as few information as possible it is resistant against potential criticism that too much emphasis is placed on a particular aspect.

"From the viewpoint of defensibility, a noninformative prior is ideal. From the viewpoint of realism, however, a noninformative prior can be defective"(Atwood, 1994, p.1) because the posterior mean is influenced by the prior mean.

In order to take the wind out of the critics' sails Martz & Waller (1982, p.189) suggest five key elements for a satisfactory Bayesian analysis:

1. Detailed justification/analysis of the chosen prior distribution
2. Comprehensive documentation of data sources used to derive the prior distribution
3. Preposterior analysis of the prior distribution assessing its impact with hypothetical sample data
4. Posterior distribution must be clearly defined
5. Sensitivity analysis of the inferences with regard to the selected prior distribution.

In summary, the Bayesian framework is exposed to criticism due to its subjective notion of probability. This critique is justified, as the explicit consideration of prior information introduces a possibility to directly influence the outcome of the analysis. The same possibility is given in the frequentist approach, but as the procedures are more restricted to the obtained data, direct manipulation becomes less of an issue, although the results can still be influenced, for example through the choice of models. Consequently, if a Bayesian analysis is conducted there is an increased requirement for detailed and accurate documentation of the analysis steps, in particular with regard to the prior distribution.

4.4 Bayesian inference in reliability applications

4.4.1 Literature review

The benefit of the Bayesian methodology is being demonstrated by a number of reliability applications. The Bayesian approach has been applied for a number of different applications across a range of industries. A few representative examples will be briefly reviewed in the following and are summarised in Table 4.2.

Table 4.2: Summary of Bayesian applications in different industries.

Industry / component	Application	Reference
Electronic devices	Updating of past field failure rates with results of Accelerated Life Tests	Pan (2009)
Rail industry; train axle wheel	Validation and updating of numerical fatigue life simulations with full scale tests results	Akama (2002)
Pressure vessels	Refinement of generic failure rates with analyst judgement	Shafaghi (2008)
Nuclear reactor database	Hierarchical Bayesian model incorporating multiple types of information	Pörn (1996), Bunea *et al.* (2005)
Power plant boilers	Updating of industry failure rate data with data from non-destructive tests and inspections	Heising & Shwayri (1987)
Oil refinery process plant	Updating of generic failure rate with plant specific operation data	Yang *et al.* (2010b)
Automotive mechanical components	Updating of past failure rate data with reliability test results for new components	Guida & Pulcini (2002), Guida *et al.* (2009)

Pan (2009) examines the matter of reliability predictions for a new product which are based on field failure rates of previous products and Accelerated Life Tests (ALT).

In cases where ALT do not entirely replicate field use conditions, failure rates established in the lab and experienced in the field vary considerably. Consequently, test results need to be adjusted to accurately predict field failures. Bayesian inference is used to combine the available reliability information from precedent products and the results from ALT for the modified product. An adjustment factor estimated with the proposed Bayesian procedure has the potential to improve the accuracy of reliability predictions, but was only illustrated with temperature accelerated tests of an electronic device and notional field failure results. Hence the method was theoretically applied and shows the capability of the Bayesian inference to improve reliability predictions but was not proven to be successful with actual field failure data. Regarding the suitability of this approach to the marine energy case, there is not enough operational experience to refine the correlation between ALT failures and field failures. However, the joint utilisation of different sources of reliability information is promising to yield e.g. improved failure estimates. However, the refinement of failure rates is likely not to be as precise as a calibration between ALTs and field failures.

An application of Bayesian inference to improve failure probability predictions of train wheel axles is reported by Akama (2002). The axle fatigue life was estimated by a numerical simulation of probabilistic fracture mechanics. These calculations were based on experimentally determined crack propagation rates of small-scale specimens. The numerical results were not deemed robust, as the simulation does not adequately replicate the load and boundary conditions. Additionally, scale effects for the material strength were identified as a source of uncertainty. For these reasons experimental verification through full-scale experiments was carried out. The Bayesian approach was the statistical tool of choice, because the data resulting from full-scale tests is typically too scarce for a conventional statistical analysis. The fatigue life distribution estimated in the numerical simulation and modelled as 3-parameter Weibull distribution was employed as a prior. The likelihood distribution was derived from the full-scale fatigue life test data. The resulting posterior distribution of crack propagation rates were used to rerun the numerical simulation in order to determine the updated failure probabilities. The outcome of this Bayesian inference was a decrease of the failure probability (approx. -30% compared to the original calculations) but more importantly the confidence into the failure probabilities were significantly increased. Not only did the full-scale

result verify the numerical calculations, but the variance of the distribution parameters was reduced in all cases (see Fig. 4.2). This case successfully illustrates the capability of the Bayesian approach to combine different sources of information/data in order to improve reliability estimates. Furthermore, this example demonstrates how numerical calculations may be verified through the effective use of sparse full-scale test results.

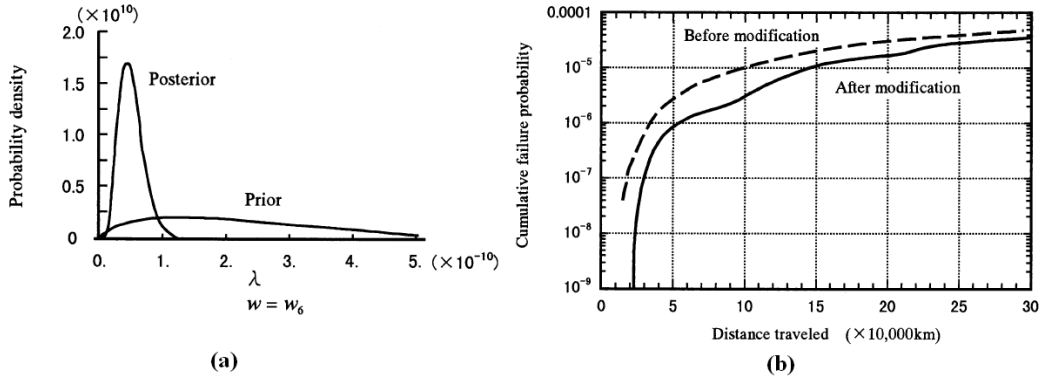

Figure 4.2: Bayesian inference results for axle failure probabilities (reproduced from Akama (2002)); (a) Improvement of Weibull scale parameter distribution; (b) Comparison of failure probabilities.

Shafaghi (2008) uses a Bayesian estimation procedure to determine the failure frequencies of pressure vessels for the disruptive and non-disruptive failure mode case. The method applies analyst judgement (by means of a weighted average) about generic failure rate information to establish a prior information. The prior distribution is modelled by a Gamma Γ pdf, while the likelihood information is assumed as Poisson distribution with notional data points. The study concludes that the amount of specific data effects the resulting posterior probability for both failure mode cases. While the disruptive failure proved to be within reasonable agreement with the prior distribution, the non-disruptive failure results differed by as much as an order of magnitude between prior and posterior.

A Bayesian procedure with reoccurring applications is the 2 stage (or hierarchical) Bayesian model which incorporates different types of information (e.g. engineering knowledge, past performance of similar equipment and performance of the particular

component). In the first stage a prior distribution is established form the generic information. The prior distribution itself is regarded as uncertain and necessitates a so-called hyperprior distribution to characterise the uncertainty of the prior (Bunea *et al.*, 2005). This approach is e.g. implemented in two large reliability databases, the German Centralised Reliability and Events Database (ZEDB) as well as the Swedish T-Book database (Pörn, 1996).

Heising & Shwayri (1987) estimated the outages of oil fired power plant boilers based on an extensive database of plant-specific information containing historical failure data, the results from non-destructive testing (NDT) and inspection protocols. This data was used as likelihood distribution to update a more generic database of 127 boilers in the US, in order to assess possible life extension measures. The outage estimate of the particular plant (i.e. the posterior distribution) showed to be significantly higher than the outage calculated from the generic data (Prior distribution).

In the processing industry accurate failure rates are also of high importance to estimate the potential downtime of the processing plant. Yang *et al.* (2010b) provide an example for a distillation unit in a refinery plan. The initial, generic failure rate estimates for a pump and valve failure are updated every few years with the operational failure data of the plant itself. They show how the knowledge about the specific component failure rates is improved through Bayesian updating. Although the mean event probability for the top event, release of flammable liquid, is not significantly altered, the standard deviation is reduced through the Bayesian updating process. This application is an example of how the event probability can be reduced when field reliability data is directly used instead of component test results.

The usefulness of the Bayesian inference also shows in a common industrial and commercial setting where cost and time allow only a few tests to be conducted for reliability demonstration purposes. In these cases, a frequentist approach would result in a reliability estimate with a low confidence level attached to it. Guida & Pulcini (2002) and Guida *et al.* (2009) sketch such a situation for the automotive industry and demonstrate how a Bayesian approach can exploit the available knowledge about a previous/similar component to yield appropriate reliability estimates.

In Guida & Pulcini (2002) reliability demonstration test results for mechanical components are used as likelihood distribution. The prior distribution is established from past failure rate data and engineering knowledge about the design and manufacturing adjustments in order to mitigate observed failure modes. Based on this information, the failure probability of the component is estimated for the end of the warranty period. An emphasis of this paper is the careful determination of the prior distribution from failure rate data that was observed under different environmental conditions such as different car makes and mileage. The available data is represented as Bernoulli likelihood distribution, where the failure frequency is modelled by a 2-parameter Weibull function. The expertise of the engineers is collected as rectangular distribution and modelled as Beta distribution.

In the paper by Guida *et al.* (2009) a similar approach is presented, but the effect of different prior distributions is also investigated for a real world case study. The resulting posterior failure probabilities have been compared for different levels of prior knowledge. Based on the real world data, it is shown that a higher level of prior knowledge (informative prior) allows to reduce the uncertainty of the reliability estimate (see figure 4.3).

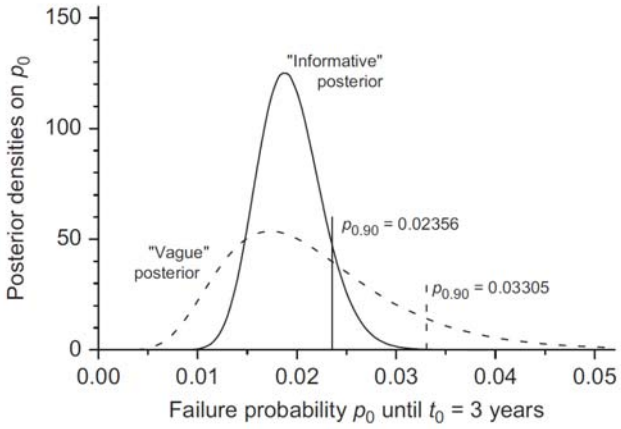

Figure 4.3: Posterior failure probability densities of an automotive component with informative and vague prior knowledge, reproduced from Guida *et al.* (2009, p.1617).

When comparing these examples from the automotive industry to the application at hand for marine renewable components, one major difference must be noted, which

is the quality of the prior information. The car industry can rely on decades of experience and development and a mass production with established failure rate records. In Guida & Pulcini (2002) approx. 243,000 vehicles with 1,383 failures of the investigated component formed the data basis for the prior distribution. In this context the Bayesian approach is used to recalibrate the already available information to a redesigned or similar component. Such a detailed and applicable pool of data is not available for the marine renewable case, due to its still early development at prototype stage. Consequently, a Bayesian approach for marine renewable components cannot yet yield highly accurate results, but should improve the reliability estimates to indicate the correct order of magnitude.

4.4.2 Rationale for the use of the Bayesian approach

While it is easy to get involved into a philosophical dispute about the respective merits and shortcomings of the classical and Bayesian approach there are pragmatic reasons to choose a Bayesian approach. If the task is to assess the reliability of a marine energy device the overruling question is which data shall be used to conduct the analysis. The general task is not revolutionary, but the specific assessment of marine energy converters is novel. The same chore is being faced in other industries which have two sources of data available:

- Generic reliability data, usually reported in industry wide databases.
- Specific reliability information for the particular application.

The dilemma from an analyst's point of view is that there might be enough generic information available to establish a reasonable point estimate of e.g. failure rates but the data might not be appropriate for the particular application. Inversely specific data is scarce and therefore does not lend itself to classical, frequentist statistical estimates. Shafaghi (2008, p.87) states that the sole use of specific- or generic data can lead to inappropriate reliability estimates, because "(...) plant specific data is statistically invalid due to a short duration of data collection or limited population of equipment. Generic data, on the other hand, does not reflect the characteristics and conditions of the plant that the equipment is operated under." The Bayesian framework is a possibility to overcome this dilemma as the generic data can be updated and 'married' with specific information that becomes available to give an improved reliability estimate.

4.5 Reduction of failure rate uncertainty through Bayesian updating

This section aims to apply the Bayesian framework to the estimation of failure rates. The model performs a Bayesian updating procedure that has been coded in Matlab. The source code is given in Appendix B.

The updating is performed in a discrete manner, which is most applicable in practice, as no conjugated pairs need to be found analytically to reach a closed solution.

For the discrete Bayesian updating case, Bayes' theorem can be written as

$$Pr(H_k|D) = \frac{\Pr(D|H_k)\Pr(H_k)}{\sum_{i=1}^{n}(\Pr(D|H_i)\Pr(H_i))} \tag{4.4}$$

The numerical model comprises of three parts, a section to establish the prior distribution, a part to model and establish the likelihood distribution and finally the computation of the posterior distribution. The presented procedure is generic, but in order to illustrate the process, actual data is used for the prior distribution and two cases are presented how the initial data might be updated.

The chosen example aims to establish a failure rate estimate for a dynamic marine power cable, also termed umbilical. The Bayesian method allows to combine information that is available before a particular test/experiment/field observations is conducted, with the data and information that is obtained during that test. While the initial information is used to establish a prior distribution. The observed data is then used to adjust the earlier distribution, establishing the posterior distribution.

4.5.1 Establishing the prior distribution

As prior information a failure rate estimate for an umbilical given in the OREDA handbook (SINTEF, 2002, p.811) is used. There are considerable differences between the cases reported in OREDA and the marine energy application. Oil and gas production umbilicals often comprise not only electrical but also multiple hydraulic supplies. The connection cables used for floating marine energy applications will be exposed to more energetic sea conditions as these are required for effective energy production. Despite these differences the OREDA data constitutes a good starting point as prior reliability information. The handbook summarises the data from 9 umbilical units with 2 reported failures, external leakage and transmission failure. The mean failure rate is given as

$\lambda = 4.2669/10^6 h$ with a standard deviation $\sigma = 4.8281/10^6 h$. The number of hours denote the time aggregated in service.

OREDA assumes a constant failure rate, i.e. the bottom of the bathtub-curve and expresses the sampling variability between the various installations by a Γ distribution (see equation 4.5).

$$\pi(\lambda|\alpha,\beta) = \frac{1}{\Gamma(\alpha)}\ \lambda^{\alpha-1}\ \beta^{-\alpha}\ e^{-\frac{\lambda}{\beta}} \tag{4.5}$$

Where $\beta = \frac{\sigma^2}{\mu}$ and $\alpha = \frac{\mu}{\beta}$; with $\Gamma(\alpha) = \int_0^\infty t^{\alpha-1}e^{-t}dt$ for $\alpha > 0$.

The mean μ and the variance σ^2 of the Γ pdf are calculated as (comp. Tobias (2006)):

$$\mu = \alpha\beta \tag{4.6}$$

$$\sigma^2 = \alpha\beta^2 \tag{4.7}$$

Hence the distribution parameters can be calculated as:

$$\beta = \frac{\sigma^2}{\lambda} \tag{4.8}$$

$$\alpha = \frac{\mu}{\beta} \tag{4.9}$$

Computing the Γ parameters accordingly for the dynamic umbilical yields: $\alpha = 0.781$ and $\beta = 5.4631$. The resulting Γ pdf $\pi(\lambda|\alpha,\beta)$ with the mean failure rate and an indication of the 90% confidence interval is depicted in figure 4.4. In the following analysis this distribution is used as prior distribution function.

4.5.2 Likelihood distribution

As a second step the likelihood distribution needs to be established. As source for additional information, different data may be obtained. This comprises failure rate data obtained during field trials, prototype or component testing of the actual component, as well as engineering knowledge. The aim here is to examine how new information may be incorporated into the prior distribution and how this will effect the updated

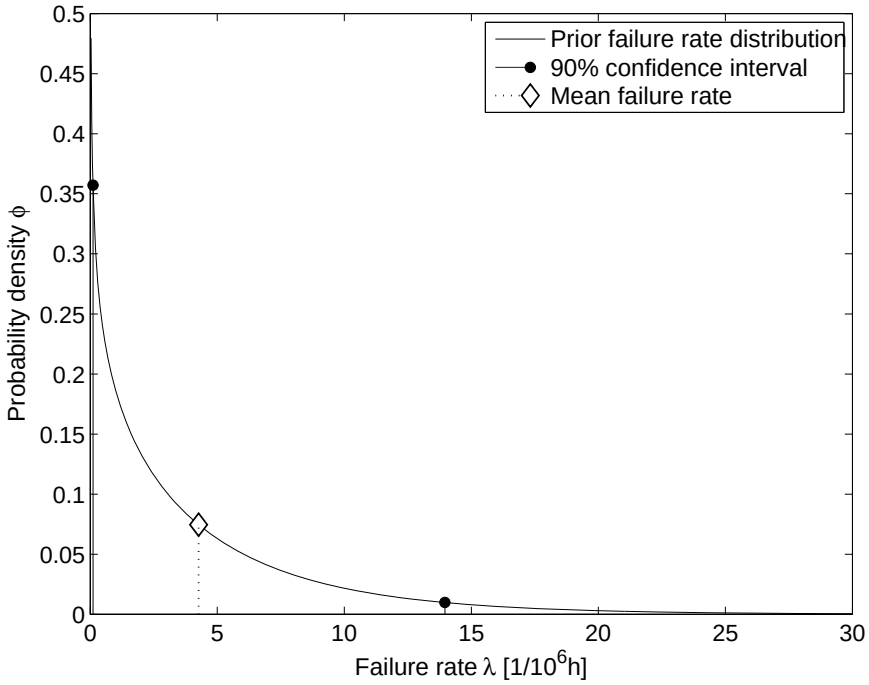

Figure 4.4: Prior distribution of umbilical failure rate, data sourced from SINTEF (2002, p.811), $\lambda_{Mean} = 4.2669/10^6 h$, 90% confidence interval $CI_{90} = [0.2, 14]$.

posterior distribution.

The likelihood distribution is modelled with a two-parameter Weibull distribution, equation 4.10 (see also section 2.1.3.2, p.53). The mean μ and variance σ^2 of the failure rate distribution are computed using Equations 4.11 and 4.12.

$$f(\lambda|a,b) = ba^{-b}\lambda^{b-1}e^{-\left(\frac{\lambda}{a}\right)^b} \tag{4.10}$$

$$\mu(f) = a\left(\Gamma(1+\frac{1}{b})\right) \tag{4.11}$$

$$\sigma^2(f) = a^2\left(\Gamma(1+\frac{2}{b}) - \Gamma(1+\frac{1}{b})^2\right) \tag{4.12}$$

In the following two examples are presented to illustrate two important, distinct failure scenarios:

1. *Modelling the effect of fatigue type failures.*

   Physical component tests may provide an indicative component failure rate. Accelerated fatigue tests subject the component to a certain number of load cycles that can be related to a distinct operational time. Through repeated tests a mean failure rate may be established. To illustrate how such information may be incorporated with existing knowledge a mean failure rate $\mu_{fatigue} = 10/10^6 h$ with $\sigma^2_{fatigue} = 26/10^6 h$ shall be assumed. The likelihood function can thus be modelled as a Weibull pdf with $a = 11$ and $b = 2$. These values are chosen so that $\mu_{fatigue}$ is close to the upper confidence limit of the prior distribution and $\sigma^2_{fatigue} < \sigma^2_{prior}$. Thus the assumed MTTF for the likelihood distribution is about 11 years and one has a stronger confidence in the test results as opposed to the prior information.

2. *Modelling the effect of unknown failure modes.*

   The application of components in new environments bears the risk that additional failure modes (FM) arise which have not been considered in the design phase. Such an unknown, overlooked failure mode may typically lead to a failure rate increase by an order of magnitude. Such information may become available from

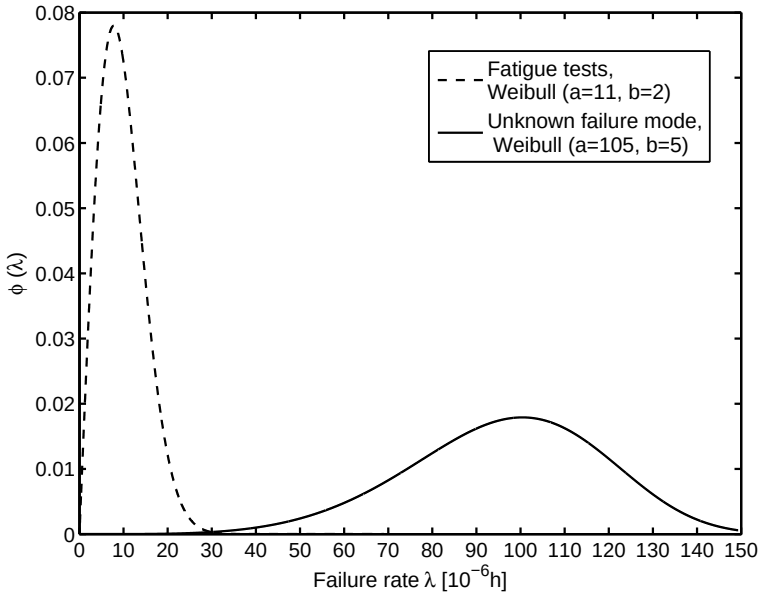

Figure 4.5: Likelihood distribution for two illustrative cases. Mean failure rates λ and associated variance σ^2 are given in Table 4.3.

initial field installations, but may also be modelled as 'engineering knowledge' to explore the effect of a potentially unknown failure mode. For the case illustrated here, it is assumed that the upper confidence limit of the prior distribution is exceeded by an order of magnitude, and fraught with a large degree of uncertainty. Thus, the likelihood function is modelled as Weibull pdf with the parameters $a = 105$ and $b = 5$. This yields $\mu_{FM} = 96/10^6 h$ and $\sigma^2_{FM} = 487/10^6 h$.

The distribution parameters for both cases are summarised in Table 4.3 and graphically presented in figure 4.5.

Table 4.3: Weibull distribution parameters modelling the assumed failure rate likelihood distribution.

Description	Weibull pdf		Measures $[\frac{1}{10^6 hours}]$	
Case 1: Fatigue tests	$a = 11$	$b = 2$	$\mu = 10$	$\sigma^2 = 26$
Case 2: Unknown failure mode	$a = 105$	$b = 5$	$\mu = 96$	$\sigma^2 = 487$

Beyond this application of 'engineering knowledge' one must resort to component testing, where the distribution of failure rates is likely to be derived from a limited

number of test points. To illustrate this the assumed likelihood distributions were used to generate 5 sample points for each case from which the likelihood distribution is subsequently evaluated. The modelling procedure is illustrated in figure 4.6. The two main steps comprise:

1. Drawing a random sample from the distribution specified for the two cases (defined in Table 4.3) to reflect the fact that any additional information will have a limited number of data from which the likelihood distribution can be estimated. For the cases considered here, a sample size of $n = 5$ was chosen, the question what sample size is required to satisfy a given reliability target is discussed in detail in (Meeker & Escobar, 1998, chap. 10).

2. The likelihood distribution is established by fitting a two-parameter Weibull distribution to the simulated data. This is somewhat trivial for the case study, as the data was generated from a Weibull distribution. However, fitting a distribution to measured test results is a crucial step in the application of real experimental data. In this case there is no physical reason to choose the Weibull distribution but it is employed because it provides a reasonable fit to a range of observed data and is thus widely used for reliability applications. Figure 4.7 shows an example of the sampled failure rates and the fitted Weibull distribution; as expected the fit indicates good agreement. To establish an adequate statistical fit to the data is likely to be not as straight forward for an actual data set, but usually the Weibull distribution proves to be flexible enough.

4.5.3 Resulting posterior distribution

Once the prior and likelihood distribution are established, the posterior distribution can be computed via Bayes' theorem (equation 4.4).

Figure 4.8 shows the updating process and posterior distribution results for case 1 and 2. Each plot shows the prior distribution (dashed line), the fitted likelihood distribution (dotted line) and the updated posterior distribution (solid line, with 90% confidence interval). The plot shows how the initial prior distribution is updated with the likelihood function, which yields the posterior probability distribution. The confidence intervals before and after the Bayesian updating are summarised in Table 4.4.

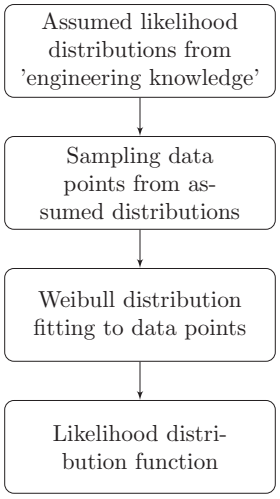

Figure 4.6: Modelling procedure to establish likelihood distribution function.

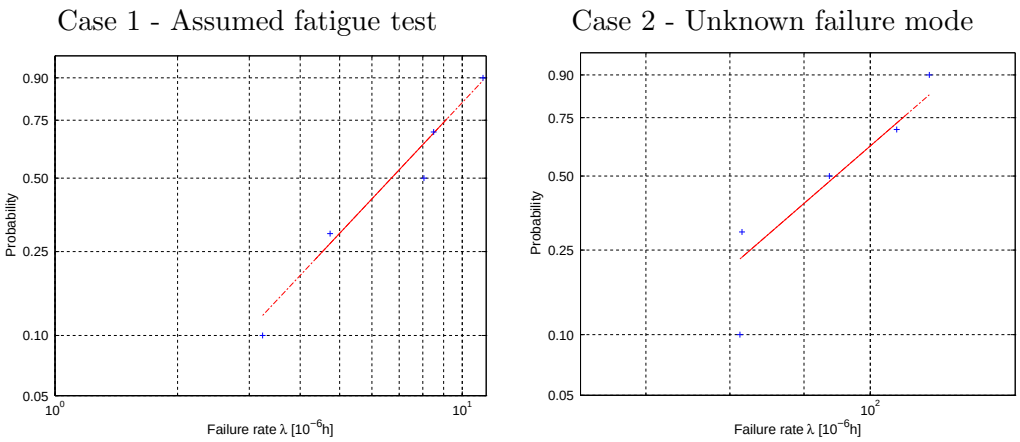

Figure 4.7: Weibull Probability plot, showing the sampled data points and the fitted distribution.

Table 4.4: Summary of 90% confidence interval for prior and posterior distribution.

	Prior distribution	Posterior distribution	
		Case 1 - Fatigue	Case 2 - Unknown failure mode
Lower bound [10^{-6}h]	0.2	1	9
Upper bound [10^{-6}h]	14	11	46

Case 1 - Assumed fatigue tests

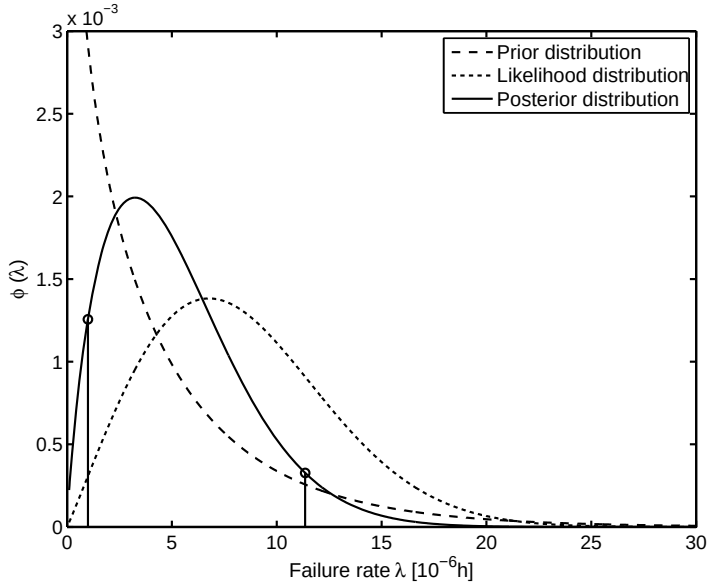

Case 2 - Unknown failure mode

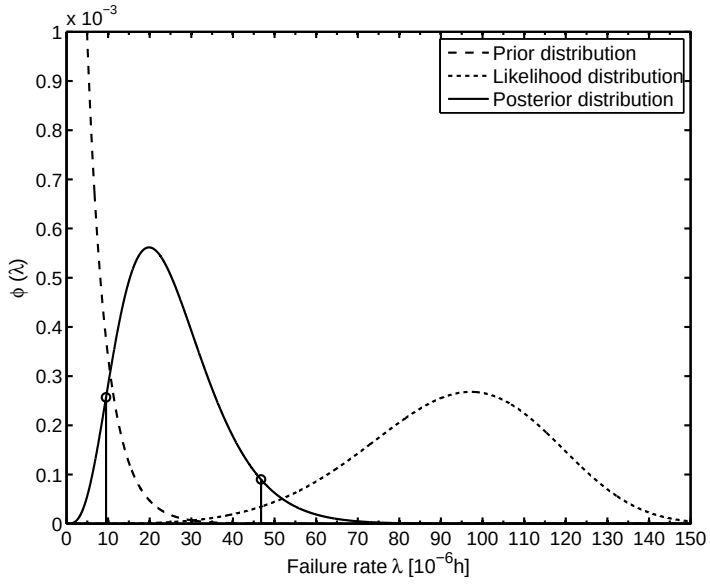

Figure 4.8: Prior, likelihood and posterior distribution for umbilical failure rate update. 90% confidence interval indicated for posterior distribution.

For case 1 the posterior distribution yields a 90% confidence interval $CI_{posterior,1} = [1, 11]$. This is a reduction compared to the confidence interval of the prior distribution $CI_{prior} = [0.2, 14]$. The initial Γ distribution is amended to a distribution with similar shape to a Weibull distribution. This illustrates, how the failure rate uncertainty may be reduced when applicable data with a limited variance, i.e. a reasonably strong belief in the data, is available to update generic failure rate information.

For case 2 the posterior distribution does not clearly resemble either distribution. The reason for this is the relatively large variance σ^2 for both the prior and the likelihood distribution. Due to the significantly larger mean failure rate modelled for the unknown failure mode likelihood distribution, the posterior distribution is shifted to the right of the prior, yielding a 90% confidence interval $CI_{posterior,2} = [9, 46]$. Thus, in the light of the additional information the failure rate uncertainty would increase.

Both examples indicate the updating procedure when an initial distribution with large uncertainty is updated with additional information. Depending on the 'belief' in the additional information, which is expressed by the variance σ^2 of the likelihood distribution, the uncertainty about the failure rate distribution is decreased when $\sigma^2_{prior} > \sigma^2_{likelihood}$ and increased if $\sigma^2_{prior} < \sigma^2_{likelihood}$.

4.6 Discussion

The Bayesian statistical framework offers a capable method to remedy the quandary of scarce specific failure rate data. Such a situation prevails not only in the design of a wave energy converter, but also throughout the period where the first prototypes and installations provide initial application specific failure and reliability information.

During the early development and design stages of wave energy converters when there is a lack of specific, appropriate failure rate data, generic failure data may be combined with additional information.

The benefit of a Bayesian approach to failure rate data is that the analyst not only operates with simplified point estimates, but has to employ probability distributions for both the underlying prior information and the established likelihood distribution. The reliability estimate is thus not constrained to the absolute failure rate value but

receives an assessment with regard to the amount of 'belief' one can have in the failure rate. This information is of high importance to decision makers, as it highlights areas of ignorance, i.e. epistemic uncertainty, or inherent, aleatory uncertainty.

Two general situations are conceivable, which have been demonstrated above. Either the certainty about the reliability parameter is improved through the Bayesian updating or it is reduced. In the former case this may reinforce an acceptable, low failure rate or an unacceptably high value which provides the decision maker with some confidence in the existing design or emphasises the need to improve the failure rate or amend the system. The latter case of reduced certainty over the failure rate would highlight necessary further investigations to improve the understanding of the failure behaviour and the identification of all potential failure modes. Reduced certainty over an acceptable low failure rate would question the validity of the prior estimate, while less certainty over an unacceptable high failure rate gives an insight to achievable failure rate levels.

When initial failure and reliability information becomes available the Bayesian approach enables the analyst to perform a regular update of the failure rate information, on which reliability and availability models are based. Such a regular update has the benefit to supply the latest 'best estimate', with the potential to identify components that over- or under perform compared to the initial design specification. The evidence in form of a Bayesian update can not only inform the search for a potential root cause, but also presents valuable input information for the planning of operation and maintenance procedures.

The literature reports the successful application of the Bayesian approach to solve a number of different questions, ranging from the validation of numerical simulations over the refinement of generic failure rates, to continuous updating and calibration of reliability information. However, in order to yield robust and meaningful results the information that is used to establish the likelihood information must be of high quality and directly related to the application in question. The reason for this lies in the deductive nature of the Bayesian inference, where the inference is reached through the combination of general (prior) knowledge with more specific data. Thus, the Bayesian approach 'promises' an improved reliability estimate, but still relies on the generation

and interpretation of appropriate, meaningful and highly specific data, which serve as representative 'sampling points' around which the likelihood distribution can be fitted. As a consequence, the scarcity of data is shifted from the failure rate or reliability information to the likelihood information. The information required to determine the likelihood distribution may be established through a combination of physical and numerical investigations. Three approaches to derive specific reliability information for components employed in a wave energy device are explored in the following chapters.

- Experimental wave tank tests to determine mooring loads
- Numerical modelling of mechanical loads for a dynamic marine power cable
- Specific, service-simulation, component testing

Part III

Physical and numerical investigations

Chapter 5

Experimental and modelling procedures

This chapter sets out the background and procedures for the experimental and numerical work that was carried out, in order to determine the specific load conditions experienced by WECs. Physical wave tank tests of a 1:20 scale OWC are presented in section 5.1. Results were subsequently utilised to establish a numerical model describing the mechanical load regime for marine power cables in such an application. The computational model is outlined in section 5.2.

Another experimental strand that was established is a component test rig that is specifically designed to replicate the forces and motions of marine applications. Section 5.3 lays out the rationale, specification and capabilities of this test facility.

5.1 Mooring load tank tests

As part of the SuperGen Marine initiative, physical model tests of a generic WEC were undertaken in the NTNU Trondheim wave basin. The tests were carried out in October 2008 and were funded by the European programme Hydralabs III. The test objectives were to gather data which would serve the validation of numerical models, and to investigate potential interactions when the devices are deployed in array configuration (Ashton *et al.*, 2009; Bryden & Linfoot, 2010; Krivtsov & Linfoot, 2010; Vickers, 2012). The tests were carried out at 1:20 scale with a generic floating OWC converter which was subjected to a range of operational sea states.

For this thesis the data for a single device is analysed to assess the tension and fatigue loading of the mooring lines. In the following the experimental set-up and test procedure are briefly described. It must be noted that the author was not present at the actual tank tests. A more detailed description of the complete experimental set-up and procedures as well as the calibration testing performed can be found in the PhD thesis by Vickers (2012).

The methodology applied to the data analysis and the results are presented in the subsequent chapter 6, section 6.1.

5.1.1 Wave tank

The NTNU Ocean Basin is a rectangular 80x50m tank with a variable depth of up to 10m. For the conducted tests the 80m side with 144 hinged single-flaps were used to generate the waves. The flaps are individually controlled and electronically driven. Figure 5.1 shows the tank dimensions (5.1(a)), and the definition of the coordinate system (5.1(b)). The water depth was set to 2.8m, and the surge motion of the WEC device (x-axis) has been defined positive in opposition to the wave maker; sway motion is defined by the y-axis and heave motion is defined as z-axis.

In the tank, the position of the converter (WEC1) has been defined as the origin of the data coordinate system. The device is moored to the bottom of the tank with three mooring lines attached at the welded anchor positions (A1, A2, A3).

5.1.2 Generic wave energy converter

The wave energy converters used in the tests were generic, cylindrical floating devices of the OWC type (see figure 5.2). The power take-off was modelled with an orifice plate at the top of the cylinder. The plate could be adjusted to change the damping properties of the device. The physical height of the cylindrical column is $h = 1.1m$ with a diameter of $d = 0.8m$. The orifice plate is fitted to the top of the cylinder, while a damping plate is mounted to the bottom of the converter. The displacement force of the device is $\Delta = 0.85kN$.

The Froude scaling law applies to most wave energy applications, as the relative influence of viscous forces F_v is small in comparison to the influence of the gravitational force F_g. This is the case when the modelled device has a compact form, i.e. the wetted surface area is small in relation to the immersed volume (Payne, 2008).

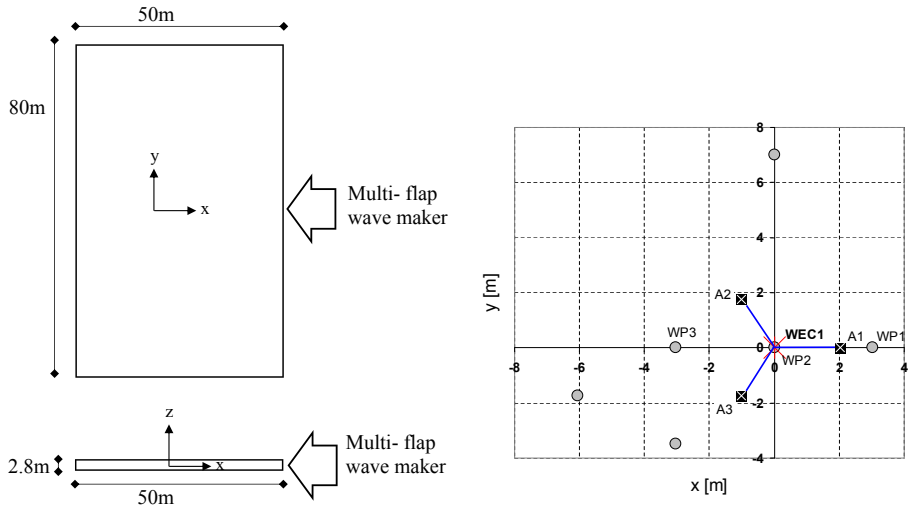

(a) Wave tank dimensions. Top - plan view; bottom - side view

(b) Coordinate system of wave probes (WP), anchor points (A) and converter (WEC)

Figure 5.1: Experimental set-up for tests carried out at Marintek Ocean Basin, NTNU, Trondheim.

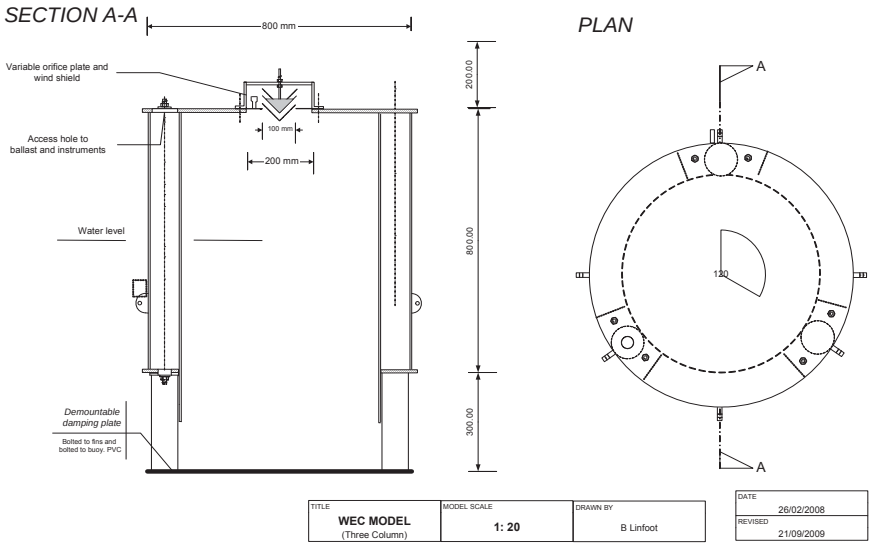

Figure 5.2: Drawing of principal dimensions of wave energy converter model.

Using Froude's scaling law, the physical dimensions of the 1:20 model relate to the full-scale values shown in table 5.1. The values and results in the following are expressed in full-scale dimensions.

Table 5.1: Experimental dimensions and Froude scaling laws with $s = 20$.

Dimension	Model scale	Scaling factor	Full scale
Height [m]	1.1	s	22
Diameter [m]	0.8	s	16
Water depth [m]	2.8	s	56
Displacement force [kN]	0.85	s^3	6800
Mooring line diameter [mm]	3.5	s	70
Mooring elastic modulus E [GPa]	13.8	s	276

5.1.3 Mooring configuration

The WEC was moored with three mooring lines, which incorporate a top floater each and were attached via shackles to the WEC and the anchoring point (figure 5.3).

The mooring line consisted of 3 strand Aramid Core rope with a 16 plait polyester cover of a diameter, $d_{line,model} = 3.5mm$. The initial elongation of the cord from zero load is governed by the polyester cover as it restrains the core during the bedding-in process and the load range at model scale ($F_{tension,\,model} < 18$ kg force) is relatively small compared to the rope minimum break load of $MBL_{model} = 570$ kg (Dyer, 2011). Under full-scale conditions the mooring line diameter would be $d_{line,full-scale} = d_{line,model} \cdot s = 70mm$. Another important parameter that requires a conversion to full-scale is the axial line stiffness. Axial stiffness, k, is defined as the tensile elasticity modulus, E, multiplied by the cross-sectional area ,A, of the rope and divided by the length l, i.e.:

$$k = \frac{EA}{l} \tag{5.1}$$

Under Froude scaling laws, a force, F, scales with a factor of s^3. Now, as EA expresses a force ($Pa \cdot m^2 = \frac{N}{m^2} \cdot m^2 = N$), and is divided by a length, l, the axial stiffness, k, scales as (Fernandes & Rossi, 2005):

$$\frac{k_{full-scale}}{k_{model}} = \frac{s^3}{s} = s^2 \tag{5.2}$$

The tensile elastic modulus for polyester mooring lines, $E_{polyester}$, depends on the specific yarn and rope construction as well as the applied loading. Flory *et al.* (1992) give an average value of $E_{Polyester} = 13.8GPa$, while the Viking 113mm diameter polyester rope is characterised with $E_{Polyester} = 7.2GPa$ for the lower load cycle range (10-30% of MBL) (VIKING, 2010).

Rearranging equation 5.1 for E and forming the ratio of $E_{full-scale}$ and E_{model} yields:

$$\frac{E_{full-scale}}{E_{model}} = \frac{\frac{k_f l_f}{A_f}}{\frac{k_m l_m}{A_m}} \tag{5.3}$$

Replacing the parameters with the associated scaling factors ($k_f/km = s^2$, $l_f/lm = s$ and $A_m/A_f = 1/s^2$ leaves:

$$\frac{E_{full-scale}}{E_{model}} = s^2 \cdot s \cdot \frac{1}{s^2} = s \tag{5.4}$$

Thus the elastic modulus scales with a factor s giving a range of

$$E_{full-scale} = E_{model} \cdot s = [7.2, 13.8]GPa \cdot 20 = 144 - 276GPa \tag{5.5}$$

Therefore, the fatigue load estimates will be considered for steel mooring materials, as the Young's modulus of steel of about $200 - 215GPa$ lies well within the potential range of the full-scale mooring characteristics (Ashby, 2005, p. 522).

5.1.4 Instrumentation

The experiment was extensively instrumented to determine the wave conditions, the converter movements in six degrees of freedom (DOF), the mooring forces, and power absorption. For the one device considered here, this comprises (compare table 5.2):

- 6 wave probes
- 1 internal water level sensor
- 1 pressure transducer
- 6 mooring line load cells
- 1 non contact motion tracking system

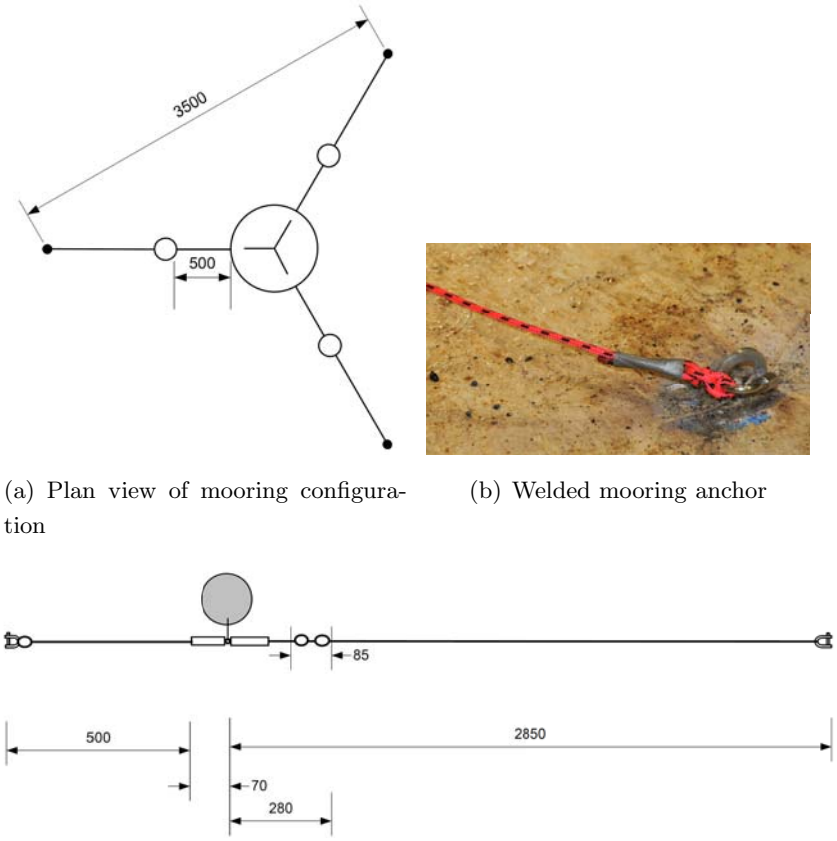

(a) Plan view of mooring configuration

(b) Welded mooring anchor

(c) Mooring line arrangement

Figure 5.3: Experimental mooring set-up of generic floating OWC, dimensions in [mm].

The data output of each unit was recorded as a time series. The Marintek CATMAN data aquisistion system filtered and stored the data with a frequency of 80Hz under experimental conditions. The data was automatically upscaled using Froude's scaling law.

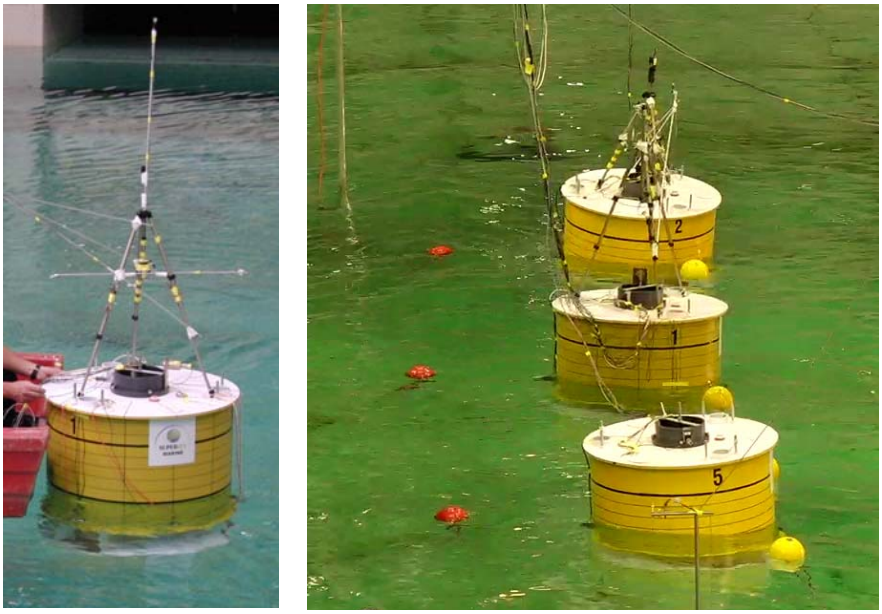

(a) Non contact motion tracking system

(b) Converter set-up in tank

Figure 5.4: Experimental set-up of generic OWC devices.

5.1.5 Test regime

The test regime considered here consisted of four consecutive steps:

1. Wave calibration test
2. Device characterisation
3. Tests with one device in regular (monochromatic) waves
4. Tests with one device in irregular (polychromatic) waves

The simulated sea states had a significant wave height (at full scale) of $H_s = 2-6m$ and a wave period, $T_p = 5 - 13s$. The actual simulated sea states are depicted in

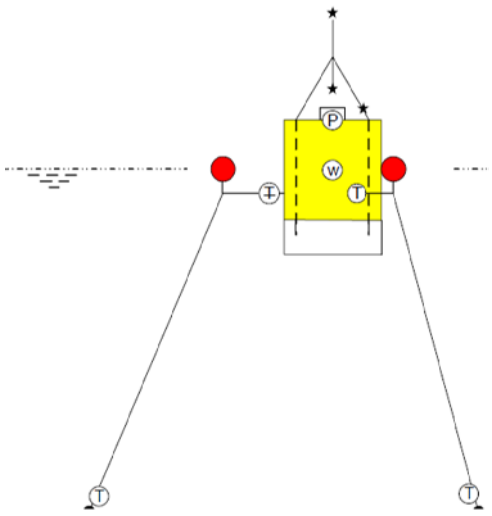

	Item	Quantity
T	Tension load cell [200N]	6
T̶	Mooring line angle sensor	1
P	Pressure transducer	1
w	Internal water level sensor	1
⋆	IR relflectors	5
•	Fixed mooring point	3

Table 5.2: Side view of generic OWC and instrumentation.

figure 5.5. The test duration for regular waves was set to $t_{reg} = 6min$ while irregular sea states were simulated for $t_{irreg} = 27min$. In between sea states the tank was left to settle for $t_{settle} = 15min$.

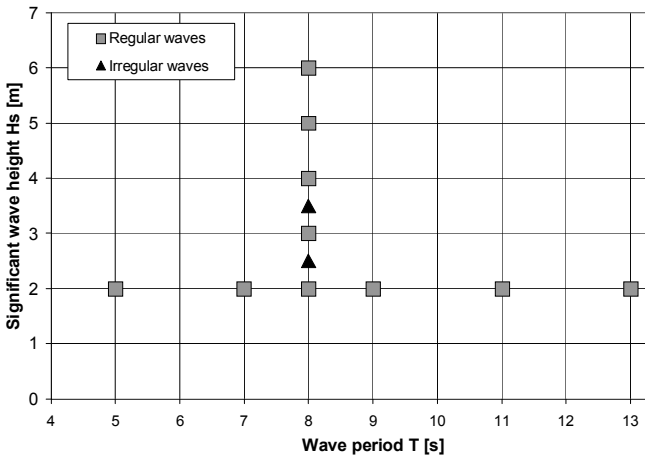

Figure 5.5: Range of sea states simulated in the tank experiments.

5.2 Numerical modelling of marine umbilical cable loads

Electricity has been transmitted across the sea with subsea power cables for more than a century, and is a well established technology (Worzyk, 2009). In the offshore industry

an 'umbilical' denotes the link between a floating structure and submarine equipment and installations. It provides the required supply (chemicals, power, hydraulics), and control (electric signal, fibre optics), to the submarine equipment.

In general, two different types of power cables can be distinguished:

- Static cable: This type of cable provides the connection between subsea connection points and is not subject to cyclic loading.
- Dynamic cable: This cable type connects a floating structure and subsea equipment through the water column and is therefore subject to considerable cyclic loading conditions induced by the movement of the floating body, the waves and the currents.

However, present dynamic power cables are not designed for situations where the top structure is subjected to large excursions, and this is often the case for motion dependent wave energy devices, making the cable susceptible to fatigue failures. This section briefly describes the design of marine power cables, assesses likely failure modes in a wave energy application, and outlines the computational model which has been developed in the proprietary hydrodynamic analysis package, OrcaFlex (Orcina, 2011).

5.2.1 Marine power cables

5.2.1.1 Design

There is a range of different designs and configuration types for specific applications but the cable generally comprises of several layers which are assembled around the conductor core (Alegría *et al.*, 2009; Green *et al.*, 2007; Worzyk, 2009). An example of a 3.3kV AC subsea power umbilical that has been supplied for an installation of the OPT PowerBuoy is shown in figure 5.6. Seven typical layers can be identified:

1. Conductor core: The cable core carries the electrical current and consists of further wires, made out of either copper or aluminium.
2. Electrical insulation: The electrical insulation can be achieved by three different design/material types. Oil impregnated paper, Cross-linked polyethylene (XLPE) and Ethylene propylene rubber (EPR). Due to their favourable mechanical and dielectric properties XLPE and EPR are considered to provide the most suitable electric insulation for dynamic applications.

3. Screen: A semi-conducting layer of paper/extruded polymer around the core to minimise electric field strength and to avoid field concentration zones.

4. Sheath: The sheath acts as a water barrier and protects the cable against fault currents.

5. Armature: The cable is surrounded with metallic armature (usually galvanised steel wires) to provide the required mechanical strength and impact protection.

6. Optic fibre: Fibre optic cables provide the capability for data transmission and monitoring purposes.

7. Protective sheath: The outer layer consists of polypropylene for abrasion resistance.

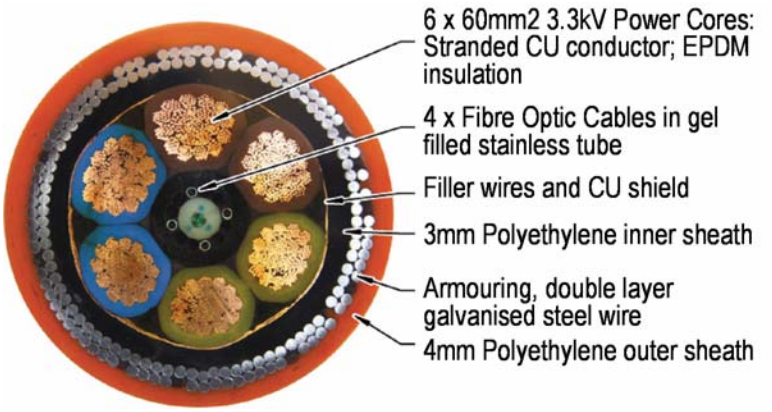

Figure 5.6: 60mm^2 Cross-section of a HVAC 3.3kV marine power umbilical supplied for Ocean Power Technology PowerBuoy installation, reproduced with courtesy of JDR (2010).

It must be noted that the multitude of materials and configurations result in complex mechanical behaviour of marine cables under load and make it difficult to predict the service life with confidence. It is also important to note that there is no standardised marine cable, and that manufacturers usually tailor-make submarine cables to the application at hand. In this process the cable layers listed above are combined in cylindrical and/or helical configuration with varying diameters and differing cross-sectional designs.

Another important design choice is the subsea geometry of the cable, which is dependant on the water depth and the anticipated loading regime. Some standard configurations which are used in the oil and gas industry are shown in figure 5.7. The two configurations that are investigated in the following are the simple free hanging (so-called catenary) shape and the Lazy-Wave shape where the cable is supported with buoyancy floats to create a long radius curve in order to absorb the top-end motion (see also figure 5.10).

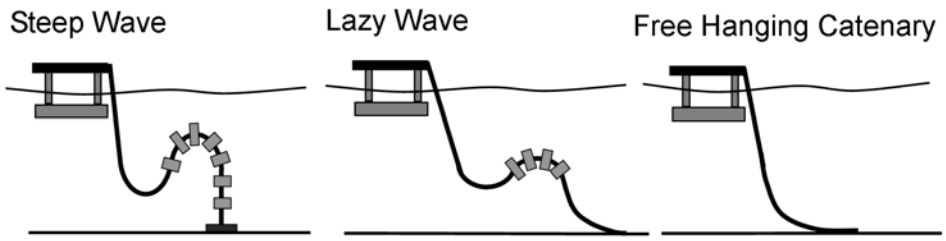

Figure 5.7: Standard flexible riser configurations for floating offshore structures, based on Clausen (2001).

5.2.1.2 Failure modes

A number of failure modes have been reported for marine cables and umbilicals. The Umbilical Manufacturers' Federation (UMF, 2004) accounts failures of control umbilicals for a 5 year period (1995 - 2000). The failure definition names incidents that are detrimental to the functionality of the fluid conduits, electrical conductor or fibre optical cable. The umbilicals in this study were mainly of the electro-hydraulic type. A total of 21 incidents were reported, with the majority of 17 failures during installation and commissioning and almost half the failures associated to manufacturing and installation errors. Most mechanical failures were associated to the failure of attachment/hang-off points.

Patel (2008) summarises the outcome of a reliability study of electrical cables in umbilicals, which lists a total of 62 failures. Approximately 50% of the failures are deemed to be caused by incorrect installation and loadout, followed by electrical faults, incorrect operation or design flaws. Other named failure causes were fatigue failures, poor manufacturing, marine life (marine growth, shark attacks), and accidents.

This highlights the importance of careful installation of umbilicals, and it also emphasises the fact that mechanical failures do occur if either; not all load parameters are considered in the design process or, the umbilical itself does not meet the required strength.

The results from an extensive measurement campaign, which was undertaken for the dynamic umbilical of the Foinhaven FPSO vessel, are analysed and reported by Trarieux *et al.* (2006). They investigated the relative contribution of the prevailing excitation forces to the fatigue damage of the umbilical. According to their bandwith measure, the fatigue damage is mainly caused through the wave excitation forces, followed by the vortex induced vibration and the mooring induced motions.

For the extract presented in figure 5.8, showing the normalised relative contribution of each component for bending fatigue, the bending due to wave excitation is the main contributing force. According to the author this was the case for all of the recorded measurement period (Trarieux, 2010).

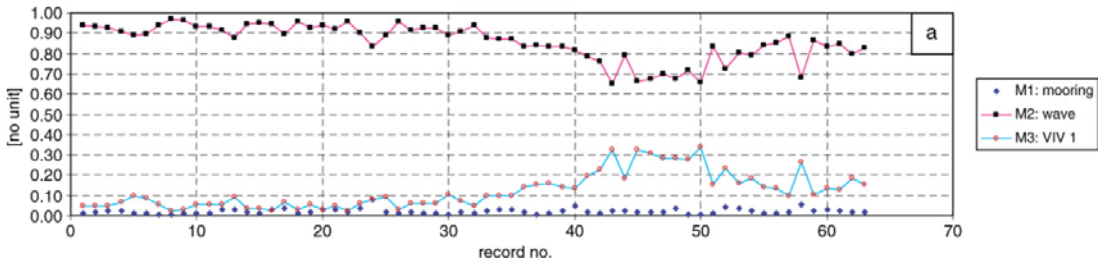

Figure 5.8: Normalised measured contribution to umbilical fatigue damage for Foinaven dynamic umbilical, reproduced from Trarieux *et al.* (2006, p.1689).

Table 5.3 lists a number of mechanical failure modes for marine power cables, and evaluates their applicability for WEC applications. Three mechanical failure modes are likely to be of concern for floating wave energy converters, all of which are most likely to occur near the top-end and along transition points.

1. Exceedance of axial tension limits,

2. over bending of the umbilical,

3. degradation due to cyclic loading.

Table 5.3: Umbilical mechanical failure modes after (Patel, 2008) and applicability to marine energy converters.

Mechanical failure modes	Applicability to wave energy devices
Severe axial tension or torque	Likely for motion dependent devices
Over bending	Likely at attachment points and buoyancy intersection
Crushing due to extreme external pressure	Not likely due to moderate water depth
Hose/tube bursting by excessive internal pressure	Not likely for power cables
Layer separation and instability	Possible
Birdcaging	Possible if umbilical under compression
Loop formation and kinking	Possible during installation process
Mechanical degradation due to wear and fatigue	Can be expected for motion dependent devices
Material degradation	Mainly due to corrosion
Termination problems	Connectors likely to be critical part

5.2.2 Modelling marine cable dynamics

Three different approaches to model the dynamics of marine cables can be distinguished (Vassalos & Huang, 1996):

1. Finite difference methods: Cable motions are described by non-linear hyperbolic equations and are being approximated through finite differences. The equations are solved in the time-domain.

2. Finite element methods: The cable is divided into a number of discrete elements

3. Analytic methods: Simplification of non-linear and coupled cases.

Huang (1999) proposes an analytical model to analyse the stability of the heave motion for cable-body systems. The system is simplified to one degree of freedom

in order to model only the vertical motion with a forced sinusoidal oscillation at the top end. The cable is modelled as spring of bi-linear stiffness and the fluid damping is linearised. It is shown that the system may become unstable for small damping coefficients.

Worzyk (2009, p. 79) presents a simplified approach to estimate the maximum occurring tension forces during the cable laying process (see equation 5.6). The maximal top tension force F_{max} is estimated as the sum of the static tension force F_S (due to the cable weight) and the dynamic Force F_D (due to the ship movement, which is governed by the wave elevation). The maximum vertical acceleration b_{max} is estimated for a sinusoidal heaving motion.

$$\begin{aligned} F_{max} &= F_S + F_D \\ &= w \cdot D + m \cdot b_{max} \\ &= w \cdot D + m \cdot \frac{1}{2} h \cdot \left(\frac{2\pi}{T}\right)^2 \end{aligned} \tag{5.6}$$

Where w = unit weight of cable in water; D = water depth; m = mass of cable; h = heave amplitude; T = movement period; b_{max} = maximum vertical acceleration

While the static force is governed by the unit weight in water, the dynamic force is due to inertia and is therefore dependent on the mass of the cable. Although this equation gives an indication of the maximum tension forces the assumption of sinusoidal movements does not always hold. The wave elevation of real waves does not necessarily follow a sinusoidal motion and has steeper wave fronts. In such cases the resulting forces will be significantly larger than calculated with equation 5.6.

To estimate the umbilical loads a computational model, based on the proprietary marine dynamics software OrcaFlex (Orcina, 2011), has been used. The software is a three-dimensional, non-linear, time domain, finite element program, which employs a lumped mass element approach to solve the dynamic behaviour of line objects.

The modelling of line objects is illustrated in figure 5.9. The umbilical is represented as a series of segments with a node at each end. While the segments carry the axial and torsional characteristics, all other properties such as mass, weight and buoyancy are attributed to the nodes. The occurring forces and moments are applied at the

nodes, while the segments are treated as straight, massless elements, with axial and torsional spring-damping characteristics. The end of each segment additionally carries a rotational spring-damping system that models the bending characteristics.

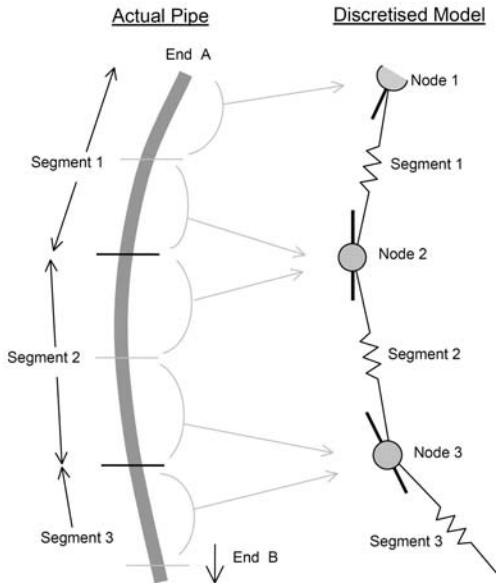

Figure 5.9: Representation of OrcaFlex line model, reproduced from Orcina (2011, p.155).

The algorithm then solves the equation of motion (equation 5.7) for each mid-node of the specified line segments in 5 subsequent steps. The tension forces are computed first, followed by the bending moment, shear forces, torsional moment and total load (Orcina, 2011, p.162 ff.). The simulation considers all geometric non-linearities as the system geometry is recomputed at every time step. Such a dynamic model allows the accurate estimation of realistic loads, i.e. going beyond the simplified sinusoidal estimation which might under predict loads. To achieve this however, the input parameters for the simulation must be highly accurate.

$$M(p,a) + C(p,v) + K(p) = F(p,v,t) \tag{5.7}$$

Where $M(p,a)$ = system inertia load; $C(p,v)$ = system damping load; $K(p)$ = system stiffness load; $F(p,v,t)$ = external load; p = position vector; v = velocity vector; a = acceleration vector and t = simulation time.

5.2.3 Computational model in OrcaFlex

In order to estimate the loads for a typical dynamic power cable attached to a wave energy converter, a model in OrcaFlex has been set up, comprising the following elements:

- OWC device modelled as a vessel object with six degrees of freedom,
- umbilical cable modelled as line object,
- attachment point at the bottom centre of the OWC device, modelled as flexjoint,
- anchor point on the seabed.

The umbilical has been modelled as a double armoured power cable in two configurations, i) catenary as shown in figure 5.10(a) and ii) Lazy-Wave (figure 5.10(b)). In order to achieve the Lazy-Wave shape, additional floats have been covered around the cable. The double armour configuration provides the tension stability and mechanical protection. The total cable length is 120m (catenary) and 130m (Lazy-Wave) in a water depth of 57m which approximately relates to the WaveHub site with 44-60m below chart datum (Penrose *et al.*, 2009). The properties of the umbilical and the buoyancy section are given in table 5.4.

The additional input data for the numerical simulation, describing the motions of the OWC device in six degrees of freedom, is taken from the experimental tank tests described above in section 5.1. The measurements were recorded by the non-contact motion tracking system. A typical time series is shown in figure 5.11, depicting a 30s excerpt of the motion data, recorded during a test run of irregular waves with significant wave height, H_s = 3.5m and wave period, T_p = 8.0s. The translational and rotational response for every motion axis is depicted against the measured wave elevation. The vertical displacement (heave) and rotation of the x-axis (pitch) constitute the main movements of the device. As the OWC device approximately follows the wave elevation, and the x-axis was defined perpendicular to the incoming wave front, the governing motions agree with general expectations.

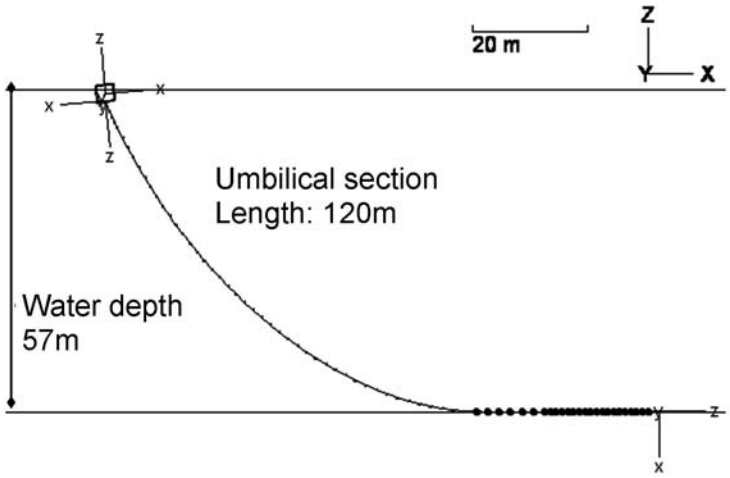

(a) Catenary

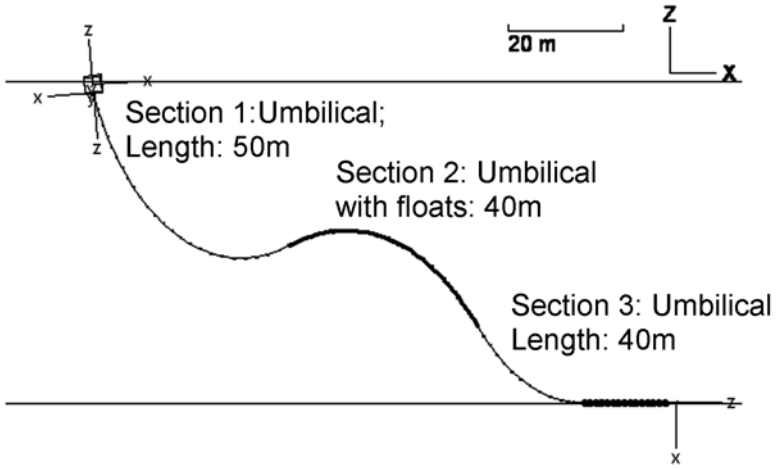

(b) Lazy wave

Figure 5.10: Visualisation of OrcaFlex model configurations, showing armoured umbilical attached to six degrees of freedom floating buoy.

Table 5.4: Characterisation parameter for modelled umbilical; armoured cable properties after Martinelli *et al.* (2010); connection after stiffness Randolph & Quiggin (2009).

Name	Unit	2-Armoured cable	Buoyancy section
Total length	m	50 (section 1) 30 (section 3)	40 (section 2)
Outside diameter	mm	200	306
Nominal weight in air	N/m	706	423
Nominal weight in seawater	N/m	390	-316
Bending stiffness	kNm^2	10	10
Axial stiffness	MN	700	700
Torsional stiffness	kNm^2/deg	600	600
Minimum Breaking Load	kN	100	100
Minimum bend radius (MBR)	m	2	2
Connection stiffness	kNm/deg	x-bend: 10 y-bend: stiff	x-bend: 10 y-bend: stiff

The motions are superimposed on the floating six degrees of freedom buoy with the connected umbilical. Hence the assumption made for the model is that the umbilical itself does not significantly alter the motion of the floating device. As the mass of the device is much larger in comparison to the mass of the umbilical cable, this assumption is considered to be reasonable. The integration time step was set to 0.02s, which is sufficiently small to capture high frequency responses. The numerical simulation was subsequently run for each of the 12 different sea states described in section 5.1.5, figure 5.5.

5.3 Dynamic Marine Component test rig

For the present thesis there was always a question to what extent dedicated component testing is needed to assess the reliability of wave energy converters, and how this may be facilitated and implemented. This section aims to provide a substantiated rationale for the development of a novel test rig, the Dynamic Marine Component test rig [DMaC]. As with most engineering projects, the development and implementation of the DMaC

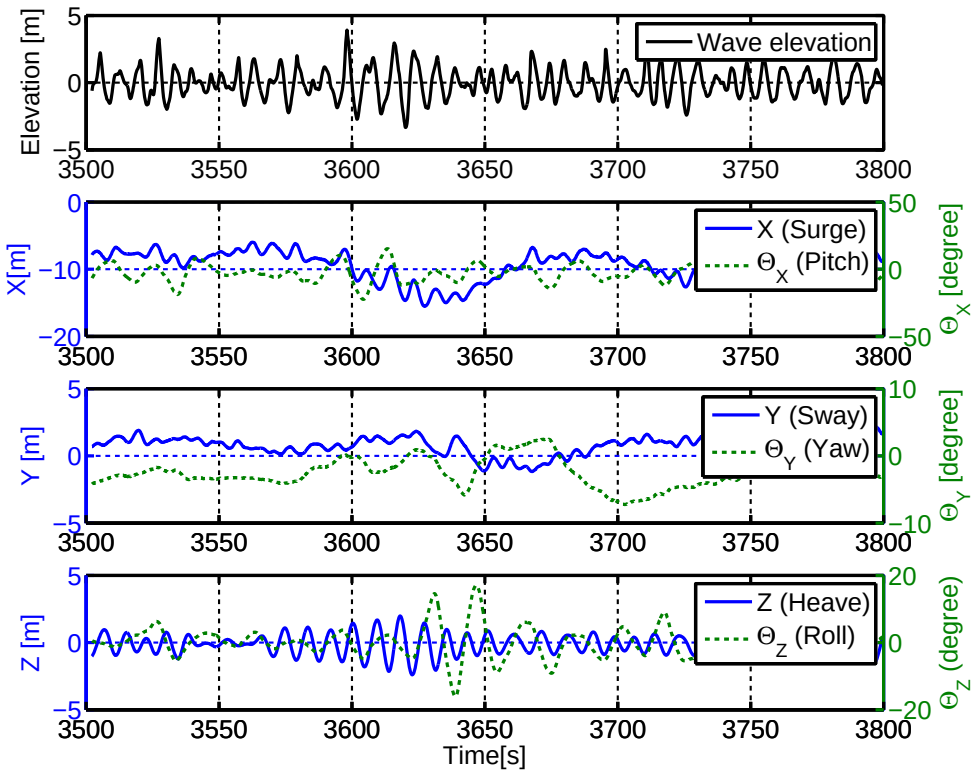

Figure 5.11: Sample section for six degrees of freedom motion used as input data for numerical simulation; top - wave elevation; three lower plots - translational and rotational displacement for each axis. Translational motions (X, Y, Z) on left ordinate and rotational motions (Θ_X, Θ_Y, Θ_Z) on right ordinate. Motions recorded during irregular wave spectrum, $H_s = 3.5$m and wave period, $T_p = 8.0$s.

was the effort of a team of engineers. The authors contribution was mainly made in form of the conceptualisation, the specification of test requirements and as the initial user of the test rig. The actual engineering, i.e. detailed system design, manufacturing and assembly was undertaken by Event Horizon Ltd., Somerset, who were awarded the contract following a European tender process.

5.3.1 Rationale for a novel test rig

Component reliability testing is carried out in most industry sectors to verify that the products meet the specified reliability targets and customer expectations. In the case of electronic components, systematic tests have been carried out for decades to determine the relationship between stressors and the associated time to failure (Meuleau, 1965).

Industry sectors such as the automotive, aviation, offshore oil and gas, or mining, have to meet safety requirements as well as a specified operational reliability. In order to provide the necessary assurance, reliability testing of components and complete systems has been extensively used. A bibliographic list can be found in Dhillon (1992, 2007).

The need for extensive component testing as a means to improve the reliability of marine energy devices has been repeatedly emphasised by various authors (Callaghan & Boud, 2006; Mueller & Wallace, 2008; Salter, 2003b; Wolfram, 2006). In general, component testing promises the opportunity to reveal and investigate occurring failure modes, to optimise the component design, and to collect the data required to estimate more appropriate failure rate probabilities through consideration of expected operational and environmental loads.

There is a multitude of different reliability tests. A general classification regarding the test purpose is reported by Schijve (1985):

- Testing of full-scale structures,
- testing of specimens,
- comparative tests,
- model validation testing.

A further useful distinction, with a view of how accurate field loads are replicated and how they are accelerated, is made by Klyatis & Klyatis (2006):

- Field testing of complete systems with accelerated operating conditions
- Laboratory testing of systems by means of physical simulation of field loads
- Computer simulation of system and field loads

Both classifications can also be ranked in order of cost and complexity. It is certainly the most expensive and most complex operation to test the complete full-scale structure under (accelerated) operating conditions. At the other end of the scale, a virtual, computer-aided test is a less costly alternative but may not provide the required level of assurance. In this respect, the kind of testing that is targeted with the DMaC should accommodate full- or large-scale components that are tested under physically simulated and, if possible, accelerated load conditions.

The question of how test type, load acceleration and safety factors are related to each other has been explored by Raath (1997). He suggests that the type of test determines the level of the required safety factor, with high safety factors for highly accelerated single axis tests, medium factors for multiple loading and medium acceleration and low safety factors for service load simulation and in service testing (see table 5.5). Service simulation testing applies selected field loads to approximate the field load conditions.

Experience in reliability engineering has shown that dedicated component testing is able to improve the accuracy of reliability estimates (Elsayed, 2003). Thus, accurate service load simulation tests can contribute to reduce costly safety factors of components and obtain reliability information at the same time. It therefore is a promising test approach for wave energy converters.

However, most test efforts that have been reported for wave energy systems are mainly concerned with demonstrating the power take-off performance. An implicit assumption may be that the reliability behaviour of the components will be similar to that experienced in other application fields. Yet, it is important to consider the particular problems imposed when components are incorporated into WEC system. For example,

the mooring system or the umbilical cable will be exposed to unusual load time histories as part of the dynamic system, which will impact on the component reliability. Component failures described in the technology review in section 2.2 had in common, that field load conditions were not anticipated for allegedly reliable components.

An example where extensive component testing is performed in order to avoid unexpected failures in a marine environment, is in the assessment of offshore moorings. Specific operational conditions such as the tension-torsion fatigue behaviour of wire ropes is carried out by Ridge (2009), while TTI (2006) engages in detailed examination and tensile testing for internal wear and Williams *et al.* (2002) test damaged mooring ropes in order to determine their damage-tolerance behaviour. These tests apply traditional tension testing to determine component reliability under specified load conditions.

A simple tensile test is not sufficient to investigate the particularities of wave energy converters. The experimental and numerical studies reported in this thesis, and evidence gathered in field tests, such as the South West Mooring Test Facility [SWMTF] (Johanning *et al.*, 2008, 2011), suggest that at least three degrees of freedom are required to replicate the dynamic mechanical load regime that a floating system is subjected to. The component test rig described below, aims to replicate the dynamic movements of mooring assemblies, and other components/sub-systems, in order to assess the reliability implications of operational field loads.

Table 5.5: Test type and required safety factors, after (Raath, 1997).

Test	Acceleration	Loading	Safety factor
In-service	None	Actual	Low
Service load simulation	Low	Selections of true loading	Low
Cyclic multi axis	Medium	Multiple level	Medium
Cyclic single axis	High	Single level	High

From simulation tests in the automotive and other industries Weltin (2009) identifies four key steps:

- Measuring realistic load data

- Identify representative loading regimes
- Testing a (representative) sample on a laboratory test rig
- Root cause analysis and statistical evaluation of test results

Realistic load data is ideally measured in situ. For example, the loads that a component is subjected to during operation, at the installation site of the device. As field deployments incur considerable installation cost, alternative data sources for realistic loads may be real sea test facilities or large scale tank tests.

Once representative load data is established, the most severe load cycles can be used to derive a loading regime for laboratory testing. For fatigue tests, such a load regime may be generated by means of a Rainflow cycle count (described in section 6.1.3.1).

Heuler & Klätscke (2005) describe how standardised load spectra and load-time histories have been generated for a range of industries, to assess the fatigue behaviour of structures and components. This service simulation testing is deemed necessary when simple constant amplitude load assumptions do not provide a sufficient level of confidence. This is particularly the case if the load spectra significantly differs in amplitude and mean-stress variations when compared to constant amplitude loading and multiaxial loading. Due to the irregular nature of realistic wave profiles, the associated loads for most wave energy components meet the conditions required to advocate a service simulation test approach. A number of standardised load-time histories are in use, which cover the representative fraction of the expected in-service spectrum in order to facilitate fatigue analysis and testing. Standardised load sequences and load time histories have been proposed for aircrafts (TWIST, FALSTAFF), helicopters (HELIX), cars (CARLOS), wind turbine blades (WISPER/WISPERX) and offshore structures (WASH). This thesis attempts to estimate the annual load spectrum for mooring lines in a wave energy application (see section 6.2).

The laboratory tests are typically performed on a purpose built test rig that subjects the component under investigation to the representative load regime. In order to complete the testing within justifiable time and cost budgets, the load signal is usually reduced and if possible accelerated. Accelerated testing cycles the items under more severe stresses than the expected normal operation, which leads to earlier failures

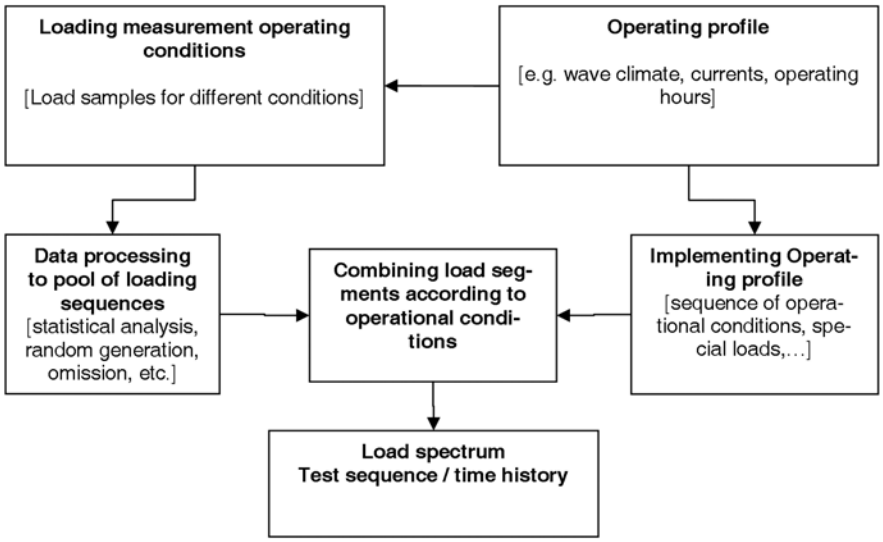

Figure 5.12: General simplified approach for the generation of standardised load-time histories for service simulation testing, based on Heuler & Klätscke (2005).

and hence reduced testing periods. It is important that the failure mode of normal operation and accelerated conditions stays the same (Lydersen & Rausand, 1987).

Escobar & Meeker (2006) distinguish four general possibilities that can be applied to accelerate reliability tests, by increasing the following characteristics:

- Use rate of the component, e.g. increased load cycle frequency,
- radiation exposure intensity, e.g. increased UV radiation,
- ageing rate of the component, e.g. increasing the chemical degradation process through higher levels of humidity,
- test stress levels, e.g. increased load force ranges compared to normal operating conditions.

The development and implementation of a purpose built marine component test rig that is capable of performing service simulation tests is described in the remainder of this section, while the results for initial tests with a marine power cable are reported in section 7.

The service simulation test approach can thus be summarised in four steps (see also figure 5.12):

1. Characterise the environmental climate of a specific installation location.
2. Measure realistic load and response characteristics for the component.
3. Analyse and extract representative/severe load cycles and combine load segments according to environmental conditions.
4. Conduct laboratory component testing with established load spectrum.

5.3.2 Design requirements

At the heart of the design requirement for any component test rig lies the test cycle that can be performed.

> A cycle with a high degree of simulation is more complex and is closer to the actual conditions of use (...). A high degree of simulation is recommended when the outcome of the test is crucial, for example, when failure consequences are critical in terms safety and economic loss (...) (BS 5760-10.2:1995, 1995).

The objective for the DMaC was to replicate the marine environmental load conditions as closely as possible, to enable a service simulation approach. The specific design requirements of the component test rig have evolved with time, incorporating restraints with regards to cost, physical size and performance capabilities, but the specifications were guided by the following requirements.

On a machine level the design requirements were those of a conventional test rig:

- Force transmission: The subsystem that directly acts on the specimen/component.
- Drive/Actuation: In order to transmit the forces necessary for component deformation the point of force transmission needs to be actuated; this is achieved with a servo-hydraulic system.
- Control: The drive has to be controlled for a systematic deformation of the specimen.

- Response structure: The actuated forces need to be balanced with a structural frame.
- Measuring instruments: To control the actuation and acquire the specimen response, all relevant parameters have to be measured.
- Data acquisition system.
- Programmable Logic Controller (PLC): To enable the control and comparison of set-point and actual value of the specimen response, the PLC must provide the set-points.

Beyond that, the proposed test rig should have unique features to facilitate the dynamic testing of components in large scale, under a controlled environment whilst applying realistic motion characteristics. The three features allowing such advanced testing are:

1. Constructing the test rig with a system to immerse the tested component
2. Construction of a three degrees of freedom moving headstock to allow replication of dynamic response as seen by component in realistic application
3. A linear hydraulic actuator at the far end to provide necessary axial loading.

5.3.3 Concept design

The initial idea for the concept design of the novel test rig emerged from the six degrees of freedom motion table, which has been invented by Stewart (1965), and has since found wide application in flight simulators and shaking tables.

The general working principle is depicted in figure 5.13. The motion platform is attached to three hydraulic actuators through tri-axial joints. Each actuator is mounted on the foundation with a biaxial joint, where one of the axes is controlled, and the other is free to rotate. This design is capable of producing controlled six degrees of freedom motions with high accelerations, but the excursions are restricted to the length of the hydraulic actuator. Another restriction for the component testing objectives sketched above is that the mechanical forces acting on the component, such as bending moments, or tension forces, can not be replicated.

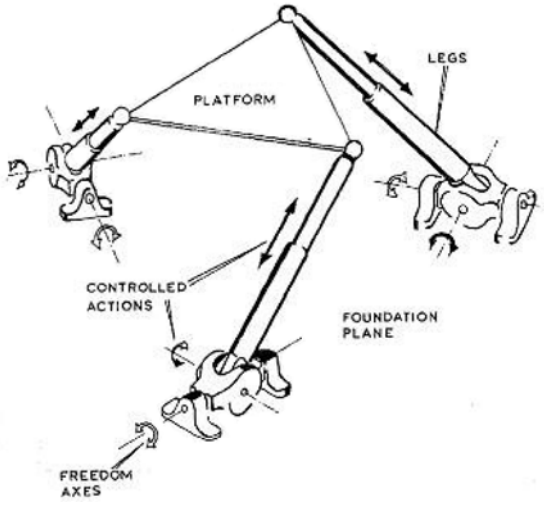

Figure 5.13: General principle and arrangement of a 6 degree of freedom (6DOF) moving table, reproduced from Stewart (1965, p.372).

The initial design concept for DMaC emerged as an amalgamation of the six degrees of freedom motion table and a conventional tensile test rig. The early concept design is depicted in figure 5.14. The rig comprises three main elements:

- A moving vertical platform which is termed 'moving headstock' to replicate motions for three degrees of freedom, i.e. pitch, yaw and roll motions, which are referred to as x-bending, y-bending and z-rotation.

- A linear actuator to provide the axial loading in z-direction, referred to as z-force.

- A reaction frame to resist the forces and motions induced by the test rig.

Both a three degrees of freedom moving platform, and the tensile testing arrangement, are being used for purposes such as motion simulators, and simple material tests. The unique feature of this test rig is to combine these two test methods to replicate dynamic loading under immersed conditions. To be able to replicate the motion and forces experienced by a WEC, or sub component, the test rig provides a pulling and pushing force (z-force) together with motions in three degrees of freedom, imposed by the moving headstock, to represent the loading conditions induced by the wave motion.

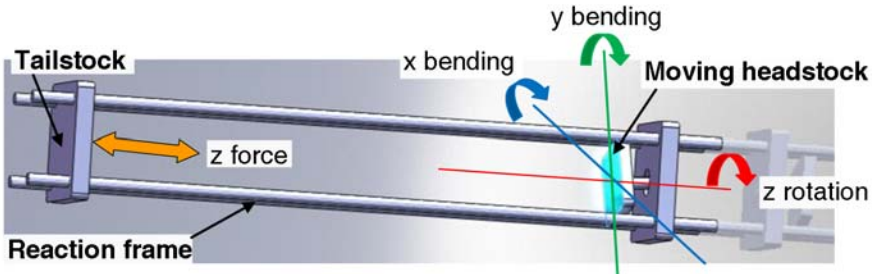

Figure 5.14: Illustration of initial test rig concept with four degrees of freedom, drawing courtesy of D. Parish.

5.3.4 Specification development

After the general working principle and the concept design are established, the specific physical dimensions of the rig, as well as the load envelope for the desired capabilities of the test rig, must be established. The main source of information that served as a reference load case is the load data described in section 6.1 and 6.3. A simple hydraulic model was developed to estimate the required flow and pressure for different load cases. A high level overview of the model layout is presented in Annex D.

The requirement for the definition of a load envelope was twofold:

1. Specification of required excursions and force that can be applied
2. Specification of frequency ranges for particular displacement or force

From the tank experiments, a superposition of high and low frequency tensile loads could be observed. As a result, two distinct reference cases were defined, i) a relatively stiff component which would not allow large amplitude extensions, but has higher frequency oscillatory loads and ii) a relatively elastic member which would have larger tensile displacements at lower frequencies. A total of four cases has been specified for compound sine waves, as listed in table 5.6. The two cases where the displacement signal is a superposition of two signals, consisting of a larger, low frequency displacement and a smaller, high frequency displacement, are illustrated in figure 5.15 below.

To specify the headstock capability, the desired bending angles have been determined based on the numerical simulations results of experimentally measured motions (see sections 5.1 and 5.2.3). Across the range of tested sea states, the angles at the top end of the power cable have not been outside a relative range of 60°. Figure 5.16 shows

Table 5.6: Design cases for the capabilities of the linear actuator displacement signal design for the DMaC test rig.

Case	Amplitude 1 [m]	Frequency 1 [Hz]	Amplitude 2 [m]	Frequency 2 [Hz]
Elastic 1	0.5	0.1		
Elastic 2	0.25	0.1	0.05	1
Stiff 1	0.05	1		
Stiff 2	0.025	1	0.005	10

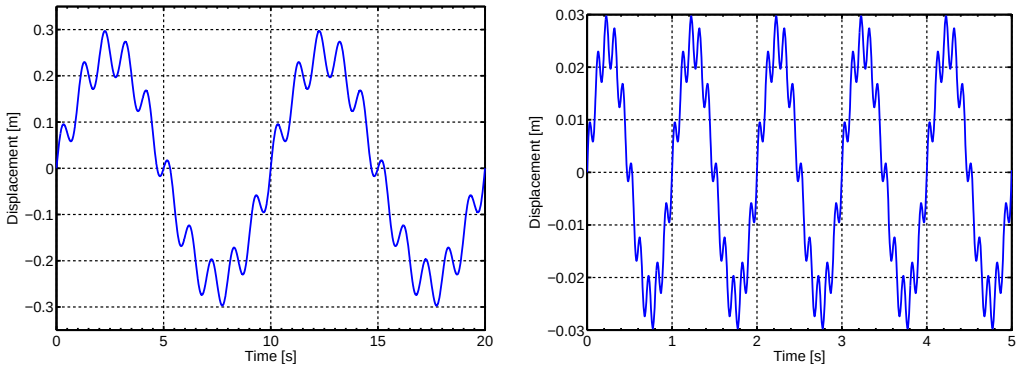

(a) Elastic member (b) Stiff member

Figure 5.15: Load case specification for superimposed amplitude signal for linear actuator.

a plot of two angles, Ezx- and Ezy-plane, which represent the two bending regimes (x- and y-bend). It can be seen that a relative angle of $\pm 30°$ is not surpassed in the case of irregular or large waves.

The required bending frequency for the headstock was similarly specified from the combination of experimental and numerical tests. A frequency of $f_{bend} = 0.5Hz$ was deemed to be sufficient. The angle of the Ezx-plane in figure 5.17 oscillates at a frequency, f, of approximately 0.15Hz, in an irregular sea state with $T_p = 8s$.

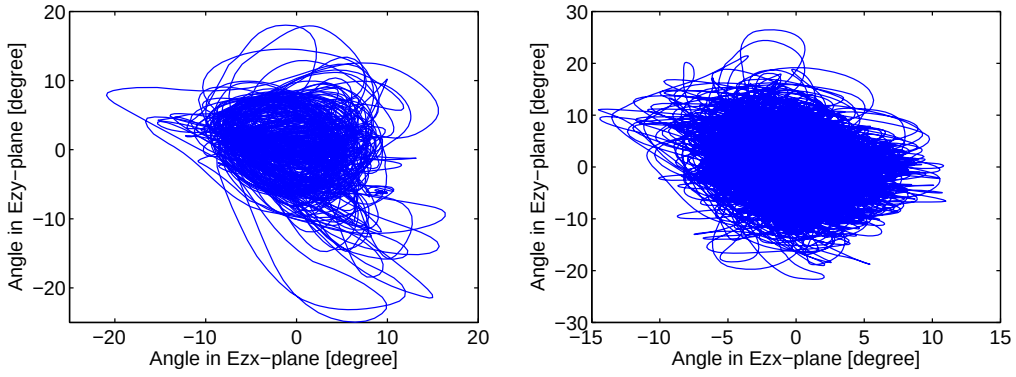

(a) $H_s = 6.0m$; $T = 8s$, regular (b) $H_s = 3.5m$; $T = 8s$, irregular

Figure 5.16: Demeaned top end angle ranges from numerical WEC model using experimental motions.

Through consultation within the design team and potential supply companies, further technical parameters of the rig have been specified as follows:

- Linear z-actuator: Maximum tensile force $F_{max} = 30t$
- Test bed: 6m working length
- Headstock test bed: diameter of 600mm with component mounting arrangement
- Headstock x-bend: +30° to -30° in 2s
- Headstock y-bend: +30° to -30° in 2s
- Headstock z rotation: continuously

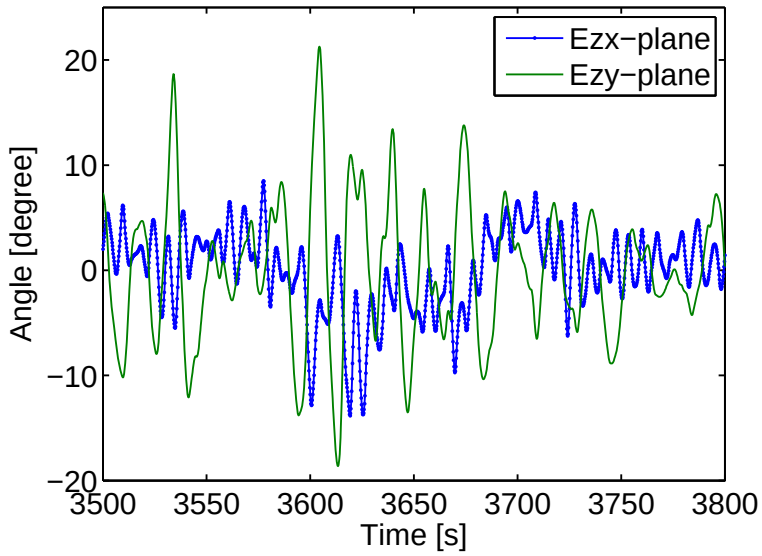

Figure 5.17: Time series of demeaned top end angles for DMaC specification, $H_s = 3.5m$; $T_p = 8s$, irregular waves.

5.3.5 Tender process and contract award

The University of Exeter must adhere to The Public Contracts Regulations when it contracts supplies and services. As such, for contract volumes above a the threshold of £139,000 (as of 2009), the contract must be publicly tendered in the Official Journal of the European Union (EU, 2009b). This journal is the official document in which public sector tenders are advertised.

As the available budget for the design, manufacturing, installation and commissioning of the test rig, was above this threshold, the project was subject to European tender in the OJEU, too.

Thus, a prior information notice was issued on 20/10/2009 ((EU, 2009c), which announced the upcoming tender for "machines and apparatus for testing and measuring". On the 25/11/2009, the subsequent contract notice was issued (EU, 2009a) and called for any interested company to submit a project proposal.

Four companies submitted their proposals and anticipated project cost. The evaluation of the various proposals was conducted in form of a panel scoring exercise for a range of criteria, specified in table 5.7. The content and evaluation of the tender

have been made available to the participating parties in form of a evaluation document (Clifford *et al.*, 2010). However, the details of the proposals are confidential and no further detail can be provided here.

The company Event Horizon Ltd. (2010) based in Somerset, Devon, were awarded the contract to design, manufacture, install and commission the test machine (University of Exeter, 2010).

Table 5.7: Award criteria for the evaluation of DMaC tenders.

Criteria	Possible
Cost	10
Specification	
Tailstock actuation and capacity	15
Headstock functionality	15
Software (test schedule, operation, post processing)	10
Functional guarantee and warranty	8
Specimen wetting system	3
Training, manuals and documentation	5
SCADA hardware	5
Maintenance/servicing	3
Energy use and installed electrical power capacity	5
Personnel and machine safety systems	3
Discretionary award for additional technical aspect	5
Delivery lead-time	8
Vendor questionnaire	3
Local procurement / sub-contracting	2
TOTAL	100

5.3.6 Implementation and Capabilities

The initial concept design was further developed in collaboration with Event Horizon, who conducted the system engineering for the test rig. In the following, the detailed design and capabilities of main sub-systems are described. These are the reaction frame and test bed, the moving headstock, the tailstock (z-force), the hydraulic power system

and the control and measurement capabilities.

An overview of the overall dimensions and layout of the test rig is shown in figure 5.18. The forces generated and applied through the four degrees of freedom are fully reacted by the frame. The frame itself is approximately 10m in length and hosts a test bed of maximal 6m in length. The length of the test bed, i.e. the distance between the two force application points, is adjustable between 1-6m. The frame itself is surrounded by a sealed outer housing which enables a test operation under wet conditions, where the item is submersed in fresh water.

The moving headstock is realised through a two-plane-gimble system. The inner gimble is pivot-mounted to the outer gimble ring, which itself is pivot-mounted to the main frame of the rig. Figure 5.19 shows the design and assembly arrangement for the gimble system. The outer ring is pivoted on the horizontal axis and thus performs the y-bending, while the inner ring is pivoted on the vertical axis and conducts the x-bending movement (figure 5.19(c)). Each axis has an angle encoder fitted to monitor and control the angular position of both rings.

The rings are driven by four hydraulic actuators which are pivot-mounted on the inner ring (see figure 5.20) and are reacted by the brace of the headstock. The superposition of linear displacements by the hydraulic actuators achieves the desired angular motion of the inner and outer ring. The maximum angular displacement of the two gimbles is $\pm 30°$, with a frequency, $f = 0.25$Hz, exerting a maximum off-axis bending moment in relation to the centre point, $M_{max} = 10kNm$. The dimension of the test specimen is constrained by the brace at the headstock, allowing a maximum diameter $D_{max} = 800mm$.

At the other end of the rig, the z-force is applied by a single hydraulic actuator, which is mounted on a moveable trolley that is bolted down to the main frame at the desired position (figure 5.21). In this way the available test bed can be varied in length to accommodate different specimen lengths and/or to allow potential preloads. The key functional parameters are listed in table 5.8. The main limiting factors are the maximum displacement stroke of 1m and a maximum applicable force of 45t in static conditions, or 30t under dynamic conditions.

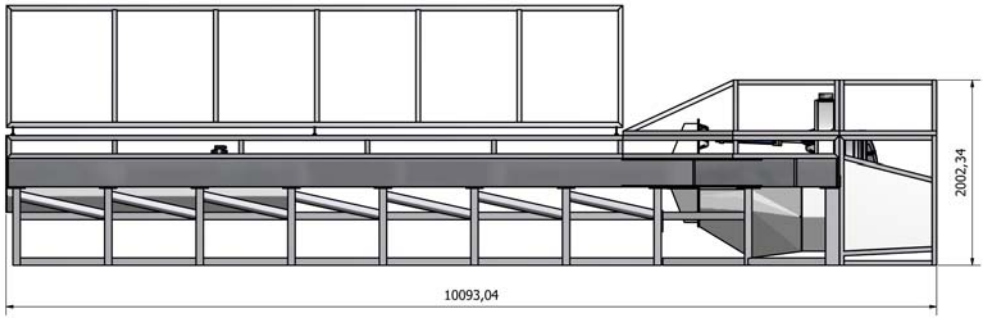

(a) Side view, dimensions in (mm)

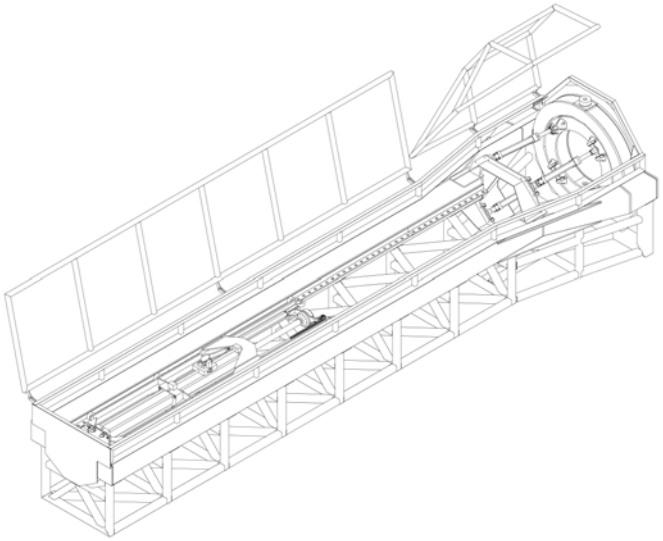

(b) Elevated view

(c) Assembled machine

Figure 5.18: Dynamic Marine component test rig.

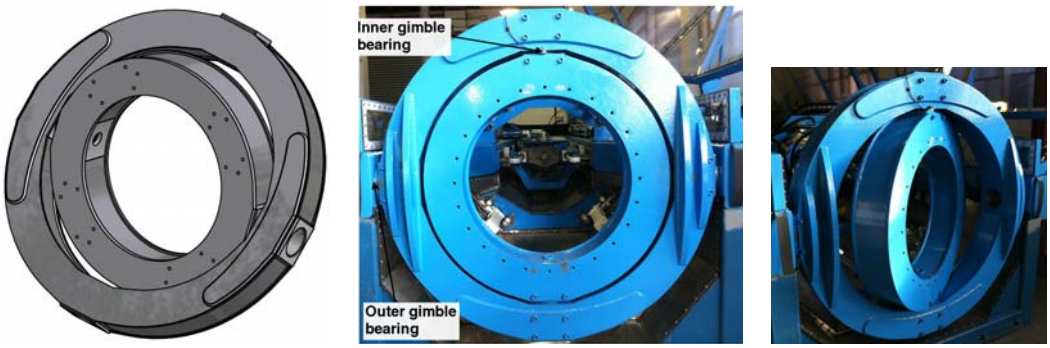

(a) Design drawing (b) Plane rings (c) Tilted inner ring

Figure 5.19: Moving headstock gimble system of Dynamic Marine Component test rig.

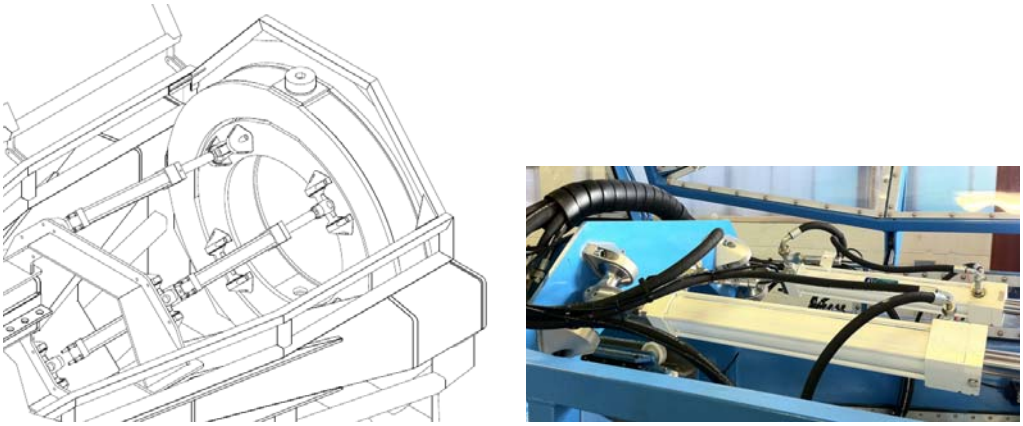

(a) Design (b) Assembled actuators

Figure 5.20: Moving headstock hydraulic actuator arrangement of Dynamic Marine Component test rig.

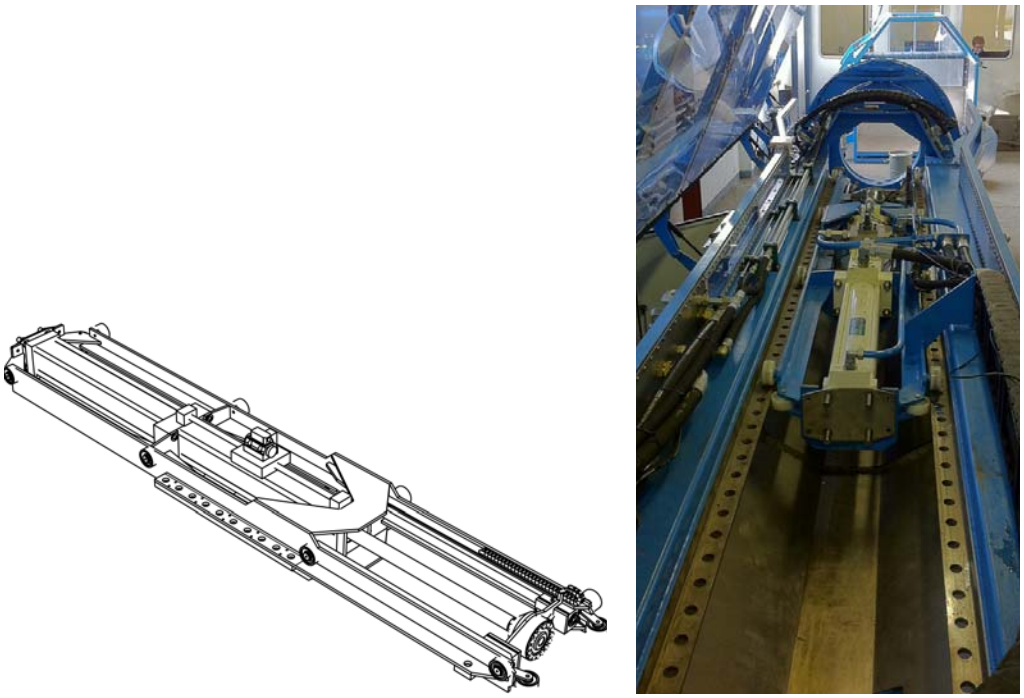

(a) Design

(b) Assembled linear actuator, short test bed position

Figure 5.21: Linear actuator arrangement with moveable trolley to adjust test bed.

Table 5.8: Functional capabilities and dimensions of hydraulic actuator supplying force at tailstock of Dynamic Marine Component test rig.

Parameter	Value
Maximum stroke	1m
Rod diameter	70 mm
Bore	160 mm
Maximum Dynamic Force	30 t
Maximum Static Force	45 t
Servo-hydraulic control valve	462 l/min
Pre-load force	14 t
Maximum specimen length	6 m
Maximum specimen diameter	800 mm
Maximum specimen weight	1000 kg

The test rig is connected to a 130kW electrical supply, with a voltage of 415V, which supplies the hydraulic power pack unit. The hydraulic power is generated with 2 variable displacement pumps that supply the pressure to both the hydraulic actuator circuit (140 bar) and the pilot circuit (210 bar), to operate the hydraulic control valves. The maximum achievable flow rate is about 360 l/min (see also table 5.9).

Table 5.9: Rated power of electrical supply and hydraulic power system for Dynamic marine component test rig.

Electrical Power Supply		Hydraulic Power Unit	
Parameter	Value	Parameter	Value
Power	130 kW	2 x Induction motors	55kW each
Voltage	415 V	2 x variable displacement pumps	
		Drive Circuit Pressure	140 bar
		Flow Rate	362 l/min
		Pilot Circuit Pressure	210 bar

The control and measurement capabilities are listed in table 5.10. The rig can be operated in two distinct modes in which either the force exerted on the specimen or the displacement is chosen as control parameter. Depending on the chosen control mode, the linear force (z-force) and the exerted bending moment are controlled, or the linear displacement together with the angular motion of the headstock. The position control frequency reaches 120kHz. The data acquisition system offers 32 analogue inputs, 8 differential inputs for strain gauges together with a total of 32 digital and 16 analogue outputs. The maximum sampling frequency is 250kHz.

5.3.7 Umbilical cable test

The experiment was carried out at the DMaC test site located at A&P Falmouth, Docks. The test specimen was provided courtesy by JDR cable systems and is a typical subsea umbilical. Although the actual components of the umbilical will vary for wave energy converters, the construction, armouring and general properties are comparable.

The cable was connected to the test rig at the moving headstock and the tensile forcing end of the rig. At the moving headstock the cable is secured into a steel socket,

Table 5.10: Measurement and control capabilities of Dynamic marine component test rig.

Item	Description
Programmable test design	Force or Displacement driven control
Data acquisition and control channels, National Instruments Compact RIO / Labview system	32 analogue inputs, 8 differential strain gauge inputs, 64 digital inputs, 32 Digital Outputs, 16 Analogue Outputs
Sampling frequency	250 kHz
Position control frequency	120 kHz

using resin, fabricated by JDR. In order to connect the socket to the bottom plate of the test rig, a circular steel plate has been welded onto the socket. The socket is bolted to the bottom plate of the head stock to make a rigid connection (figure 5.22).

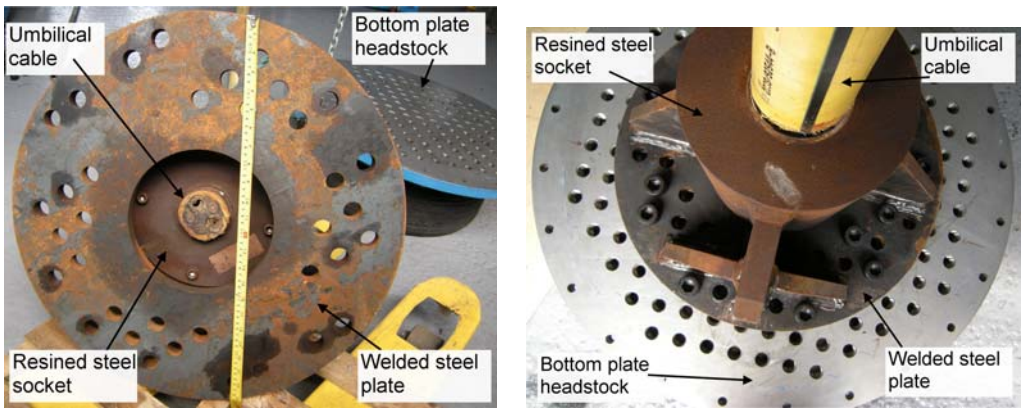

(a) Rear view (b) Top view

Figure 5.22: Umbilical cable connection to headstock plate.

At the other end, where the tensile force is exerted, the cable is clamped by two cylindrical steel sections which are fitted with internal rips that grip the cable. The clamp is tightened with bolts at either side and is connected to the load cell on the

hydraulic linear cylinder, using a pin joint connection (figure 5.23).

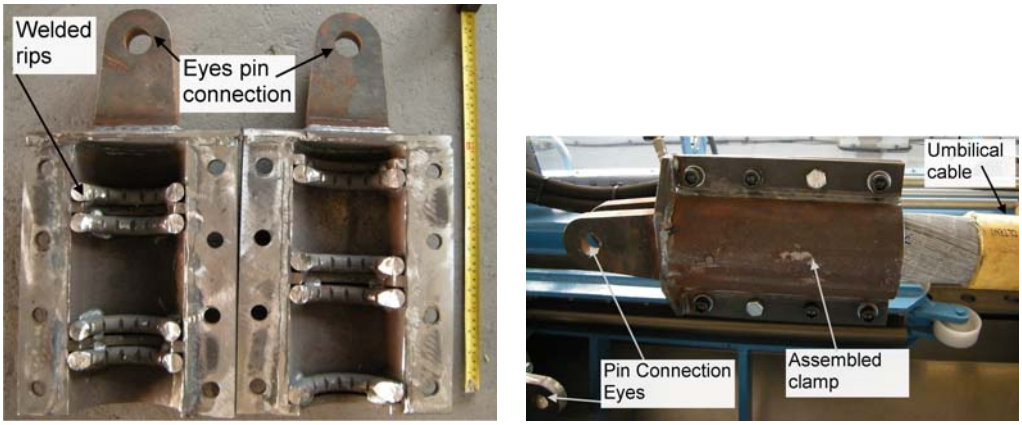

(a) Inside view (b) Clamp assembled

Figure 5.23: Umbilical cable clamp to linear cylinder.

Figure 5.24 shows the experimental set-up with the cable fitted to the test rig. The rig is instrumented with the following measurement equipment:

- Force load cell measuring the tensile/compressive force that the specimen experiences at the end of the linear cylinder.
- Linear displacement encoder measuring the stroke position of the linear actuator.
- Rotary encoder measuring the angle of the x-bend and y-bend plane.
- Pressure transducers at each of the hydraulic actuators.

Before the experiment, it was ensured that the displacement settings of the x-bend and the y-bend ring where set to an angle $\Theta = 0$ degree. The linear tensile force cylinder was also set to a displacement $D = 0$, where 0 was chosen as the midpoint of the 1m stroke. Thus, a retraction of the cylinder is defined as negative displacement, while an extension is read as a positive value.

The sign convention for the force reading of the load cell considers tensile forces as negative values and compression as positive. Positive angles on the y-bend axis are defined that the top of the ring bends leans towards the test bed. While for the x-bend ring a positive angle means that the outer right hand side bends towards test bed.

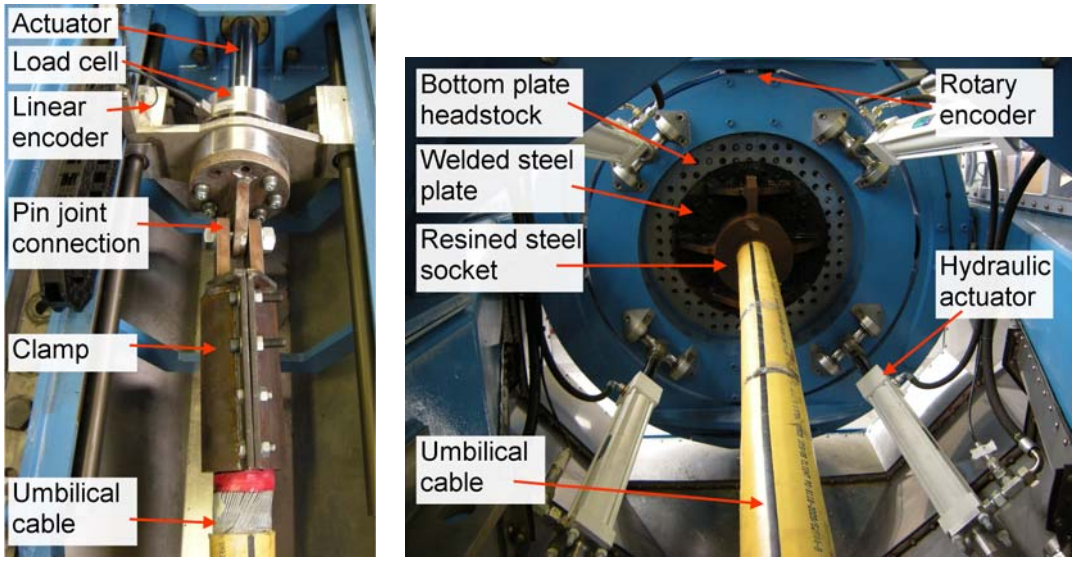

(a) Linear actuator (b) Moving headstock

Figure 5.24: Experimental set-up with umbilical cable fitted to test rig.

The test procedure for each conducted test was as follows:

1. Defining the test signal, specifying displacement or force parameters for each of the three axis.
2. Saving and importing test signal as Comma Separated Values (CSV) file format.
3. Choice of displacement and force parameters, sampling rate, interpolation method for the time series, control parameters and data logging channels and time steps.
4. Test data is sent to the rig controller and written to the input file of the controller.
5. Start of the test.
6. Test observation by visual control, camera recording and real time data streaming of the output signals.
7. Downloading and archiving of logged data file.

Chapter 6

Determination of component load conditions

This chapter aims to determine operational load conditions of components. The components considered, moorings and marine power cables, were chosen because they generically apply to floating wave energy converters. Even though the presented results are specific to the type of device and the considered test conditions, some general findings can be made.

The chapter covers different setups which are representative for typical early development stages of WECs. Experimental wave tank tests form the basis of initial concepts and yield data on device performance and component loads at laboratory scale. The results of experimental mooring tests are analysed in section 6.1. The results are further used to estimate the annual field load conditions that the moorings would experience at a particular site section 6.2. The experimental information is further used for a hydrodynamic numerical model to predict and evaluate component loads which were not considered during the experimental tests. This allows to model changes in component configurations while the hydrodynamic properties of the floating device are kept constant. Section 6.3 assesses the mechanical load conditions for two power cable configurations.

6.1 Mooring load analysis

The mooring load analysis covers two aspects that are crucial from a reliability perspective. Firstly, the peak loads need to be assessed to ensure the occurring loads do not surpass the maximum strength of the moorings. Secondly, the cyclic load conditions which hold the potential for fatigue failures are assessed. Both aspects have their peculiarities in the wave energy case. Extreme loads may occur under operational conditions and fatigue is one of the most likely failure modes to be of relevance for marine energy devices due to the highly oscillatory nature of induced motions and forces.

The section falls into three distinctive parts. The initial assessment of mooring loads seeks to illustrate the interrelation of incident waves, device motions in six degrees of freedom and tension loads. This is followed by identifying the maximum mooring loads where extreme, so called snap loadings, are observed for the range of sea states. Thirdly, the rainflow cycle analysis method is being applied to estimate the fatigue damage.

6.1.1 Interrelation of waves, motions and tension loads

As a first investigation of the data, the relationship between incident waves, induced device motion and resulting tension loads are of interest. For this reason an automated plot showing the incident wave elevation and mooring forces in all three mooring lines was used.

Figure 6.1 shows a typical 25 second window for the 3030 test with an irregular sea state of $H_s = 3.5m$ and $T_p = 8s$. It can be seen, that the tension force of the leading mooring Line L1A closely follows the shape of the incident wave record. Another observation is that the tension increases in line L1A with an incoming crest and decreases towards the trough. The rear mooring lines L2A and L3A show increased tensions towards the wave trough and become slack, i.e. are not tensioned, with incoming crests. The plot also reveals the high sample frequency adopted to ensure a satisfying resolution of dynamic events.

A more detailed investigation of the governing device motions which lead to the observed mooring loads is achieved with a simple plot of wave elevation, tension force of the leading mooring line and device motions in all 6 DOFs. Figure 6.2 plots a 500s window with a high tension event at around 3,630s. It is evident that the device motion is a superposition of low and high frequency components.

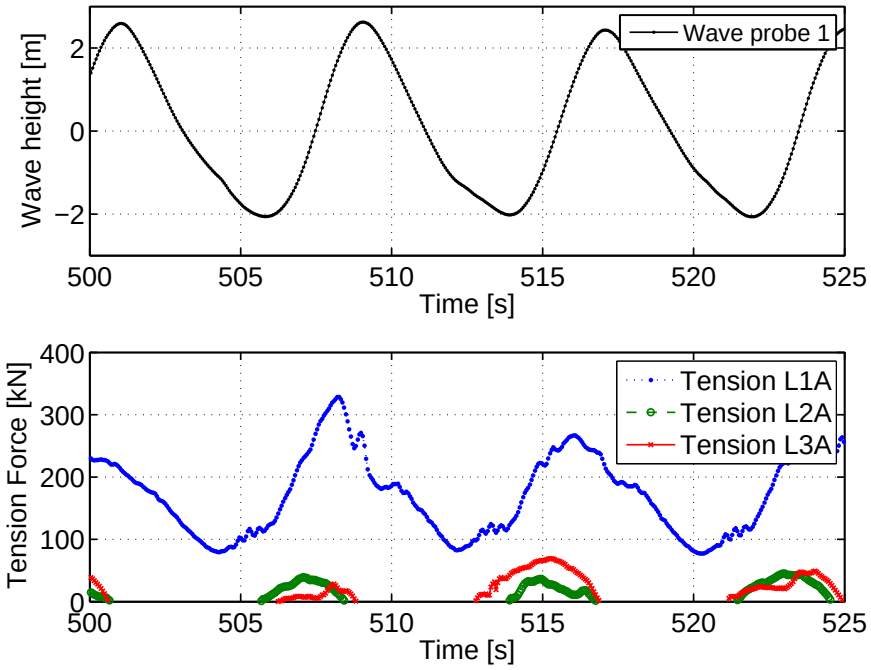

(a) Regular waves $H_s = 4m$, $T_p = 8s$

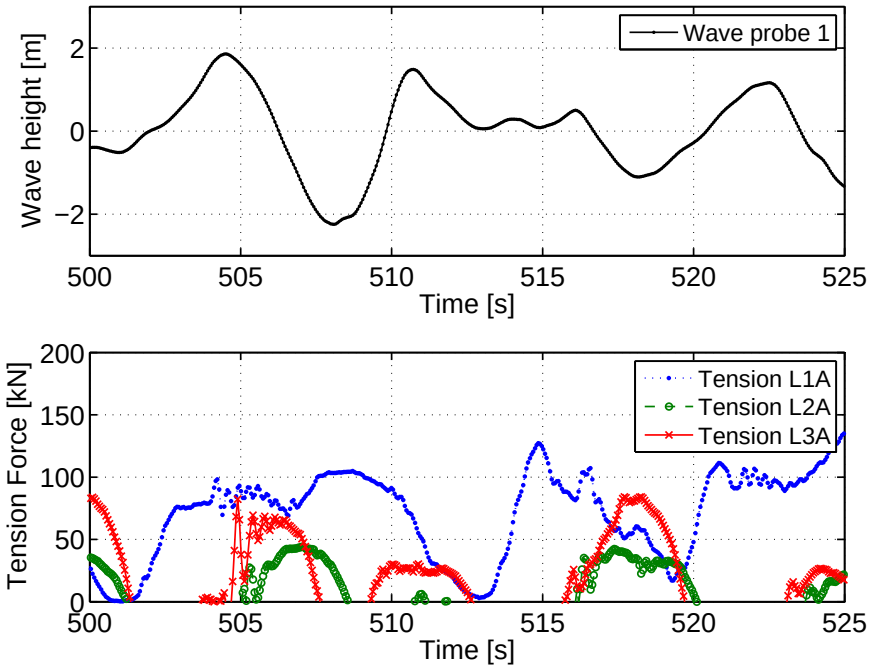

(b) Irregular waves $H_s = 3.5m$, $T_p = 8s$

Figure 6.1: Typical time series of wave elevation and mooring line tension force.

The translational motions are dominated by heave and surge components while there is only a limited amount of sway. It is also shown that there is a significant offset in the X position which is due to the incoming waves which push the device away from its origin position.

For the rotational motions, pitching and rolling motions are more pronounced with amplitudes of up to 20°. Under the simulated conditions yaw motion is small. While this type of plot gives some information about the prevalent device motions it is difficult to identify the motion characteristics that are associated with high load events for the entire time series.

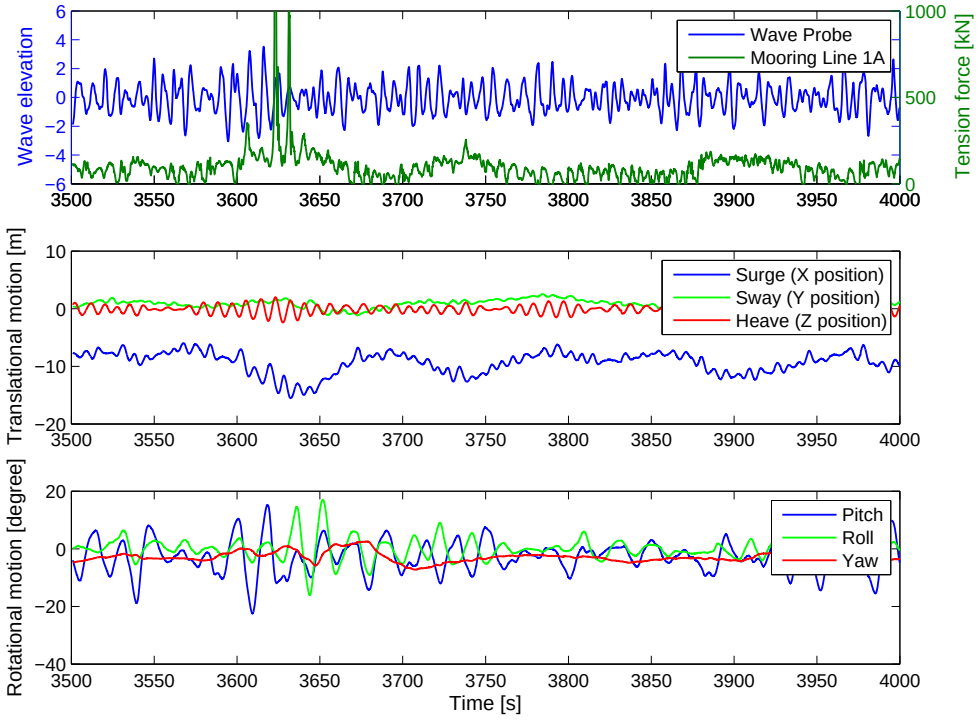

Figure 6.2: Wave elevation, mooring tension force and device motion.

The question, which motions are associated with high load events, may be assessed through scatter plots which correlate the magnitude of tension forces with translational and rotational motions close to the event. The scatter plots in figure 6.3 show all data points collected during the 3030 test. For the translational motion (6.3(a)) the highest mooring loads coincide with large negative values in surge (x-position) and the largest excursions in heave direction (z-position). This is expected, because when the device

moves further away (in x and z direction) from the anchor point, the mooring load of the leading line increases. However, from the scatter plot that illustrates the rotational motions (6.3(b)) it appears that the pitching motion of the device is strongly related to the high load events, too. Mooring loads increase for more negative pitching values, i.e. when the devices pitches away from the anchoring point A1. No clear correlation becomes apparent for the roll and yaw motions.

Thus, high load events of mooring loads are not only caused by large heave motions, but an interaction of other degrees of freedom. In the present case high load events are associated with strong pitching movement, large surge excursions and positive heave.

6.1.2 Peak mooring loads

Similarly to extreme wave heights it is important to assess peak mooring loads in order to inform the mooring design process (Eik & Aksnes, 2010). The simple visualisation of mooring tension in the time domain highlighted the presence of extreme load events in relatively moderate operational conditions for the tested device. This type of extreme sudden impact loading is known as snap or snatch loading, where the mooring line or cable becomes slack and experiences a fast transition to become taut again. The reason for this is that the mooring line cannot resist compressive forces which are induced by the oscillatory motion of the wave converter. Liu (1973) distinguishes three types of cable loading (compare figure 6.4).

- Static load - the weight of the mooring arrangement
- Dynamic load - Load caused by the motion of the system
- Snap/Snatch load - Sudden tensioning of a slack mooring line

Dynamic loads are generated by the system oscillation, i.e. surge, heave and sway movements of the wave energy device. The snap load occurs when the mooring line is slack and suddenly becomes taut again. This is particularly the case when the motion of the floating device is subject to high frequencies and/or large amplitudes.

According to Niedzwecki & Thampi (1991, p. 2) snap load events can be "several orders larger than the normal static and dynamic loading and are the dominant design consideration when known to exist." This is important to note, as repeated snap loading

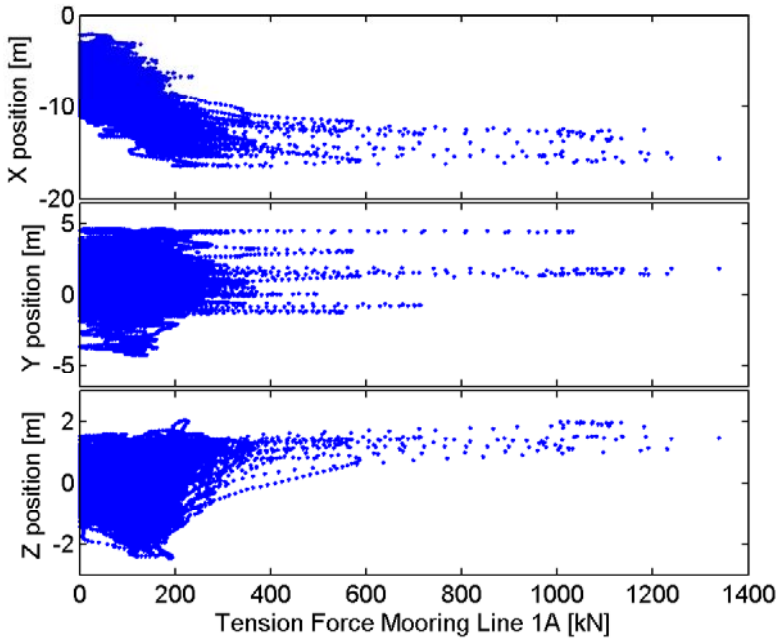

(a) Tension and translational motion

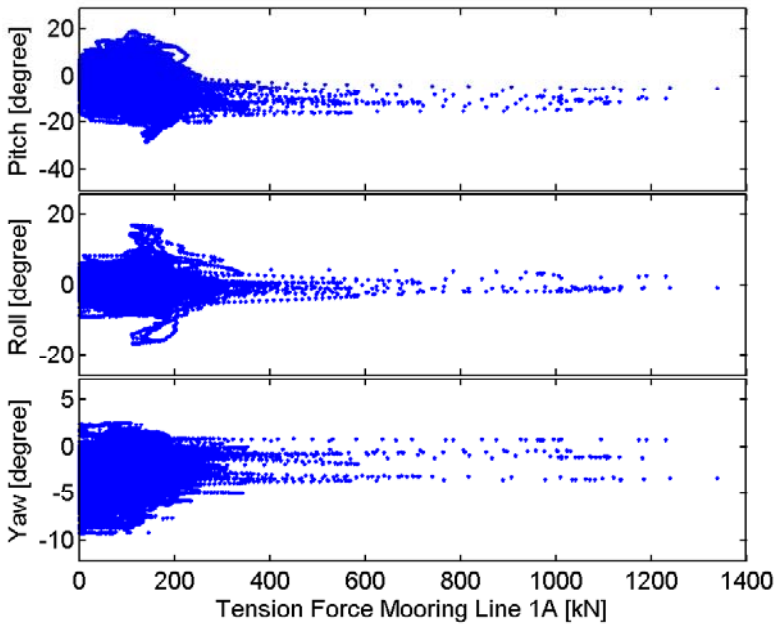

(b) Tension and rotational motion

Figure 6.3: Scatter plot of mooring line tension and device motions for 3030test.

in operational sea states would significantly reduce the life of a mooring line, because the extreme cyclic loading would lead to fatigue failure.

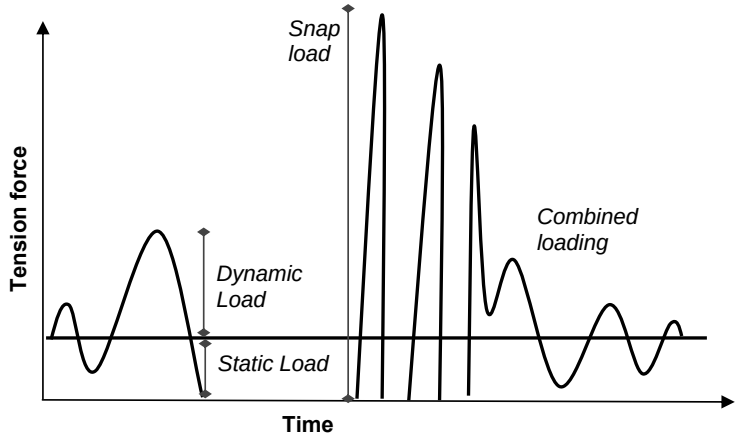

Figure 6.4: Qualitative illustration of typical mooring line loads, after Liu (1973).

The test results were further analysed with regard to the occurrence and magnitude of peak mooring loads for different test conditions. The analysis was automated with a MatLab script that made use of some functionality in the Wafo toolbox to identify the peaks of a given time series (WAFO-group, 2000). Within the time series all peaks are identified and a threshold value can be set to exclude peaks of smaller amplitude. The rationale behind this is that a noisy signal might lead to peaks that do not correspond to actual peaks but are due to the signal noise. A plot showing the identified peaks (given a threshold value $P_{min} = 20kN$) is shown in figure 6.5.

To allow a good graphical representation and a simple comparison of mooring load magnitudes under different test regimes, the largest 50 peaks are extracted from each signal which showed to be sufficient to capture both snap load events and regular dynamic peaks. Figure 6.6 displays the highest 50 peaks that occurred in all three mooring lines during two regular (6.6(a), 6.6(b)) and two irregular (6.6(c), 6.6(d)) wave tests.

It can be seen that the leading mooring line L1A has to withstand the largest tension forces among the three mooring lines. The rear mooring lines L2A and L3A experience only small loads $F_{Peak}(L2A, L3A) < 200kN$.

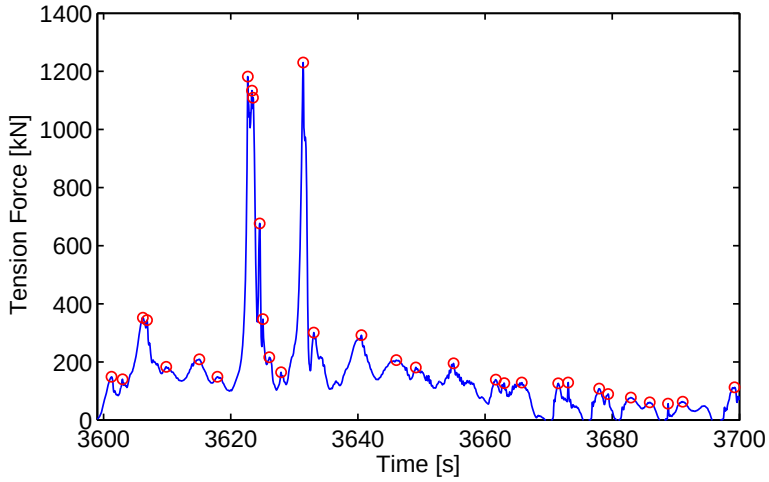

Figure 6.5: Example of peaks identified in time series; amplitude threshold value $P_{min} = 20kN$.

For the two cases on the left pane 6.6(a) and 6.6(c) mooring line L1A is subject to moderate tension loads. However, slightly larger sea states 6.6(b), 6.6(d) lead to an extreme increase of peak loads, indicating the occurrence of snap loads $F_{Peak}(L1A) > 1000kN$. In tested sea states with $H_s \leq 3m$, no snap loading occurred but in all situations where $H_s \geq 3.5m$ snap loads are observed. This type of loading would be of concern for a full-scale device and occurrences of snap loads have been reported for two wave energy prototypes, the Danish WaveDragon (Kofoed *et al.*, 2006) and the Australian Oceanlinx device (Ferrario *et al.*, 2004). The repeated snap loads are likely to be the root causes of the mooring line failures these devices suffered.

The analysis so far has shown, that early tank testing may reveal conditions under which snap loads arise. This information is of importance as repeated snap loading may lead to mooring failure. This may either be due to the fact that the maximum mooring strength is exceeded through an extreme event, or that repeated cyclic loading leads to fatigue failure. The former case can be assessed by comparing the design specifications against the measured forces. In general, snap loading conditions may be mitigated through elastic mooring configurations, but the exact configuration can only be determined through a dedicated mooring design process as described by Johanning *et al.* (2005).

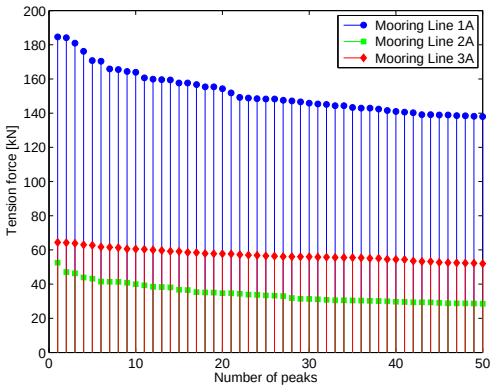

(a) Regular wave test 2060, $H_s = 3m$

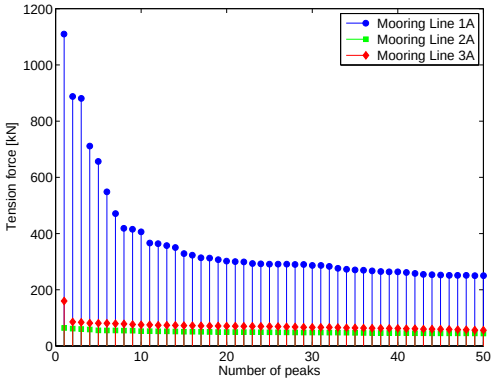

(b) Regular wave test 2070, $H_s = 4m$

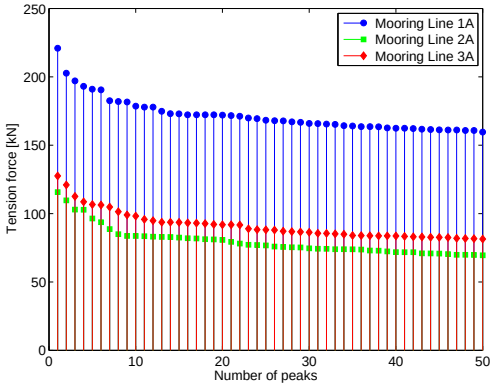

(c) Irregular wave test 3000, $H_s = 2.5m$

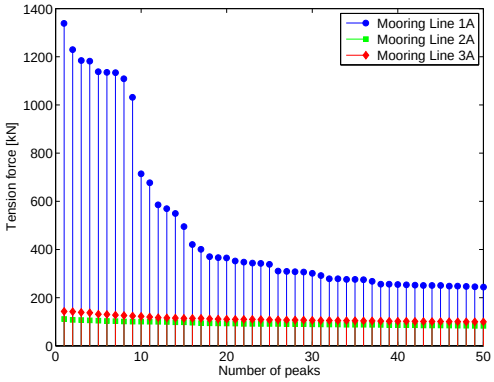

(d) Irregular wave test 3030, $H_s = 3.5m$

Figure 6.6: Largest 50 tension force peaks of mooring lines for regular and irregular sea states, $T_p = 8s$.

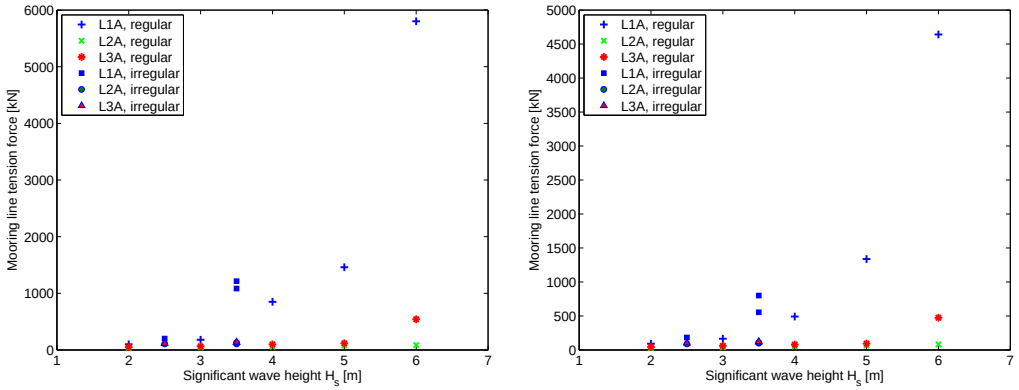

(a) N=5

(b) N=20

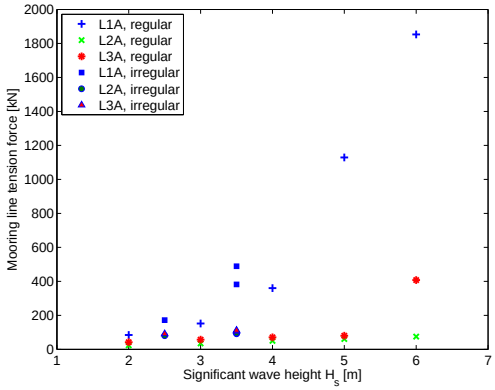

(c) N=50

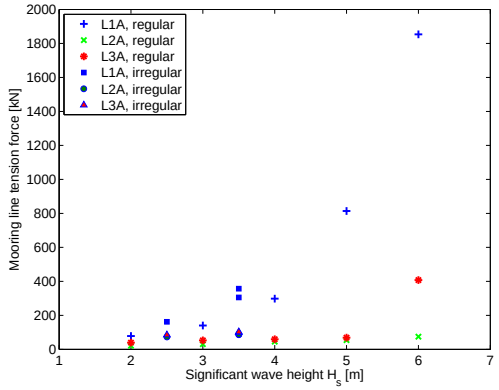

(d) N=100

Figure 6.7: Change of mean peak tension force (highest N peaks) with H_s for mooring lines L1A, L2A, L3A. $T_p = 8s$, irregular sea states plotted as solid markers.

The further investigation in this thesis is dedicated to the contributions of snap loads to mooring line fatigue (section 6.1.3).

6.1.3 Fatigue loads

6.1.3.1 Rainflow cycle method

There are different methods to characterise fatigue load signals. Common methods are level crossing and range counting procedures, where the load signal is assessed regarding the crossing of a specific reference level or its load amplitudes. When the load cycles are of randomly varying amplitude the so-called rainflow count method is commonly used to evaluate fatigue damage, as it realistically considers the fatigue damage caused by each individual load cycle. It identifies and counts the stress ranges corresponding to individual hysteresis loops (Schijve, 2009). Thus, the rainflow cycle count methodology is used here.

It pairs high maxima with low minima, where each local maximum is used as the maximum of an hysteresis loop that has the amplitude computed by the rainflow algorithm. The algorithm is based on the definition for a rainflow cycle by Rychlik (1987) which is illustrated in figure 6.8. "From each local maximum (...) one shall try to reach above the same level (...) with an as small downward excurcsion as possible."

Starting from a local load maximum Max_k ,two minima are identified before and after Max_k, i.e. Min_{k+} and Min_{k-}. That minimum having the smaller deviation from Max_K is chosen as the rainflow minimum $Min_{k,RFC}$, giving the k:th rainflow cycle $(Min_{k,RFC}, Max_k)$. This algorithm is then repeated over the entire time series t. Additionally a threshold level can be set for the rainflow amplitude, i.e. $Max_k - Min_{k,RFC}$ so that only pairs greater than the threshold are considered.

Further, with t_k as the time of the k:th local maximum and the rainflow amplitude characterising the amplitude of the hysteresis loop, the total damage $D(t)$ can be calculated by the Pålmgren-Miner rule (Miner, 1945; Pålmgren, 1924). It is also known as the linear cumulative fatigue damage rule and assumes that the each load cycle causes a damage of $1/N(S_{k,RFC})$. The fatigue damage is then calculated as the sum of

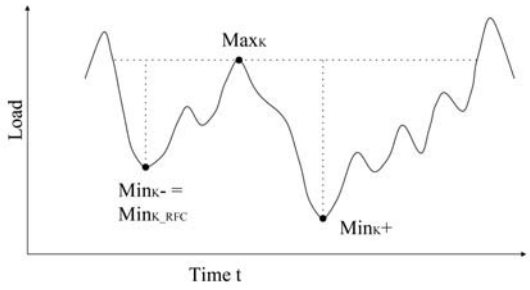

Figure 6.8: Rainflow cycle count definition after (Rychlik, 1987).

the individual blocks of constant load amplitude:

$$D(t) = \sum_{t_k \leq t} \frac{1}{N(S_{k,RFC})} = \frac{1}{K} \sum_{t_k \leq t} (S_{k,RFC})^{\beta} \tag{6.1}$$

Where $N(S_{k,RFC})$ is the number of cycles during the time t, K represents a random variable to account for material uncertainties and β is usually taken to be a fixed constant describing the shape of the material's S-N curve:

$$N(S) = \begin{cases} K \cdot S^{-\beta} & S > S_{\infty} \\ \infty & S \leq S_{\infty} \end{cases} \tag{6.2}$$

With $N(S)$ number of load cycles; S stress amplitudes.

It is worth noting that β is usually in the range from 3 to 5 for many components and thus, from equation 6.1, when the amplitude of a load cycle doubles the amount of fatigue damage increases by a factor of between 8 and 32. Another implication is that fatigue damage caused by small load cycles is negligible compared with those by the largest load cycles.

6.1.3.2 Mooring line fatigue properties

The two primary factors to affect fatigue reliability are the material's fatigue strength and the applied cyclic loading. While the fatigue strength is an intrinsic material and mechanical characteristic, the applied loading describes an extrinsic process. Two approaches are common to evaluate fatigue reliability (Wang *et al.*, 1997):

- The crack growth model examines the fracture behaviour of mechanical elements under dynamic loading, where failures occur if dominant cracks have grown to a critical length.

- The stress-life (S-N) approach considers the cumulative fatigue damage, where a failure occurs after a number of loading cycles N, at a particular stress range S.

S-N curves describe the fatigue properties of different materials. These curves are found empirically through fatigue tests and show the number of cycles to failure N, as a function of the cyclic stress S. The fatigue life design for offshore structures is commonly based on the use of S-N diagrams (Stacey & Sharp, 2007) and is adopted here.

Fatigue curves are modelled with a power law, that stems from a linear regression of fatigue test results. The number of cycles $N(S)$ to failure for a particular cyclic stress range S is described by 6.2.

This power law equation becomes a linear relationship if the logarithm is taken:

$$log\,(N(S)) = log\,(K) - \beta \cdot log\,(S) \tag{6.3}$$

where $N(S)$ is the number of cycles at a certain stress, S is the constant amplitude cyclic stress, K is the intercept parameter of the S-N curve and β describes the slope of the S-N curve. Care has to be taken how the stress range S is specified. These may be stress amplitudes S_a or stress ranges S_r, where $S_r = 2S_a$. Moreover, the stress may be given as nominal stress values, e.g. in $MPa = \frac{N}{mm^2}$, or as relative value e.g. a ratio of applied cyclic stress and maximum tensile strength.

The design S-N curves for tension-tension fatigue of different mooring line materials are given in DNV-OS-E301 (2010), a standard for position mooring, and are plotted in table 6.1. The graph shows the reference fatigue design curves for steel wire ropes and chain. The given values imply that the chain is exposed to the corrosive influence of seawater, while the curves for steel wire rope assume corrosive protection e.g. through outer sheath lining. From the four mooring types, spiral steel wire rope has the most favourable fatigue properties followed by the stranded wire, the studded and the studless chain.

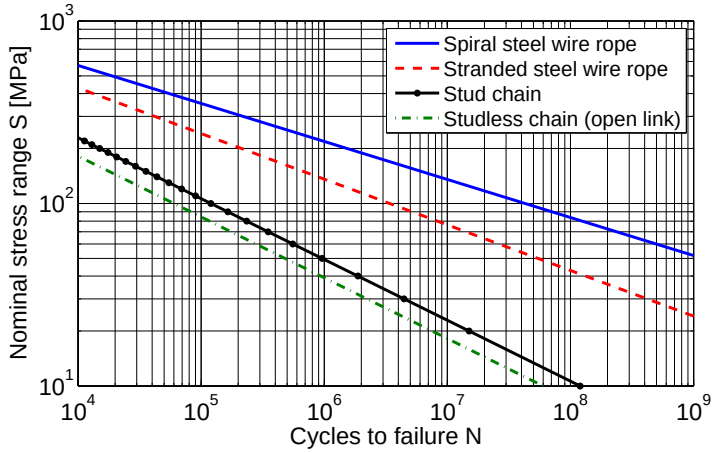

Parameters

Type	K	β
Spiral	$1.7 \cdot 10^{17}$	4.8
Stranded	$3.4 \cdot 10^{14}$	4.0
Stud	$1.2 \cdot 10^{11}$	3.0
Studless	$6.0 \cdot 10^{10}$	3.0

Table 6.1: Nominal S-N fatigue curve for different mooring types after DNV-OS-E301 (2010). Parameters shown for: $log\,(N(S)) = log\,(K) - \beta \cdot log\,(S)$.

As the S-N curves are given in terms of the nominal stress range, the measured tension load signal was converted to a nominal stress using:

$$\sigma_{NOM} = \frac{F_{Moor}}{A} \tag{6.4}$$

σ_{NOM} is the nominal stress [MPa], F_{Moor} is the measured mooring force [N] and A is the cross-sectional area of the mooring line $[mm^2]$. For a full-scale line diameter of $d = 70$mm with $A = 3.85 \cdot 10^3\ mm^2$

6.1.3.3 Rainflow cycle count and damage calculation

The rainflow cycle analysis of the mooring tensions has been carried out with the WAFO Matlab toolbox (WAFO-group, 2000).

The calculation comprises two subsequent steps for each measured load time history of the individual sea states. Only the leading mooring line L1A is considered as it was shown to carry the main load.

1. Rainflow cycle count in order to compute the rainflow matrix, showing the amount of load cycles for different stress ranges.

2. Fatigue damage calculation, which computes the accumulated damage based on the rainflow matrix and the fatigue properties of the mooring line (comp. equation 6.1).

The results of the rainflow cycle count are exemplarily shown for the irregular wave conditions (test 3000, $H_s = 2.5m$, $T_p = 8s$). Figure 6.9 shows 4 plots of the unfiltered load signal. The load cycles of the mooring line tension are plotted as point process with the minimum and the maximum of each cycle. The contour lines indicate the number of cycles (6.9(a)). The rainflow cycles can be further discretised for each matrix cell which yields the rainflow matrix (6.9(b)). The abscissa mark the stress range of the load cycle while the colour scheme indicates the number of load cycles for each cell.

The cumulative distribution of load amplitudes irrespective of their individual trough and peak location is plotted in figure 6.9(c). For the given example it shows a total number of 5,200 cycles. The fourth plot (6.9(d)) shows the normalised load amplitudes, which allows a comparison of different load cases.

The majority of load cycles have an amplitude smaller than 10kN. Whilst these small amplitude cycles dominate the rainflow matrix, the contribution to fatigue damage is insignificant. For this reason and to reduce potential signal noise, the smallest load cycles are filtered out in the data processing. The threshold value was set to $F_{TH} = 20kN$. This filtering reduces the amount of load cycles and yields a filtered rainflow matrix as shown in figure 6.10. The calculations have been performed accordingly for all other sea states.

The generated rainflow matrix forms the basis of the fatigue damage calculation as defined by the Pålmgren-Miner rule in equation 6.1. Both the filtered rainflow matrix and the corresponding fatigue damage matrix for a simple chain are shown in figure 6.11. As expected, the load cycles with larger amplitudes ($> 250MPa$ nominal stress in the chain) result in significantly larger fatigue damage.

6.2 Estimation of annual field load conditions for moorings

After the load conditions have been assessed for individual sea states, the question arises how this corresponds to actual field load conditions. More precisely, how can the fatigue life be estimated using the available data? This section aims to estimate the annual field load conditions with regard to mooring line tensions if the full-scale version of the device described in section 5.1.2 would be deployed at a particular site.

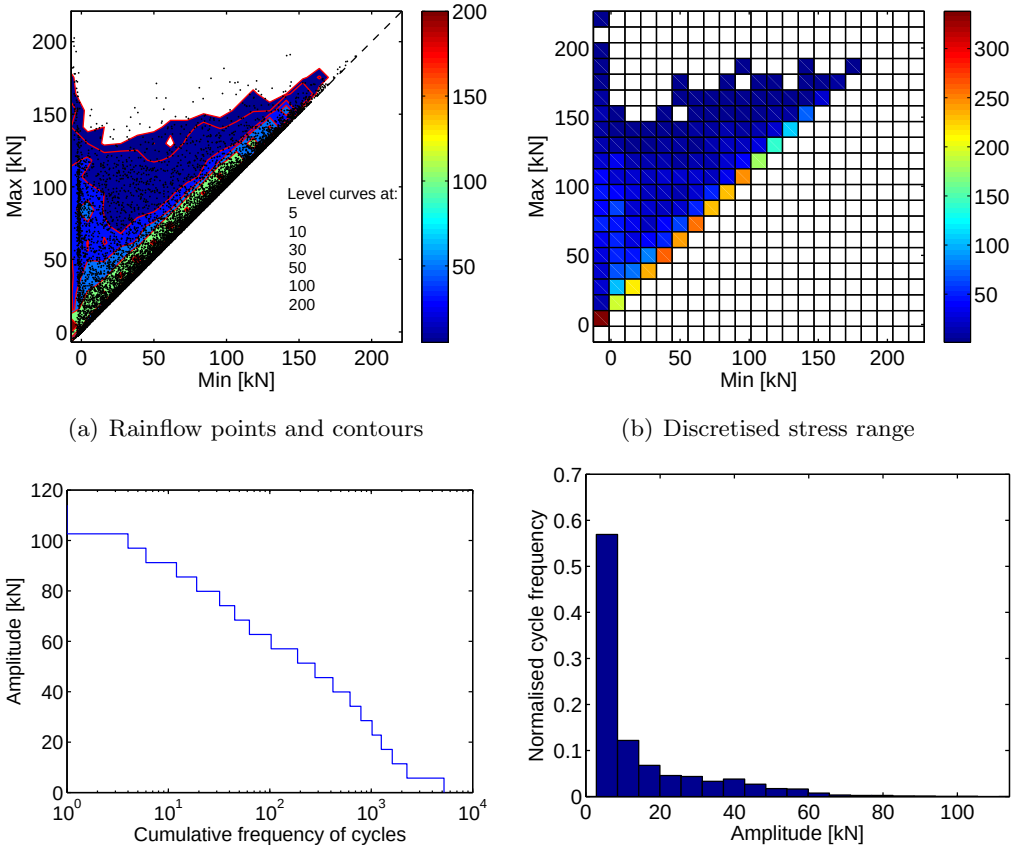

(a) Rainflow points and contours

(b) Discretised stress range

(c) Cumulative amplitudes

(d) Normalised amplitude frequency

Figure 6.9: Unfiltered rainflow cycle matrix indicating the occurrence of mooring line tension load cycle [kN]. 135 min irregular wave test with $H_S = 2.5m$ and $T_p = 8.0s$, leading mooring line L1A.

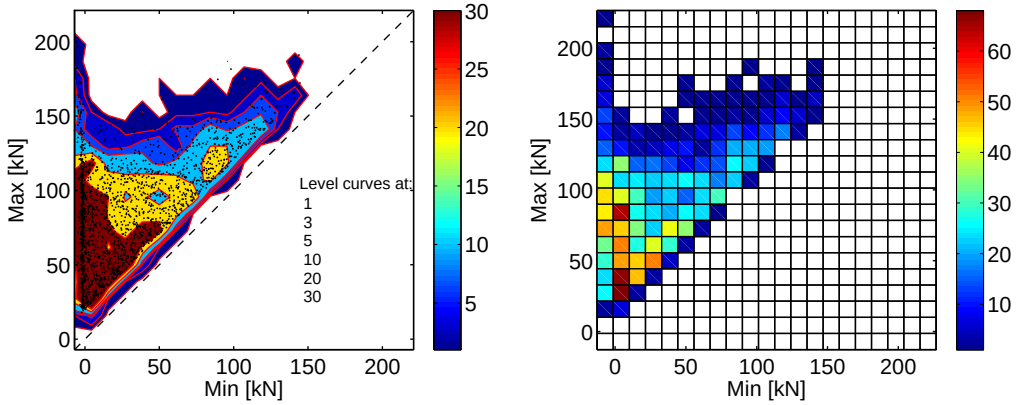

(a) Rainflow points and contours

(b) Discretised stress range

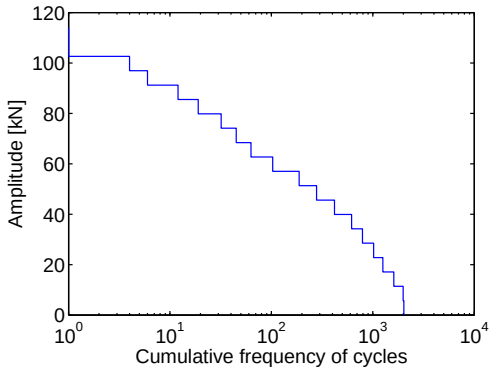

(c) Cumulative amplitudes

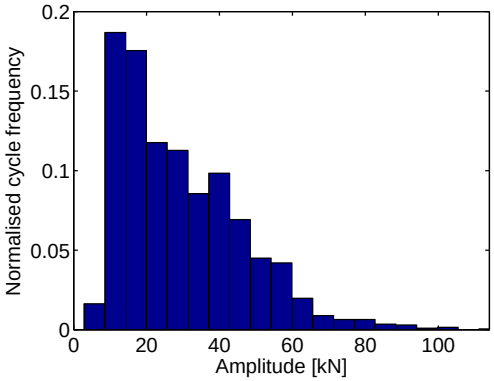

(d) Normalised amplitude frequency

Figure 6.10: Filtered rainflow cycle matrix showing mooring line tension load cycles [kN], filter threshold $F_{TH} = 20kN$. 135 min irregular wave test with $H_S = 2.5m$ and $T_p = 8.0s$, leading mooring line L1A.

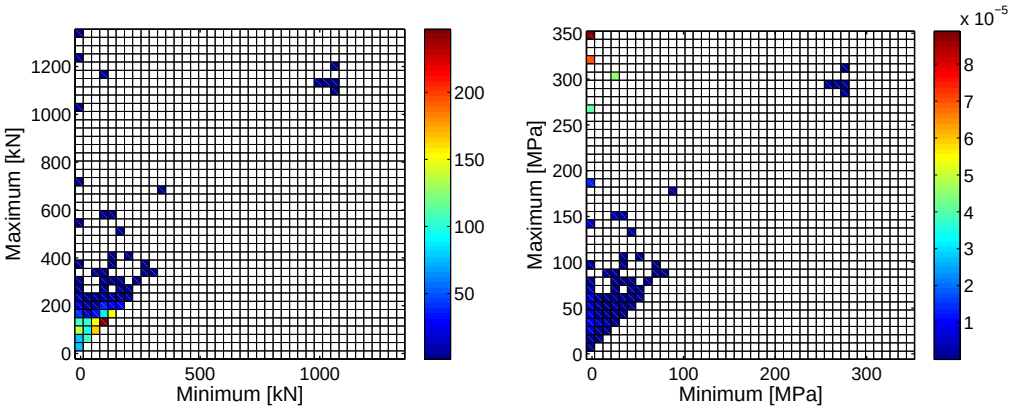

(a) Filtered rainflow matrix

(b) Damage matrix

Figure 6.11: Rainflow cycle and damage matrix for 120min irregular wave test with $H_S = 3.5m$ and $T_p = 8.0s$. Damage results shown for studless chain with $K = 6 \cdot 10^{10}$ and $\beta = 3$.

6.2.1 Annual load spectrum generation

Some additional information and subsequent calculations are required to generate an annual load spectrum from the individual sea states. Firstly, the annual wave characteristics of the deployment site are required. The wave climate is typically characterised by a so called scatter plot which bins the continuous wave elevation into sea states described by wave period T and significant wave height H_s and reports the occurrence of each condition. From these scatter plots the annual probability of the individual sea states can be obtained.

As a second step the probability of each sea state is assigned to the experimental sea states. The objective is to derive a multiplicative factor for each experimental sea state in order to replicate the annual wave climate at the site regarding the accumulated load cycles, using the available experimental load data such that:

$$P_{site}(H_s, T_p) \mapsto RFM_{test}(H_s, T_p) \cdot M \tag{6.5}$$

where $P_{site}(H_s, T_p)$ is the annual probability of a given sea state at the site (specified through H_s and T_p), $RFM_{test}(H_s, T_p)$ is the calculated rainflow matrix of the experi-

mental test and M is the adjusting multiplying factor with

$$M = P_{assign}(H_s, T_p) \cdot 8760h\frac{1}{2} \tag{6.6}$$

$P_{assign}(H_s, T_p)$ is the assigned annual probability for an experimental sea state. Effectively this is the sum of $P_{site}(H_s, T_p)$ assigned to an experimental sea state. The factors relate to the number of hours for a year (8760h) and account for the fact that the RFMs are calculated for 2 hour intervals.

One difficulty that is likely to arise here, is that the experimental tests do not cover the entire range of sea states. The scatter plots investigated below contain 40-90 different sea states. These are already classified through bins (typically H_s interval of $0.5m$ and T_p interval of $1s$) and thus are a simplification of the actual occurring wave conditions. However, experimental load cases may be even less than the number of populated scatter bins. This is the case for the experimental data presented earlier, which investigated a total of 12 different sea states.

In order to still estimate the expected annual load spectrum, two approaches have been followed:

- Calculation of a fractional year that is representative of the experimentally tested conditions
- Estimation of full annual spectrum through reducing the wave conditions to wave height H_s only, i.e. assigning P_{site} irrespective of Tp.

The first approach adheres to the available data and should thus yield a sound estimate of expected loads for the fraction of the year where sea states are similar to the experimental conditions. However, if experimental data is scarce no annual load estimate can be derived. If the assumption is acceptable, that the majority of fatigue damage is associated with increased wave heights rather than the incident wave period, then the annual load spectrum may be estimated with the second approach.

During the experimental tests the wave period was only varied for $H_s = 2m$ but not for larger wave heights, leading to the situation where not all scatter cells are populated. However, comparing the influence of H_s and T_p on the accumulated fatigue damage for the experimental tests, the variation of wave heights showed to have the dominant influence compared to variations in wave period (comp. figure 6.12 and 6.13).

Thus, the approach to constrain wave conditions to H_s has been pursued in order to demonstrate the methodology to obtain an initial fatigue estimate at an early design stage. The shortcomings and limitations of this reduced approach are further discussed in section 6.2.3.4.

6.2.2 Case study for typical site

To provide an example here, the operational fatigue loads have been calculated for a typical site where annual wave characteristics are readily available. A scatter plot that is derived from a measurement campaign from 2005-2006 at the Wave Hub site is published in (Pitt *et al.*, 2006). For the same site a long term wave climate has been predicted by Phillips *et al.* (2008) who used the measured data in conjunction with modelled wave data (from a 18 year period) in a Measure-Correlate-Predict analysis. The long term estimate will be used in the following as it describes the long-term average wave conditions and is thus better suited to assess the long-term fatigue conditions. As the experimental tests are not available for the desired range of sea states, covering all combinations of period *and* wave height, the wave climate is curtailed to the probability distribution of the significant wave height, H_s. The wave climate with regard to H_s that is used for the following calculations is shown in table 6.2.

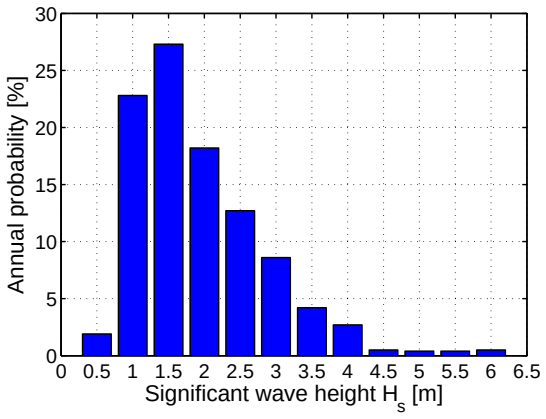

H_s [m]	P_{annual} [%]
6.0	0.5
5.5	0.4
5.0	0.4
4.5	0.5
4.0	2.7
3.5	4.2
3.0	8.6
2.5	12.7
2.0	18.2
1.5	27.3
1.0	22.8
0.5	1.9
Total	100.0

Table 6.2: Annual probability distribution P_{annual} of significant wave height H_s, data after Phillips *et al.* (2008)

Each experimental test is assigned an annual probability, P_{assign}, that corresponds to the same wave height in the scatter plot. The assignment for each experimental sea state is tabulated in table 6.3.

The annual load cycle matrix is then computed as:

$$\sum_{i=1}^{i=5} RFM(H_s) \cdot M_i \tag{6.7}$$

Where i denotes the corresponding sea state. The estimated annual field load conditions can thus be thought of as a linear combination of individual experimental sea states.

Table 6.3: Assignment of annual probabilities, P_{assign} represents the assigned annual probability of the experimental test condition, M is the multiplication factor for the corresponding rainflow matrix

i	Test	$H_s[m]$	P_{assign} [%]	M
1	2020	2	82.8	3626
2	2060	3	12.7	559
3	2070	4	3.2	141
4	2080	5	0.8	33
5	2090	6	0.5	21

6.2.3 Damage estimates

In this section the numerical results of the above case study for the estimation of annual field loads are presented. It must be noted that these findings are specific to the generic device and the taut mooring configuration. The results cannot be directly transferred to other types of devices. However, the approach and analysis are applicable to other MECs in order to estimate the expected fatigue damage for a particular configuration and potential deployment site. Still, the presented findings highlight that fatigue considerations are crucial for marine renewable applications which operate in the wave environment. The gained information allows to reiterate or approve the fatigue design of components.

Three aspects are presented, the fatigue damage caused by individual sea states, the estimated annual mooring load spectrum and the resulting annual accumulated fatigue damage for different mooring materials.

6.2.3.1 Damage for individual sea states

The rainflow analysis procedure described above has been applied to the range of tested sea states. The accumulated damage for each sea state is calculated. Two different

mooring lines are considered under full-scale conditions, steel wire rope (in spiral and stranded configuration) and steel chain (in studdless and studded configuration). The S-N material properties are given in table 6.1, page 204. The accumulated fatigue is calculated for a 2 hour interval of each sea state. This then allows a comparison of the resulting fatigue damage with regards to incident wave height H_s and wave period T_p.

Figure 6.12 shows the accumulated fatigue damage D plotted against the significant wave height H_s for steel wire and chain configurations. A logarithmic scale has been applied for D to allow the large range of values to be displayed. The transparent markers indicate regular sea states and solid markers show irregular sea states. It is apparent that the fatigue damage drastically increases with higher H_s. This is attributed to the occurrence of snap loads, which were identified in particular for $H_s > 3m$ and account for the majority of the caused fatigue damage. Thus, for $H_s = 6m$ the studless chain consumes almost 30% of its fatigue life, while for $H_s = 2m$ it consumes only 0.01%. The spiral steel wire exhibits a better fatigue life performance and consumes 1% and $2 \cdot 10^{-8}$ % of its fatigue life at $H_s = 6m$ and $H_s = 2m$ respectively.

Another observation is that the spread of damage values for the different mooring materials and configurations declines for larger wave heights. Still the ranking order that steel wire shows the better fatigue behaviour over chain is consistent.

The relationship between fatigue damage and wave period T_p is shown in figure 6.13. In order to enable a direct comparison with the earlier figure 6.12 the damage is also plotted on logarithmic scale. No clear relation seems to be eminent for damage and wave period. The accumulated damage differs by an order of magnitude across the different wave periods with slightly larger damages for smaller T_p and decreased damage values for $T_p > 9s$. The small effect of the incident wave period on the fatigue damage may be explained by the natural period of the moored device. The response analysis by Vickers (2012) yielded natural periods of $T_{N,Surge} = 268.0s$, $T_{N,Pitch} = 19.5s$ and $T_{N,Heave} = 11.3s$. Large surge and pitch motions induce the larger tension load cycles which cause the majority of the fatigue damage. Both natural periods (surge and pitch) are well above the incident wave periods and thus do not significantly effect the mooring line tension and subsequently the accumulated fatigue damage. This however may be different for other devices where the natural frequencies are closer to the incident wave

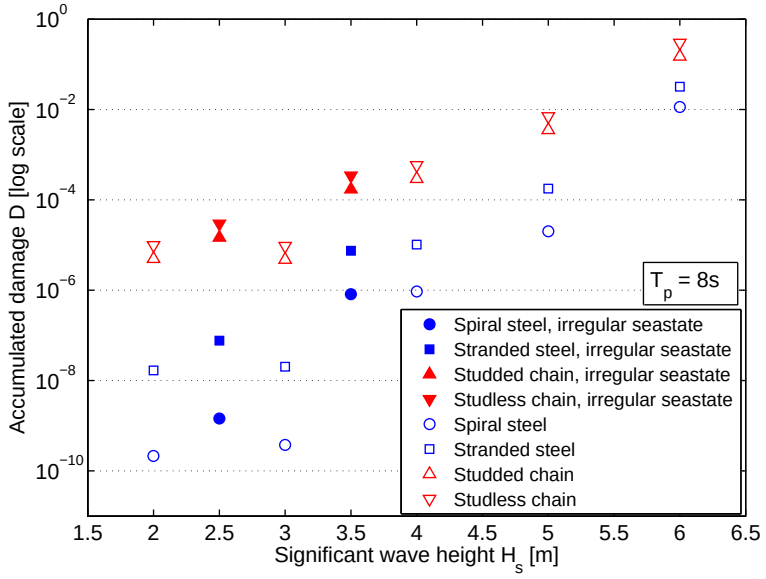

Figure 6.12: Mooring line fatigue damage for different wave heights H_s. Duration of sea state $t = 2h$, wave period $T_p = 8s$.

periods.

Thus, when comparing the impact of the different sea state parameters H_s and T_p on the accumulated fatigue damage for the tested generic wave converter, the incident H_s appears to be the dominant factor for the resulting fatigue damage D. For the presented case this is mainly due to the occurrence of large snap loads for larger wave heights.

6.2.3.2 Annual load spectrum

The annual tension load spectrum for the leading mooring line is calculated as linear combination of the individual experimental sea states. It comprises all load cycles the mooring line experiences for a typical year of operation at the chosen deployment site. Figure 6.14 shows the annual load spectrum in form of the rainflow matrix (6.14(a)) and the distribution of load amplitudes (6.14(b)). In the rainflow matrix, those load cycles with a large tension range i.e. small minima and large maxima, are plotted in the upper left corner of the matrix. Cycles with smaller load ranges at a higher load level are plotted near the centre of the matrix. The amplitude distribution plot shows

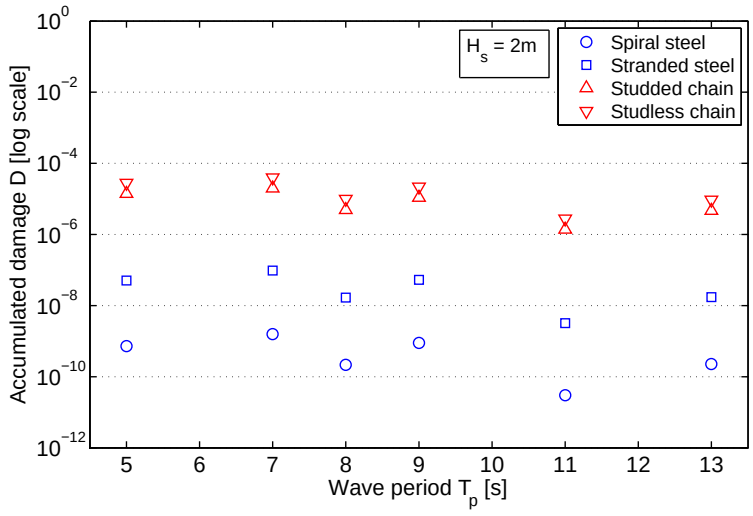

Figure 6.13: Mooring line fatigue damage for different wave periods T_p. Duration of sea state $t = 2h$, wave height $H_s = 2m$.

the occurrence of different load amplitudes. It gives a better view of the number of cycles at different load magnitudes. The total number of cycles amounts to $N_{annual} = 3.29 \cdot 10^6/year$. The smallest load amplitudes ($< 50kN$) are estimated to occur in the order of 10^6 times a year while the largest amplitudes ($> 900kN$) are expected to occur in the order of 10^3.

6.2.3.3 Annual accumulated fatigue damage

The annual damage matrix has the same pattern as the underlying rainflow matrix. It differs with regard to the stress ranges which are converted to the nominal stress of the mooring line and the colour bar, which represents the accumulated fatigue damage for each cell.

Figure 6.15 depicts the damage matrix for spiral steel wire that has the best fatigue properties of the mooring lines compared here. The total accumulated annual fatigue damage is estimated as $D_{annual} = 6.96 \cdot 10^{-3}$. The majority of the fatigue damage stems from the largest amplitude cycles ($A > 250MPa$) which contribute a total damage of $D = 5.34 \cdot 10^{-3}$. This accounts for over 75% of the annual fatigue damage.

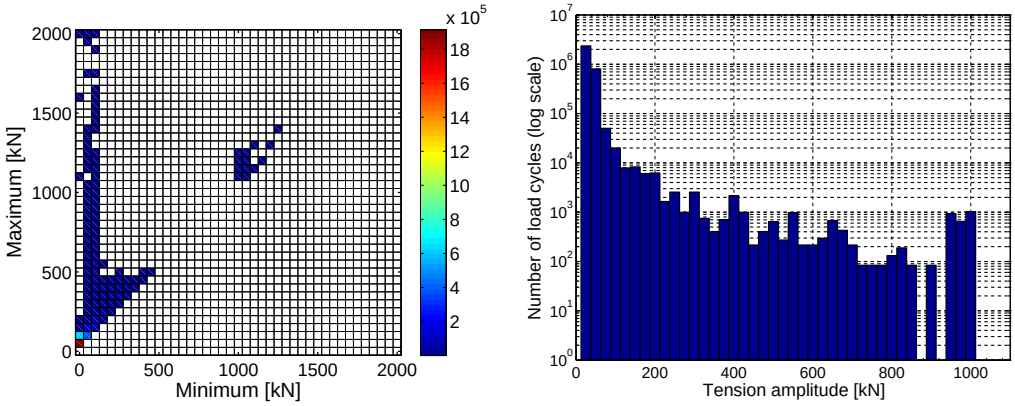

(a) Rainflow matrix (b) Amplitude distribution

Figure 6.14: Annual load spectrum for leading mooring line irrespective of wave period T_p.

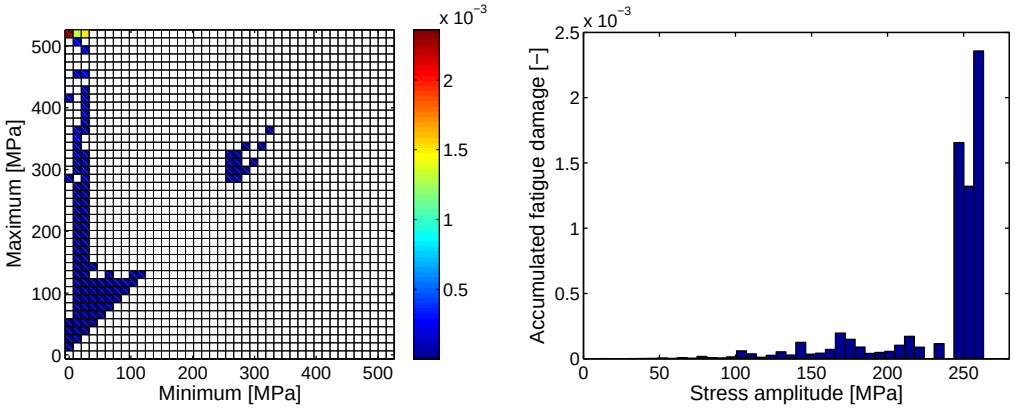

(a) Damage matrix (b) Stress amplitudes

Figure 6.15: Annual damage matrix for spiral steel mooring line, total accumulated damage for the hypothetical year of operation $D_{annual} = 6.96 \cdot 10^{-3}$.

The estimated fatigue damage for the different mooring lines is summarised in table 6.4. This is a projection of the estimated annual fatigue damage for a number of years, assuming that the typical year reoccurs. In reality, there will be inter-annual variations but as the long term wave climate was used here, it is reasonable to calculate with the average year to obtain an indication of damage fatigue for different design year projections.

Spiral steel wire performs well and would stay within the design limit for fatigue. Stranded steel wire comes close to $D = 1$ in the 20 year case. The chosen chain diameter seems to be inappropriate for the modelled application, this is mainly due to the high snap loads. Again it should be noted here that these figures should be treated with caution as they are very specific to the modelled device and are subject to the assumptions outlined in section 6.2.3.4.

The safety factors for the fatigue limit state (FLS) are specified in DNV-OS-E301 (2010, p. 38) and typically range between 1 and 10 for steel moorings. Considering the highest safety actor, only the spiral steel mooring would be within the fatigue limit for the 5 and 10 year case.

Table 6.4: Estimated accumulated fatigue damage for different mooring lines and design years. After Miners law, damage values $D \geq 1$ indicate fatigue failure.

Design years	Spiral steel	Stranded steel	Studded chain	Studless chain
1	0.01	0.05	0.65	1.30
5	0.03	0.23	3.26	6.52
10	0.07	0.46	6.52	13.05
15	0.10	0.69	9.79	19.57
20	0.14	0.92	13.05	26.10

It is of interest to assess the composition of the total fatigue damage i.e. which sea states have caused the most severe fatigue damage. Those load conditions could then e.g. be replicated in service simulation tests. The contribution to total fatigue damage for each type of mooring line is shown in figure 6.16. The bars are grouped for each sea state, while the different colours indicate the mooring type. The contributions for each mooring type sum up to 1, which is the reference value given in table 6.4. The largest sea state with $H_s = 6m$ clearly causes the most severe fatigue damage (between

72% and 88% of the total annual damage), irrespective of the mooring type. The contribution for $H_s = 5m$ ranges between 10% and 19% of the total damage. Thus, these two sea states alone cause over 90% of the fatigue damage.

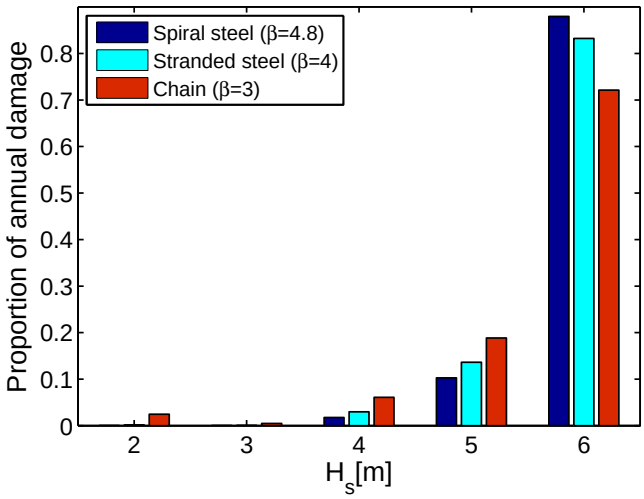

Figure 6.16: Contribution of different sea states to accumulated fatigue damage for different mooring line materials.

6.2.3.4 Discussion of annual field load and fatigue estimates

The calculation of annual field loads and fatigue damage estimates are subject to a number of assumptions which have been touched upon but are summarised and discussed in the following.

The calculation of annual field loads, i.e. the annual load spectrum assumes that there is only a single wave direction, collinear to the leading mooring line. This is not the case in reality, as can be seen from figure 6.17. More than 60% of the incident waves come from the prevailing WSW direction (between 270° and 240°). Thus, almost 40% of the incident wave are not collinear with the leading mooring line. In this respect, the assessment provides a worst case estimate for the annual field loads in that 100% of the incident waves are collinear with the leading mooring line L1A.

To generate annual load spectra and in turn annual fatigue estimates, the experimental sea states need to be assigned to the joint probabilities of the wave climate at

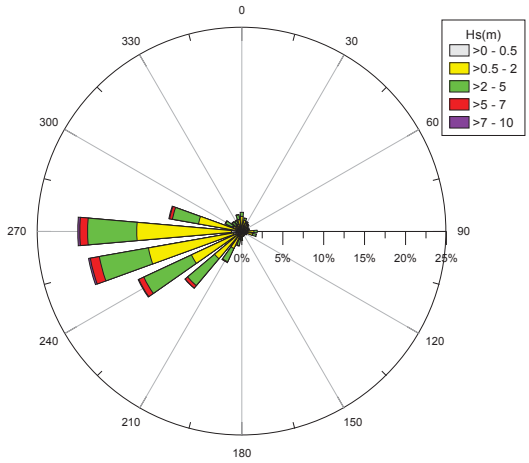

Figure 6.17: Offshore wave direction rose for sample site, after (Black, 2007).

the deployment site. This assignment is conducted only in terms of wave height H_s and irrespective of the wave period T_p. To describe long term environmental conditions by discrete sea states is common practice (compare, e.g. DNV-OS-E301 (2010, p. 36)) but the required number of reference sea states ranges between 10 to 50. The experimentally tested sea states only varied the wave period for one wave height. Additionally, the tests comprised both regular and irregular waves. To ensure the annual load calculations were consistent, the choice was made to consider only the regular sea states at different wave heights H_s. This leaves five sea states to estimate the annual load conditions. The presented procedure may appear coarse due to the scarcity of test data but it may be easily refined if more data is available in different assessments and would make the fatigue results more robust.

The procedure that has been performed to assign the sea states recorded in the scatter diagram to the tested sea states had to ignore the wave period of sea states. The assignment leads to the implicit assumption that all sea states have a dominant wave period of $T_p = 8s$, which is a simplification due to the scarce wave tank test data. This approximation is still deemed reasonable for the presented case as it could be shown that the fatigue damage is dominated by the wave height, rather than the wave period (compare figure 6.12 and 6.13). In order to back this argument the relative error that is introduced through the simplification of wave periods has been estimated, based

on the experimental data where the wave period was varied with $T_p = 5, 7, 8, 9, 11, 13$ for $H_s = 2m$. Using equation 6.8 the relative error ΔD_{ij} is calculated for the different mooring materials. The results are shown as relative error factors in table 6.5. The mean error for the different materials varies between a factor of -0.9 and -1.8, i.e. the simplified assignment of wave periods leads to a underestimation of fatigue damage. In comparison with the safety factors stated in DNV-OS-E301 (2010), the degree of underestimation is considered to be moderate.

$$\Delta D_{ij} = \frac{D_{R,\,i} - D_{ij}}{D_R} \quad i = 1, 2, 3, 4;\ j = 5, 7, 8, 9, 11, 13 \tag{6.8}$$

Where ΔD_{ij} is the relative error, $D_{R,\,i}$ is the damage of the reference case, D_{ij} is the damage of the actual sea states with $T_p \neq 8s$, i denotes the mooring type and j denotes the wave period.

Table 6.5: Relative error factors introduced through assigned wave period.

	T_p	Stranded	Spiral	Studded	Studdless
	5	-2.4	-2.0	-1.8	-1.8
	7	-6.4	-4.7	-3.0	-3.0
	8	0	0	0	0
	9	-3.2	-2.2	-1.2	-1.2
	11	0.9	0.8	0.7	0.7
	13	0	0	0	0
Mean		-1.8	-1.4	-0.9	-0.9

6.3 Marine umbilical load modelling

The results of the computational model described in section 5.2 are presented and discussed in the following with regards to i) the response and load behaviour and ii) a reliability assessment of maximum loads and fatigue life estimation.

6.3.1 Response and load behaviour

The four main points under consideration are i) the determination of maximum load points, ii) load patterns near the attachment point, iii) analysis of cyclic loading, as well as iv) the influence of wave parameters on the mechanical loads.

6.3.1.1 Maximum loading

The range graph in figure 6.18 shows points of maximum loading along the length of the umbilical. The maximum, mean and minimum tension forces for both configurations (catenary and Lazy-Wave shape) are depicted. For the catenary configuration the area of highest tension is located at the hang-off point, where the allowable tension is surpassed. Furthermore, the line of minimum tension shows that the umbilical experiences compression loads, in particular at the touchdown point.

In case of the Lazy-Wave, the highest forces also occur near the attachment point as well as at the transition points of the buoyancy section. In comparison to the catenary shape, forces are reduced and compression is avoided. The maximum tension is reduced by a factor of 5. However, this load reduction has the expense of two local load peaks at the transition points of the buoyancy section.

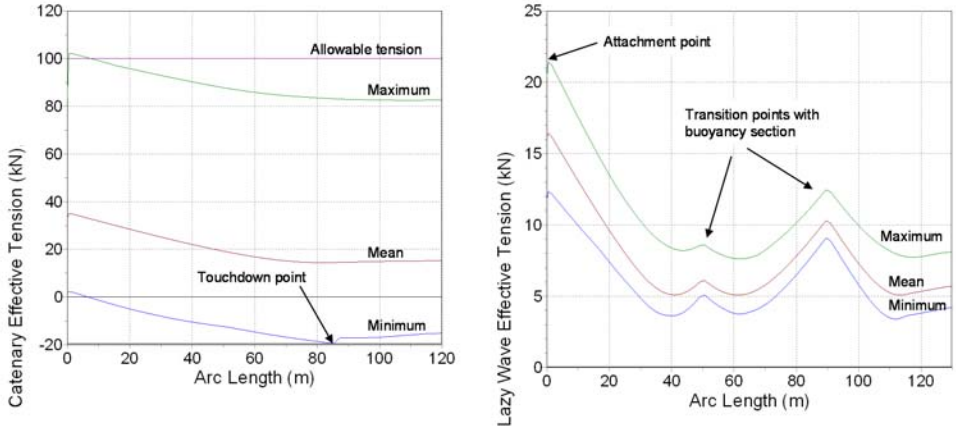

Figure 6.18: Maximum, mean and minimum tension force (compression) along the length of the umbilical in a moderate, irregular sea state of $H_s = 3.5m$, $T_p = 8s$. Left - catenary; right Lazy Wave.

6.3.1.2 Tension and bending near attachment point

Figure 6.19 shows the time series of tension force near the attachment point resulting from the WEC motions. Although both umbilical configurations are subjected to identical motions of the floating buoy, the resulting tension forces are very dissimilar. While for the catenary cable the high peak tension forces ($> 100kN$) are induced, the

compliant design of the Lazy-Wave shape absorbs the movements and exhibits only a moderate increase of tension force ($< 22kN$) for the shown wave group.

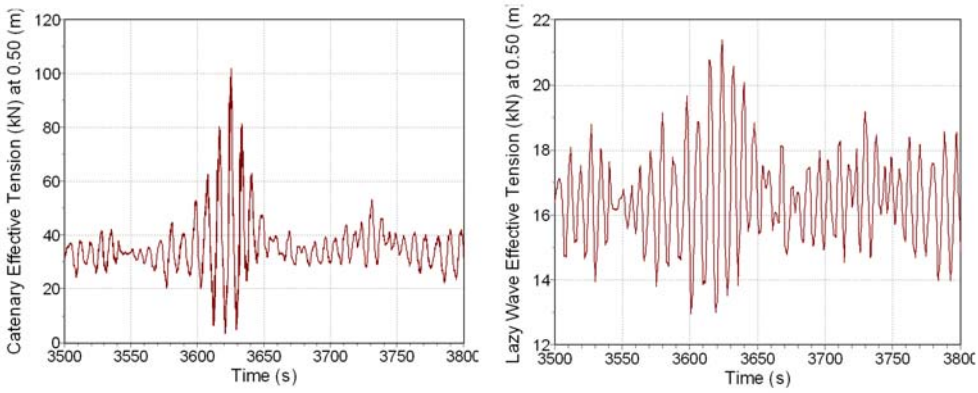

Figure 6.19: Time series of the effective tension 0.5m off the attachment point. Left - catenary; right - Lazy-Wave configuration. N.B. different scales of y-axis.

For the same wave group the bending behaviour near the attachment point is depicted in figure 6.20. The largest bending moments (Fig. 6.20(a)) are just under 6kNm (catenary) and 4kNm (Lazy-Wave), respectively. The bending moment correlates to a bending radius (Fig. 6.20(b)) of the umbilical which is typically used as a design parameter. For the modelled cable the minimum bend radius is given as MBR = 2m, i.e. the bend radius must not be smaller in order not to damage the cable. The bend radius falls below the critical value of 2m for the catenary shape (1.7m) but remains within the allowable limit for the Lazy-Wave shape (2.5m).

6.3.1.3 Cyclic loading

The presented time series demonstrate that the power cable is subject to considerable cyclic load conditions. The rainflow cycles (refer to section 6.1.3.1) of the WEC's motion response and the power cable's load cycles have been counted and are summarised in table 6.6.

The motion response cycles are reported for each degree of freedom while the load cycles are distinguished by load type (tension/bending) and by cable configuration (catenary/Lazy-Wave). The comparison shows that the computed load cycles are more numerous than would be expected from solely considering any of the motion responses in a single degree of freedom approach. This is the case for both tension forces and

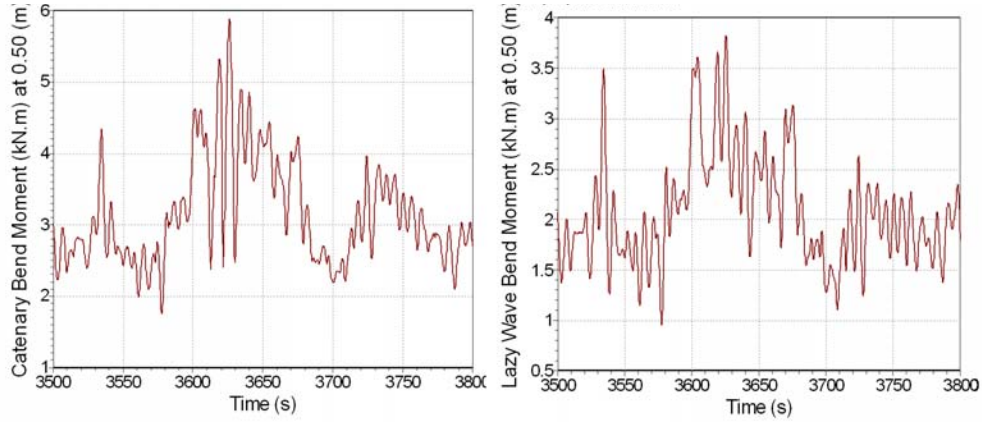

(a) Bending moment

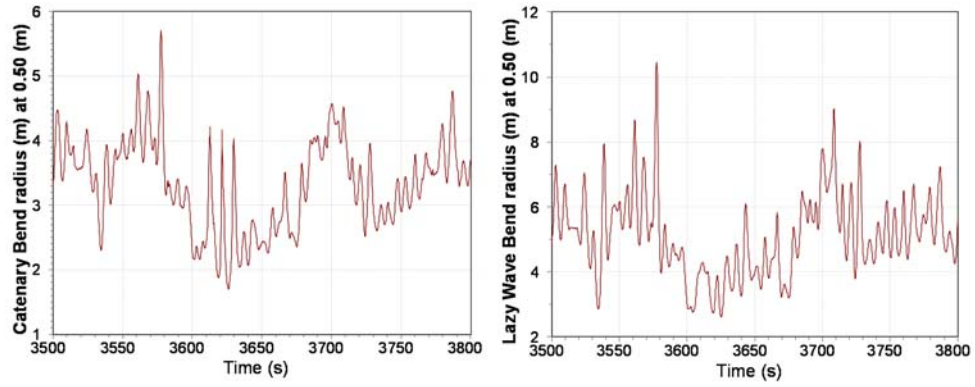

(b) Bend radius

Figure 6.20: Time series of bending behaviour 0.5m off the attachment point. Left - catenary; right - Lazy-Wave configuration.

Table 6.6: Rainflow cycles for motion response of floating converter and umbilical tension/bending cycles 0.5m off attachment point. Length of the simulation is 135 min; irregular waves with $H_s = 3.5m$, $T_p = 8s$.

Motion response of device		Type	Umbilical load cycles	
Surge (X)	2,214		Catenary	Lazy wave
Sway (Y)	2,275	Tension force	3,846	3,124
Heave (Z)	1,856	Bending moment	3,603	2,677
Pitch (Θ_X)	1,198			
Yaw (Θ_Y)	1,480			
Roll (Θ_Z)	1,262			

bending moments. For example, the heave motion response of the device amounts to approximately 1,800 half cycles, while there are more than twice as many tension and bend moment half cycles. Thus all 6 degrees of freedom must be considered in the design analysis, which is the case for the coupled computational analysis.

6.3.1.4 Effect of wave parameters

The analysis so far considered the motion and load response of the device for a particular irregular sea state. To assess the load conditions for varying operating environments, different wave states must also be assessed. In the following, the sensitivity of maximum loads and fatigue cycles is shown with respect to the significant wave height and the wave period.

Figure 6.21 shows the relationship between wave height and the resulting maximum tension near the attachment point for both cable configurations. As it would be expected, an increase in wave height is associated with an increased maximum tension force.

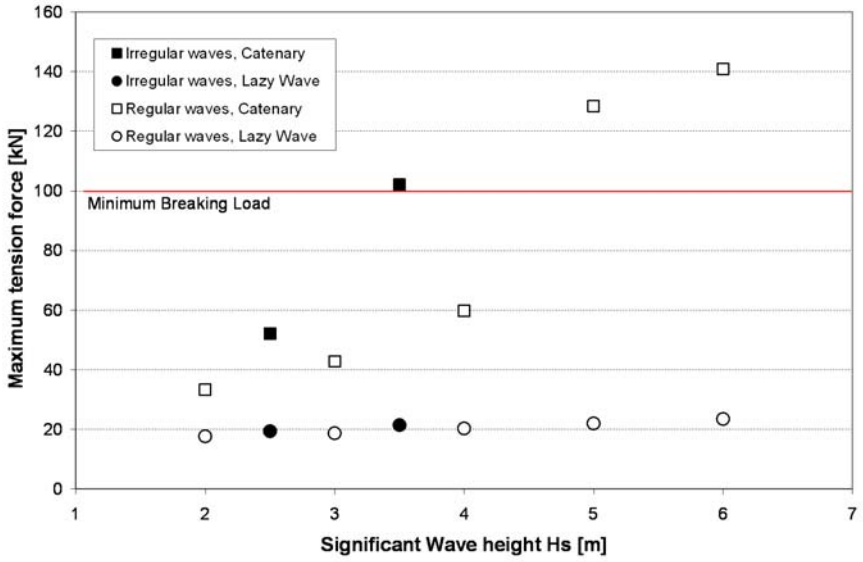

Figure 6.21: Maximum tension force (0.5m off attachment point) for different wave heights and cable configurations.

While the maximum tension for small waves is comparable for both cable configurations, the catenary cable is subject to a steep increase of tension loads for larger wave

heights. The Lazy-Wave shape only shows a slight increase of tension loads for higher waves. In fact a threefold increase of H_s leads to a one-third increase of maximum loads for the Lazy-Wave shape compared to a fourfold increase for the catenary case.

The maximum tension force that was modelled for the sea state with $H_s = 6m$ is $F_{max,lazy} = 23.4kN$ and $F_{max,catenary} = 140.9kN$, respectively. The Lazy-Wave configuration reduces the maximum tension force by up to a factor of six for the modelled conditions.

If we turn to the bending moment, increased wave heights also lead to a higher bending moment. This correlates with a reduction of the occurring cable bending radii. This relationship is depicted in figure 6.22. The minimum bending radius decreases in the more realistic irregular sea states for the catenary shape, i.e. the cable is subjected to larger bending moments in irregular seas.

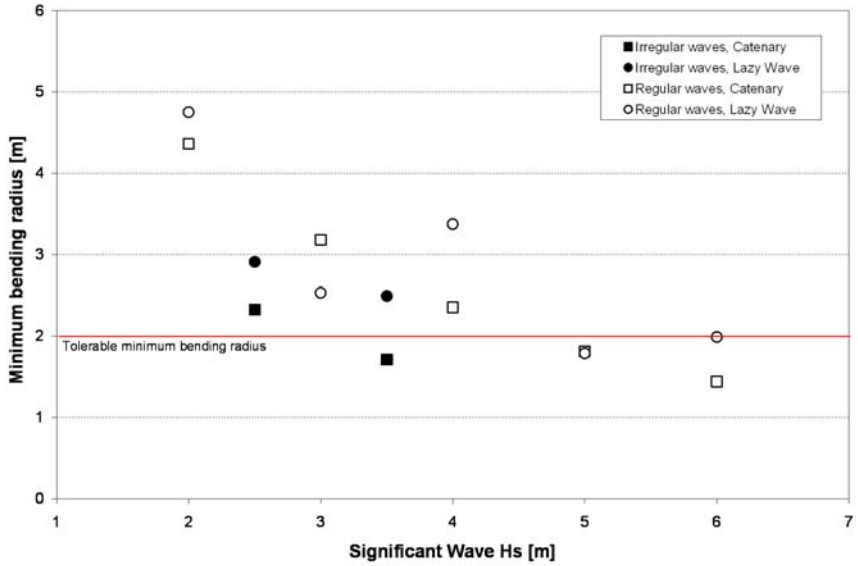

Figure 6.22: Minimum bending radius (0.5m off attachment point) for different wave heights.

While the device motion response for different wave heights influences the load amplitude, it does not have a considerable effect on the number of load cycles. For a modelled 25min period, approximately 500 (600) half cycles are counted for the tension force in regular (irregular) sea states. There are slightly less bending half cycles of

approximately 400 (500) in regular (irregular) seas.

The wave period has a direct effect on the number of load cycles. Figure 6.23 shows the counted rainflow cycles for both tension force and bending moment for different wave periods. An increasing wave period reduces the number of load cycles, as the motion response frequency of the device is governed by the incident wave period. An increase of wave period from 5s to 13s reduces the number of counted load cycles by approximately a factor of two. The resonance effects at 9s (half of the device natural frequency) can be identified in the pronounced drop in load cycles, as larger amplitude, lower frequency oscillations dominate the motion response. Tensional load cycles tend to be more numerous than bending moment cycles.

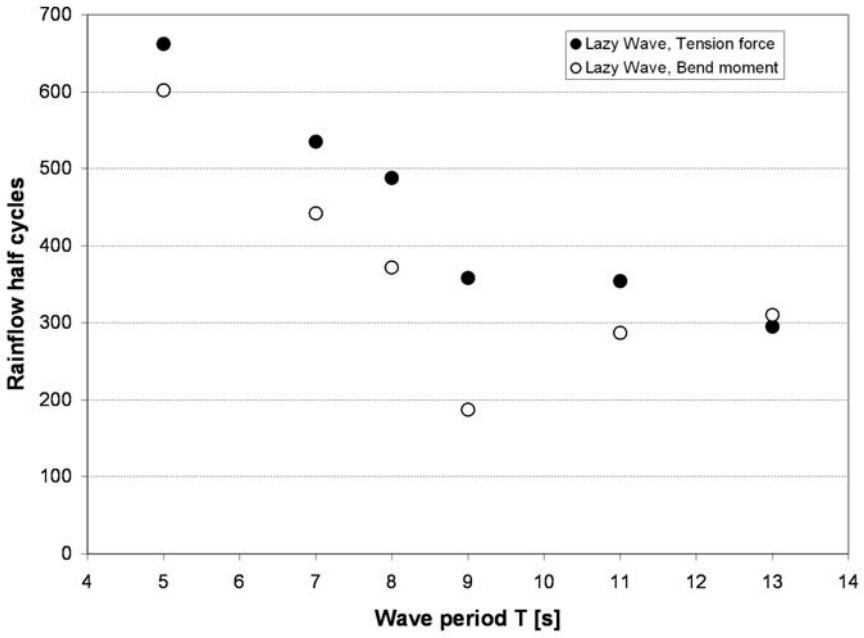

Figure 6.23: Rainflow half cycles of Lazy-Wave configuration for different wave periods (regular sea states, Hs = 2m, calculated 0.5m off attachment point, duration of 25 min).

6.3.2 Reliability assessment

The performance assessment of a system regarding reliability, availability and maintainability (RAM) provides crucial information for decisions on project investment, design

alternatives, and maintenance strategies and the identification of necessary improvements. Two general approaches can be distinguished, measurement-based techniques and model-based assessments. The approach applied here is a combination of both using experimental measurements and numerical modelling tools to assess the reliability of the marine cable in a wave energy application. The considered reliability aspects are i) compliance with maximum design load limits and ii) estimation of fatigue life for the copper conductor core of the cable.

6.3.2.1 Maximum load assessment

There are two main mechanical design specifications that must not be exceeded to maintain the integrity of the cable. The minimum breaking load (MBL) is given at $MBL = 100kN$ while the minimum bend radius (MBR) is specified as $MBR = 2m$ (Martinelli *et al.*, 2010).

The maximum tension force for both cable configurations in a number of sea states were shown in figure 6.21. The tension force for the free hanging catenary cable exceeds the MBL in a number of cases and by up to 40% of the MBL in the most extreme case of $H_s = 6m$. The tension force in case of the Lazy-Wave shape does not exceed the cable strength in any of the modelled sea states. In comparison to the catenary shape, forces are reduced and compression is avoided.

The bending radius of the cable in the modelled sea states is plotted in figure 6.22. With a MBR of 2m it can be seen that the cable has the potential to suffer damage for wave heights larger than 4m for both the catenary and umbilical configuration. The comparison of regular and irregular sea states shows more extreme bending radii for the catenary shape in realistic, irregular seas. This indicates that the Lazy-Wave configuration might be more suitable in field conditions.

It is of interest to compare the results of the simple sinusoidal approximation with the outcomes of the numerical simulation. For the simple relationship, suggested by Worzyk (2009) (section 5.2.2), the maximum tension force at the hang-off point is estimated with equation 5.6, assuming pure sinusoidal motions of the top-end. This is done for both configurations, the simple catenary, and the Lazy-Wave shape.

Table 6.7 compares the results with the maximum tensions computed in the dynamic simulation. The highest tension force for the Lazy-Wave shape is $F_{max,dynamic,lazy} = 21.4kN$, which is below the maximum force estimated with the sinusoidal approximation. The opposite is the case for the catenary configuration. The approximation estimate is $F_{max,sinus,lazy} = 32.6kN$ while the simulation yielded a maximal tension force $F_{max,dynamic,lazy} = 102.0kN$.

Table 6.7: Comparison of maximum tension forces near umbilical hang-off point for different geometric configurations and calculation methods.

Calculation method	Geometric configuration	
	Lazy wave	Catenary
Sinusoidal approximation	26.5kN	32.6kN
Dynamic simulation	21.4kN	102.0kN

While the sinusoidal approximation is in reasonable agreement with the simulation results for the Lazy-Wave, the approximation does considerably under predict the maximum tension force for the catenary shape, i.e. the sinusoidal assumption does not hold in the latter case. Moreover, the sinusoidal approximation does not provide any load information along the length of the cable as it is given by a dynamic simulation.

6.3.2.2 Fatigue life estimation

The initial analysis of the load patterns (section 6.3.1.3) indicated that a large number of annual load cycles, in the order of 10^6, may be expected for the power cable. Therefore a more detailed fatigue assessment is presented here that was carried out for the copper conductor of the Lazy-Wave umbilical configuration.

Electrolytic Tough Pitch (ETP) copper is most commonly used for power conductors (Mendenhall & Schmidt, 1998) and is assumed as conducting material in the following. The main factors that influence the conductor fatigue life are the tensile strength and the number of wire strands. Cable construction parameters such as lay length or construction type influence the fatigue life to a lesser extent. In this respect, the assumption of a single ETP copper conductor can be considered as a lower bound for fatigue life.

The fatigue life estimation is performed in three sequential steps:

1. Cycle count for modelled sea states
2. Estimation of accumulated cycles for assumed load conditions at the Wave Hub site
3. Assessment of fatigue limit through material fatigue curves

Strain-cycle $\epsilon - N$ fatigue curves Empirically derived S-N curves are the conventional point of reference for fatigue assessments, showing the number of cycles a material can withstand until failure, depending on the stress range. However, copper is characterised by non-linear stress-strain behaviour and stress relaxation. For this reason Karlsen *et al.* (2009) suggest the use of a strain-cycle $\epsilon - N$ curve for ETP copper. The $\epsilon - N$ fatigue curves account for the elastic and plastic strain the material undergoes. The so-called Coffin-Manson relationship (equation 6.9) denotes the total strain amplitude ϵ_a as the sum of plastic $\epsilon_{a,pl}$ and elastic strain $\epsilon_{a,el}$ (Schijve, 2009, p.165).

$$\epsilon_a = \epsilon_{a,pl} + \epsilon_{a,el} = C_1 N^{-\beta_1} + C_2 N^{-\beta 2} \tag{6.9}$$

Where C and β are material constants that describe the shape of the fatigue curve.

The Strain-cycle $(\epsilon - N)$ fatigue curve for copper is plotted in figure 6.24. The material dependent variables for the two distinct linear sections are: $C_1 = 0.7692$, $\beta_1 = 0.5879$, $C_2 = 0.0219$ and $\beta_2 = 0.1745$.

Strain calculation and rainflow cycle count For the stress/strain calculation, OrcaFlex models the cable as a cylinder of uniform material. The parameter that may be used to count the number of rainflow cycles is the 'maximum strain range zz' which denotes the maximum bending strain the cable is exposed to at the outer diameter. A time series of the strain cycles near the attachment point of the power cable is shown in figure 6.25.

In order to compute the number of cycles for the copper conductor some additional calculations were performed. If a cable cross-section similar to the one shown in figure 5.6 is assumed, the location of the copper conductor is about half the diameter

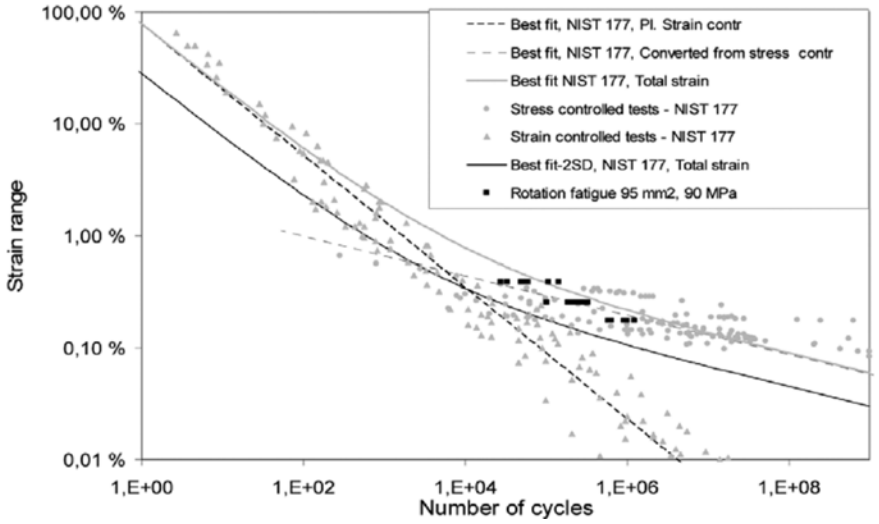

Figure 6.24: Strain-cycle $\epsilon - N$ fatigue curve for copper conductor. Graph shows results from Simon *et al.* (1992) for different copper qualities (under stress and strain controlled conditions) and results from rotational fatigue tests by Karlsen *et al.* (2009). Figure reproduced from Karlsen *et al.* (2009).

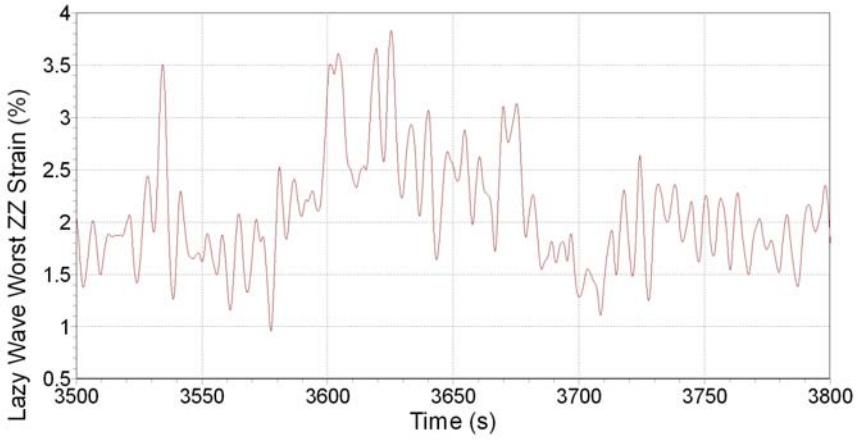

Figure 6.25: Time series of umbilical strain at its outer diameter, 0.5m off the attachment point; worst ZZ strain relates to the maximum strain ϵ.

away from the umbilical centre point, which means that the strain as calculated at the outer diameter, is a very conservative estimate for the conductor. If the cable is treated as a simple beam, following the Euler-Bernoulli hypothesis (i.e. plane sections stay plane), the stress can be calculated as given in equation 6.10 (Bruhns, 2003). For a constant Young's Modulus E the conductor is subjected to a strain ϵ which is half of the outside diameter strain (worst zz strain); since $\epsilon = \sigma/E$.

$$\sigma = \frac{M_x}{I_x} \cdot y \tag{6.10}$$

Where σ = stress, M = moment for a given axis, I = second moment of area and y = distance from the centreline.

As the smallest load cycles do not significantly contribute to fatigue damage, small strain cycles are not considered for this analysis. The threshold is chosen at 1% strain, as this represents the region of elastic-plastic transition (compare figure 6.24).

After these adjustments, the rainflow count was performed following the procedure described in section 6.1.3. The rainflow plots for the two irregular sea states are shown in figure 6.26 and 6.27 respectively. Each matrix shows the number of cycles that occur within each bin for a particular strain minimum and maximum. For $H_s = 2.5m$, three load cycles larger than the 1% strain level occur (Fig. 6.26(b)). A total of 29 full load cycles larger than the 1% threshold strain range are counted for the conductor at $H_s = 3.5m$ (Fig. 6.27(b)).

Annual load cycle estimation To estimate the expected annual load cycles of the cable conductor the modelled cases are assigned to the associated sea sates at the Wave Hub site. The assignment is graphically illustrated in figure 6.28 which shows the underlying scatter plot and the sum of the annual occurrence for the considered sea sates, $\sum(H_s = 2-4m,\, T_e = 7-9s) = 21.3\%$.

The number of load cycles for each sea state is calculated for the annual occurrence probability of the respective sea state interval (equation 6.11). The resulting estimated conductor strain cycles for the modelled range of sea states, together with

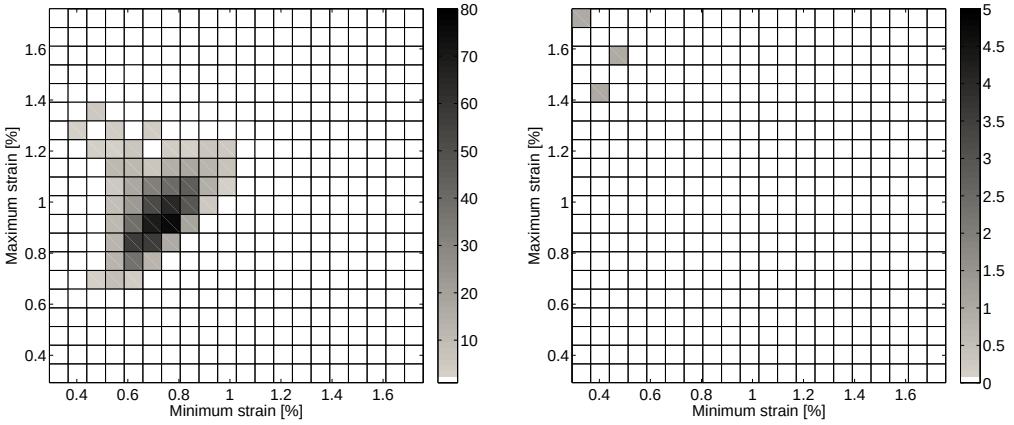

(a) Unfiltered (b) Filtered

Figure 6.26: Rainflow strain cycle matrix for copper conductor. Filter threshold of 1%; sea state $H_s = 2.5m$, $T_p = 8s$, duration $t = 2.25h$.

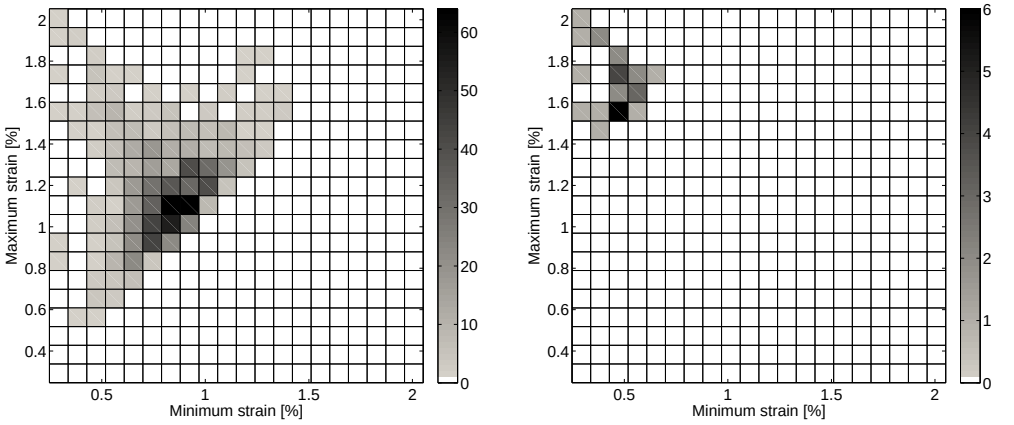

(a) Unfiltered (b) Filtered

Figure 6.27: Rainflow strain cycle matrix for copper conductor. Filter threshold of 1%; sea state $H_s = 3.5m$, $T_p = 8s$, duration $t = 2.25h$.

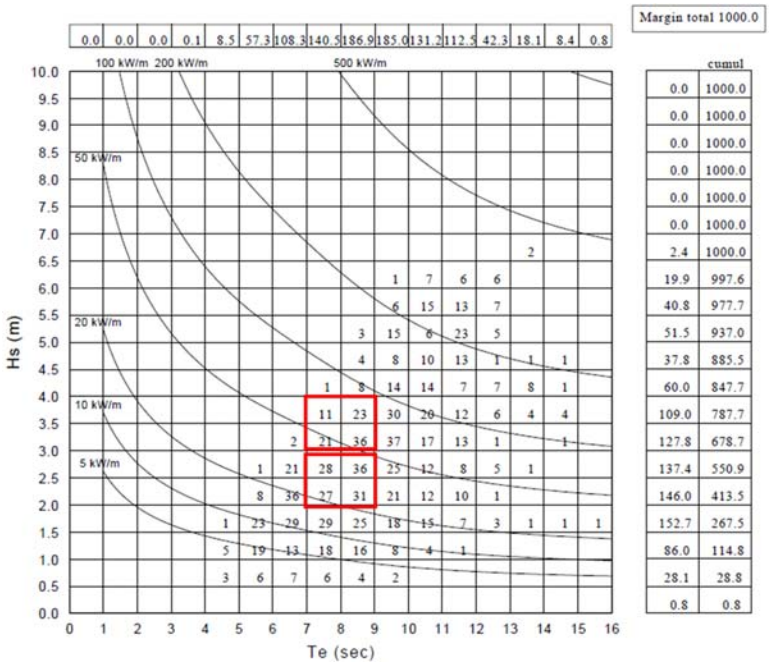

Figure 6.28: Wave climate characteristics at the Wave Hub site, and assigned annual occurrences for modelled sea states, adapted from Pitt *et al.* (2006).

the copper fatigue limits at constant 1% strain amplitudes, are given in table 6.8 and are graphically presented in figure 6.29.

$$N_{annual}(H_s) = N_{experiment} \cdot \frac{t_a}{t_{experiment}} \cdot P(Hs) \tag{6.11}$$

Where $N_{annual}(H_s)$ = number of strain cycles during a typical year for a particular sea state, t_a = 8760h, $t_{experiment}$ = experimental time [h] and $P(H_s)$ = occurrence probability of a particular sea state.

Although the results are approximations of the copper conductor strain cycles, the number of cycles surpass the conservative fatigue limits of the $\epsilon - N$ curve at 1% strain range (Best fit - 2 standard deviations). The best-fit fatigue limit is exceeded for an annual probability of 21.3%. This is especially of concern as the site specific evaluations for the Wave Hub site do only constitute fractions of a year. The hypothetical full year at a sea state of $H_s = 3.5m$ lies considerably beyond the specified fatigue life.

Even though it must be noted that the actual number of cycles is device and site

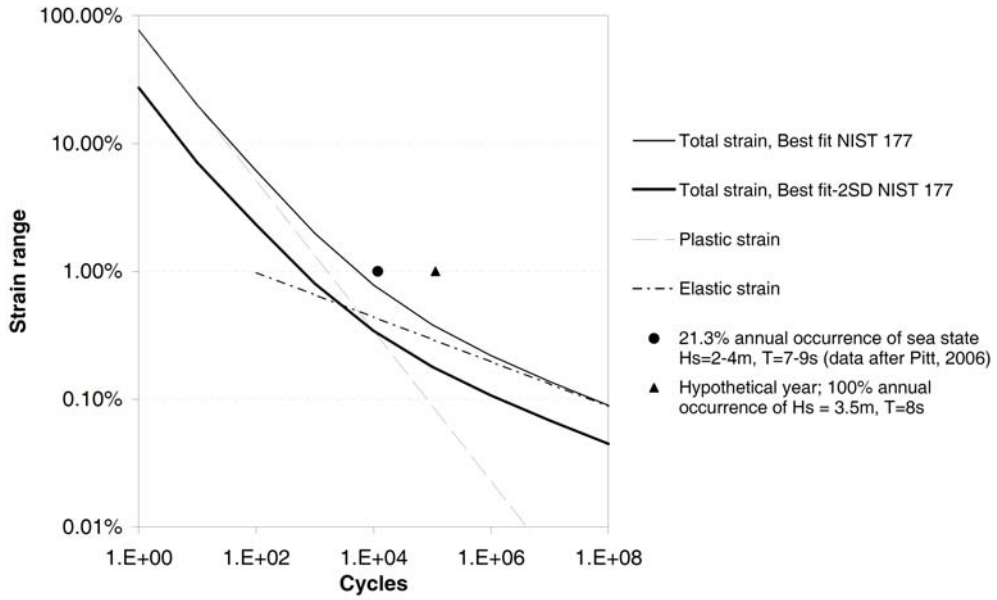

Figure 6.29: Strain - cycle $\epsilon - N$ copper fatigue curve and expected number of conductor load cycles $> 1\%$ strain range for typical year of operation (data: own calculations after (Karlsen *et al.*, 2009; Pitt *et al.*, 2006)).

Table 6.8: Strain cycles (exceeding 1% range) for copper conductor in Lazy-Wave double armoured umbilical - experimental tests and annual accumulated cycles for sea state at Wave Hub site.

Sea state		Tank test		Annual accumulated cycles, N_{annual}	Fatigue limit $\epsilon - N$ curve	
H_s [m]	T [s]	Time t_{exp}	Cycles N_{exp}	after Pitt *et al.* (2006)	Best fit	Best fit-2SD
3.5	8	2.25h	29	10,275		
2.5	8	2.25h	3	1,425		
				$\sum(11,699)$	5,100	590

specific, the results presented quantify the potential fatigue failure for a generic wave energy converter at a particular site and lead to the conclusion that the copper conductor of a typical dynamic power cable would have an unacceptable short fatigue life of less than one year.

6.3.2.3 Discussion of results

This section showed that high peak tensions in dynamic marine cable applications can be avoided with a Lazy-Wave configuration, while the catenary configuration is subject to severe peak loads induced by the dynamic motion response of the floating wave device. However, the Lazy-Wave shape introduces two local load peaks at the buoyancy transition points (compare figure 6.18). This is consistent with the advice given in DNV (2004) for compliant riser systems which identify the area in the wave zone, hog and sag bends and terminations as the most critical and failure-prone locations.

Due to the limitations of available information regarding the extent of experiments and constraints in the numerical modelling of the cable cross-section, this case study is subject to some necessary simplifications:

- simplified power cable design, i.e. cable modelled as cylinder of uniform material;
- the response and load behaviour have been determined for only a limited number of sea states;
- the numerical model does not allow a coupled assessment of the floater/cable;
- no fluid loading by waves and currents is applied to the cable.

It is inherent that these simplifications will affect the specific outcomes of the assessment, however the general method can be easily adapted to more detailed analysis which will be part of further work.

The simplified stress/strain calculations in OrcaFlex model the cable as a cylinder of uniform material. Hence friction stresses of different cable layers are not considered. As a consequence, the calculated stress/strain results are not directly applicable to composite structures, such as multi-layered umbilicals. There are a number of software tools available that perform the cross-sectional stress analysis with more specific FEA

models (Ekeberg *et al.*, 2006; Knapp *et al.*, 2002), which is the subject of further work described in section 8.2.

As wave energy converters will be typically deployed in more energetic sea conditions than the operational conditions modelled here, the study strongly indicates the requirement for a bend stiffener to restrict the bending and avoid kinking/damaging the cable near the attachment point. The implementation of dedicated bend stiffeners require careful design and are specifically tailored to the predicted load cases (Lane *et al.*, 1995), and have not been further considered in this thesis.

In more general terms, the usefulness of the applied methodology combining i) experimental tank tests, ii) numerical modelling and iii) site specific characteristics was shown. It allows to estimate the environmental loading conditions of components in the absence of field experience. As a result, the design information and data can be enhanced and an initial estimate of the operational lifetime can be made prior to deployment in testing, yet unchartered dynamic conditions.

Chapter 7

Marine umbilical cable tests

7.1 Characterisation tests

The stiffness properties of marine umbilicals are important design parameters for marine umbilicals. They determine the load response and are required to evaluate the expected loading through numerical models. Thus, the reliability estimate of the cable is dependent on an accurate evaluation of the cable stiffness. Two stiffness parameters of particular importance for umbilicals are experimentally determined in the following:

1. Tensile stiffness EA

2. Bending stiffness EI

For simple structures of uniform material, the tensile stiffness can be analytically derived as the product of Young's modulus E and the cross-sectional area A. In the case of the bending stiffness, E is multiplied with the area moment of inertia I.

Umbilicals are constructed from a range of different layers and materials which makes this calculation difficult. Even though specialist software exists to model the stiffness characteristics (Ekeberg *et al.*, 2006), the results require validation through experimental tests.

This test also provides a worthwhile initial test to demonstrate the basic capability of the test rig and investigate the stiffness behaviour of the umbilical cable.

7.1.1 Axial stiffness

The calculation of the spring constant k is well known, e.g. (Shigley, 2004), as:

$$k = \frac{\partial F}{\partial \delta} = \frac{EA}{l_0} \tag{7.1}$$

where F is the tensile force acting on the specimen, δ is the elongation of the specimen and l_0 is the original length of the specimen.

7.1.1.1 Experimental setup

For this simple tension test, the angles at the moving headstock are kept constant at $\Theta_x = \Theta_y = 0$. Each set point is then held for a period of $t = 20s$. Starting with a force of $F_0 = 10$kN, the tension is incrementally increased to set points in steps of 5kN. To ensure that enough data is collected to perform a linear regression, and the holding capacity of the clamp is not exceeded, a total of nine independent tests were conducted with subsequently higher maximum tension forces, as tabulated in table 7.1.

Force [kN]	10	15	20	25	30	35	40	60	80
Test	I	II	III	IV	V	VI	VII	VIII	IX

Table 7.1: Axial stiffness test schedule, maximum tension forces and test number.

For each test the tension force F, and the displacement of the linear cylinder D have been recorded at 10Hz sample frequency. The recorded measurements during all nine tests are shown in figure 7.1. The tension force record which is plotted in 7.1(a) shows that the intended force steps are closely followed and reproduced by the rig. There were only three occasions (test II, IV and IX) where the 'ramping down' part of the curve is slightly noisy. This effect is attributed to sticktion forces occurring in the linear bearings of the hydraulic actuator, which lead to a disturbed feed-back signal and subsequent adjustments through the control algorithm. However, this does not effect the test results for the axial stiffness test, as only the steady state point for each set point is used in the following calculations.

In figure 7.1(b) it can be seen that the increased tension force correlates with the resulting displacement of the actuator, i.e. the cable is extended in small steps. Furthermore, two observations which have been made during the experiment are clearly reflected in the extension. The first incident was a small slippage (10mm) of the cable

out of the connection clamp at the linear actuator. This happened at the end of test I, when the actuator suddenly retracted back due to its control default position. This was resolved through a different end position of the cable which requests $F_{end} = 0$ instead of $F_{I,end} = -500N$. The amount of slippage D_{slip} can be calculated from the measurements as $D_{slip} = D(I, 10kN) - D(II, 10kN) = 6.6mm$. The displacement of all other tests (II-IX) is very close, some minor slippage (0.7mm) at the cable clamp occurred during test VIII.

The second observation which was made is a continuous cable slip from the clamp at $F > 65kN$, leading to a displacement signal which is very similar to the behaviour seen for material yielding. However, in this case it is a matter of the connection strength which is exceeded that leads to the noticeable behaviour at the end of test IX. The test was aborted at this point. The amount of slippage after test I and IX is pictured in figure 7.2. The exit of the cable clamp was marked and observed for each test to ensure the clamping force was sufficient.

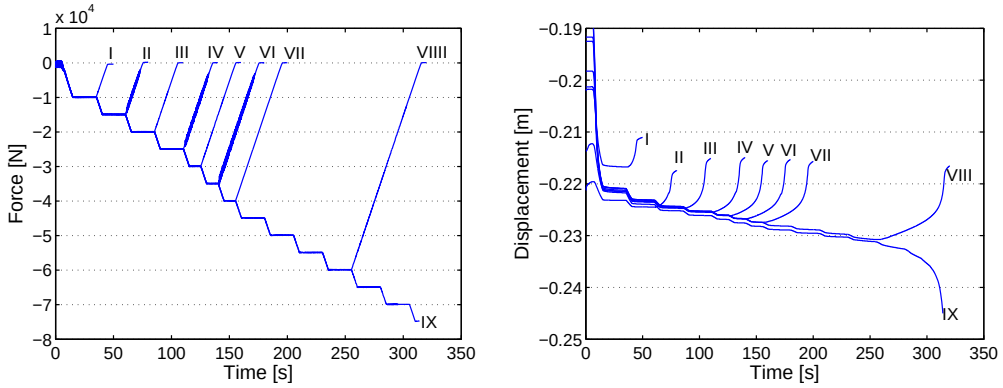

(a) Force

(b) Displacement

Figure 7.1: Logged data signals of axial stiffness test series, showing the measured tension force 7.1(a) and the position of the linear cylinder 7.1(b).

7.1.1.2 Calculations and results

In order to determine the linear stiffness the stationary points for each experiment are extracted from the measurements with regards to cylinder displacement D and tensile force F. This yields a first approximation of the cable stiffness, plotted in figure 7.3(a).

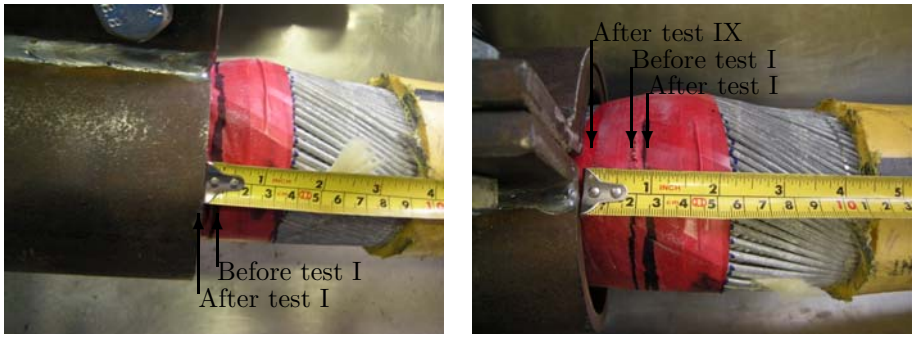

(a) Test I (b) Test IX

Figure 7.2: Cable clamp slippage, pictured at the end of test I and IX.

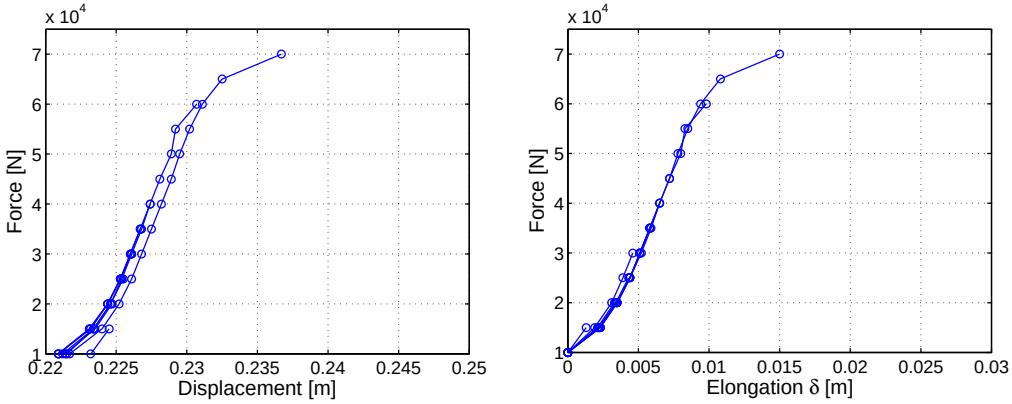

(a) Position of linear cylinder (b) Cable elongation δ

Figure 7.3: Measured position of linear cylinder 7.3(a) and calculated cable elongation 7.3(b) for different axial force set points.

To compensate for the observed cable slippage, the cable elongation for each stationary force step δ_i is calculated with respect to the initial position D_0 with $F = 10kN$.

$$\delta_i = D_i - D_0 \;\; i = 1 \dots 12 \tag{7.2}$$

This calculation is performed for each of the conducted tests. The compensated stiffness behaviour is plotted in figure 7.3(b). It can be seen, that the values follow a characteristic curve and overlay each other, indicating that the tests reproduce the stationary stiffness values. The plot can be separated in three distinct regions. First, the nonlinear region at the lower part of the curve, up to a force value of approximately $F = 20kN$. In this region the cable is still sagging slightly, due to its own weight. Thus, the observed displacement can be attributed mostly to the fact that the cable is straightened. Second, a region of constant linear stiffness up to about $F = 50kN$. Third, for $F > 50kN$ a yielding behaviour can be observed, which is due to the umbilical slipping out of the clamp. As both the nonlinear and the plastic region are influenced through the described factors, they do not describe the actual stiffness of the umbilical cable. Thus, the linear part is used in the following to derive the cable stiffness.

The linear part of the curve has been fitted with a linear regression model in MatLab, yielding the estimator for the force $\hat{F}$ (figure 7.4).:

$$\hat{F} = 6.76 \cdot 10^6 \frac{N}{m} \cdot \delta - 3.62 \cdot 10^3 \tag{7.3}$$

Thus, the axial stiffness is estimated as $k_{Umbilical} = 6.76 \frac{MN}{m}$. The goodness of fit can be assessed by the coefficient of determination R^2 which is calculated as (Draper & Smith, 1981, p. 90):

$$R^2 = \frac{\sum (\hat{F}_i - \bar{F})^2}{\sum (F_i - \bar{F})^2} \tag{7.4}$$

where $\hat{F}$ is the estimated fit, $\bar{F}$ denotes the mean and i denotes the measurement points. For the presented linear regression $i = 31$ and $R^2 = 0.988$. As $R^2 = 1$ describes a perfect fit, it can be seen that the linear fit provides an accurate model for the linear stiffness for higher tension forces, $F > 20kN$. Moreover, an extrapolation is usually valid until material yielding processes start to occur, for steel wire the yield stress at 0.2% strain $\sigma_{0.2}$ is typically in the region of $\sigma_{0.2} = 460MPa$ (Custõdio & Vaz, 2002).

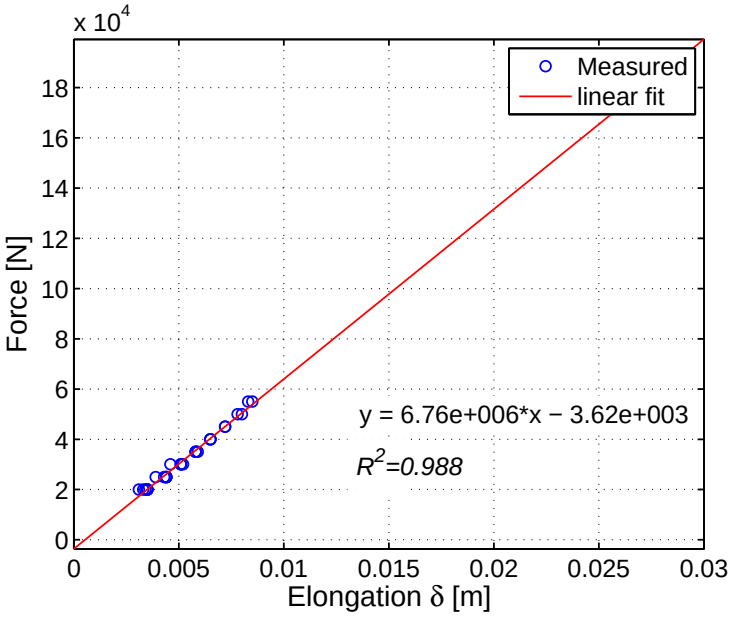

Figure 7.4: Axial tension stiffness test, linear regression for chosen measurements.

7.1.2 Bending stiffness

The bending stiffness test aims to determine the bending characteristics of the umbilical cable. The bending stiffness EI expresses the bending moment in relation to the deflection of the cable. The Euler-Bernoulli bending theory defines the bending moment M for a deformed bar of linearly elastic material, with for the exact curvature κ, as (Pilkey, 2005):

$$M = EI \frac{\left(\frac{\mathrm{d}^2 d}{\mathrm{d}x^2}\right)}{\left(1 + \left(\frac{\mathrm{d}d}{\mathrm{d}x}\right)^2\right)^{\frac{3}{2}}} \tag{7.5}$$

where M denotes the bending moment, E is the modulus of elasticity, I is the area moment of inertia, d is the deflection and x is the axis coordinate.

For cases where the change in $\frac{\mathrm{d}d}{\mathrm{d}x}$ can be considered small, equation 7.5 can be linearised to:

$$M = EI \frac{\mathrm{d}^2 d}{\mathrm{d}^x 2} \tag{7.6}$$

and thus the bending stiffness can be rewritten as,

$$EI = \frac{M}{\kappa} \tag{7.7}$$

The conducted bending test varies the bending moment through different vertical angles at the headstock, and measures the cable deflection to calculate the corresponding cable curvature κ. To evaluate the effect of varying tensile loads, the test has been repeated for different tensile forces $F = [2500, 3000, 3500, 5000]N$.

In each case, the tensile force F is kept constant and the x-plane angle Θ_x at the headstock is varied in steps of $\Delta\Theta = 5^\circ$ over a range of $\Theta_x = \pm 30^\circ$. The y-plane angle is also kept constant at $\Theta_y = 0$.

7.1.2.1 Experimental set up

Ideally, the bending moment brought upon the specimen, and the resulting deflection, would be measured directly throughout the experiment. However, the instrumentation of the rig at this early stage only allowed the measurement of directly associated parameters from which the desired parameters could be derived. The measured parameters were:

- the angles Θ_x, Θ_y at the headstock by two angle encoders,
- the vertical distance of the cable to a fixed measurement height above the rig,
- the hydraulic pressure in all four cylinders which induce the bending moment on the headstock, p_i, where $i = 1, 2, 3, 4$,
- tension force F of the linear cylinder.

The cable deflection d was measured manually with a hand-held laser distance meter, Leica Disto DXT (figure 7.5). The measuring range is $m = 0.05 - 70m$ at an accuracy of 1.5 mm. The device was placed at a fixed height above the cable, using a bar across the test rig which was adjustable along the length of the cable. The readings were taken at each angle set point, and determined the distance between the cross bar and the cable. A reference point in the middle of the cable was marked, as the

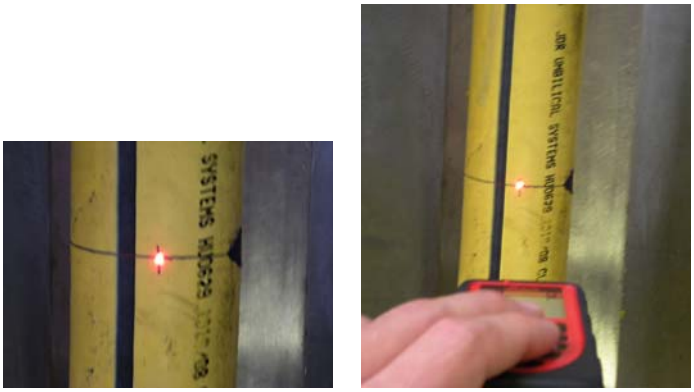

(a) Cable marking (b) Distance measurement

Figure 7.5: Laser point measurement of cable deflection.

maximal deflection was expected at this position. For this reason the cable was marked at $l = 2750mm$, to ensure readings are taken consistently at the same position.

The input test signal that prescribes the angular position of the headstock for all bending stiffness tests is shown in figure 7.6. It shows the close agreement of desired position (drive signal) and actual, measured position of the headstock, which was observed in all tests. The plotted signal shows one complete test, which has been conducted in two steps.

1. Positive angles - the top of the headstock leans towards the cable, causing the cable to deflect downwards.

2. Negative angles - the bottom of the headstock leans towards the cable, causing the cable to deflect upwards.

The reason for this distinction is the gravitational effect that is caused by the horizontal fitting of the cable in the test rig. The distinction in positive and negative angles allows to assess and compensate for the gravitational effects. While the deflection induced by the positive angles is assisted by gravity, the deflection for negative angles is opposed by the weight of the cable. By taking the mean of the measured deflection for a given positive and negative angle the, gravitational effect cancels out.

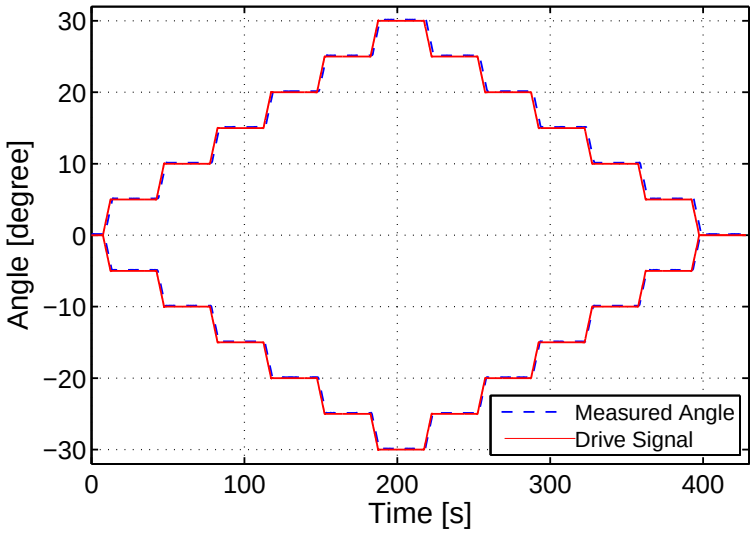

Figure 7.6: Bending stiffness test drive signal and measured headstock angle.

7.1.2.2 Calculations

As mentioned earlier, not all necessary parameters could be measured directly. The curvature κ and the bending moment M are calculated from the obtained measurements through the following considerations.

The curvature is derived from the geometric relationship between the headstock angle Θ_y and the measured deflection d under the idealised condition that the cable describes a circular arc. Using the conventions given in figure 7.7 (Papula, 2003), the length of the chord l is calculated as:

$$l = 2 \cdot \sqrt{d(2R - d)} \tag{7.8}$$

Expanding and rearranging of the equation yields an expression of R in terms of the initial cable length l and the measured deflection d.

$$R = \frac{l^2 + 4d^2}{8d} \tag{7.9}$$

The curvature κ is simply the inverse of the radius R, thus:

$$\kappa = \frac{1}{R} = \frac{8d}{l^2 + 4d^2} \tag{7.10}$$

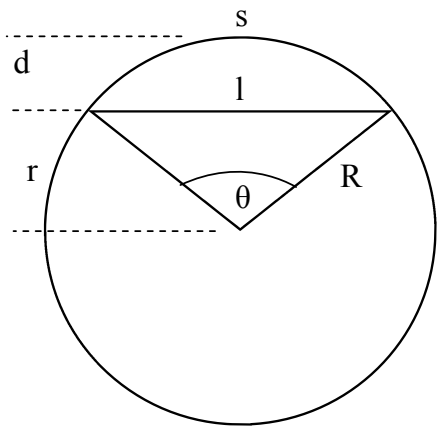

Figure 7.7: Circular segment conventions.

The bending moment M is derived from the pressure readings p_i and the position of the headstock Θ_x. For this purpose, an empirical calibration has been established through previous experimental tests that relate measured pressure differentials at given headstock angles to the exerted bending moment at the centre of the base plate. The pressure differential Δp is calculated from the measured pressure delivered to the headstock cylinders. The pressure differential for each axis results in a bending moment M. The measurements presented in figure 7.8 are based on data reported by Clifford (2011). For a range of different headstock angles both Δp and the corresponding bending moment M have been measured across the entire test capacity. A linear regression is performed for each angle and the parameters are shown in table 7.2. The correlation coefficient $R^2 \approx 1$ for all angles, which indicates that a linear fit is reasonable. In the following, the presented linear relationship $\Delta p \propto M$ is assumed, i.e. the measured pressure differential is used to calculate the corresponding bending moment for each bending angle.

7.1.2.3 Results

In this section the results are firstly presented in their measured form to provide the basis for the required calculations. Secondly, the calculated results for the bending stiffness are presented.

The deflection that was measured at the given angular setpoints for different tensile forces is plotted in figure 7.9. As explained earlier the tests were conducted both for

Table 7.2: Linear regression result parameters for bending moment M calibration test, $M = m \cdot \Delta p + t$.

AngleΘ	m	t	R^2
0	133	741	0.9995
5	146	-823	0.9971
10	133	-1207	0.9937
15	133	-2365	0.9973
20	120	-2631	0.9917
25	109	-3307	0.9978
30	97	-3765	0.9979

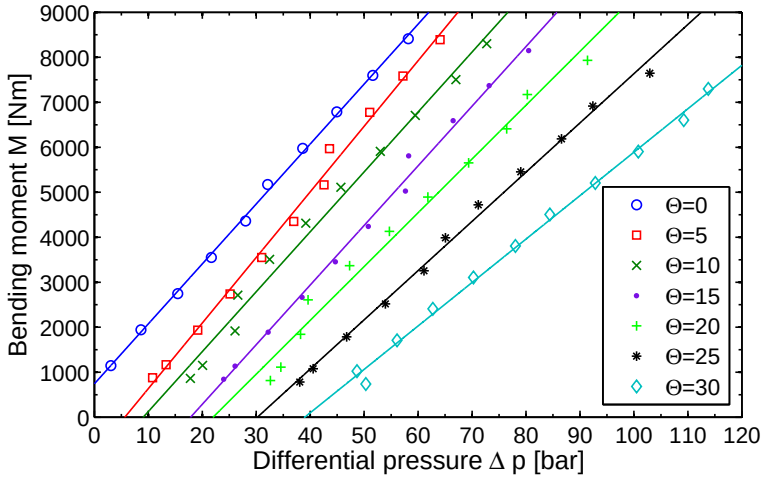

Figure 7.8: Bending moment calibration results. Plot shows measured data points for different headstock angles Θ and linear regression fits. Regression parameters are presented in table 7.2.

positive 7.9(a) and negative 7.9(b) angles. It can be seen that with positive angles the distance between measurement reference point and cable increases, i.e. the cable is deflected downwards for increased angles. In analogy to this, the positive angles mean a decreased distance, i.e. the cable bends towards the reference point of the measurement. As the deflection at $\Theta_x = 0$ varies for the different tensile forces, the relative deflection d_{rel} is computed with regard to the initial deflection d_0 for each tensile force case,

$$d_{rel,i} = |d_i| - |d_0| \quad \text{for } i = 0 \dots 12 \tag{7.11}$$

Where i denotes the number of headstock angles.

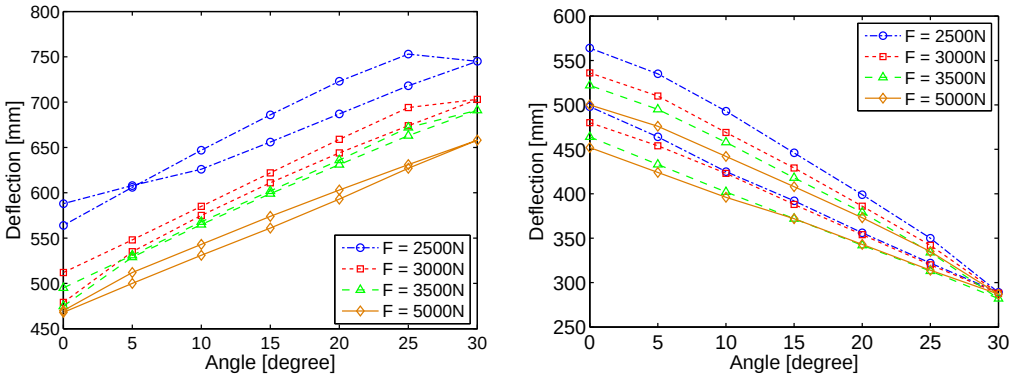

(a) Positive bending angle (b) Negative bending angle

Figure 7.9: Measured cable deflection for different bending angles.

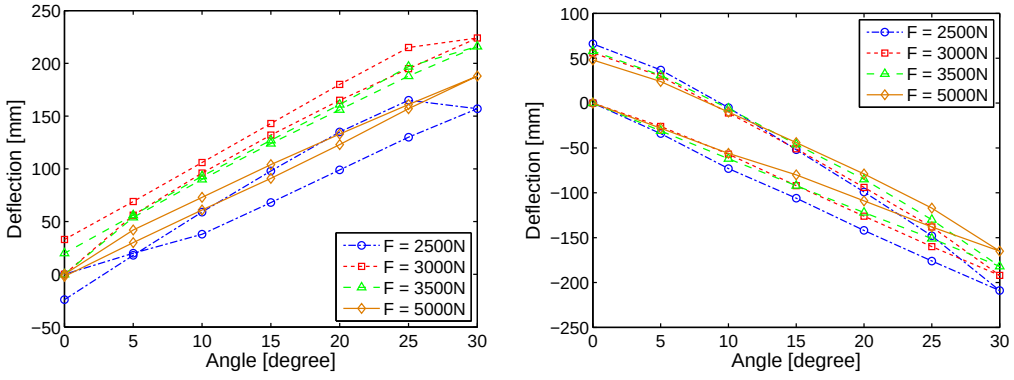

(a) Positive bending angle (b) Negative bending angle

Figure 7.10: Calculated relative cable deflection for different bending angles and tensile force.

The relative deflection, shown in figure 7.10, allows a comparison between the different tensile forces. The main points to consider are:

- Each test run starts at $\theta_x = d = 0$ and follows the plotted curve.
- As expected, the positive angle tests 7.10(a) are subject to a larger deflection than the negative angle tests 7.10(b) due to the assistance of gravity.
- All curves indicate a hysteresis effect. The deflection for decreasing headstock angles ($\Theta_x 30° \rightarrow 0°$) is higher than for increasing angles ($\Theta_x 0° \rightarrow 30°$).

As a third step, the objective was to eliminate the influence of gravity on the measured deflection. For this purpose, the mean relative deflection $\overline{d_{rel}}$ values of the positive and negative tests were computed for each headstock angle,

$$\overline{d_{rel,i}} = \frac{d_{rel,i,positive} + d_{rel,i,negative}}{2} \tag{7.12}$$

The results are plotted in figure 7.11, which show the close correlation between bending angle and deflection, as well as the similar gradient of all tests.

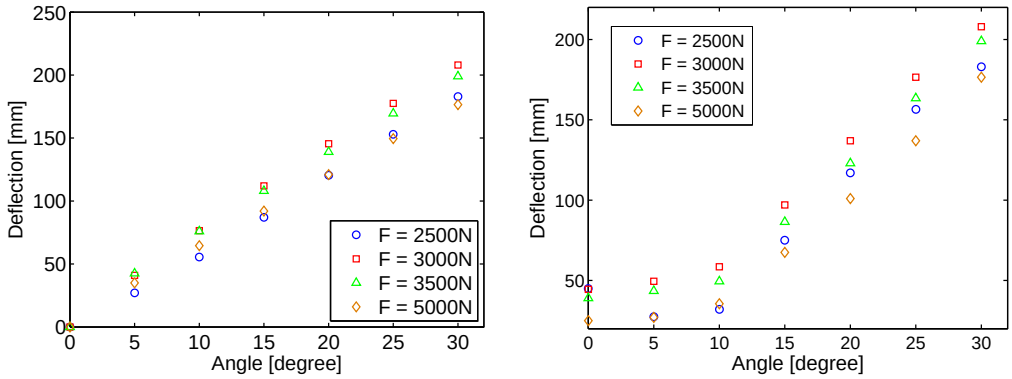

(a) Increasing angle

(b) Decreasing angle

Figure 7.11: Calculated mean cable deflection for different tensile forces, showing increasing part of the bending cycle and decreasing part.

The bending stiffness of the cable is described by the slope of the curvature - bending moment (κ-M) relationship. The bending moment for each angle setpoint is calculated using the measured pressure difference between the hydraulic actuators Δp together with the linear relationship that was established earlier and is given in table 7.2.

The curvature κ is calculated after equation 7.10 using the mean relative deflection $\overline{d_{rel,i}}$ for each headstock angle. Figure 7.12 shows the κ-M curves for the different tensile forces. In all cases a hysteresis effect is observable. For increasing headstock angles the bending moment leads to a linear increase of the cable curvature. After the maximum bending point at $\Theta_x = 30°$ is reached, the cable resists the reversed bending. This can be seen in the fact that the data points for increasing angles form the lower part of the curve, while decreasing angles constitute the upper part of the curves. Thus, an increased bending moment M is required to induce the same curvature κ when the cable bending is reversed. This behaviour of armoured, multi-layered cables has been termed as "bi-linear hysteretic bending moment against curvature relationship arising from the progressive activation of friction and consequential slipping between adjacent layers" (Vaz & Patel, 2007, p.470).

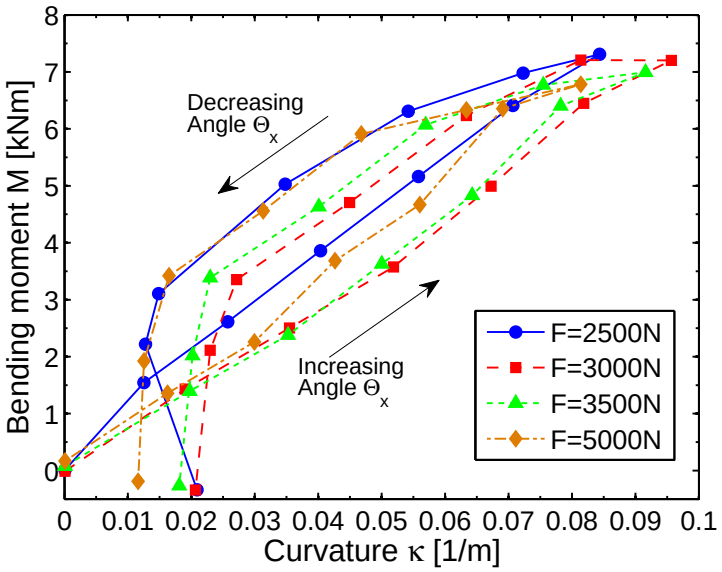

Figure 7.12: Calculated bending stiffness. Plot shows data points for different tensile force settings. Slope of the linear regression lines represents bending stiffness. Regression parameters are presented in table 7.3.

Table 7.3: Linear regression result parameters for bending stiffness.

Force [N]	Bending stiffness EI $[Nm^2]$	t [Nm]	R^2
2500	10142	151	0.89
3000	9766	82	0.93
3500	10352	91	0.93
5000	11537	135	0.93

7.2 Service simulation test

A major objective of the umbilical test was to demonstrate the capability of DMaC to replicate the operational load conditions which would be expected for components in a wave energy application. As part of the collaboration with the marine cable manufacturer JDR Cable Systems, the load envelopes for an umbilical cable, designed and modelled for a wave energy project were made available to perform such a service simulation test. The load information stems from an in-house OrcaFlex simulation from JDR. The simulations are similar to those described earlier in section 5.2 but use more precise values for the cable parameters and motion characteristics of a realistic, full-scale floating wave energy device.

Figure 7.13 displays a screen shot of the numerical model using a lazy wave configuration for the umbilical cable. Also of interest is the bend stiffener at the top-end attachment point of the cable which restricts the bending of the cable. The use of the bend stiffener moves the critical bending point of the cable to the end of the bend stiffener. The experimental load conditions at this position were replicated in the service simulation test.

7.2.1 Time series input

The input load data for the service simulation test was provided in the form of time series that describe typical mechanical load conditions for the cable section just after the bend stiffener. The input parameters are briefly presented in the following, and are summarised in table 7.4:

- Effective Tension

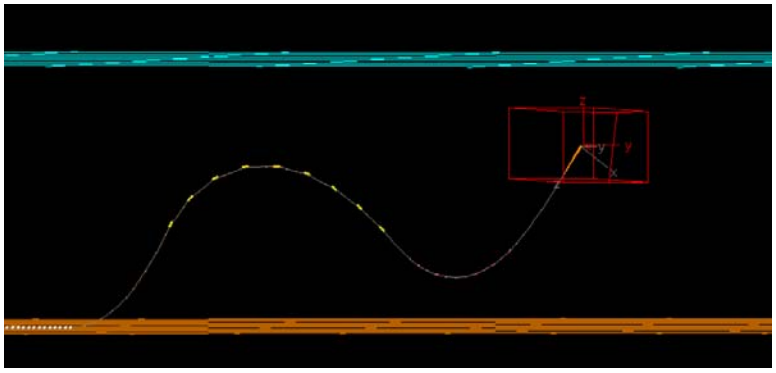

Figure 7.13: Screen shot of numerical simulation of power umbilical cable for full-scale floating WEC, courtesy of JDR.

- Angle between cable section and adjacent section plane (resolved for angle with zx-plane (Ezx), which corresponds to y-bend; and zy-plane (Ezy), corresponding to x-bend.

Only a short load signal with a duration of 5 minutes was employed in the initial tests presented here, which had the purpose to demonstrate the capability of the rig, rather than to fatigue test the cable, which is beyond the scope of this thesis.

The effective tension signal is plotted in figure 7.14(a). The negative values denote the tensile force experienced by the cable section which varies between -2.8kN and -5.3kN. The tension force is highly cyclic, with a total of 122 load cycles. This effective tension is combined with bending angles at the headstock which are depicted in figure 7.14(b). The angles are also highly cyclic and follow the five incident wave groups with a range between $-16.4°$ and $14.5°$.

The tests were carried out with the experimental setup described in section 5.3.7, with a total of four independent test runs and a sampling frequency of 50Hz to ensure the repeatability of the results and the test rig performance. The measured load and displacement data is presented and assessed in the following.

7.2.2 Test results and simulation accuracy

The test results are presented in a way that evaluates the accuracy to which the desired load signals are replicated through the experimental setup. For the comparison and

Table 7.4: Statistical properties of umbilical test input parameters, 5min signal, given for cable section after bend stiffener, courtesy of JDR.

Type	Tension force [N]	y-bend angle (Ezx) [°]	x-bend angle (Ezy) [°]
Minimum	-2813	-16.4	-12.6
Maximum	-5324	12.4	14.5
Mean	-4058	-0.7	1.2
SD	444	4.8	5.3
Range	2511	28.8	27.1

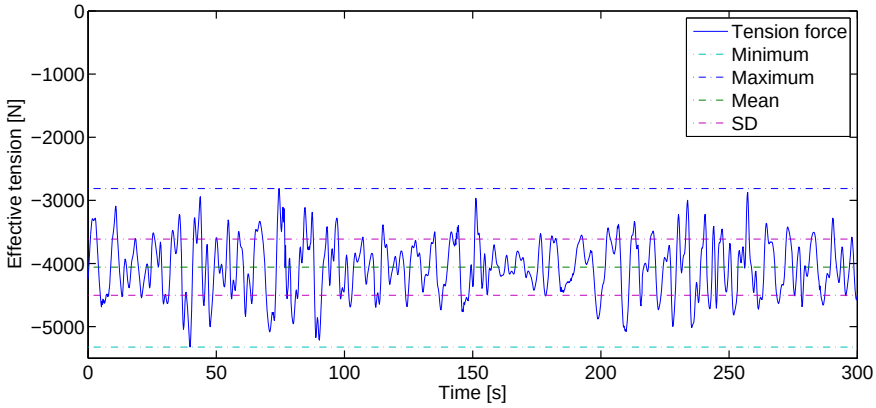

(a) Force

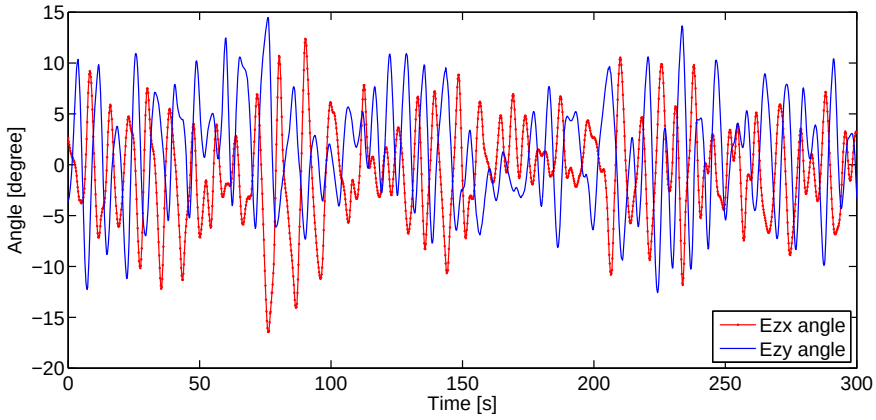

(b) Headstock angles

Figure 7.14: Umbilical service simulation test signals, showing the effective tension force, 7.14(a), and the associated headstock angles, 7.14(b), for cable section below bend stiffener, data courtesy of JDR.

validation of time series a variety of measures have been described in the literature (Hamilton, 1994; Mayer & Butler, 1993). In the following assessment, a combined qualitative and quantitative approach is used to assess the accuracy of the service simulation test signals.

7.2.2.1 Qualitative assessment

As a first, qualitative measure the data is visually examined through two types of plots:

- A simple time series plot which shows both, the desired input signal and the measured signal. This plot allows an instant impression of the simulation accuracy. It is however, only practical for short time series.
- Entire time series can be conveniently compared when the measured data X is plotted against the desired input signal Y. Together with the line that indicates a perfect correlation, i.e. $Y = X$, this plot allows a visual assessment of larger data sets. The vertical distance from the ideal line directly shows how well the signal is reproduced.

Time series plots The time series plots for the headstock angles are shown in figure 7.15 (Ezy angle, x-bend) and figure 7.16 (Ezx angle, y-bend). Each figure depicts the input drive signal and the measured angles for all four independent tests and consists of 2 subplots for the full 300s time series and an excerpt of 15s. For both axis, there is close agreement between the drive signal and the measured angles. For figure 7.15(a) and 7.16(a) the agreement is so close that the 4 tests and the drive signal cannot be distinguished. Only the enlarged 15s plots indicate that the Ezy angle is slightly larger than the drive signal, figure 7.15(b), and the measured angles for Ezx are slightly smaller than requested, figure 7.16(b).

The input signal and measured tension force at the tailstock of the rig are illustrated in figure 7.17, showing the full time signal, figure 7.17(a), and a 60s excerpt, figure 7.17(b). The measured test signals follow the drive signal reasonably well, but have a tendency to overshoot around the peaks, in particular towards smaller, i.e. less negative, tension forces. There is good agreement between the four tests and a random

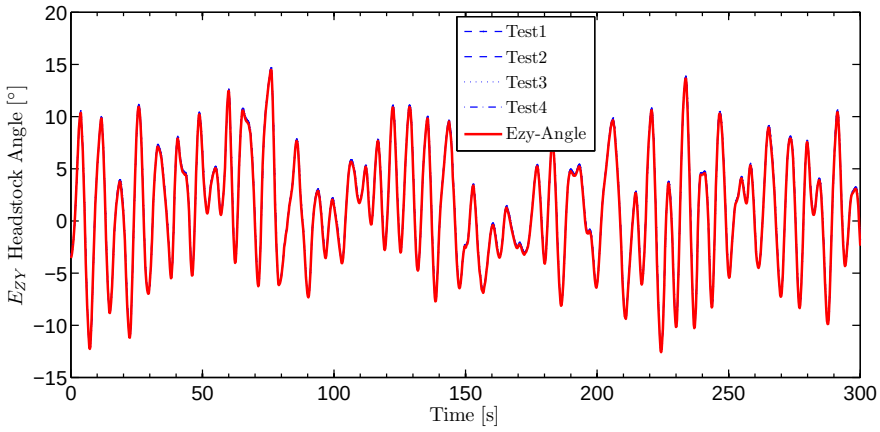

(a) Full signal

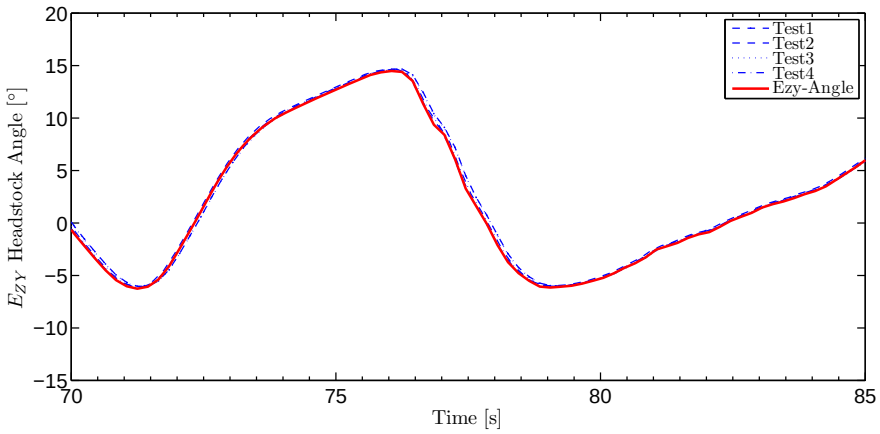

(b) Excerpt

Figure 7.15: Umbilical service simulation test, time series comparison of input and measured x-axis (Ezy-angle) signal.

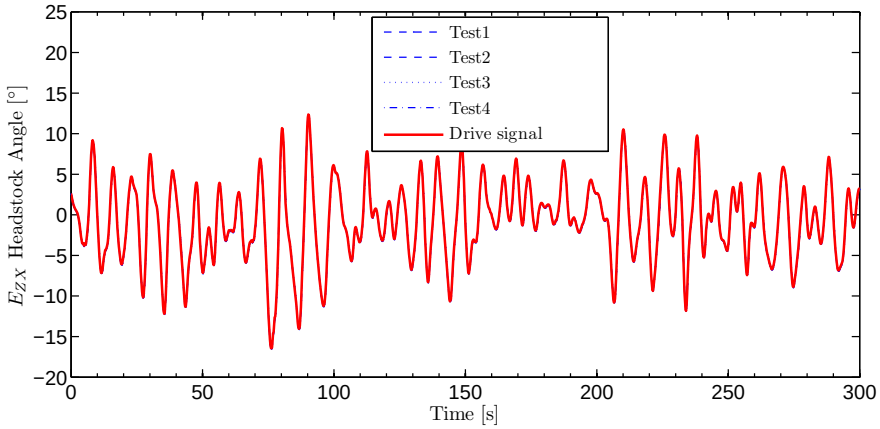

(a) Full signal

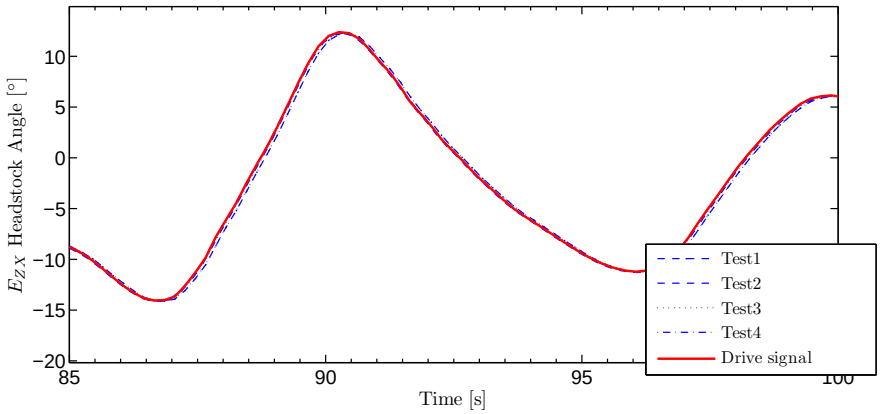

(b) Excerpt

Figure 7.16: Umbilical service simulation test, time series comparison of input and measured y-axis (Ezx-angle) signal.

fluctuation of this overshooting behaviour can thus be ruled out. The largest overshooting events occur around $t = 40s$, $80s$, $210s$, $240s$, which appears to coincide with some of the largest headstock angles.

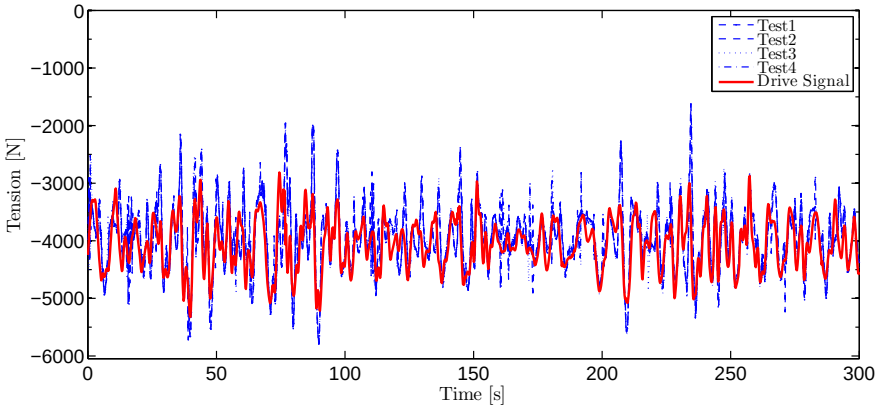

(a) Full signal

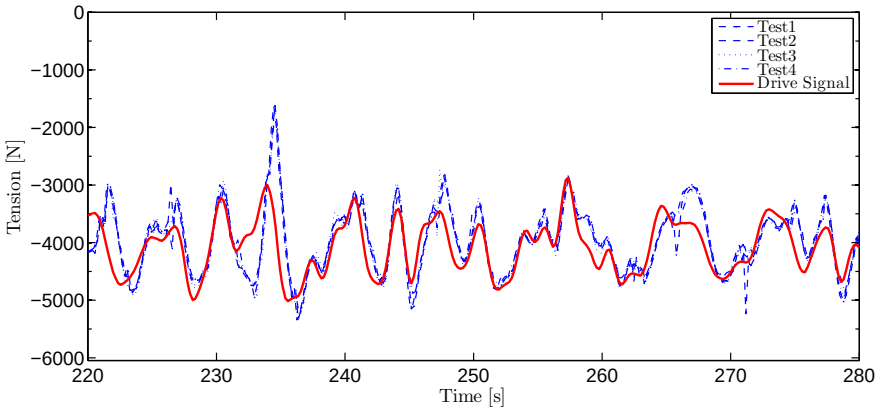

(b) Excerpt

Figure 7.17: Umbilical service simulation test, time series comparison of input and measured tension force signal.

Correlation plots The correlation plots of the headstock angles for all 4 tests are given in figures 7.18, Ezx-angle (y-axis), and 7.19, Ezy-angle (x-axis). Points above the ideal correlation line $Y = X$ show that the measured parameter is below the value that was requested by the input signal. In analogy, points below the perfect fit line show that the measured value is above the one requested. For both angles there is very good agreement with all measured points close to or on the ideal line, confirming

the close replication of the input signal which was shown in the simple time series plots.

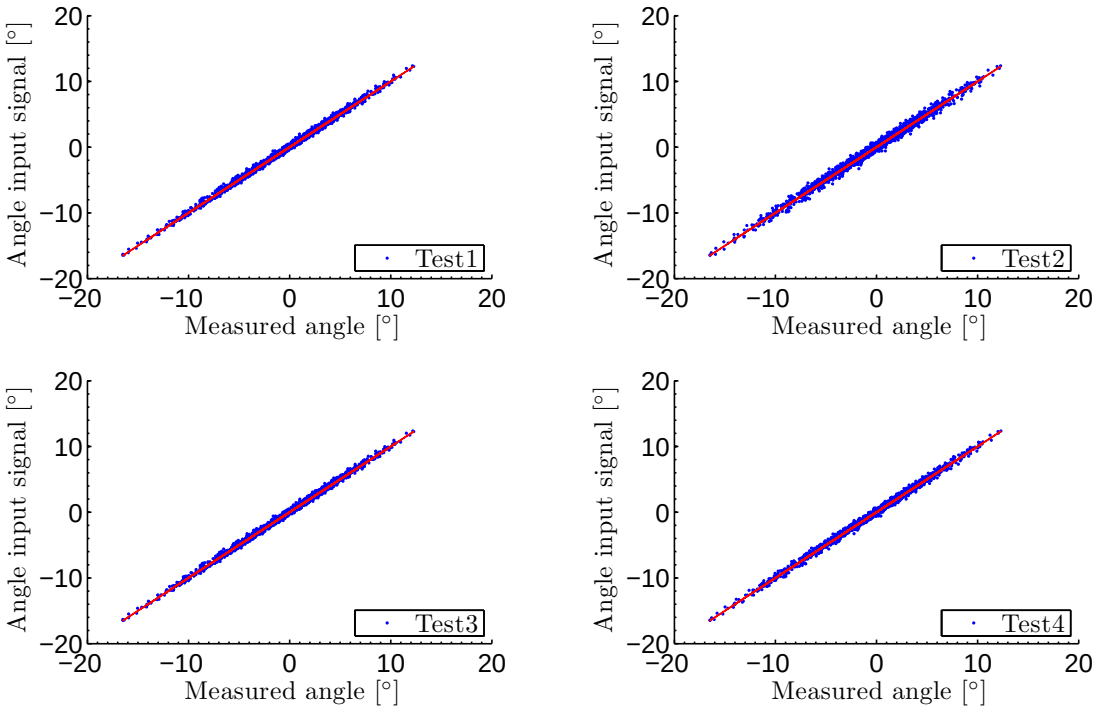

Figure 7.18: Correlation plots of input signal and measurement for Ezx-angle (y-axis).

Figure 7.20 depicts the correlation plot for the tension force. In comparison to the close correlation of the measured angles, there is a significant amount of scatter evident for the tensile force, with a considerable amount of data points away from the ideal line. The larger deviations appear to be below the ideal line, thus the measured tensile force has been less than requested. The indication that the tensile force is not replicated accurately is reinforced through these correlation plots.

7.2.2.2 Quantitative assessment

As a second step, quantitative measures have been calculated to assess the simulation accuracy of the test rig. Two suitable parameter to quantify the accuracy depicted in the scatter plots above are the Pearson correlation coefficient r, defined in equation 7.13,

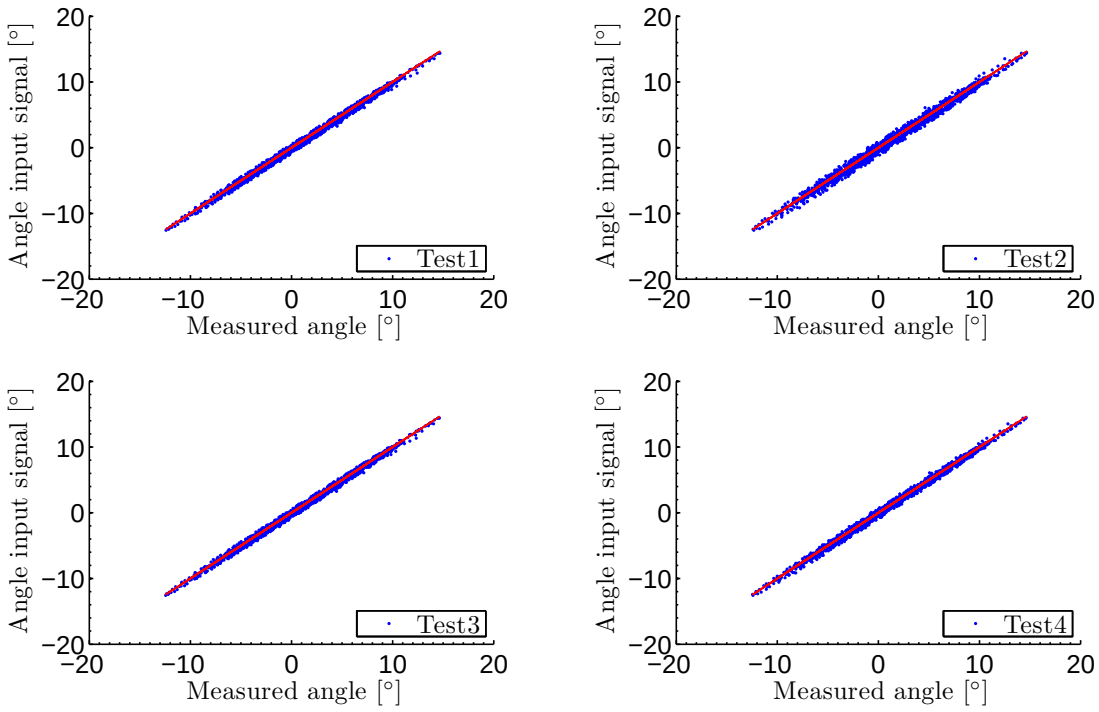

Figure 7.19: Correlation plots of input signal and measurement for Ezy-angle (x-axis).

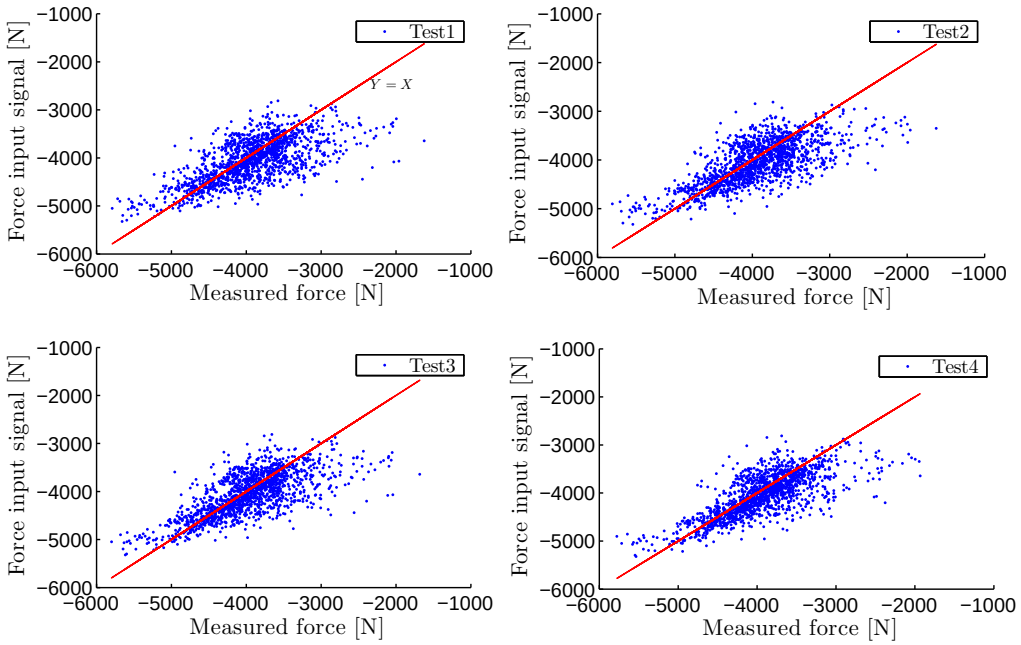

Figure 7.20: Correlation plots of input signal and measurement for tension force.

and the mean absolute error (MAE), equation 7.14.

$$r = \frac{\sum_{i=1}^{n}(X_i - \bar{X})(Y_i - \bar{Y})}{\sqrt{\sum_{i=1}^{n}(X_i - \bar{X})^2}\sqrt{\sum_{i=1}^{n}(Y_i - \bar{Y})^2}} \tag{7.13}$$

Where X_i, Y_i denote the individual sample points and $\bar{X}$, $\bar{Y}$ are the means for each sample set, n denotes the number of sample points.

$$MAE = \frac{1}{n}\sum_{i=1}^{n}|X_i - Y_i| \tag{7.14}$$

Where X_i, Y_i denote the individual sample points.

Correlation coefficient The Pearson correlation coefficient r for the three parameters across all four tests is given in table 7.5. The tension forces do not show a very high correlation, with $0.663 < r < 0.744$ and are not replicating the tension forces to a satisfying level. The bending angles display very high correlation values close to $r = 1$, indicating an accurate replication of the given input signals.

Table 7.5: Correlation coefficient for service simulation test results, correlating measured signal and input load signal.

Test Nr.	Tension force	y-bend angle (Ezx)	x-bend angle (Ezy)
1	0.663	0.998	0.998
2	0.707	0.995	0.996
3	0.702	0.998	0.998
4	0.744	0.998	0.998

Mean absolute error For the second quantitative measure the MAE has been calculated and is tabulated in table 7.6. With regard to the tension force, MAE values between 329N and 267N are reached during the four tests. Considering the less favourable value of 329N, this equates to a mean relative error of 11.7% with respect to the minimum tension force of the input signal, 8.1% in relation to the mean force and 6.2% relative error of maximum tension force. In the more favourable case the values the relative error lies between 9.5%-5.0% with a mean value of 6.6%. There is some improvement of the MAE throughout the tests, but the error is still unacceptably large, in particular if compared to the MAE computed for the angles, which are all significantly smaller than 0.5°. The relative error with respect to the maximum angle is in the order of ±2%.

Table 7.6: Mean absolute error (MAE) of service simulation test results, comparing measured parameter and input load signal.

Test Nr.	Tension [N]	y-bend angle (Ezx) [°]	x-bend angle (Ezy) [°]
1	329.69	0.26	0.31
2	313.36	0.38	0.43
3	294.79	0.25	0.28
4	267.59	0.27	0.31

7.2.2.3 Potential causes of limited tension force replication

The simulation accuracy of the headstock angles are satisfactory, but the replication of the tension force is not as good as expected and thus initiated some further investigation to potential causes.

An inspection of the time series shown above (Figures 7.15-7.17) shows that the overshooting seems to be caused by a coupled behaviour, where a large headstock excursion induces an overshooting of the tension force, as the cable is pulled away and pushed into the tailstock. However, the PID control of the tailstock force should be fast enough to adjust to these changes.

To confirm that the PID control values are not the root cause for the observed overshooting, a step function for critical PID values, established with the Ziegler-Nichols method (Ziegler & Nichols, 1942), has been tested but the force following could not be improved in this way.

Another potential cause was attributed to the bearing stiction force which is a known disadvantage of linear bearings as opposed to rotational bearings. Stiction forces describe the physical behaviour, that the friction force between two surfaces under load is higher in a static position, i.e. when there is no movement between the surfaces, as opposed to lower friction forces when the surfaces are in motion (Harnoy, 2003). The friction factor f is typically described by the Coulomb model that relates the friction force F_f which is tangential to the sliding surfaces and the normal load on the contact surface F_n:

$$f = \frac{F_f}{F_n} \tag{7.15}$$

A typical relation between the sliding velocity of the contact surfaces and the change in friction factor f is shown in figure 7.21. The friction factor is the largest at velocities close to zero and then rapidly declines. Even though the figure shows values from an experiment with journal bearings, a similar behaviour will occur for the two linear bearings of the test rig. The actuator has to overcome the initial stiction force each time that the actuator is moved from a static position or when it must change its direction.

To confirm the possible influence of stiction, forces a combined plot of tension force signal, actuator velocity and displacement is examined (figure 7.22). For the three largest overshoot occurrences highlighted in the plot, it can be seen that the actuator displacement changes direction which correlates to a brief moment of zero velocity and hence a higher friction force that the actuator has to overcome.

The reason that this stiction force is transmitted to the load cell measurement is due to the location of the load cell, as can be seen in figure 7.23. The load cell is

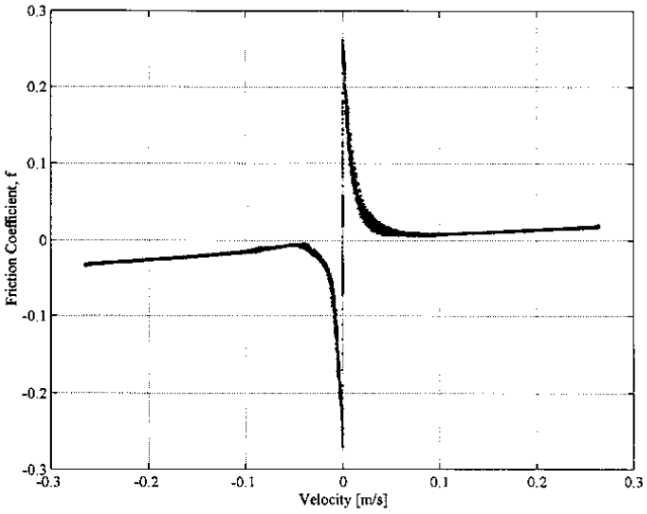

Figure 7.21: Friction coefficient f versus sliding velocity U, illustrating stiction forces, i.e. high f at low velocities. Graph reproduced from Harnoy (2003, p.534). Displayed results are based on experiments for sinusoidal oscillating velocity ($\omega = 0.0055\frac{rad}{s}$) of a journal bearing with $d = 25mm$ and $L/D = 0.75$. Steel on brass with SAE10W-40 lubricant.

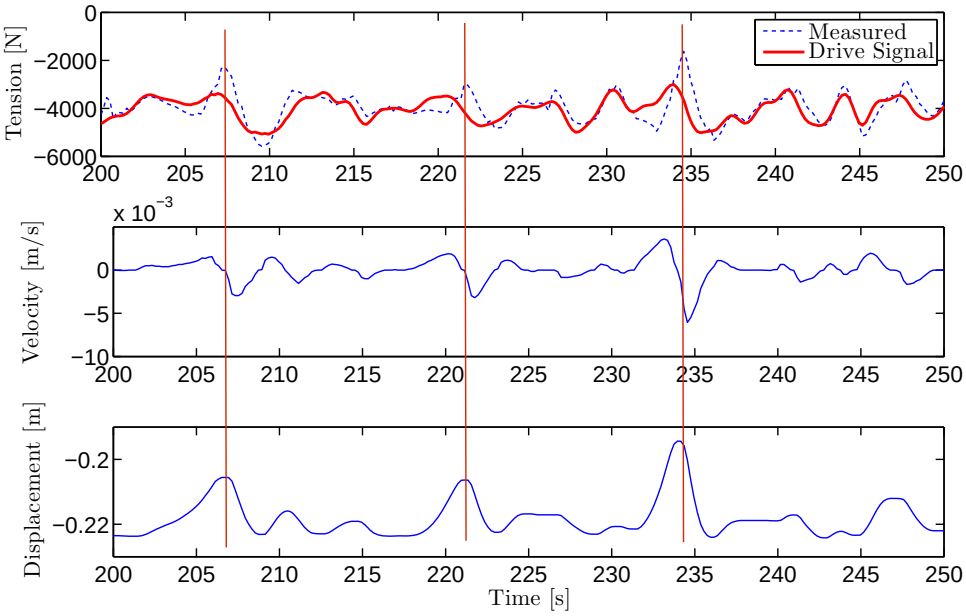

Figure 7.22: Tension force, actuator velocity and displacement to investigate the possible contribution of stiction forces on the force measurement. Plot shows measurements during Test 1.

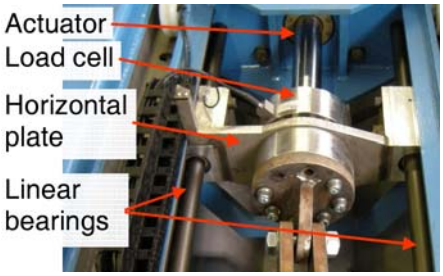

Figure 7.23: Load cell assembly on the DMaC, showing the location behind a horizontal runner plate connected to the linear bearings.

positioned between the actuator and the horizontal runner plate, that in turn is connected to the linear bearings on either side. Therefore, the load cell is subjected to the additional force that the actuator has to apply to overcome the stiction force, which is the case when the actuator changes its direction. When the actuator extends and then retracts the measured force signal will exhibit a spike from decreasing tension forces to a suddenly increasing force, and vice versa for the case when the direction of the actuator changes from retraction to extension. In fact, the PID control constantly tries to adjust the actuator displacement to reach the correct force value. However, any change of direction causes the measured force to overshoot, because the higher force required to move the actuator is transmitted and measured by the load cell.

In conclusion, it is recommended that the location of the load cell is changed from behind the horizontal runner plate to the front of the plate. This will ensure, that the stiction forces are not transmitted to the load cell, as it is not subjected to the load path between linear bearings and actuator.

Part IV

Concluding remarks

Chapter 8

Discussion and conclusion

8.1 Discussion of results

Most of the preceding chapters included a brief discussion at the end. However, it is considered useful to bring the main results of this thesis together in this section and to discuss them in a coherent way.

Reliability prediction The review of different reliability prediction methods in chapter 2 led to the choice of a Reliability Block Diagram (RBD) analysis, a bottom-up statistical approach. The decision was made on the grounds of practical considerations, including the type of available failure information and the degree to which specific load conditions were available for the analysed hydraulic wave energy converter. Although a single reliability prediction method was carried out in the case study presented in chapter 3, it is important to note that this is not the only approach to assess the reliability for marine energy converters. A particularly promising, but information-intensive approach, is for example the bottom-up physics of failure approach suggested by the MechRel (2004) handbook. This approach focuses on the individual mechanical components and would thus complement and inform a system-based RBD analysis.

It is also important to note that depending on the desired outcome, other methods of reliability assessment may prove useful. For example, if the objective is to estimate the occurrence probability of a singular critical fault, a fault tree analysis may be more useful. If more specific information of the system under investigation is available in the

form of statistical distributions that describe the time to failure and the time to repair for individual components, a discrete event simulation may be performed which yields an availability estimate.

A generic availability model to estimate the levelised cost for offshore wave energy conversion is described by Malcolm (2010). With a deterministic assumption of five failures, for different access constraints, the levelised cost was shown to increase between 32% and 81% compared to the 'no failure' reference case. Even though the loss of production and the associated repair cost assumed fixed values, the study highlights the importance of developing an improved understanding of both the type and the rate of component failures which are to be expected. This thesis makes a contribution in identifying potential uncertainty ranges of failure rate distributions and their quantification on system reliability. A simple constant failure rate assumption may significantly over- or underestimate the system reliability and is thus questionable for a robust reliability assessment.

Abdulla *et al.* (2011) present a statistical availability model for wave energy converters using Monte Carlo simulation techniques and provide a case study for the Oyster device developed by Aquamarine Power. They acknowledge the criticality of failure rates, but do not state the used values and associated statistical distributions or sensitivities, but mainly aim to establish maintenance and access criteria to achieve acceptable availability levels.

As discussed in chapter 3 and Thies *et al.* (2009), the scarcity of appropriate failure data for wave energy converters is evident due to limited field deployments and no prolonged periods of operation. This poses a challenge to traditional reliability prediction methods. Yet, this lack of information should not hinder the attempt to assess and improve the reliability at an early design stage. The work presented in this thesis will be useful to a range of stakeholders who require reliability information for MECs, to either improve their design, optimise maintenance strategies or to evaluate the technical and economic risk.

This thesis has presented a range of experimental, numerical and statistical methods to establish, and continuously improve, the reliability information for MECs. An indi-

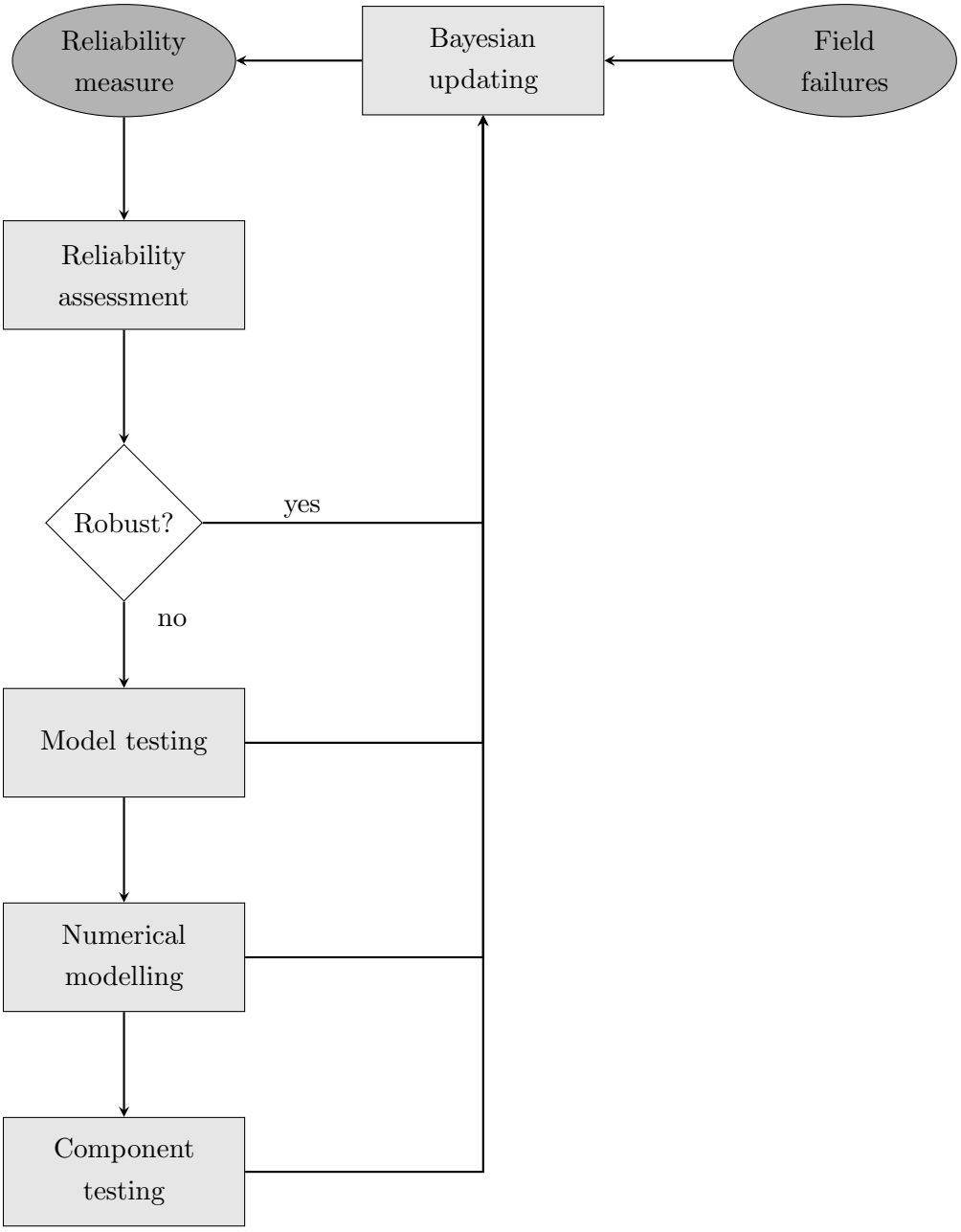

Figure 8.1: Improvement of reliability information through Bayesian updating, incorporating results from model tests, numerical modelling and component testing to compensate a potential scarcity of field failure information.

cation of the overall process is shown in figure 8.1. Reliability measure are the starting point for initial reliability assessments. If the reliability assessment yields results that are deemed to be not sufficient or robust enough, the reliability measure must be improved with regard to its absolute value or its confidence level. Thus a combination of methods including model testing, numerical modelling and physical component testing can be applied to establish additional reliability information or validate the increased reliability of an improved design. Through the Bayesian updating approach this additional information can then be feed back into the initial reliability metrics, such as the MTTF, to provide a new best estimate. Once field failure information becomes available, it can also be included by means of Bayesian updating. Once the reliability assessment is considered to be robust, the reliability metrics can be continuously updated with field failure information.

The presented research does not provide a definitive answer to the question of how reliable a WEC will be. Nonetheless, it identifies and addresses the most important challenges that must be addressed to ensure reliable, and thus economically viable, WECs:

- Reduction of failure rate uncertainties;
- Explicit examination of environmental and operational conditions to avert field failures;
- Design verification of components with measured and anticipated field load conditions;
- Specific component testing to ensure component reliability *prior* to deployment.

Mooring load analysis The mooring tension loads and the fatigue conditions for a three leg mooring configuration of a floating OWC-type device have been analysed in chapter 6. This load analysis is based on experimental tank tests (section 5.1) and is therefore limited by the experimental sea states ranging between $2m \leq H_s \leq 6m$, the chosen mooring configuration and the type of floating device.

Johanning *et al.* (2006) propose a design spiral for WEC moorings. As a first iterative process, suitable mooring materials and arrangements must be chosen to achieve

an acceptable footprint area, excursions and natural frequencies. The second iteration then assesses the structural integrity of the mooring system with regard to its ultimate limit state (ULS) and fatigue limit state (FLS). The research presented here, does contribute an evaluation procedure to estimate the fatigue life for a proposed mooring system and is considered to be an important step within the second iteration 'spiral', in which design calculations are experimentally validated.

An important finding of this thesis is that very high mooring loads can occur in operational sea states. These high snap loads were also found to be the dominant fatigue life contribution. As a consequence, the occurrence of snap loads may lead to mooring failures prior to envisaged project lifetimes of typically 15-20 years.

The occurrence of snap loads during field deployments of scaled prototypes have also been noted by Kofoed *et al.* (2006) and Ferrario *et al.* (2004). In both cases the wave devices suffered a mooring line failure during deployment. This thesis has shown that if snap loads are not mitigated, they are not only of concern with regard to the ultimate limit state, but will considerably shorten the fatigue life and lead to mooring failure.

Mechanical loading of marine power cables Little work has been published on the application of marine power cables in floating wave energy systems. This thesis presents an approach to assess the expected load behaviour based on the motion characteristic of the floating structure. It was shown that the lazy wave shape is the favourable configuration to cross the water column, compared to a simple catenary shape. The lazy wave configuration reduces the tension forces at the attachment point, avoids compression at the touchdown point, which would damage the cable, and reduces the occurring bending moment. For the modelled sea states the mechanical loading was shown to remain within the design specifications stated by Martinelli *et al.* (2010). It was further shown that fatigue failures are also of concern for marine power cables, so that bend stiffeners will be required to reach acceptable fatigue lives, in particular near the attachment point.

The specific load behaviour for the power cable will be highly device- and site specific, but the presented work identifies some of the design challenges that cable manufacturers will be confronted with. It is therefore important for device developers

to include the power cable in the overall system design at an early stage, so that the motion characteristics of the device and the mooring system can be iterated with consideration of the power cable reliability.

Dynamic Marine Component test rig One of the early findings of this thesis was that reliability information for WECs is scarce and often not appropriate. Thus, for robust reliability assessments, more application specific information is required. The need for dedicated component reliability testing was pointed out by other authors before (Mueller & Wallace, 2008; Salter, 2003b) but has not been carried out for wave energy converters before.

This thesis informed and contributed to the design and implementation of a unique test rig that is capable of replicating the force and motion envelopes expected for marine energy components, such as mooring assemblies and power cables.

The time required to design, contract, manufacture and assemble the test rig only allowed for initial tests to be carried out during the time frame of this thesis. However, these tests provided relevant operating experience, aided in establishing testing procedures and initiated improvements for the user-interface and operability of the rig.

The stiffness characteristics of a marine power cable were successfully determined, together with initial service simulation tests which prompted amendments to the positioning of the main load cell to improve the force-following characteristics.

Service simulation testing is routinely applied in other industries (Heuler & Klätscke, 2005; Schijve, 2009) and has proved beneficial for the continuous reliability improvement of components. The work presented here substantiates one of the first attempts to implement this service simulation test approach for marine renewable energy converters. This effort will benefit the industrial and academic research, and has attracted interest from academic and industrial stakeholders.

8.2 Further work

8.2.1 Industrial research and development

Reliability data base for marine renewable energy During this thesis, a failure rate data base, which was originally established during SuperGen Marine Phase I,

was continued and extended (see Appendix C). Industrial research and development to further populate and improve this data base would be beneficial for future reliability assessments in the marine renewable sector. One difficulty in sharing such information among device developers and stakeholders, is that the 'lessons learnt' are considered as a competitive advantage. Yet, it is crucial during the transition towards commercial installations, that the experiences from first deployments are shared to avoid the duplication of efforts and failures. Such a database could be hosted by an independent third part such as a consortia of certification agencies or the operators of installation sites.

An example of such a dedicated measurement and data collection campaign to assess the performance and reliability of generating assets, is the joint wind offshore energy project *alpha ventus* (DOTI, 2010). It is the first German offshore wind farm which was commissioned in 2010 and is jointly owned and operated by the utility companies E.ON, EWE and Vattenfall under the Deutsche Offshore-Testfeld- und Infrastruktur GmbH & Co. KG (DOTI). Since 1999, the operation of wind farms in Germany is accompanied by the Scientific Measurement and Evaluation Program (WMEP), funded by the federal government, with the objective to collect statistically relevant data on the practical use of wind turbines, including plant reliability and failure reporting. All participating operators provide standardised monthly reports to the Fraunhofer Institute for Wind Energy and Energy System Technology (IWES), which holds the data under consideration of confidentiality clauses. This measurement and reporting programme is continued as Offshore-WMEP at alpha ventus, to obtain a substantial pool of data (Brune *et al.*, 2010; Faulstich *et al.*, 2010). This is achieved through close collaboration of all stakeholders, including operators, manufacturers, suppliers and scientists. Ultimately such a campaign does not only allow continuous reliability assessment and improvement, but also forms the foundation for future political decision-making about offshore wind energy.

For the case of wave- and tidal energy in the UK, there is no comparable scheme. However, institutional bodies such as the Crown Estate would be in a position to make the scientific measurement and evaluation of deployments a requirement for the lease consent of deployment sites.

Qualification of components for the marine energy application The presented work has shown that components and sub-assemblies which are used in a marine energy application are likely to be subject to new and potentially unknown failure modes as compared to their conventional use in established industries. It was also shown that unknown failure modes may alter the anticipated failure rate level by as much as an order of magnitude. Thus, there is a need to qualify, adapt, and possibly redesign both, proven and unproven components to ensure their suitability *prior* to their field deployment in numbers. This needs the close collaboration between device developers and component manufacturers in order to combine their application specific and component specific knowledge. Third parties such as research institutes and certification agencies may be of further assistance to facilitate such efforts.

8.2.2 Academic research

This thesis provides the basis for further academic research that makes use of the existing facilities and extends the application of the proposed methodologies and approaches.

Fatigue load estimation with measured field data The procedure to calculate the fatigue load spectrum and to establish a fatigue life estimate for mooring components, presented in chapter 6, will be performed with more detailed field measurements undertaken at the South West Mooring Test facility (SWMTF). A first data set of a 18 month deployment is already available and a second data set is currently being gathered. The duration of the deployment allows to establish the load envelopes of multiple sea states and establish a 'load library' to predict the fatigue life for a variety of metocean conditions at the deployment site and beyond. Such an improved data set will alleviate the uncertainties, which were introduced by the assumptions due to the smaller experimental data set available for this thesis, and allow a detailed analysis of the governing fatigue parameters.

The fatigue load estimation approach also holds the potential to process the load data gathered during planned device deployments at the Wave Hub and FaBTest sites. For large amounts of data, the analysis would only need minor additional development to become fully automated.

Site specific availability model Another important aspect to ensure the viability of marine energy converters will be to optimise both the reliability and maintenance strategy in order to achieve a high technical availability of devices and entire farms. The research presented in this thesis, in the form of a system reliability assessment, represents one input factor to such availability models. Maintenance strategies, metocean conditions (Ashton, 2012; Smith *et al.*, 2012), weather windows and accessibility (Walker *et al.*, 2011) and cost will also be incorporated. This work is envisaged to be performed within the research group at the University of Exeter and with potential collaboration of colleagues at Strathclyde University (Lazakis *et al.*, 2010).

Such a suitable site and device specific availability model would allow to optimise the availability prior and during the deployment, based on the underlying reliability, access, and maintenance parameters.

Peak mooring load analysis and mitigation The possible occurrence of peak mooring loads under operational conditions was an important finding but was only based on scaled experimental tests of a generic device. As mentioned, such snap loads have also been reported in the field for the case of Wavedragon in Kofoed *et al.* (2006). Conversations with the researchers at Aalborg University give an indication to extend and validate these findings through analysis of the mooring load data gathered during the Wavedragon deployment. This work could not only aim to validate the occurrence and impact of snap loads for floating wave energy converters but could also provide an opportunity to develop mooring systems that mitigate this damaging load behaviour.

Component and reliability testing The results and recommendations from the initial component tests presented in chapter 7 will be used for further development of the test rig itself, but also to conduct further specific component tests.

Several specific component tests are envisaged, which continue some of the work described in this thesis. Among the planned tests are two collaborations with component manufacturers, which require validation and/or qualification of their components for the marine energy applications. Beyond those specific tests it is envisaged to develop, use and assess the suitability of accelerated component tests for mooring assemblies, so that potential fatigue estimates can be validated. Alternatively, the performance of

redesigned components can be assessed and verified on the tests rig before field deployment.

A medium-term task is to work towards a third party certification of the test rig installation and test procedures. "On the basis of a review and a decision, a third party issues a written statement confirming that fulfilment of specified requirements has been demonstrated" (DNV, 2007). As an example, Det Norske Veritas offers two applicable standards, a "Certification of components and materials (CMC)" (DNV, 2007) and a certification guideline for companies which are engaged in non destructive testing on offshore projects and offshore units/components (DNV, 2008). Such an independent assessment and certification will ensure the compliance of the test rig and experimental procedures with common standards in the offshore industry, which will foster the confidence in the capability of the rig and contribute to its reputation.

Beyond this machine and process certification, a further accreditation with the United Kingdom Accreditation Service (UKAS), the authoritative body for lab accreditations, is advisable. Such an accreditation is based on the ISO/IEC 17025:2005 standard (ISO, 2005), which stipulates general requirements to validate the technical capability of the personnel, the technical compliance of the test machine and the appropriateness of management structures. This will be beneficial to the credibility of the test facility which has the potential to become a dedicated marine energy component reliability test centre for the South West of the UK and beyond.

References

Abdulla, K., Skelton, J., Doherty, K., OKane, P., Doherty, R. & Bryans, G. (2011). Statistical availability analysis of wave energy converters. In I.S. of Offshore & P.E. (ISOPE), eds., *Proc. of the 21st Int. Offshore and Polar Engineering Conf.*, 572–578, Maui, Hawaii, USA, june 19-24. 268

Akama, M. (2002). Bayesian analysis for the results of fatigue test using full-scale models to obtain the accurate failure probabilities of the Shinkansen vehicle axle. *Reliability Engineering & System Safety*, **75**, 321–332. 132, 133, 134

Akhmedjanov, F.M. (2001). Reliability databases: State-of-the-art and perspectives. Tech. Rep. R-1235, Risø National Laboratory. 94

Al-Habaibeh, A., Su, D., McCague, J. & Knight, A. (2010). An innovative approach for energy generation from waves. *Energy Conversion and Management*, **51**, 1664 – 1668. 38

Alegría, I.M., Martín, J.L., Kortabarria, I., Andreu, J. & no, P.I.E. (2009). Transmission alternatives for offshore electrical power. *Renewable and Sustainable Energy Reviews*, **13**, 1027 – 1038. 159

AME (1992). Reliability and availability assessments of wave energy devices. Technical Report ETSU WV 1690 - P1, Advanced Mechanics & Engineering [AME], report for the Energy Technology Support Unit [ETSU]. 33, 105, 109, 112, 310

Arnold, A. (2010). Port kembla wave generator on sea floor. Illawarra Mercury. 37

Ashby, M.F. (2005). *Materials Selection in Mechanical Design*. Elsevier, 3rd edn. 155

Ashton, I., Johanning, L. & Linfoot, B. (2009). Measurement of the effect of power absorption in the lee of a wave energy converter. In *Proc. ASME 28th International Conference on Ocean, Offshore and Arctic Engineering*, Honolulu, Hawaii, USA. 151

Ashton, I.G. (2012). *Spatial variability of wave fields over the scale of a wave energy test site*. Ph.D. thesis, University of Exter. 275

Atwood, C.L. (1994). Constrained noninformative priors. Tech. Rep. INEL-94/0074, Idaho National Engineering Laboratory, prepared for the U.S. Nuclear Regulatory Commission Office for Analysis and Evaluation of Operational Data Reliability and Risk Analysis Branch. 131

Ayyub, B.M. & McCuen, R. (2003). *Probability, statistics, and reliability for engineers*. CRC Press, 2nd edn. 64

Barlow, R. & Proschan, F. (1975). *Statistical Theory of Reliability and Life Testing. Probability models*. Holt, Rinehart & Winston, New York. 126

Barnard, G.A. & Bayes, T. (1958). Studies in the History of Probability and Statistics: IX. Thomas Bayes's Essay Towards Solving a Problem in the Doctrine of Chances. *Biometrika*, **45**, 293–315, reproduced from: The Philosophical Transactions (1763), 53, pp. 370-418. 123

Black, K.P. (2007). Review of Wave Hub technical studies: Impacts on inshore surfing beaches. Tech. rep., ASR Marine Consulting and Research, report provided for: South West of England Regional Development Agency. 218

Boake, C.B., Whittaker, T.J.T., Folley, M. & Ellen, H. (2002). Overview and initial operational experience of the LIMPET wave energy plant. In *Proc. of the 12th International Offshore and Polar Engineering Conference*, The International Society of Offshore and Polar Engineers, Kitakyushu, Japan. 80

Bond, R. (2009). Wave power machine capsize at sea. BBC News, monday, 21 September. 83

Brito-Melo, A., Sarmento, A., Clément, A. & Delhommeau, G. (1999). A 3D Boundary Element code for the analysis of OWC wave-power plants. In *Proc. 9th Int Offshore and Polar Engineering Conf. ISOPE*, vol. I, 188–195, Brest, France. 76

Brito-Melo, A., Neumann, F. & Sarmento, A. (2007). Full-scale data assessment in OWC Pico plant. In *Proc. of the Sixteenth International Offshore and Polar Engineering Conference ISOPE*, 447–454, Lisbon, Portugal. 81

Brooke, J. (2003). *Wave energy conversion*, vol. 6 of *Elsevier Ocean engineering book series*. Elsevier. 78

Bruhns, O.T. (2003). *Advanced Mechanics of Solids*. Engineering online library, Springer. 230

Brune, D., Faulstich, S., Hahn, B. & Lyding, P. (2010). A collaborative reliability database for maintenance optimisation. In *Proc. of European Wind Energy Conference and Exhibition (EWEC)*, 20-23 Apr, Warsow, Poland. 273

Bryden, I. & Linfoot, B. (2010). Wave and current testing of an array of wave energy converters. In *Proc. of the HYDRALAB III Joint User Meeting*, Hannover, Germany. 151

BS 5760-10.2:1995 (1995). Reliability of systems, equipment and components. Guide to reliability testing. Design of test cycles. Standard, British Standards Institution [BSI]. 175

BS 5760-4:2003 (2003). Reliability of systems, equipment and components. Guide to the specification of dependability requirements. Standard, British Standards Institution [BSI]. 45

BS 5769-0:1986 (1986). Reliability of constructed or manufactured products, systems and components. Part 0: Introductory guide to reliability. Tech. rep., British Standard Institute [BSI]. 127

Bunea, C., Charitos, T., Cooke, R. & Becker, G. (2005). Two-stage Bayesian models - application to ZEDB project. *Reliability Engineering & System Safety*, **90**, 123 – 130, selected papers from ESREL 2003. 132, 135

Cadwallader, L.C. (2001). Comparisons of facility-specific and generic component failure rates for tritium-bearing components used in fusion research. *Fusion Engineering and Design*, **54**, 353–359. 102

Callaghan, J. & Boud, R. (2006). Future marine energy - results of the marine energy challenge: Cost competitiveness and growth of wave and tidal stream energy. Tech. rep., The Carbon Trust. 39, 170

Caraher, S. (2011). *Bearing options, including design and testing, for direct drive linear generators in wave energy converters*. Ph.D. thesis, The University of Edinburgh, School of Engineering. 83

Caraher, S., Chick, J., Mueller, M., Steynor, J. & Stratford, T. (2010). Test rig design and development for linear bearings in direct drive generators. In *Proc. of 3rd Int. Conference on Ocean Energy ICOE*, 6th-8th October, Bilbao, Spain. 83

Chakrabarti, S.K. (2005a). Loads and responses. In S.K. Chakrabarti, ed., *Handbook of Offshore Engineering*, chap. 4, 79 – 131, Elsevier, London. 65, 68, 69, 71, 72, 74

Chakrabarti, S.K. (2005b). Ocean environment. In S.K. Chakrabarti, ed., *Handbook of Offshore Engineering*, chap. 3, 133 – 196, Elsevier, London. 70

Choi, Y.J., Gilbert, R.B., Ding, Y. & Zhang, J. (2006). Reliability of mooring systems for floating production systems. OTRC Library Number: 1/06C166 Project Number 423, Minerals Management Service (MMS). 121

Christensen, L., Friis-Madsen, E. & Kofoed, J. (2005). The wave energy challenge - the wave dragon case. In *PowerGen 2005 Europe Conference, Milan, Italy, June 2005*. 86, 87

Clausen, T. (2001). Dynamic risers key component for deepwater drilling, floating production. *Offshore*, **61, (5)**, 89–93. 161

Clément, A., McCullen, P., Falcão, A., Fiorentino, A., FredGardner, Hammarlund, K., Lemonis, G., Lewis, T., Nielsen, K., Petroncini, S., Pontes, T., Schild, P., Sjöström, B.O., Sørensen, H.C. & Thorpe, T. (2002). Wave energy in europe: current status and perspectives. *Renewable and Sustainable Energy Reviews*, **6**, 405 – 431. 64

Clifford, T. (2011). Empirical bending moment calibration of dynmic marine component test rig, internal report. 246

Clifford, T., Johanning, L. & Thies, P.R. (2010). DMaC tender evaluations. Tech. rep., University of Exeter, confidential report. 182

Clifton, P.C.J., McMahon, R.A. & Kelly, H.P. (2010). Design and commissioning of a 30 kW direct drive wave generator. In *Proc. of 5th IET Int. Conference on Power Electronics, Machines and Drives PEMD*, 1–6, Brighton, UK. 82

Cox, D.C. & Baybutt, P. (1981). Methods for Uncertainty Analysis: A Comparative Survey. *Risk Analysis*, **1**, 251–258. 102

Cox, S. & Tait, R. (1998). *Safety, reliability, and risk management: an integrated approach*. Butterworth-Heinemann, Oxford, 2nd edn. 101, 116

Cruz, J. (2008). *Ocean Wave Energy: Current Status and Future Perspectives*. Green Energy and Technology, Springer. 64, 79

Cruz, J., Rea, M., Sarmento, A., Thomas, G. & Henderson, R. (2008). Numerical and experimental modelling of WECs. In J. Cruz, ed., *Ocean Wave Energy*, Green Energy and Technology, 133–188, Springer, Berlin. 72

Custõdio, A.B. & Vaz, M.A. (2002). A nonlinear formulation for the axisymmetric response of umbilical cables and flexible pipes. *Applied Ocean Research*, **24**, 21 – 29. 241

Dalton, G., Alcorn, R. & Lewis, T. (2010). Case study feasibility analysis of the Pelamis wave energy convertor in Ireland, Portugal and North America. *Renewable Energy*, **35**, 443 – 455. 32

Danielsson, O. (2006). *Wave Energy Conversion - Linear Synchronous Permanent Magnet Generator*. Ph.D. thesis, Faculty of Science and Technology, Uppsala University. 82

Dasgupta, A. & Pecht, M. (1991). Material failure mechanisms and damage models. *IEEE Transactions on Reliability*, **40**, 531–536. 60

De Backer, G. (2009). *Hydrodynamic design optimization of wave energy converters consisting of heaving point absorbers*. Ph.D. thesis, Ghent University. 76

de O. Falcão, A.F. (2000). The shoreline OWC wave power plant at the Azores. In *Proc. of 4th European Wave Energy Conference EWTEC*, B1, Aalborg, Denmark. 80, 81

de O. Falcão, A.F. (2004). First-generation wave power plants: Current status and R&D requirements. *Journal of Offshore Mechanics and Arctic Engineering*, **126**, 384–388. 30

de O. Falcão, A.F. (2010). Wave energy utilization: A review of the technologies. *Renewable and Sustainable Energy Reviews*, **14**, 899 – 918. 64, 65

Debray, B., Piatyszek, E., Cauffet, F. & Londiche, H. (2004). Frequencies and probabilities data for the fault tree. Accidental risk assessment methodology for industries in the framework of SEVESO II directive (ARAMIS), Armines, École Nationale Supérieure de Mines de Saint Etienne, France. 100

DECC (2010). Marine Energy Action Plan 2010 - Executive Summary & Recommendations. Tech. rep., HM Government, Department of Energy and Climate Change. 27, 29

Delorm, T.M., Zappal'a, D. & Tavner, P.J. (2011). Tidal stream device reliability comparison models. *Proc. of the Institution of Mechanical Engineers, Part O: Journal of Risk and Reliability*. 122

Denniss, T. (2009). The Oceanlinx wave energy technology. In *Proc. of 3rd Int Symposium Ocean Energy*, EVE - Ente Vasco de la Energia, Bilbao, Spain. 80

Deyuan, L., Zhiquan, Y., Yan, C. & Nengsheng, B. (2003). Load spectrum and fatigue life analysis of the blade of horizontal axis wind turbine. *Wind Engineering*, **27**, 495–506. 68

Dhillon, B. (1992). Reliability testing: Bibliography. *Microelectronics Reliability*, **32, 8**, 1115–1135. 170

Dhillon, B. (2007). *Applied reliability and quality: fundamentals, methods and applications*. Series in reliability engineering, Springer, London. 170

DNV (2004). Recommended practice dnv-rp-f205: Global performance analysis of deep-water floating structure. Tech. rep., Det Norske Veritas. 234

DNV (2005). Guidelines on design and operation of wave energy converters. Tech. rep., Det Norske Veritas, Carbon Trust. 32, 69, 84

DNV (2007). Standard for certification No. 1.1 - General description of the CMC services. Certification of Materials and Components (CMC). 276

DNV (2008). Standard for certification no 2.9 - firms engaged in non destructive testing (ndt) on offshore projects and offshore units/components. Programme No. 402B. 276

DNV-OS-E301 (2010). Offshore standard - position mooring. Standard, Det Norske Veritas DNV. 203, 204, 216, 218, 219

Dorrell, P. (2004). *Reliability and availability of marine energy converters*. Master's thesis, Heriott-Watt University, Edinburgh. 104

DOTI (2010). Alpha ventus - the building of an offshore wind farm. Tech. rep., Deutsche Offshore-Testfeld und Infrastruktur GmbH & Co. KG, Berlin, www.alpha-ventus.de. 273

Draper, N.R. & Smith, H. (1981). *Applied Regression Analysis*. Wiley-Interscience, 2nd edn. 241

Drew, B., Plummer, A.R. & Sahinkaya, M.N. (2009). A review of wave energy converter technology. *Proc. of the Institution of Mechanical Engineers, Part A: Journal of Power and Energy*, **223 (8)**, 887–902. 64

Dunnett, D. & Wallace, J.S. (2009). Electricity generation from wave power in Canada. *Renewable Energy*, **34**, 179–195. 31

Dyer, P. (2011). Specification, KT3 rope, personal communication, e-mail 14/06/2011. 154

Eik, K. & Aksnes, V. (2010). Characterisation of peak loads on a moored production vessel in ice. In *Proc. of 20th IAHR International Symposium on Ice*, Lahti, Finland. 195

Ekeberg, K.I., Ottesen, T. & Aarstein, J. (2006). Predicting, measuring and implementing friction and bending stresses in dynamic umbilical design. In *Proc. Offshore technology conference OTC*, paper nr. 17986-MS., OTC, Houston, Texas, USA. 235, 237

Elsayed, E.A. (2003). *Handbook of reliability engineering*, chap. Accelerated Life Testing, 415–426. Springer. 171

EMEC (2011a). Full scale prototype testing. Tech. rep., European Marine Energy Centre EMEC. 36

EMEC (2011b). Nursery facilities for scale testing. Tech. rep., European Marine Energy Centre. 35

EMEC (2011c). Nursery facilities for scale testing. Tech. rep., European Marine Energy Centre. 36

EPSMA (2005). Reliability - guidelines to understanding reliability prediction. Tech. rep., European Power Supply Manufacturers Association. 55

Eriksson, M., Isberg, J. & Leijon, M. (2005). Hydrodynamic modelling of a direct drive wave energy converter. *International Journal of Engineering Science*, **43**, 1377 – 1387. 76, 82

Escobar, L.A. & Meeker, W.Q. (2006). A review of accelerated test models. *Statistical Science*, **21, 4**, 552–577. 174

EU (2009a). Contract notice: machines and apparatus for testing and measuring. In *Official Journal of European Union (OJEU)*, 2009/S 227-326052. 181

EU (2009b). Ojeu - the official journal of the european union. 181

EU (2009c). Prior infromation notice: machines and apparatus for testing and measuring. In *Official Journal of European Union (OJEU)*, 2009/S 202-290626. 181

EVENT HORIZON LTD. (2010). Precision energetics engineering. www.precisionenergetics.co.uk/engineering.html. 182

FAB TEST (2011). Falmouth Bay test site, marine renewables comissioning site. description of site characteristics and eligible test installations. Tech. Rep. FHC / FT / 104 (issue 1), Falmouth Harbour commissioners and University of Exeter. 35, 36

FARADIP (2006). Failure rate data in perspective. http://www.m2k.com/failure-rate-data-in-perspective.htm. 310

FAUDOT, C. & DAHLHAUG, O.G. (2011). Tidal turbine blades: Design and dynamic loads estimation using CFD and blade element momentum theory. In *Proc. of 30th Int Conference on Ocean, Offshore and Arctic Engineering OMAE*, vol. 2011, 599–608, ASME, Rotterdam, The Netherlands. 68

FAULSTICH, S., HAHN, B. & LYDING, P. (2010). Offshore-WMEP - Monitoring offshore wind energy use. In *Proc. of European Wind Energy Conference and Exhibition (EWEC)*, 20-23 Apr, Warsow, Poland. 273

FERNANDES, A. & ROSSI, R. (2005). Distorted polyester lines for model testing of offshore moored platforms. *Ocean Engineering*, **32**, 817 – 825. 154

FERRARIO, S., KING, D. & GOULD, J. (2004). The technical challenges in designing, building and installing a moored wave energy device at Port Kembla, New South Wales. Tech. rep., J P Kenny. 198, 271

FLEMING, K.N., MOSLEH, A. & DEREMER, R.K. (1986). A systematic procedure for the incorporation of common cause events into risk and reliability models. *Nuclear Engineering and Design*, **93**, 245 – 273. 63

FLINN, J. & BITTENCOURT, C. (2008). Reliability estimation method for wave and tidal energy converters. In *Proc. of 2nd Int. Conference on Ocean Energy ICOE*, 15th-17th October, Brest, France. 92, 95, 102

FLORY, J.F., MCKENNA, H.A. & PARSEY, M.R. (1992). Fiber ropes for ocean engineering in the 21st century presented at the civil engineering in the oceans conference,

American Society of Civil Engineers, 1982. In R.T. Hudspeth, ed., *Proc. of Civil Engineering in the Oceans*, vol. 5, 934–947, American Society of Civil Engineers, New York, N.Y. 155

Foucher, B., Boullié, J., Meslet, B. & Das, D. (2002). A review of reliability prediction methods for electronic devices. *Microelectronics Reliability*, **42**, 1155 – 1162. 57, 62

Funnemark, E., Eldor, J. & Haugom, G. (2006). Identification and review of databases for reliability data. Tech. Rep. Deliverable 4.4, WP4 HyApproval, HyApproval - Handbook for Approval of Hydrogen Refuelling Stations (European Commission FP6 contract Nr 019813). 94

Graw, K.U. (1995). *Wellenenergie - eine hydromechanische Analyse*. Bericht Nr. 8 des Lehr- und Forschungsgebietes Wasserbau und Wasserwirtschaft, Bergische Universität - GH Wuppertal. 65, 67

Green, A. & Bourne, A. (1978). *Reliability Technology*. Wiley, New York. 105, 310

Green, J., Bowen, A., Fingersh, L.J. & Wan, Y.H. (2007). Electrical collection and transmission systems for offshore wind power. In *Proc. of the conference on Offshore Technology*, OTC19090, 10, Houston, Texas. 159

Grimwade, J. (2010). Ensuring reliability for marine renewable drive train systems nautilus testing facilities. In *Proc. of 3rd Int. Conference on Ocean Energy ICOE*, Bilbao. 38

Guida, M. & Pulcini, G. (2002). Automotive reliability inference based on past data and technical knowledge. *Reliability Engineering & System Safety*, **76**, 129 – 137. 132, 135, 136, 137

Guida, M., Pulcini, G. & Vianello, M. (2009). Early inference on reliability of upgraded automotive components by using past data and technical information. *Journal of Statistical Planning and Inference*, **139**, 1604 – 1618, Spec. Iss. on Degradation, Damage, Fatigue and Accelerated Life Models in Reliability Testing. 132, 135, 136

Gullo, L. (1999). In-service reliability assessment and top-down approach provides altemative reliability prediction method. In *Reliability and Maintainability, Annual Symposium - RAMS*, 365–377, Los Angeles. 59

Hamada, M., Wilson, A., Reese, C. & Martz, H. (2008). *Bayesian Reliability*. Springer Series in Statistics, Springer. 124, 126, 127, 129, 130

Hamilton, J.D. (1994). *Time Series Analysis*. Princeton University Press. 254

Harnoy, A. (2003). *Bearing design in machinery: engineering tribology and lubrication*. Marcel Dekker, New York. 262, 263

Harris, R., Johanning, L. & Wolfram, J. (2004). Mooring systems for wave energy converter: A review of design issues and choices. In *Proc. of 3rd Int. Conference on Marine Renewable Energy MAREC*, Blyth, UK. 65, 107

Hasham, N. (2010). Port Kembla wave generator wrecked. *Illawarra Mercury*, 15 May. 82

Heising, C.D. & Shwayri, N. (1987). An application of the two-stage Bayesian method to estimate the outage rate of oil-fired boilers. *Reliability Engineering*, **18**, 23–33. 132, 135

Henderson, R. (2006). Design, simulation, and testing of a novel hydraulic power take-off system for the Pelamis wave energy converter. *Renewable Energy*, **31**, 271–283. 38, 84

Heuler, P. & Klätscke, H. (2005). Generation and use of standardised load spectra and load-time histories. *International Journal of Fatigue*, **27**, 974–990. 173, 174, 272

Hitziger, T. (2007). *Übertragbarkeit von Vorkenntnissen bei der Zuverlässigkeitstestplanung*. Ph.D. thesis, Institut für Maschinenelemente IMA, University Stuttgart. 59

Holthuijsen, L.H. (2007). *Waves in oceanic and coastal waters*. Cambridge University Press, New York. 70

Hopson, C. (2009). Wave generator capsizes as it is being towed for trial. RECHARGE News. 37

HUANG, S. (1999). Stability analysis of the heave motion of marine cable-body systems. *Ocean Engineering*, **26**, 531 – 546. 163

HUDSON, J.A., PHILLIPS, D.C. & WILKINS, N.J.M. (1980). Material aspects of wave energy converters. *Journal of materials science*, **15**, 1337–1363. 33, 87, 88

HUDSON, J.C. & KAPUR, K.C. (1982). Reliability theory for multistate systems with multistate components. *Microelectronics and Reliability*, **22**, 1 – 7. 46

ISO (2005). Iso/iec 17025:2005 general requirements for the competence of testing and calibration laboratories. 276

JDR (2010). Dynamic power umbilical for wave energy buoy. website, www.jdrcables.com/SubseaPowerCables/RenewableEnergySolutions. 160

JEFFREY, D., RICHMOND, D., SALTER, S. & TAYLOR, J. (1976). Second year interim report on Edinburgh Wave Power Project, "Study of mechanisms for extracting power from sea waves". Tech. rep., University of Edinburgh, Department of Mechanical Engineering. 72

JOHANNING, L., SMITH, G.H. & WOLFRAM, J. (2005). Towards design standards for WEC moorings. In *Proc. of 6th European Wave and Tidal Energy Conference EWTEC*, Glasgow. 198

JOHANNING, L., SMITH, G.H. & WOLFRAM, J. (2006). Mooring design approach for wave energy converters. *Proc. of the Institution of Mechanical Engineers, Part M: Journal of Engineering for the Maritime Environment*, **220**, 159 – 174. 68, 270

JOHANNING, L., SMITH, G.H. & WOLFRAM, J. (2007). Measurements of static and dynamic mooring line damping and their importance for floating wec devices. *Ocean Engineering*, **34**, 19181934. 108

JOHANNING, L., SPARGO, A. & PARISH, D. (2008). Large scale mooring test facility a technical note. In *Proc. of 2nd Int. Conference on Ocean Energy ICOE*, Brest, France. 172

JOHANNING, L., THIES, P.R., PARISH, D. & SMITH, G.H. (2011). Offshore reliability approach for floating renewable energy devices. In *Proc. of 30th Int. Conference*

on Ocean, Offshore and Arctic Engineering OMAE, OMAE2011-49844., Rotterdam, Netherlands. 36, 172

Karlsen, S., Slora, R., Heide, K., Lund, S., Eggertsen, F. & Osborg, P. (2009). Dynamic deep water power cables. In *Proc. of the 9th Int. Conference and Exhibition for oil and gas resources development of the Russian Arctic and CIS continental shelf, RAO/CIS Offshore*, 184–203, St. Petersburg. 228, 229, 233

Klaassen, K.B. & van Peppen, J.C.L. (1989). *System Reliability: Concepts and Applications*. Edward Arnold. 310

Klyatis, L. & Klyatis, E. (2006). *Accelerated quality and reliability solutions*. Elsevier, London. 171

Knapp, R., Das, S. & Shimabukuro, T. (2002). Computer-aided design of cables for optimal performance geometric modelling and finite element software for structural design of cables. *Sea Technolgy*, **43**, 4146. 235

Kofoed, J., Frigaard, P., E., F.M. & Sørensen, H. (2006). Prototype testing of the wave energy converter Wave Dragon. *Renewable Energy*, **31**, 181–189. 198, 271, 275

Krivtsov, V. & Linfoot, B. (2010). Physical model investigations of mooring loads in arrays of wave energy converters. In *Proc. of Int. Association for Hydro-Environment Engineering and Research conference IAHR*, Edinburgh, UK. 151

Krivtsov, V. & Wasiloff, J. (2000). Classical vs. Bayes reliability growth in theory and practice. In *Proc. of ASQ 54th Annual Quality Congress*, 311–316. 130

Lane, M., McNamara, J., Gibson, R. & Tyrer, A. (1995). Bend stiffeners for flexible risers. In *Proc. of the Conference on Offshore Technology OTC*, Houston, Texas, 7730-MS. 235

Lazakis, I., Turan, O. & Aksu, S. (2010). Increasing ship operational reliability through the implementation of a holistic maintenance management strategy. *Ships and Offshore Structures*, **5**, 337–357. 275

Limbourg, P., Savić, R., Petersen, J. & Kochs, H.D. (2006). *Safety and Reliability for Managing Risk*, chap. Approximating Failure Rates from Similar Components Using Artificial Neural Networks, 911–919. European Safety and Reliability Conference ESREL, Taylor & Francis. 60

Liu, F. (1973). Snap loads in lifting and mooring cable systems induced by surface wave conditions. Tech. Rep. AD-772 515, Naval Civil Engineering Laboratories. 195, 197

Lydersen, S. & Rausand, M. (1987). A systematic approach to Accelerated Life Testing. *Reliability Engineering*, **18, 4**, 285–293. 174

Mackie, G. (2004). Operation, Reliability and Maintainability of LIMPET. In *HIE Offshore Renewables Operation & Maintenance Seminar*. 80

Malcolm, D. (2010). Reliability, maintainability and levelised cost of offshore wave energy. In *Proc. of Int. Conf. Marine renewable and offshore wind energy, The Royal Institution of Naval Architects (RINA)*. 268

Martinelli, L., Lamberti, A., Ruol, P., Ricci, P., Kirrane, P., Fenton, C. & Johanning, L. (2010). Power umbilical for ocean renewable energy systems - feasibility and dynamic response analysis. In *Proc. of 3rd Int. Conference on Ocean Energy ICOE*, Bilbao, Spain. 168, 226, 271

Martz, H.F. & Waller, R.A. (1982). *Bayesian reliability analysis*. Wiley Series in Probability and Mathematical Statistics: Applied Probability and Statistics, John Wiley & Sons, Chichester. 47, 126, 127, 128, 129, 130, 131

Mayer, D. & Butler, D. (1993). Statistical validation. *Ecological Modelling*, **68**, 21–32. 254

McCabe, A.P. (2004). An appraisal of a range of fluid modelling software. Workpackage 2 T2.3.4, SuperGen Marine, Lancaster University. 71

MechRel (2004). Handbook of reliability prediction procedures for mechanical equipment. Www.mechrel.com. 61, 267

Meeker, W.Q. & Escobar, L.A. (1998). *Statistical Methods for Reliability Data*. Wiley Series in Probability and Statistics, John Wiley & sons. 126, 130, 143

Mendenhall, H. & Schmidt, R. (1998). *Handbook of materials selection*, chap. Copper and its alloys, 59 – 69. John Wiley & Sons, Chichester. 227

Meuleau, C. (1965). High reliability testing and assurance for electronic components. *Microelectronics and Reliability*, **4**, 163–177. 170

Mil-Hdbk-217F (1995). *Reliability Prediction of Electronic Equipment, Military Handbook 217 F*. United States Department of Defence. 55, 57, 58, 99, 310

Mill, A. (2004). Archimedes wave swing evaluation of test procedures and results from deployment in Portugal 2004. Report AM/EMEC/0100, European Marine Energy Centre EMEC. 82

Miner, M.A. (1945). Cumulative damage in fatigue. *Journal of Applied Mechanics*, **12**, A159–A164. 201

Morison, J., O'Brien, M., Johnson, J. & Schaaf, S. (1950). The force exerted by surface waves on piles. *Petroleum Transactions, American Institute of Mining Engineers*, **189**, 149–154. 69

Mueller, M. & Wallace, R. (2008). Enabling science and technology for marine renewable energy. *Energy Policy*, **36**, 4376–4382. 37, 170, 272

Mueller, M., Jeffrey, H., Wallace, R. & von Jouanne, A. (2010). Centers for marine renewable energy in europe and north america. *Oceanography*, **23**, 42–52. 35, 36, 39

Neumann, F., Didier, A.B.M.E. & Sarmento, A. (2007). Pico OWC recovery project: Recent activities and performance data. In *Proc. of 7th European Wave and Tidal Energy Conference EWTEC*, Porto, Portugal. 81

Niedzwecki, J.M. & Thampi, S.K. (1991). Snap loading of marine cable systems. *Applied Ocean Research*, **13**, 2 – 11. 195

Noble Denton (2006). Floating production system JIP FPS mooring integrity. Research report 444, Health and Safety Executive HSE. 107, 310

Oberkampf, W.L., Helton, J.C., Joslyn, C.A., Wojtkiewicz, S.F. & Ferson, S. (2004). Challenge problems: uncertainty in system response given uncertain parameters. *Reliability Engineering and System Safety*, **85**, 11–19. 100

Ocean Navitas (2007). Hydraulic linear wave simulator. Website, www.oceannavitas.com/technology/wave$_s imulator.html, accessedon$26/01/10.

O'Connor, P.D. (1995). Quantifying uncertainty in reliability and safety studies. *Microelectron. Reliab.*, **35**, 1347–1356. 100

O'Connor, P.D.T. (2008). *Practical reliability engineering*. Wiley, 4th edn. 39, 49, 55, 64, 92, 113

OGP (2010). Guide to finding and using reliability data for QRA. Risk Assessment Data Directory 434 20.1, International Association of Oil & Gas Producers. 94, 96

Orcina (2011). *OrcaFlex Manual*. Daltongate, Ulverston, Cumbria, LA12 7AJ, UK, version 9.5a. 159, 164, 165

Pålmgren, A. (1924). The fatigue life of ball bearings. *Zeitung Verein deutscher Ingeneure ZVDI*, **68**, 339–441, in german. 201

Pan, R. (2009). A Bayes approach to reliability prediction utilizing data from accelerated life tests and field failure observations. *Quality and Reliability Engineering International*, **25**, 229–240. 132

Papanikolaou, A. & Eliopoulou, M.N. (2006). Impact of hull design on tanker pollution. In *Proc. 9th Int. Marine Design Conference IMDC*, Ann Arbor, Michigan, USA. 108

Papula, L. (2003). *Mathematische Formelsammlung fr Ingenieure und Naturwissenschaftler*. Vieweg Teubner, 8th edn. 55, 245

Patel, D. (2008). Subsea umbilicals and power cables. STEEGE Lecture 44, BPP-TECH. 161, 163

Payne, G. (2008). Guidance for the experimental tank testing of wave energy converters. Tech. rep., SuperGen Marine, The University of Edinburgh. 76, 152

PCCI (2009). Wave end current energy generating devices - criteria and standards. Tech. Rep. Contract No. M08PC20032., Minerals Management Service MMS. 32

Peacock, D. (2011). TC 114 - Marine energy - Wave, tidal and other water current converters. Strategic Business Plan SMB/4555/R, International Electrotechnical Commission IEC. 33

Pecht, M. & Jie, G. (2009). Physics-of-failure-based prognostics for electronic products. *Transactions of the Institute of Measurement and Control*, **31**, 309–322. 60

Pelamis (2011). Development history. website, www.pelamiswave.com/our-technology/development-history, accessed 01/05/2011. 85

Penrose, R., Elliott, A., Henden, E., Rainbow, B. & Hanham, J. (2009). Wave Hub hydrographic survey for archaeological assessment. Tech. Rep. 08/J/1/02/1329/0829, Emu Ltd. 166

Phillips, J., Cruz, J., Rawlinson-Smith, R., Parkes, J. & Holbrow, R. (2008). Defining the long-term wave resource at Wave Hub: The role of measurements and models. In *Proc. of 27th Int. Conf. on Offshore Mechanics and Arctic Engineering OMAE*, OMAE2008-57349, Estoril, Portugal. 210

Pierce, D. & Brusius, P. (1997). Electromigration: A review. *Microelectronics Reliability*, **37**, 1053 – 1072. 61

Pilkey, W.D. (2005). *Formulas for Stress, Strain, and Structural Matrices*. John Wiley & Sons., 2nd edn. 242

Pitt, E., Saulter, A. & Smith, H. (2006). The wave power climate at the Wave Hub site. Tech. rep., Applied Wave Research report to the SWRDA. 210, 232, 233

Polinder, H., C., D.M.E. & Gardner, F. (2005). Design, modelling and test results of the AWS PM linear generator. *European Transactions on Electrical Power*, **15**, 245–256. 82

Polinder, H., Mueller, M., Scuotto, M. & de Sousa Prado, M.G. (2007). Linear generator systems for wave energy conversion. In *Proc. of the 7th European Wave and Tidal Energy Conference EWTEC*, Porto, Portugal. 83

PÖRN, K. (1996). The two-stage bayesian method used for the t-book application. *Reliability Engineering & System Safety*, **51**, 169 – 179. 132, 135

PREVISIC, M. & BEDARD, R. (2004). Methodology for conceptional level design of offshore wave power plants. Report e21 EPRI WP 005 - US, Electrical Power Reseach Institute EPRI. 31

PREVISIC, M., BEDARD, R. & HAGERMANN, G. (2004a). Offshore wave energy conversion devices. E21 EPRI Asessment WP-004-US-Rev1, Electrical Power Research Institute EPRI. 31

PREVISIC, M., BEDARD, R., HAGERMANN, G. & SIDDIQUI, O. (2004b). System level design, performance, and costs for San Francisco California Pelamis offshore wave power plant. Tech. rep., Electrical Power Research Institute EPRI. 31

RAATH, A.D. (1997). A new time domain parametric dynamic system identification approach to multiaxial service load simulation testing in components. *Int. Journal of Fatigue*, **19**, 409–414. 171, 172

RAMANI, A.S.S. & TRIVEDI, K.S. (2000). Availability models in practice. In *Proc. of Int. Workshop on Fault-Tolerant Control and Computing (FTCC-1)*, Seoul, Korea. 91

RANDOLPH, M. & QUIGGIN, P. (2009). Non-linear hysteretic seabed model for catenary pipeline contact. In *Proc. of the 28th Int. Conference on Ocean, Offshore and Arctic Engineering OMAE*, OMAE2009-79259, ASME, Honolulu, Hawaii, USA. 168

RAUSAND, M. & HØYLAND, A. (2004). *System reliability theory. Models statistical methods and applications.*. Series in probability and statistics, Wiley, 2nd edn. 46, 47, 52, 63, 94, 96, 125

RENEWABLEUK (2010). Channelling the energy - a way forward for the UK wave & tidal industry towards 2020. Tech. rep. 29

RIAC (1995). Nonelectronic parts reliability data NPRD. Tech. rep., Reliability Information Analysis Center. 310

RIDGE, I. (2009). Tension-torsion fatigue behaviour of wire ropes in offshore moorings. *Ocean Engineering*, **36**, 650 – 660. 172

RUDD, H. (2003). Technical and economic feasibility study of a frond type wave power generator. Tech. Rep. DTI report V/06/00200/REP URN 04/1858, Engineering Business. 28

RYCHLIK, I. (1987). A new definition of the rainflow cycle counting method. *Int. Journal of Fatigue*, **9**, 119–121. 201, 202

SALTER, S. (2003a). Research requirements for fourth generation wave energy devices. In *Results from the work of the European Thematic Network on Wave Energy (WaveNet)*, 194–224, European Community. 37

SALTER, S., TAYLOR, J. & CALDWELL, N. (2002). Power conversion mechanisms for wave energy. *Pro. of the Institution of Mechanical Engineers, Part M: Journal of Engineering for the Maritime Environment*, **216**, 1–27. 64

SALTER, S.H. (2003b). Proposals for a component and sub-assembly test platform to collect statistical reliability data for wave energy. In *Proc. of the 4th European Wave Energy Conference EWTEC, Cork*. 37, 170, 272

SCARR, D., KOLLEK, R. & COLLIER, D. (2001). Wave energy: Technology transfer & generic R & D recommendations. ETSU V/06/00187//REP DTI Pub/URN 01/799, Arup Energy & Partners Int. 65

SCHAUMANN, P., KLEINEIDAM, P. & WILKE, F. (2004). Fatigue design bei Offshore-Windenergieanlagen. *Stahlbau*, **73, 9**, 716–726, in German. 34

SCHIJVE, J. (1985). The significance of flight-simulation fatigue tests. Tech. rep., Delft University of technology, report No. LR-466. 170

SCHIJVE, J. (2009). *Fatigue of structures and materials*. Springer. 201, 228, 272

SCOTLAND HERALD (1995). Storm wrecks wave-power Osprey. online archive, http://www.heraldscotland.com/sport/spl/aberdeen/storm-wrecks-wave-power-osprey-1.664677. 37

SDC (2005). Wind power in the UK. Tech. rep., Sustainable Development Comission, www.sd-commission.org.uk, accessed on 25/03/2011. 66

Shafaghi, A. (2008). Equipment failure rate updating - Bayesian estimation. *Journal of Hazardous Materials*, **159**, 87–91. 132, 134, 137

Sharp, J., Strutt, J. & Pereira, D.B.A. (2005). State of the art report and gap analyses quality and reliability. Tech. Rep. 2005 1721, Det Norske Veritas DNV. 94, 96

Shigley, J.E. (2004). *Standard Handbook of Machine Design*. McGraw-Hill, 3rd edn. 238

Simon, N., Drexler, B. & Reed, R. (1992). *Properties of copper and copper alloys at cryogenic temperatures*. NIST Monograph 177, National Institute of Standards and Technology, Gaithersburg, Maryland. 229

SINTEF (1984). *OREDA - Offshore Reliability Data Handbook*, vol. Volume 1 Topside Equipment, Volume 2 Subsea Equipment. Det Norske Veritas DNV, 5th edn. 310

SINTEF (1997). *OREDA - Offshore Reliability Data Handbook*, vol. Volume 1 Topside Equipment, Volume 2 Subsea Equipment. Det Norske Veritas DNV, 5th edn. 310

SINTEF (2002). *OREDA - Offshore Reliability Data Handbook*. Det Norske Veritas DNV, 4th edn. 97, 110, 138, 140

Smith, D.J. (2005). *Reliability, Maintainability and Risk - Practical Methods for Engineers*. Elsevier. 97, 101, 310

Smith, H.C., Pearce, C. & Millar, D.L. (2012). Further analysis of change in nearshore wave climate due to an offshore wave farm: An enhanced case study for the Wave Hub site. *Renewable Energy*, **40**, 51 – 64. 275

Snieckus, D. (2010). Pelamis is ready to ride the next wave. *Recharge*, 16–17. 37, 85

Spooner, E. & Mueller, M. (2001). Comparative study of linear generators and hydraulic systems for wave energy conversion,. ETSU Report V/06/00189/REP, University of Durham, School of Engineering. 82

STACEY, A. & SHARP, J.V. (2007). Safety factor requirements for the offshore industry. *Engineering Failure Analysis*, **14**, 442 – 458. 203

STARLING, M. (2009). Guidelines for reliability, maintainability and survivability of marine energy conversion systems. Tech. rep., The European Marine Energy Centre EMEC. 33

STEWART, D. (1965). A platform with six degrees of freedom. *Proc. of the Institution of Mechanical Engineers*, **180**, 371–386. 176, 177

STIESDAL, H. & MADSEN, P.H. (2005). Design for reliability. In *Proc. of Copenhagen Offshore Wind Conference*, 26 - 28 Oct., Copenhagen, Denmark. 117

SUPERGEN (2007). Supergen marine energy research. Tech. Rep. Grant GR/S26958/01, University of Edinburgh. 29, 30

SWRDA (2011). Invitation to express an interest in deploying at Wave Hub in 2012. www.wavehub.co.uk, South West Regional Development Agency, accessed on 28/12/2011. 36

TAVNER, P.J., XIANG, J. & SPINATO, F. (2007). Reliability analysis for wind turbines. *Wind Energy*, **10**, 1–18. 91

TECHET, A.H. (2004). Morrison's equation. Tech. Rep. 13.42, Massachusetts Institute of Technology [MIT]. 69

TEDD, J. (2007). *Testing, analysis and control of Wave Dragon, wave energy converter*. Phd thesis, Aalborg University. 37, 86

THIES, P.R., FLINN, J. & SMITH, G.H. (2009). Is it a showstopper? Reliability assessment and criticality analysis for wave energy converters. In *Proc. of 8th European Wave and Tidal Energy Conference EWTEC*, Uppsala, Sweden. 268

THOMAS, G. (2008). *The Theory Behind the Conversion of Ocean Wave Energy: a Review*, chap. 3, 41–91. Green Energy and Technology, Springer Berlin. 76

THORPE, T.W. (1999). A brief review of wave energy. Tech. Rep. ETSU-R120, The UK Department of Trade and Industry. 31, 65

Tobias, P. (2006). *e-Handbook of Statistical Methods*, chap. 8: Assessing Product Reliability. NIST/SEMATECH. 123, 139

Trarieux, F. (2010). Personal correspondence, e-mail , dated 22nd June 2010. 162

Trarieux, F., Lyons, G. & Patel, M. (2006). Investigations with a bandwidth measure for fatigue assessment of the Foinaven dynamic umbilical including VIV. *Engineering Structures*, **28**, 1671–1690. 162

TTI (2006). Durability of polyester ropes. Final project report TTI-SJB-2005-321, Report by Tension Technology Internantional for the Mineral Management Service MMS. 172

Tucker, M.J. (1991). *Waves in Ocean Engineering*. Series in Marine Science, Ellis Horwood, Chichester. 70

UMF (2004). Experience report. control umbilicals delivered by UMF members in the period 1995-2000. Tech. rep., International Umbilical Manufacturers' Federation. 161

University of Exeter (2010). Cornwall scientists speed up marine renewable testing. Press release, 24th Feb 2010, accessed 10/03/2011. 182

U.S. Department of Energy (2011). Marine and hydrokinetic technology database. Updated and reviewed quarterly. 64

Valério, D., ao, P.B. & da Costa, J.S. (2007). Optimisation of wave energy extraction with the Archimedes Wave Swing. *Ocean Engineering*, **34**, 2330 – 2344. 82

van Bussel, G.J.W. & Zaaijer, M.B. (2001). Reliability, Availability and Maintenance Aspects of Large-Scale Offshore Wind Farms, a Concepts Study. In *Proc. of Marine Renewable Energies Conference MAREC*, vol. 113, 119–126. 310

Vassalos, D. & Huang, S. (1996). Dynamics of small-sagged taut-slack marine cables. *Computers & Structures*, **58**, 557 – 562. 163

Vaz, M. & Patel, M. (2007). Post-buckling behaviour of slender structures with a bilinear bending momentcurvature relationship. *International Journal of Non-Linear Mechanics*, **42**, 470 – 483. 250

VICKERS, A. (2012). *Improve the understanding of uncertainties in numerical analysis of moored floating wave energy converters*. Submitted, University of Exeter, College of Engineering Mathematics and Physical Sciences [CEMPS]. 151, 152, 212

VIKING (2010). Synthetic rope specification. Tech. rep., www.viking-moorings.com/Portals/96/dokumenter/fiber/fiber$_r ope.pdf$, $accessed$30/06/2011.

VINTR, M. (2007). Reliability assessment for components of complex mechanisms and machines. In J.P. Merlet & M. Dahan, eds., *Proc. 12th World Congr. Mechanism Machine Science (IFToMM)*, 17-21 June 2007, Besancon, France. 94

WAFO-GROUP (2000). *WAFO - A Matlab Toolbox for Analysis of Random Waves and Loads - A Tutorial*. Center for Math. Sci., Lund Univ., Lund, Sweden. 197, 204

WALKER, R.T., JOHANNING, L. & PARKINSON, R. (2011). Weather windows for device deployment at UK test site: Availability and cost implications. In *Proc. of 9th European Wave and Tidal Energy Conference EWTEC*, Southampton, UK. 66, 275

WANG, K.S., SHEN, Y.C. & HUANG, J. (1997). Loading adjustment for fatigue problem based on reliability considerations. *International Journal of Fatigue*, **19**, 693 – 702. 202

WATERS, R., STALBERG, M., DANIELSSON, O., SVENSSON, O., GUSTAFSSON, S., STROMSTEDT, E., ERIKSSON, M., SUNDBERG, J. & LEIJON, M. (2007). Experimental results from sea trials of an offshore wave energy system. *Applied Physics Letters*, **90, 3**, 034105 – 034105–3. 82

WAVEGEN (2002). ISLAY LIMPET Project monitoring final report. Tech. Rep. ETSU V/06/00180/00/Rep, DTI. 80

WEBB, I., SEAMAN, C. & JACKSON, G. (2005). Marine energy challenge - Oscillating Water Column wave energy converter evaluation report. Tech. rep., Arup Energy, report for the Carbon Trust. 80

WEIBULL, W. (1951). A statistical distribution function of wide applicability. *Journal of Applied Mechanics*, **18**, 293–297. 53

Weise, K. & Wöger, W. (1992). A Bayesian theory of measurement uncertainty. *Measurement Science and Technology*, **3**, 1–11. 124

Weltin, U. (2009). Reliability in engineering dynamics. Lecture notes Reliability Engineering TUHH. 172

White, M. & Bernstein, J.B. (2008). Microelectronics reliability: Physics-of-failure based modeling and lifetime evaluation. NASA Electronic Parts and Packaging (NEPP) Program, Office of Safety and Mission Assurance NASA WBS: 939904.01.11.10, National Aeronautics and Space Administration (NASA). 55, 60

Williams, J.G., Miyase, A., Li, D. & Wang, S.S. (2002). Small-scale testing of damaged synthetic fiber mooring ropes. In *Offshore Technology Conference*, 14308-MS, 13, Houston, Texas. 172

Winterbottom, A. (1984). The interval estimation of system reliability from component test data. *Operations Research*, **32**, 628–640. 130

Wolfram, J. (2006). On assessing the reliability and availability of marine energy converters: The problems of a new technology. *Proc. of the Institution of Mechanical Engineers, Part O: Journal of Risk and Reliability*, **220**, 55–68. 34, 87, 88, 93, 103, 112, 170

Worzyk, T. (2009). *Submarine Power Cables: Design, Installation, Repair, Environmental Aspects*. Springer, Berlin. 158, 159, 164, 226

Yang, G. (2007). *Life Cycle Reliability Engineering*. Wiley, New Jersey. 46, 47

Yang, L. & Moan, T. (2011). Numerical modeling of wear damage in seals of a wave energy converter with hydraulic power take-off under random loads. *Tribology Transactions*, **54, 1**, 44–56. 85

Yang, L., Hals, J. & Moan, T. (2010a). Analysis of dynamic effects relevant for the wear damage in hydraulic machines for wave energy conversion. *Ocean Engineering*, **37**, 1089 – 1102. 85

Yang, X., Rogers, W.J. & Mannan, M.S. (2010b). Uncertainty reduction for improved mishap probability prediction: Application to level control of distillation unit. *Journal of Loss Prevention in the Process Industries*, **23**, 149 – 156. 132, 135

YARD (1980). Reliability of six wave power devices. Tech. Rep. WV 1581, Energy Technology Support Unit [ETSU]. 33, 310

Yemm, R. (2003). Pelamis WEC - Full scale joint system test. DTI report V/06/00191/00/00/REP, DTI. 38, 84, 85, 105, 110

Zafiropoulos, E. & Dialynas, E. (2004). Reliability and cost optimization of electronic devices considering the component failure rate uncertainty. *Reliability Engineering and System Safety*, **84**, 271284. 115

Ziegler, J. & Nichols, N. (1942). Optimum settings for automatic controllers. *Transactions of the ASME*, 759–765, www2.eie.ucr.ac.cr/ valfaro/docs/Ziegler 262

Zimmermann, H.J. (2000). An application-oriented view of modeling uncertainty. *European Journal of Operational Research*, **122**, 190–198. 100

Zio, E. (2009). *Computational methods for reliability and risk analysis*, vol. 14 of *Series on Quality, Reliability and Engineering Statistics*. World Scientific Publishing. 102

Appendix A

Publications

A.1 Journal publications

I Thies, P.R., Johanning, L. & Smith, G.H. (2011). Towards component reliability testing for marine energy converters. *Ocean Engineering,* ***38***, 360 - 370.

II Thies, P.R., Johanning, L. & Smith, G.H. (2011). Assessing mechanical loading regimes and fatigue life of marine power cables in marine energy applications. *Spec. Iss. Proc. of the Institution of Mechanical Engineers, Part O, Journal of Risk and Reliability,* ***226***, 18 - 32.

III Thies, P.R., Smith, G.H. & Johanning, L. (2012). Addressing failure rate uncertainties of marine energy converters. *Renewable Energy,* ***44***, 359 - 367.

A.2 Conference publications

IV Thies, P.R., Flinn, J. & Smith, G.H.(2009). Is it a showstopper? Reliability assessment and criticality analysis for wave energy converters. In *Proc. of 8th European Wave and Tidal Energy Conference EWTEC*, 7 - 10 Sep, Uppsala, Sweden.

V Johanning, L., Thies, P.R. & Smith, G.H.(2010). Component test facilities for marine renewable energy converters. In *Proc. of Int. Conf. Marine renewable and offshore wind energy*, The Royal Institution of Naval Architects (RINA), 21 - 23 Apr, London, UK.

VI Thies, P.R. & Johanning, L.(2010). Development of a marine component testing facility for marine energy converters. In *Proc. of 3rd Int. Conference on Ocean Energy ICOE*, 6-8 Oct, Bilbao, Spain.

VII Thies, P.R., Johanning, L. & Smith, G.H.(2011). Assessing loading regimes and failure modes of marine power cables in marine energy applications. In Prescott, D. & Remenyte-Prescott, R. (eds.), *Proc. of 19th Advances in Risk and Reliability Technology Symposium ARTS*, pp. 237 - 251, 12 - 14 Apr, Stratford-upon-Avon, UK.

VIII Johanning, L., Thies, P.R., Parish, D. & Smith, G.H.(2011). Offshore reliability approach for floating renewable energy devices. In *Proc. of 30th Int. Conf. on Ocean, Offshore and Arctic Engineering*, OMAE2011-49844, Rotterdam, Netherlands.

IX Thies, P.R., Johanning, L. & Smith, G.H.(2012). Lifecycle fatigue load spectrum estimation for mooring lines of a floating marine energy converter. In *31st Int. Conf. on Ocean, Offshore and Arctic Engineering*, OMAE2012-84101, 01 - 06 Jul, Rio De Janeiro, Brazil.

X Weller, S., Davies, P., Thies, P.R., Harnois, V. & Johanning, L.(2012). Durability of synthetic mooring lines for ocean energy devices. In *Proc. of 4th Int. Conference on Ocean Energy ICOE*, 17-19 Oct, Dublin, Ireland.

Appendix B

Bayesian updating model

The generic Bayesian updating model that has been established as part of the work in chapter 4 is given as an annotated Matlab source code below.

Discrete Bayesian update of failure rate estimates This model presents an example of a failure rate update for an umbilicul. The Bayesian method allows to combine information that is available before a particular test/experiment/field observations is conducted, with the data and information that is obtained during that test. While the initial information is used to establish a prior distribution. The observed data is then used to adjust the earlier distribution, establishing the so-called posterior distribution.

Here a discrete Bayesian updating is performed, which is more applicable in practice, as no conjugated pairs need to be found analytically to reach a closed solution.

For the discrete Bayesian updating case, Bayes' theroem can be written as:

$$P(h_i|E) = \frac{P(E|h_i)P(h_i)}{\sum_j P(E|h_i)P(h_i)}$$

or verbally as:

$$\text{Posteriorprobability} = \frac{(\text{Likelihood})(\text{Priorprobability})}{\sum(\text{Likelihood})(\text{Priorprobability})}$$

The presented procedure is generic, but in order to illustrate the process, actual data is used for the prior distribution and notional test results are simulated as observations.

Establishing the Prior Distribution As prior information an umbilical failure rate estimate from the OREDA handbook (2002, p.811) is used. The handbook states the mean failure rate (λ_{mean}) and the standard deviation λ_σ calculated from the available component failure information. The failure rates are given per 10^6 operational hours. OREDA also only describes a constant failure rate, i.e. the bottom of the bathtub-curve.

```
% Defining \lambda_{mean}, \lambda_{\sigma}
Lmean=4.2669;    % Mean estimated failure rate from OREDA [failures/10^{6} hours];
```

```
Lsd=4.8281;      % Estimated standard deviation from OREDA [failures/10^{6} hours];
%Lmean=1000000/Lmean;%Readjusted for MTTF instead of failure rate per million hours.
%Lsd=1000000/Lsd;
Lvar=Lsd^2;     % Calculates the variance \sigma^{2}

%Calculate parameters for Gamma distribution (see OREDA, 2002, p. 29)
Theta=Lmean/Lvar;
k=Lmean*Theta;

%Generate prior
t =linspace(0,1,1001);
Rt=(1+(t./Theta)).^(-k);
ft=(k*Theta.^(k))./((Theta+t).^(k+1));
zt=k./(Theta+t);

%Plot failure rate function (Prior)
figure; plot(t,ft, 'b-', 'DisplayName', 'Probability density function f(t)')
hold on;
plot(t, zt, 'r--', 'DisplayName', 'Failure rate function z(t)');
xlabel('Time [10^{6} h]'); ylabel('f(t), z(t)'); legend('show')

figure; plot(t,Rt, 'b-', 'DisplayName', 'Reliability function R(t)');
xlabel('Time [h]'); ylabel('R(t)'); legend('show')

Prior=ft;
PriorN=Prior/sum(Prior);
```

Generate Likelihood Distribution The actual observations are hypothetical in this example. It assumes the observed a number of failure times are being observed, e.g. in an experiment. These observations are randomly drawn from a 2-paramter Weibull distribution. The actual Likelihood distribution is subsequently fitted to the synthesised data.

```
% Assumed test data results (Observations); here failure rate [per million h]
% May be assessed for different Weibull parameters a, b.
n=10;        % Number of failure rare observations
a=0.5;     % Shape parameter
b=3;      % Scale parameter
rand('state',70);  % Seed selection for random number generation
Test=wblrnd(a,b,n,1);   % Generates randum numbers within given weibull distribution

parmhat = wblfit(Test); %Distribution fitting to drawn sample;
```

```
Likelihood = wblpdf(t, parmhat(1), parmhat(2)); Generation of Likelihood function
LikelihoodN=Likelihood/sum(Likelihood); %Normalisation of likelihood function

%Weibull Plot
figure; wblplot(Test);
figure; plot(Test,zeros(n,1),'go', 'MarkerSize', 8) ; hold on; % Plots observations
plot(t,Likelihood)
legend('Observations', 'Fitted distribution');
xlabel('Time [10^{6} h]'); ylabel('f(t)'); legend('show')
```

Compute Posterior distribution The evidence is computed to normalise the posterior distribution, then the posterior distribution is computed and plotted.

```
Evidence=sum(Likelihood.*Prior);  %Computes Evidence
Posterior=(Likelihood.*Prior); % Compute posterior
%Plot Figure
figure; plot(t,Prior,'--b',t,Likelihood,'-.r',t,Posterior,'-m');
legend('Prior', 'Likelihood','Posterior');
legend('show');
```

Appendix C

List of failure rates

Table C.1: Guide to additional information for list of failure rates in table C.2.

Data source		Data quality	
Alias	Reference	Alias	Type
1	Green & Bourne (1978)	I	Prototype tests
2	Smith (2005)	Ia	Offshore sources
3	SINTEF (1984)	II	Generic database
4	SINTEF (1997)	III	Expert judgement
5	YARD (1980)		
6	AME (1992)		
7	van Bussel & Zaaijer (2001)		
8	FARADIP (2006)		
9	Mil-Hdbk-217F (1995)		
10	Klaassen & van Peppen (1989)		
11	Noble Denton (2006)		
12	RIAC (1995)		

Table C.2: List of base failure rates collected from different data sources

Part	Capacity	Failure Mode	Source	Statistical parameter	Quality	N failures	Failure rate [1/year]
Air / water turbines							
Sleeve Bearing	General	Failure	1	Mean	II	N/A	0.0438
Air / Water Turbine	General	Failure	2	Lower	II	N/A	0.2630
Air / Water Turbine	General	Failure	2	Upper	II	N/A	0.7013
Sleeve Bearing	General	Binding	2	Lower	II	N/A	0.0018
Sleeve Bearing	General	Binding	2	Upper	II	N/A	0.0175
Sleeve Bearing	General	Worn	2	Lower	II	N/A	0.0026
Sleeve Bearing	General	Worn	2	Upper	II	N/A	0.0263
Heavy Ball Bearing	General	Binding	2	Lower	II	N/A	0.0070
Heavy Ball Bearing	General	Binding	2	Upper	II	N/A	0.0701
Heavy Ball Bearing	General	Worn	2	Lower	II	N/A	0.0105
Heavy Ball Bearing	General	Worn	2	Upper	II	N/A	0.1052
Air Turbine	General	Failure	5	Mean	II	N/A	0.0127
Turbine Governor	General	Failure	5	Mean	II	N/A	0.0244
Air Turbine	General	Failure	5	Mean	II	N/A	0.0127
Bearings	General	Failure	5	Mean	II	N/A	0.0333
Driveshaft	General	Failure	5	Mean	II	N/A	0.0061
Brake Assembly	General	Failure	5	Mean	II	N/A	0.0187
Air Turbine	General	Failure	5	Mean	II	N/A	0.0367
Air Turbine	General	Failure	6	Mean	II	N/A	0.0190
Pelton turbine	General	Failure	6	Mean	II	N/A	0.1051
Bearing							
Bearing, Ball, Roller	General	Failure	12	Mean	II	5	1.8996
Bearing, Sleeve	General	Failure	12	Mean	II	1	1.2351
Cables and connections							

Continued on Next Page...

Table C.2 – Continued

Part	Capacity	FM	Source	Stats	Qual.	N	FR [1/year]
Normal	$\geq$ 1kV	Failure	1	Mean	II	N/A	0.0053
Normal	1kV - 33kV (per km)	Failure	1	Mean	II	N/A	0.0386
Normal	33kV - 275kV (per km)	Failure	1	Mean	II	N/A	0.0657
Overhead	10kV - 33kV (per km)	Failure	1	Mean	II	N/A	0.1096
Overhead	110kV - 400kV (per km)	Failure	1	Mean	II	N/A	0.0272
Busbar	11kV	Failure	2	Lower	II	N/A	0.0002
Busbar	11kV	Failure	2	Mean	II	N/A	0.0018
Busbar	3.3kV	Failure	2	Lower	II	N/A	0.0004
Busbar	3.3kV	Failure	2	Upper	II	N/A	0.0175
Busbar	415kV	Failure	2	Lower	II	N/A	0.0053
Busbar	415kV	Failure	2	Upper	II	N/A	0.0175
Overhead	$\leq$ 600V	Failure	2	Mean	II	N/A	0.0044
Overhead	600V - 15kV	Failure	2	Lower	II	N/A	0.0438
Overhead	600V - 15kV	Failure	2	Upper	II	N/A	0.1315
Overhead	$\geq$ 300kV	Failure	2	Lower	II	N/A	0.0263
Overhead	$\geq$ 300kV	Failure	2	Upper	II	N/A	0.0614
Circuit Breaker	$\leq$ 600V	Arcing and Damage	2	Lower	II	N/A	0.0004
Circuit Breaker	$\leq$ 600V	Arcing and Damage	2	Upper	II	N/A	0.0013
Circuit Breaker	$\leq$ 600V	Fail to Close	2	Lower	II	N/A	0.0002

Continued on Next Page...

Table C.2 – Continued

Part	Capacity	FM	Source	Stats	Qual.	N	FR [1/year]
Circuit Breaker	$\leq$ 600V	Fail to Close	2	Upper	II	N/A	0.0007
Circuit Breaker	$\leq$ 600V	Fail to Open	2	Lower	II	N/A	0.0018
Circuit Breaker	$\leq$ 600V	Fail to Open	2	Upper	II	N/A	0.0053
Circuit Breaker	$\leq$ 600V	Spurious Operation	2	Lower	II	N/A	0.0020
Circuit Breaker	$\leq$ 600V	Spurious Operation	2	Upper	II	N/A	0.0059
Circuit Breaker	$\geq$ 3kV	Arcing and Damage	2	Lower	II	N/A	0.0004
Circuit Breaker	$\geq$ 3kV	Arcing and Damage	2	Upper	II	N/A	0.0018
Circuit Breaker	$\geq$ 3kV	Fail to Close	2	Lower	II	N/A	0.0002
Circuit Breaker	$\geq$ 3kV	Fail to Close	2	Upper	II	N/A	0.0009
Circuit Breaker	$\geq$ 3kV	Fail to Open	2	Lower	II	N/A	0.0018
Circuit Breaker	$\geq$ 3kV	Fail to Open	2	Upper	II	N/A	0.0070
Circuit Breaker	$\geq$ 3kV	Spurious Operation	2	Lower	II	N/A	0.0020
Circuit Breaker	$\geq$ 3kV	Spurious Operation	2	Upper	II	N/A	0.0079
Circuit Breaker	$\geq$ 100kV	Arcing and Damage	2	Lower	II	N/A	0.0026
Circuit Breaker	$\geq$ 100kV	Arcing and Damage	2	Upper	II	N/A	0.0088
Circuit Breaker	$\geq$ 100kV	Fail to Close	2	Lower	II	N/A	0.0013
Circuit Breaker	$\geq$ 100kV	Fail to Close	2	Upper	II	N/A	0.0044

Continued on Next Page...

Table C.2 – Continued

Part	Capacity	FM	Source	Stats	Qual.	N	FR [1/year]
Circuit Breaker	$\geq$ 100kV	Fail to Open	2	Lower	II	N/A	0.0105
Circuit Breaker	$\geq$ 100kV	Fail to Open	2	Upper	II	N/A	0.0351
Circuit Breaker	$\geq$ 100kV	Spurious Operation	2	Lower	II	N/A	0.0118
Circuit Breaker	$\geq$ 100kV	Spurious Operation	2	Upper	II	N/A	0.0394
Circuit Breaker	$\leq$ 220V	Spurious Operation	3	Lower	I(a)	2	0.0025
Circuit Breaker	$\leq$ 220V	Spurious Operation	3	Mean	I(a)	2	0.0140
Circuit Breaker	$\leq$ 220V	Spurious Operation	3	Upper	I(a)	2	0.0447
Circuit Breaker	$\leq$ 220V	Failure	3	Lower	I(a)	3	0.0202
Circuit Breaker	$\leq$ 220V	Failure	3	Mean	I(a)	3	0.0359
Circuit Breaker	$\leq$ 220V	Failure	3	Upper	I(a)	3	0.0701
Circuit Breaker	221V - 440V	Spurious Operation	3	Lower	I(a)	6	0.0010
Circuit Breaker	221V - 440V	Spurious Operation	3	Mean	I(a)	6	0.0021
Circuit Breaker	221V - 440V	Spurious Operation	3	Upper	I(a)	6	0.0039
Circuit Breaker	221V - 440V	Fail to Open	3	Lower	I(a)	2	0.0002
Circuit Breaker	221V - 440V	Fail to Open	3	Mean	I(a)	2	0.0007
Circuit Breaker	221V - 440V	Fail to Open	3	Upper	I(a)	2	0.0021
Circuit Breaker	221V - 440V	Fail to Close	3	Lower	I(a)	3	0.0003

Continued on Next Page...

Table C.2 – Continued

Part	Capacity	FM	Source	Stats	Qual.	N	FR [1/year]
Circuit Breaker	221V - 440V	Fail to Close	3	Mean	I(a)	3	0.0011
Circuit Breaker	221V - 440V	Fail to Close	3	Upper	I(a)	3	0.0025
Circuit Breaker	221V - 440V	Operated Prematurely	3	Lower	I(a)	1	0.0000
Circuit Breaker	221V - 440V	Operated Prematurely	3	Mean	I(a)	1	0.0004
Circuit Breaker	221V - 440V	Operated Prematurely	3	Upper	I(a)	1	0.0016
Circuit Breaker	221V - 440V	Contaminated	3	Lower	I(a)	2	0.0002
Circuit Breaker	221V - 440V	Contaminated	3	Mean	I(a)	2	0.0007
Circuit Breaker	221V - 440V	Contaminated	3	Upper	I(a)	2	0.0021
Circuit Breaker	221V - 440V	Failure (Total)	3	Lower	I(a)	38	0.0062
Circuit Breaker	221V - 440V	Failure (Total)	3	Mean	I(a)	38	0.0140
Circuit Breaker	221V - 440V	Failure (Total)	3	Upper	I(a)	38	0.0228
Circuit Breaker	441V - 5.5kV / 6.6kV	Fail to Close	3	Lower	I(a)	7	0.0000
Circuit Breaker	441V - 5.5kV / 6.6kV	Fail to Close	3	Mean	I(a)	7	0.0430
Circuit Breaker	441V - 5.5kV / 6.6kV	Fail to Close	3	Upper	I(a)	7	0.1052
Circuit Breaker	441V - 5.5kV / 6.6kV	Spurious Operation	3	Lower	I(a)	4	0.0066

Continued on Next Page...

Table C.2 – Continued

Part	Capacity	FM	Source	Stats	Qual.	N	FR [1/year]
Circuit Breaker	441V - 5.5kV / 6.6kV	Spurious Operation	3	Mean	I(a)	4	0.0193
Circuit Breaker	441V - 5.5kV / 6.6kV	Spurious Operation	3	Upper	I(a)	4	0.0447
Circuit Breaker	441V - 5.5kV / 6.6kV	Fail to Open	3	Lower	I(a)	2	0.0018
Circuit Breaker	441V - 5.5kV / 6.6kV	Fail to Open	3	Mean	I(a)	2	0.0096
Circuit Breaker	441V - 5.5kV / 6.6kV	Fail to Open	3	Upper	I(a)	2	0.0307
Circuit Breaker	441V - 5.5kV / 6.6kV	Contaminated	3	Lower	I(a)	4	0.0000
Circuit Breaker	441V - 5.5kV / 6.6kV	Contaminated	3	Mean	I(a)	4	0.0228
Circuit Breaker	441V - 5.5kV / 6.6kV	Contaminated	3	Upper	I(a)	4	0.0614
Circuit Breaker	441V - 5.5kV / 6.6kV	Failure (Total)	3	Lower	I(a)	35	0.0421
Circuit Breaker	441V - 5.5kV / 6.6kV	Failure (Total)	3	Mean	I(a)	35	0.1841
Circuit Breaker	441V - 5.5kV / 6.6kV	Failure (Total)	3	Upper	I(a)	35	0.3419
Cell Cable	General	Failure	5	Mean	II	N/A	0.0040
Cell Cable Connection	General	Failure	5	Mean	II	N/A	0.0053

Continued on Next Page...

Table C.2 – Continued

Part	Capacity	FM	Source	Stats	Qual.	N	FR [1/year]
Circuit Breaker	General	Failure	5	Mean	II	N/A	0.0013
Busbar	General	Failure	5	Mean	II	N/A	0.0012
Switchgear	Low Voltage	Failure	5	Mean	II	N/A	0.0012
Distribution Switchboard	General	Failure	5	Mean	II	N/A	0.0012
Bridging Switch / Busbar	General	Failure	5	Mean	II	N/A	0.0015
Cable	General	Failure	5	Mean	II	N/A	0.0040
Switchgear	High Voltage	Failure	5	Mean	II	N/A	0.0013
Switchgear	Low Voltage	Failure	5	Mean	II	N/A	0.0013
Switchgear	General	Failure	6	Mean	II	N/A	0.0020
Circuit Breaker	General	Failure	6	Mean	II	N/A	0.0036
Circuit Breaker	33kV	Failure	6	Mean	II	N/A	0.0036
Busbar	3.3kV	Failure	6	Mean	II	N/A	0.0050
Winding Connection	Low Voltage	Failure	6	Mean	II	N/A	0.0035
Fuse	3.3kV	Failure	6	Mean	II	N/A	0.0019
Busbar	33kV	Failure	6	Mean	II	N/A	0.0011
Circuit Breaker	33kV	Failure	6	Mean	II	N/A	0.0036
Overhead	132kV	Failure	6	Mean	II	N/A	0.4050
Circuit Breaker	400kV	Failure	6	Mean	II	N/A	0.0180
Subsea	400kV (per km)	Failure	6	Mean	I(a)	N/A	0.0151
Collection loop	6kV	Failure	6	Mean	II	N/A	0.0148
Bus, Connection	General	Failure	12	Mean	II	1	3.2864
Bushing, Cable, Electrical	General	Failure	12	Mean	II	1	1.9724

Continued on Next Page...

Table C.2 – Continued

Part	Capacity	FM	Source	Stats	Qual.	N	FR [1/year]
Bushing, Sleeve	General	Failure	12	Mean	II	8	0.6347
Bushing, Sleeve, Pressed	General	Failure	12	Mean	II	1	1.5831
Cable, Electrical	General	Failure	12	Mean	II	1	21.7625
Cable, Electrical Lead, Power	General	Failure	12	Mean	II	2	0.4129
Cable, Electrical Lead, Utility 480V	480V	Failure	12	Mean	II	2	1.6094
Cable, Wire Rope	General	Failure	12	Mean	II	6	2.0065
Circuit Breaker	General	Failure	12	Mean	II	6	1.1159
Gearbox							
Gear - Per Mesh	General	Binding	2	Lower	II	N/A	0.0004
Gear - Per Mesh	General	Binding	2	Mean	II	N/A	0.0035
Gear - Per Mesh	General	Binding	2	Upper	II	N/A	0.0070
Gear - Per Mesh	General	No Transmission	2	Lower	II	N/A	0.0001
Gear - Per Mesh	General	No Transmission	2	Mean	II	N/A	0.0009
Gear - Per Mesh	General	No Transmission	2	Upper	II	N/A	0.0018
Gear - Assembly	General	Binding	2	Lower	II	N/A	0.0701
Gear - Assembly	General	Binding	2	Upper	II	N/A	0.3506
Gear - Assembly	General	No Transmission	2	Lower	II	N/A	0.0175

Continued on Next Page...

Table C.2 – Continued

Part	Capacity	FM	Source	Stats	Qual.	N	FR [1/year]
Gear - Assembly	General	No Transmission	2	Upper	II	N/A	0.0877
Oil Pump	General	Leak	2	Lower	II	N/A	0.0263
Oil Pump	General	Leak	2	Upper	II	N/A	0.3068
Oil Pump	General	No Transmission	2	Lower	II	N/A	0.0263
Oil Pump	General	No Transmission	2	Upper	II	N/A	0.3068
Gearbox	General	Auxiliary Systems Leak	4	Lower	I(a)	15	0.0439
Gearbox	General	Auxiliary Systems Leak	4	Mean	I(a)	15	0.2246
Gearbox	General	Auxiliary Systems Leak	4	Upper	I(a)	15	0.5209
Gearbox	General	Auxiliary Systems Leak	4	SD	I(a)	15	0.1534
Gearbox	General	Failure While Running	4	Lower	I(a)	1	0.0029
Gearbox	General	Failure While Running	4	Mean	I(a)	1	0.0150
Gearbox	General	Failure While Running	4	Upper	I(a)	1	0.0347
Gearbox	General	Failure While Running	4	SD	I(a)	1	0.0102
Gearbox	General	Other	4	Lower	I(a)	10	0.0292

Continued on Next Page...

Table C.2 – Continued

Part	Capacity	FM	Source	Stats	Qual.	N	FR [1/year]
Gearbox	General	Other	4	Mean	I(a)	10	0.1498
Gearbox	General	Other	4	Upper	I(a)	10	0.3473
Gearbox	General	Other	4	SD	I(a)	10	0.1022
Gearbox	General	Overhaul	4	Lower	I(a)	1	0.0029
Gearbox	General	Overhaul	4	Mean	I(a)	1	0.0150
Gearbox	General	Overhaul	4	Upper	I(a)	1	0.0347
Gearbox	General	Overhaul	4	SD	I(a)	1	0.0102
Gearbox	General	Vibration	4	Lower	I(a)	3	0.0088
Gearbox	General	Vibration	4	Mean	I(a)	3	0.0449
Gearbox	General	Vibration	4	Upper	I(a)	3	0.1042
Gearbox	General	Vibration	4	SD	I(a)	3	0.0307
Gearbox	General	Failure (Total)	4	Lower	I(a)	30	0.0877
Gearbox	General	Failure (Total)	4	Mean	I(a)	30	0.4493
Gearbox	General	Failure (Total)	4	Upper	I(a)	30	1.0418
Gearbox	General	Failure (Total)	4	SD	I(a)	30	0.3067
Gearbox	General	Failure (Critical)	4	Lower	I(a)	8	0.0123
Gearbox	General	Failure (Critical)	4	Mean	I(a)	8	0.1017
Gearbox	General	Failure (Critical)	4	Upper	I(a)	8	0.2632

Continued on Next Page...

Table C.2 – Continued

Part	Capacity	FM	Source	Stats	Qual.	N	FR [1/year]
Gearbox	General	Failure (Critical)	4	SD	I(a)	8	0.0823
Brake Assembly	General	Failure	7	Mean	II	N/A	0.0500
Gearbox	General	Failure	7	Mean	II	N/A	0.3000
Coupling, Rigid	General	Failure	12	Mean	II	1	0.5040
Coupling, Shaft	General	Failure	12	Mean	II	3	0.6653
Gear Assembly	General	Failure	12	Mean	II	1	33.3897
Gear, Spur	General	Failure	12	Mean	II	1	0.6171
Roller	General	Failure	12	Mean	II	2	1.0747
Shaft, Power Transmittal	General	Failure	12	Mean	II	1	0.5488
Generators							
AC	General	Failure	1	Mean	II	N/A	0.0614
DC	General	Failure	1	Mean	II	N/A	0.0789
AC	$\geq$ 200kW	Failure	1	Mean	II	N/A	0.0877
AC	$\leq$ 200kW	Failure	1	Mean	II	N/A	0.0438
Circuit Breaker	General	Failure	1	Mean	II	N/A	0.0175
Circuit Breaker	415V - 11kV	Failure	1	Mean	II	N/A	0.0131
Circuit Breaker	33kV	Failure	1	Mean	II	N/A	0.0263
Circuit Breaker	132kV	Failure	1	Mean	II	N/A	0.0351
Circuit Breaker	275kV	Failure	1	Mean	II	N/A	0.0614
Circuit Breaker	400kV	Failure	1	Mean	II	N/A	0.0877
AC	General	Drift or Intermittent	2	Lower	II	N/A	0.0210

Continued on Next Page...

Table C.2 – Continued

Part	Capacity	FM	Source	Stats	Qual.	N	FR [1/year]
AC	General	Drift or Intermittent	2	Upper	II	N/A	0.2104
AC	General	Loss of Output	2	Lower	II	N/A	0.0053
AC	General	Loss of Output	2	Upper	II	N/A	0.0526
DC	General	Drift or Intermittent	2	Lower	II	N/A	0.0070
DC	General	Drift or Intermittent	2	Upper	II	N/A	0.0701
DC	General	Loss of Output	2	Lower	II	N/A	0.0018
DC	General	Loss of Output	2	Upper	II	N/A	0.0175
Turbine Set	General	Drift or Intermittent	2	Lower	II	N/A	0.0701
Turbine Set	General	Drift or Intermittent	2	Mean	II	N/A	1.4026
Turbine Set	General	Drift or Intermittent	2	Upper	II	N/A	5.6102
Turbine Set	General	Loss of Output	2	Lower	II	N/A	0.0175
Turbine Set	General	Loss of Output	2	Mean	II	N/A	0.3506

Continued on Next Page...

Table C.2 – Continued

Part	Capacity	FM	Source	Stats	Qual.	N	FR [1/year]
Turbine Set	General	Loss of Output	2	Upper	II	N/A	1.4026
Oil Pump	General	Leak	2	Lower	II	N/A	0.0263
Oil Pump	General	Leak	2	Upper	II	N/A	0.3068
Oil Pump	General	No Transmission	2	Lower	II	N/A	0.0263
Oil Pump	General	No Transmission	2	Upper	II	N/A	0.3068
Generator	General	Auxiliary Systems Leak	4	Lower	I(a)	17	0.0497
Generator	General	Auxiliary Systems Leak	4	Mean	I(a)	17	0.2546
Generator	General	Auxiliary Systems Leak	4	Upper	I(a)	17	0.5904
Generator	General	Auxiliary Systems Leak	4	SD	I(a)	17	0.1738
Generator	General	Excessive Noise	4	Lower	I(a)	1	0.0029
Generator	General	Excessive Noise	4	Mean	I(a)	1	0.0150
Generator	General	Excessive Noise	4	Upper	I(a)	1	0.0347
Generator	General	Excessive Noise	4	SD	I(a)	1	0.0102

Continued on Next Page...

Table C.2 – Continued

Part	Capacity	FM	Source	Stats	Qual.	N	FR [1/year]
Generator	General	Faulty Output Frequency	4	Lower	I(a)	1	0.0029
Generator	General	Faulty Output Frequency	4	Mean	I(a)	1	0.0150
Generator	General	Faulty Output Frequency	4	Upper	I(a)	1	0.0347
Generator	General	Faulty Output Frequency	4	SD	I(a)	1	0.0102
Generator	General	Faulty Output Voltage	4	Lower	I(a)	11	0.0322
Generator	General	Faulty Output Voltage	4	Mean	I(a)	11	0.1647
Generator	General	Faulty Output Voltage	4	Upper	I(a)	11	0.3820
Generator	General	Faulty Output Voltage	4	SD	I(a)	11	0.1124
Generator	General	Failure to Start	4	Lower	I(a)	40	0.1170
Generator	General	Failure to Start	4	Mean	I(a)	40	0.5991

Continued on Next Page...

Table C.2 – Continued

Part	Capacity	FM	Source	Stats	Qual.	N	FR [1/year]
Generator	General	Failure to Start	4	Upper	I(a)	40	1.3891
Generator	General	Failure to Start	4	SD	I(a)	40	0.4089
Generator	General	Fail While Running	4	Lower	I(a)	115	0.3364
Generator	General	Fail While Running	4	Mean	I(a)	115	1.7223
Generator	General	Fail While Running	4	Upper	I(a)	115	3.9936
Generator	General	Fail While Running	4	SD	I(a)	115	1.1755
Generator	General	Reduced Power Delivery	4	Lower	I(a)	15	0.0439
Generator	General	Reduced Power Delivery	4	Mean	I(a)	15	0.2246
Generator	General	Reduced Power Delivery	4	Upper	I(a)	15	0.5209
Generator	General	Reduced Power Delivery	4	SD	I(a)	15	0.1533
Generator	General	Overheating	4	Lower	I(a)	4	0.0117

Continued on Next Page...

Table C.2 – Continued

Part	Capacity	FM	Source	Stats	Qual.	N	FR [1/year]
Generator	General	Overheating	4	Mean	I(a)	4	0.0599
Generator	General	Overheating	4	Upper	I(a)	4	0.1389
Generator	General	Overheating	4	SD	I(a)	4	0.0409
Generator	General	Overhaul	4	Lower	I(a)	6	0.0175
Generator	General	Overhaul	4	Mean	I(a)	6	0.0899
Generator	General	Overhaul	4	Upper	I(a)	6	0.2084
Generator	General	Overhaul	4	SD	I(a)	6	0.0613
Generator	General	Fail to Synchronize	4	Lower	I(a)	10	0.0292
Generator	General	Fail to Synchronize	4	Mean	I(a)	10	0.1498
Generator	General	Fail to Synchronize	4	Upper	I(a)	10	0.3473
Generator	General	Fail to Synchronize	4	SD	I(a)	10	0.1022
Generator	General	Vibration	4	Lower	I(a)	11	0.0322
Generator	General	Vibration	4	Mean	I(a)	11	0.1647
Generator	General	Vibration	4	Upper	I(a)	11	0.3820
Generator	General	Vibration	4	SD	I(a)	11	0.1124
Generator	General	Other	4	Lower	I(a)	230	0.6727
Generator	General	Other	4	Mean	I(a)	230	3.4446
Generator	General	Other	4	Upper	I(a)	230	7.9873
Generator	General	Other	4	SD	I(a)	230	2.3509
Generator	General	Unknown	4	Lower	I(a)	11	0.0322
Generator	General	Unknown	4	Mean	I(a)	11	0.1647

Continued on Next Page...

Table C.2 – Continued

Part	Capacity	FM	Source	Stats	Qual.	N	FR [1/year]
Generator	General	Unknown	4	Upper	I(a)	11	0.3820
Generator	General	Unknown	4	SD	I(a)	11	0.1124
Generator	General	Failure (Total)	4	Lower	I(a)	455	1.3308
Generator	General	Failure (Total)	4	Mean	I(a)	455	6.8143
Generator	General	Failure (Total)	4	Upper	I(a)	455	15.8009
Generator	General	Failure (Total)	4	SD	I(a)	455	4.6508
Generator	General	Failure (Critical)	4	Lower	I(a)	125	0.1917
Generator	General	Failure (Critical)	4	Mean	I(a)	125	1.5888
Generator	General	Failure (Critical)	4	Upper	I(a)	125	4.1123
Generator	General	Failure (Critical)	4	SD	I(a)	125	1.2866
Cooling System	General	Auxiliary Systems Leak	4	Lower	I(a)	12	0.0351
Cooling System	General	Auxiliary Systems Leak	4	Mean	I(a)	12	0.1795
Cooling System	General	Auxiliary Systems Leak	4	Upper	I(a)	12	0.4163

Continued on Next Page...

Table C.2 – Continued

Part	Capacity	FM	Source	Stats	Qual.	N	FR [1/year]
Cooling System	General	Auxiliary Systems Leak	4	SD	I(a)	12	0.1226
Cooling System	General	Excessive Noise	4	Lower	I(a)	1	0.0028
Cooling System	General	Excessive Noise	4	Mean	I(a)	1	0.0146
Cooling System	General	Excessive Noise	4	Upper	I(a)	1	0.0338
Cooling System	General	Excessive Noise	4	SD	I(a)	1	0.0099
Cooling System	General	Failure to Start	4	Lower	I(a)	1	0.0028
Cooling System	General	Failure to Start	4	Mean	I(a)	1	0.0146
Cooling System	General	Failure to Start	4	Upper	I(a)	1	0.0338
Cooling System	General	Failure to Start	4	SD	I(a)	1	0.0099
Cooling System	General	Failure While Running	4	Lower	I(a)	28	0.0817
Cooling System	General	Failure While Running	4	Mean	I(a)	28	0.4185
Cooling System	General	Failure While Running	4	Upper	I(a)	28	0.9705

Continued on Next Page...

Table C.2 – Continued

Part	Capacity	FM	Source	Stats	Qual.	N	FR [1/year]
Cooling System	General	Failure While Running	4	SD	I(a)	28	0.2857
Cooling System	General	Overheating	4	Lower	I(a)	13	0.0381
Cooling System	General	Overheating	4	Mean	I(a)	13	0.1953
Cooling System	General	Overheating	4	Upper	I(a)	13	0.4529
Cooling System	General	Overheating	4	SD	I(a)	13	0.1333
Cooling System	General	Other	4	Lower	I(a)	14	0.0408
Cooling System	General	Other	4	Mean	I(a)	14	0.2087
Cooling System	General	Other	4	Upper	I(a)	14	0.4838
Cooling System	General	Other	4	SD	I(a)	14	0.1425
Cooling System	General	Unknown	4	Lower	I(a)	1	0.0028
Cooling System	General	Unknown	4	Mean	I(a)	1	0.0146
Cooling System	General	Unknown	4	Upper	I(a)	1	0.0338
Cooling System	General	Unknown	4	SD	I(a)	1	0.0099
Cooling System	General	Failure (Total)	4	Lower	I(a)	70	0.2047
Cooling System	General	Failure (Total)	4	Mean	I(a)	70	1.0481
Cooling System	General	Failure (Total)	4	Upper	I(a)	70	2.4303
Cooling System	General	Failure (Total)	4	SD	I(a)	70	0.7156
Cooling System	General	Failure (Critical)	4	Lower	I(a)	19	0.0291

Continued on Next Page...

Table C.2 – Continued

Part	Capacity	FM	Source	Stats	Qual.	N	FR [1/year]
Cooling System	General	Failure (Critical)	4	Mean	I(a)	19	0.2415
Cooling System	General	Failure (Critical)	4	Upper	I(a)	19	0.6251
Cooling System	General	Failure (Critical)	4	SD	I(a)	19	0.1956
Lubrication System	General	Auxiliary Systems Leak	4	Lower	I(a)	81	0.2369
Lubrication System	General	Auxiliary Systems Leak	4	Mean	I(a)	81	1.2131
Lubrication System	General	Auxiliary Systems Leak	4	Upper	I(a)	81	2.8129
Lubrication System	General	Auxiliary Systems Leak	4	SD	I(a)	81	0.8282
Lubrication System	General	Excessive Noise	4	Lower	I(a)	2	0.0059
Lubrication System	General	Excessive Noise	4	Mean	I(a)	2	0.0300
Lubrication System	General	Excessive Noise	4	Upper	I(a)	2	0.0695
Lubrication System	General	Excessive Noise	4	SD	I(a)	2	0.0204
Lubrication System	General	Failure to Start	4	Lower	I(a)	1	0.0028

Continued on Next Page...

Table C.2 – Continued

Part	Capacity	FM	Source	Stats	Qual.	N	FR [1/year]
Lubrication System	General	Failure to Start	4	Mean	I(a)	1	0.0150
Lubrication System	General	Failure to Start	4	Upper	I(a)	1	0.0347
Lubrication System	General	Failure to Start	4	SD	I(a)	1	0.0102
Lubrication System	General	Failure While Running	4	Lower	I(a)	24	0.0701
Lubrication System	General	Failure While Running	4	Mean	I(a)	24	0.3594
Lubrication System	General	Failure While Running	4	Upper	I(a)	24	0.8335
Lubrication System	General	Failure While Running	4	SD	I(a)	24	0.2454
Lubrication System	General	Reduced Power Delivery	4	Lower	I(a)	9	0.0263
Lubrication System	General	Reduced Power Delivery	4	Mean	I(a)	9	0.1348
Lubrication System	General	Reduced Power Delivery	4	Upper	I(a)	9	0.3125

Continued on Next Page...

Table C.2 – Continued

Part	Capacity	FM	Source	Stats	Qual.	N	FR [1/year]
Lubrication System	General	Reduced Power Delivery	4	SD	I(a)	9	0.0920
Lubrication System	General	Overheating	4	Lower	I(a)	2	0.0059
Lubrication System	General	Overheating	4	Mean	I(a)	2	0.0300
Lubrication System	General	Overheating	4	Upper	I(a)	2	0.0695
Lubrication System	General	Overheating	4	SD	I(a)	2	0.0204
Lubrication System	General	Other	4	Lower	I(a)	20	0.0585
Lubrication System	General	Other	4	Mean	I(a)	20	0.2995
Lubrication System	General	Other	4	Upper	I(a)	20	0.6945
Lubrication System	General	Other	4	SD	I(a)	20	0.2045
Lubrication System	General	Overhaul	4	Lower	I(a)	1	0.0028
Lubrication System	General	Overhaul	4	Mean	I(a)	1	0.0150
Lubrication System	General	Overhaul	4	Upper	I(a)	1	0.0347
Lubrication System	General	Overhaul	4	SD	I(a)	1	0.0102
Lubrication System	General	Failure (Total)	4	Lower	I(a)	140	0.4092
Lubrication System	General	Failure (Total)	4	Mean	I(a)	140	2.0950
Lubrication System	General	Failure (Total)	4	Upper	I(a)	140	4.8618
Lubrication System	General	Failure (Total)	4	SD	I(a)	140	1.4315
Lubrication System	General	Failure (Critical)	4	Lower	I(a)	39	0.0598

Continued on Next Page...

Table C.2 – Continued

Part	Capacity	FM	Source	Stats	Qual.	N	FR [1/year]
Lubrication System	General	Failure (Critical)	4	Mean	I(a)	39	0.4957
Lubrication System	General	Failure (Critical)	4	Upper	I(a)	39	1.2830
Lubrication System	General	Failure (Critical)	4	SD	I(a)	39	0.4014
Alternator	General	Failure	5	Mean	II	N/A	0.0060
Alternator Cooling	General	Failure	5	Mean	II	N/A	0.0181
Lubrication System	General	Failure	5	Mean	II	N/A	0.0403
Cooling System	General	Failure	5	Mean	II	N/A	0.0539
Lubrication System	General	Failure	5	Mean	II	N/A	0.0600
Generator & Exciter	General	Failure	5	Mean	II	N/A	0.0061
Generator Heat Exchanger	General	Failure	5	Mean	II	N/A	0.0147
Generator	General	Failure	6	Mean	II	N/A	0.0140
Generator	1.5kV	Failure	6	Mean	II	N/A	0.0840
Heat Exchanger	General	Failure	6	Mean	II	N/A	0.1100
Lubrication System	General	Failure	6	Mean	II	N/A	1.0446
Generator	16kV	Failure	6	Mean	II	N/A	0.0840
Generator	General	Failure	7	Mean	II	N/A	0.0500
Coil	General	Failure	12	Mean	II	2	14.2412
Control Assembly, Electrical	General	Failure	12	Mean	II	3	0.6171
Control Panel, Generator	General	Failure	12	Mean	II	1	3.8754

Continued on Next Page...

Table C.2 – Continued

Part	Capacity	FM	Source	Stats	Qual.	N	FR [1/year]
Electrical Motor, AC	General	Failure	12	Mean	II	7	2.6000
Electrical Motor, AC, Starter	General	Failure	12	Mean	II	5	2.0583
Motor, Selsyn	General	Failure	12	Mean	II	4	1.8295
Solenoid, Assembly	General	Failure	12	Mean	II	3	1.0958
Solenoid, Coil	General	Failure	12	Mean	II	3	1.9969
Solenoid, Coil, Brake	General	Failure	12	Mean	II	2	0.5321
Hydraulic							
Filter	General	Blockage	1	Mean	II	N/A	0.0088
Filter	General	Leakage	1	Mean	II	N/A	0.0088
Piping	General	Failure	1	Mean	II	N/A	0.0018
Pipe Joint	General	Failure	1	Mean	II	N/A	0.0044
Piston	General	Failure	1	Mean	II	N/A	0.0088
Pressure Gauge	General	Failure	1	Mean	II	N/A	0.1315
Pressure Vessel	General	Failure	1	Mean	II	N/A	0.0263
Ball Valve	General	Failure	1	Mean	II	N/A	0.0044
Accumulator	General	Failure	2	Mean	II	N/A	0.1753
Accumulator	General	Failure	2	Upper	II	N/A	1.7532
Piston	General	Failure	2	Mean	II	N/A	0.0088
Motor	General	Failure	2	Mean	II	N/A	0.0438
Non Return Valve	General	Blockage	2	Lower	II	N/A	0.0004
Non Return Valve	General	Blockage	2	Upper	II	N/A	0.0088
Non Return Valve	General	Leak	2	Lower	II	N/A	0.0013
Non Return Valve	General	Leak	2	Upper	II	N/A	0.0263
Non Return Valve	General	Passing	2	Lower	II	N/A	0.0053

Continued on Next Page...

Table C.2 – Continued

Part	Capacity	FM	Source	Stats	Qual.	N	FR [1/year]
Non Return Valve	General	Passing	2	Upper	II	N/A	0.1052
Non Return Valve	General	Sticking	2	Lower	II	N/A	0.0018
Non Return Valve	General	Sticking	2	Upper	II	N/A	0.0351
Non Return Valve	General	Failure	5	Mean	II	N/A	0.0200
Piping	General	Failure	5	Mean	II	N/A	0.0020
Motor	General	Failure	6	Mean	II	N/A	0.0184
Rams	General	Failure	6	Mean	II	N/A	0.0870
Piping	General	Failure	6	Mean	II	N/A	0.0790
Oil Cooler	General	Failure	6	Mean	II	N/A	0.2100
Coupling, Tube, Hydraulic	General	Failure	12	Mean	II	2	48.0578
Fitting, Hydraulic	General	Failure	12	Mean	II	1	16.0085
Hose, Hydraulic	General	Failure	12	Mean	II	1	1.5831
Piston, Hydraulic, Rod	General	Failure	12	Mean	II	2	0.6198
Pump, Hydraulic	General	Failure	12	Mean	II	3	5.4656
Seal	General	Failure	12	Mean	II	20	2.5904
Seal, Oil	General	Failure	12	Mean	II	3	1.3123
Seal, O-Ring	General	Failure	12	Mean	II	1	0.7802
Seal, Packing	General	Failure	12	Mean	II	2	0.8284
Tubing, Hydraulic	General	Failure	12	Mean	II	2	1.1326
Valve, Hydraulic, Solenoid	General	Failure	12	Mean	II	1	16.0085
Rolling rubber seal on hydraulic rams	General	Failure	6	Mean	II	N/A	0.0364

Continued on Next Page...

Table C.2 – Continued

Part	Capacity	FM	Source	Stats	Qual.	N	FR [1/year]
Inverters							
Inverter	General	No Output	3	Lower	I(a)	5	0.0167
Inverter	General	No Output	3	Mean	I(a)	5	0.0877
Inverter	General	No Output	3	Upper	I(a)	5	0.1841
Inverter	General	Failed to Transfer	3	Lower	I(a)	1	0.0001
Inverter	General	Failed to Transfer	3	Mean	I(a)	1	0.0068
Inverter	General	Failed to Transfer	3	Upper	I(a)	1	0.0333
Inverter	General	Frequency Outside of Spec	3	Lower	I(a)	1	0.0001
Inverter	General	Frequency Outside of Spec	3	Mean	I(a)	1	0.0068
Inverter	General	Frequency Outside of Spec	3	Upper	I(a)	1	0.0333
Inverter	General	Voltage Outside of Spec	3	Lower	I(a)	4	0.0000
Inverter	General	Voltage Outside of Spec	3	Mean	I(a)	4	0.0394
Inverter	General	Voltage Outside of Spec	3	Upper	I(a)	4	0.1140

Continued on Next Page...

Table C.2 – Continued

Part	Capacity	FM	Source	Stats	Qual.	N	FR [1/year]
Inverter	General	Failure (Total)	3	Lower	I(a)	20	0.0964
Inverter	General	Failure (Total)	3	Mean	I(a)	20	0.2279
Inverter	General	Failure (Total)	3	Upper	I(a)	20	0.3682
Inverter	General	Failure	5	Mean	II	N/A	0.0433
Inverter	General	Failure	6	Mean	II	N/A	0.0960
Inverter	General	Failure	7	Mean	II	N/A	0.3200
Miscellaneous							
Fire Water Pump System	General	Leak	2	Lower	II	N/A	0.6575
Fire Water Pump System	General	Leak	2	Mean	II	N/A	0.8766
Fire Water Pump System	General	Leak	2	Upper	II	N/A	3.5064
Fire Water Pump System	General	No Transmission	2	Lower	II	N/A	0.6575
Fire Water Pump System	General	No Transmission	2	Mean	II	N/A	0.8766
Fire Water Pump System	General	No Transmission	2	Upper	II	N/A	3.5064
Bilge System	General	Failure	5	Mean	II	N/A	0.0950
Auxiliary Electrical	General	Failure	5	Mean	II	N/A	0.0533
Auxiliary Electrical	General	Failure	5	Mean	II	N/A	0.0633

Continued on Next Page...

Table C.2 – Continued

Part	Capacity	FM	Source	Stats	Qual.	N	FR [1/year]
Bilge System	General	Failure	5	Mean	II	N/A	0.0033
Power Supply	High Voltage	Failure	5	Mean	II	N/A	0.0037
Auxiliary Electrical	General	Failure	5	Mean	II	N/A	0.0547
Bilge System	General	Failure	5	Mean	II	N/A	0.0080
Auxiliary Electrical	General	Failure	5	Mean	II	N/A	0.0037
Bolt	General	Failure	12	Mean	II	8	0.6119
Bolt, Anchor	General	Failure	12	Mean	II	2	0.5943
Brake, Electromechanical	General	Failure	12	Mean	II	8	2.5343
Brake, Shoe	General	Failure	12	Mean	II	1	33.3897
Chain, Hoisting, Bicycle Type	General	Failure	12	Mean	II	1	0.6171
Clutch	General	Failure	12	Mean	II	1	2.8893
Clutch, Friction, Power Transmittal	General	Failure	12	Mean	II	2	3.9131
Control Panel	General	Failure	12	Mean	II	1	1.0283
Drum, Wire Rope	General	Failure	12	Mean	II	1	1.5218
Gauge	General	Failure	12	Mean	II	2	1.0808
Nut, Split	General	Failure	12	Mean	II	1	20.8552
Pin, Mechanical, Gudgeon	General	Failure	12	Mean	II	1	0.8301
Programmable Logic Controller	General	Failure	12	Mean	II	2	1.9005
Receptacle, Electrical	General	Failure	12	Mean	II	1	3.7992

Continued on Next Page...

Table C.2 – Continued

Part	Capacity	FM	Source	Stats	Qual.	N	FR [1/year]
Relay	General	Failure	12	Mean	II	3	2.0881
Relay, Contact, Brake	General	Failure	12	Mean	II	1	0.7802
Relay, Contact, Signal	General	Failure	12	Mean	II	1	0.7802
Switch	General	Failure	12	Mean	II	3	2.0846
Switch, Control	General	Failure	12	Mean	II	6	1.5840
Switch, Control, Selector	General	Failure	12	Mean	II	1	2.6991
Switch, Interlock	General	Failure	12	Mean	II	1	2.8893
Switch, Limit	General	Failure	12	Mean	II	21	3.5581
Switch, Limit, Rotary	General	Failure	12	Mean	II	7	2.6131
Switch, Micro	General	Failure	12	Mean	II	2	1.2448
Switch, Transfer, Automatic	General	Failure	12	Mean	II	4	1.2255
Valve, Pilot	General	Failure	12	Mean	II	1	1.2448
Mechanical linkage	General	Failure	6	Mean	II	N/A	0.6300
FPSO Mooring, UK	General	failure	11	Mean	II	N/A	0.1851
Rectifiers							
Rectifier	General	Failure	2	Lower	II	N/A	0.0263
Rectifier	General	Failure	2	Upper	II	N/A	0.0438
Rectifier	General	No Output	3	Lower	I(a)	1	0.0000
Rectifier	General	No Output	3	Mean	I(a)	1	0.0027
Rectifier	General	No Output	3	Upper	I(a)	1	0.0149

Continued on Next Page...

Table C.2 – Continued

Part	Capacity	FM	Source	Stats	Qual.	N	FR [1/year]
Rectifier	General	Erratic Output	3	Lower	I(a)	1	0.0000
Rectifier	General	Erratic Output	3	Mean	I(a)	1	0.0359
Rectifier	General	Erratic Output	3	Upper	I(a)	1	0.0833
Rectifier	General	High Output	3	Lower	I(a)	1	0.0000
Rectifier	General	High Output	3	Mean	I(a)	1	0.0359
Rectifier	General	High Output	3	Upper	I(a)	1	0.0833
Rectifier	General	Failure (Total)	3	Lower	I(a)	1	0.0228
Rectifier	General	Failure (Total)	3	Mean	I(a)	1	0.0771
Rectifier	General	Failure (Total)	3	Upper	I(a)	1	0.1403
Rectifier	General	Failure	5	Mean	II	N/A	0.0053
Rectifier	General	Failure	5	Mean	II	N/A	0.0053
Bridge Rectifier	General	Failure	5	Mean	II	N/A	0.0053
Rectifier	General	Failure	6	Mean	II	N/A	0.0380
Tidal turbines							
Sleeve Bearing	General	Binding	2	Lower	II	N/A	0.0018
Sleeve Bearing	General	Binding	2	Upper	II	N/A	0.0175
Sleeve Bearing	General	Worn	2	Lower	II	N/A	0.0026
Sleeve Bearing	General	Worn	2	Upper	II	N/A	0.0263
Heavy Ball Bearing	General	Binding	2	Lower	II	N/A	0.0070

Continued on Next Page...

Table C.2 – Continued

Part	Capacity	FM	Source	Stats	Qual.	N	FR [1/year]
Heavy Ball Bearing	General	Binding	2	Upper	II	N/A	0.0701
Heavy Ball Bearing	General	Worn	2	Lower	II	N/A	0.0105
Heavy Ball Bearing	General	Worn	2	Upper	II	N/A	0.1052
Shaft and Bearings	General	Failure	7	Mean	II	N/A	0.0200
Blade	General	Failure	7	Mean	II	N/A	0.1600
Pitch Mechanism	General	Failure	7	Mean	II	N/A	0.2800
Transformers							
Transformer	$\geq$ 15kV	Failure	1	Mean	II	N/A	0.0053
Transformer	15kV - 33 kV	Failure	1	Mean	II	N/A	0.0175
Transformer	33kV - 132kV	Failure	1	Mean	II	N/A	0.0351
Transformer	132kV - 400kV	Failure	1	Mean	II	N/A	0.0614
Transformer	$\geq$ 415V	Open Primary	2	Lower	II	N/A	0.0018
Transformer	$\geq$ 415V	Open Primary	2	Mean	II	N/A	0.0044
Transformer	$\geq$ 415V	Open Primary	2	Upper	II	N/A	0.0307
Transformer	$\geq$ 415V	Open Secondary	2	Lower	II	N/A	0.0004
Transformer	$\geq$ 415V	Open Secondary	2	Mean	II	N/A	0.0009
Transformer	$\geq$ 415V	Open Secondary	2	Upper	II	N/A	0.0061
Transformer	$\geq$ 415V	Short Primary	2	Lower	II	N/A	0.0011

Continued on Next Page...

Table C.2 – Continued

Part	Capacity	FM	Source	Stats	Qual.	N	FR [1/year]
Transformer	≥ 415V	Short Primary	2	Mean	II	N/A	0.0026
Transformer	≥ 415V	Short Primary	2	Upper	II	N/A	0.0184
Transformer	≥ 415V	Short Secondary	2	Lower	II	N/A	0.0004
Transformer	≥ 415V	Short Secondary	2	Mean	II	N/A	0.0009
Transformer	≥ 415V	Short Secondary	2	Upper	II	N/A	0.0061
Transformer	221V - 440V	Failure	3	Lower	I(a)	2	0.0046
Transformer	221V - 440V	Failure	3	Mean	I(a)	2	0.0254
Transformer	221V - 440V	Failure	3	Upper	I(a)	2	0.0798
Transformer	441V - 5.5kV / 6.6kV	Failure	3	Lower	I(a)	5	0.0210
Transformer	441V - 5.5kV / 6.6kV	Failure	3	Mean	I(a)	5	0.0526
Transformer	441V - 5.5kV / 6.6kV	Failure	3	Upper	I(a)	5	0.1140
Transformer Cooling	General	Failure	5	Mean	II	N/A	0.0362
Transformer	General	Failure	5	Mean	II	N/A	0.0013
Transformer	General	Failure	5	Mean	II	N/A	0.0013
Transformer / Rectifier	General	Failure	5	Mean	II	N/A	0.0066

Continued on Next Page...

Table C.2 – Continued

Part	Capacity	FM	Source	Stats	Qual.	N	FR [1/year]
Isolating Transformer	General	Failure	5	Mean	II	N/A	0.0025
Transformer	3.3kV - 33kV	Failure	6	Mean	II	N/A	0.0064
Transformer	33kV - 132kV	Failure	6	Mean	II	N/A	0.0027
Transformers	132kV - 400kV	Failure	6	Mean	II	N/A	0.0037
Transformer	4.5kV - 415V	Failure	6	Mean	II	N/A	0.0064

Appendix D

Hydraulic test rig simulation

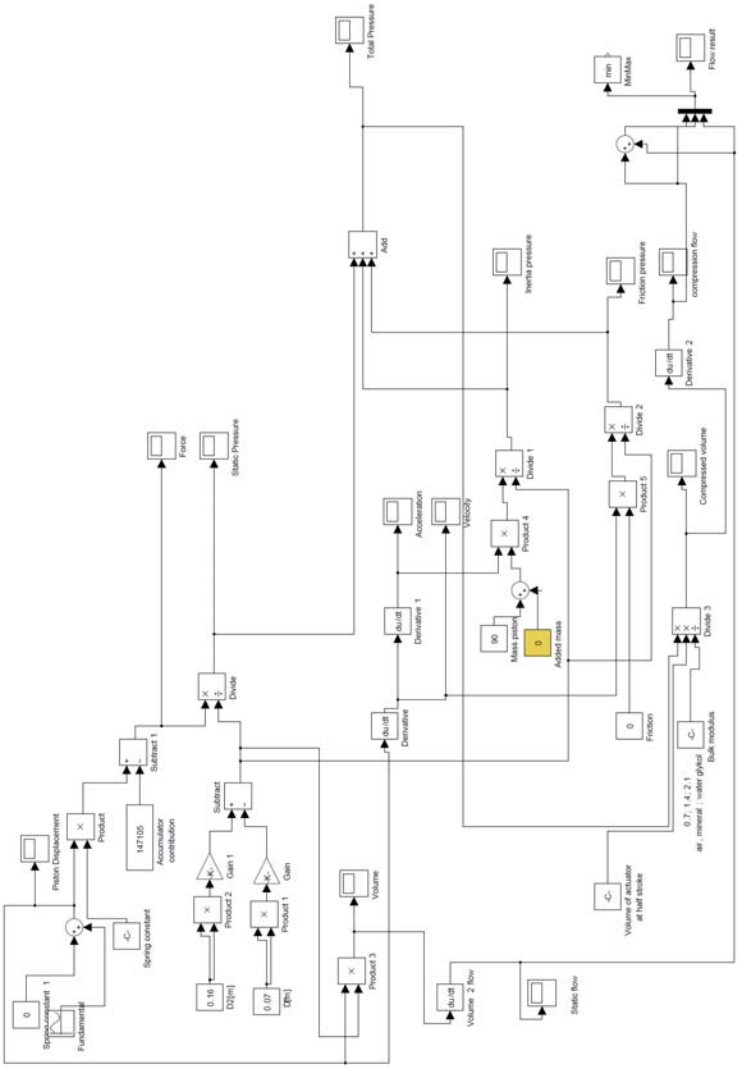
Total Pressure
Add
Inertia pressure
Friction pressure
compression flow
Flow result
MinMax
Derivative 2
Divide 2
Compressed volume
Divide 3
Bulk modulus
Force
Static Pressure
Divide 1
Acceleration
Velocity
Product 4
Product 5
Derivative 1
Mass piston
Added mass
Friction
Divide
Derivative
Subtract 1
Subtract
Piston Displacement
Product
147105
Accumulator contribution
Gain 1
Gain
Product 2
Product 1
Spring constant
Volume
Product 3
Volume of actuator at half stroke
Volume 2 flow
Static flow
Spring constant 1
Fundamental
0.16
D2[m]
0.07
d[m]